AD NUMBER
AD452983
NEW LIMITATION CHANGE
TO Approved for public release, distribution unlimited
FROM Distribution authorized to U.S. Gov't. agencies and their contractors; Administrative/Operational Use; 30 JUN 1964. Other requests shall be referred to Department of Defense, ATTN: Public Affairs Office, Washington, DC 20301.
AUTHORITY
USAEC ltr dtd 15 Jun 1966

UNCLASSIFIED

AD **4 5 2 9 8 3**

DEFENSE DOCUMENTATION CENTER

FOR

SCIENTIFIC AND TECHNICAL INFORMATION

CAMERON STATION ALEXANDRIA. VIRGINIA

UNCLASSIFIED

Quarterly Research Review No. 9

1 April through 30 June 1964

4 5 2 9 8 3

Prepared by

Solid-State Electronics Laboratory
Electron Devices Laboratory
Systems Theory Laboratory
Radioscience Laboratory

of the
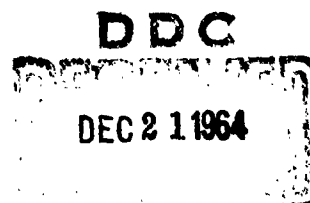
STANFORD ELECTRONICS LABORATORIES

STANFORD UNIVERSITY · STANFORD, CALIFORNIA

QUARTERLY RESEARCH REVIEW NO. 9

1 April through 30 June 1964

Prepared by
SOLID-STATE ELECTRONICS LABORATORY

under

ELECTRON DEVICES LABORATORY

under

and

SYSTEMS THEORY AND RADIOSCIENCE LABORATORIES

under

W. R. Rambo, Director

STANFORD ELECTRONICS LABORATORIES
Stanford University   Stanford, California

FOREWORD

This report contains a review of unclassified research activities of the Stanford Electronics Laboratories. This report covers the three-month period ending June 30, 1964. Because of contractual specifications, the research activities of the Systems Techniques Laboratory and portions of the Radioscience Laboratory are not included in this report but are reported separately.

SEL-64-073

PERSONNEL OF THE ELECTRON DEVICES LABORATORY

(1 April through 30 June 1964)

DIRECTOR - D. A. Dunn

FACULTY SENIOR RESEARCH ASSOCIATES, AND RESEARCH ASSOCIATES

W. W. Anderson	D. A. Dunn	R. P. Lagerstrom
P. Burger	S. E. Harris	R. J. Morris
O. Buneman	H. Heffner	D. Pigache
H. Derfler	R. Hockney	A. E. Siegman

RESEARCH ASSISTANTS AND FELLOWS

J. Allen	R. Kerr	E. J. Powers
W. A. Bares	T. C. Lee	G. Reiter
J. Bjorkholm	L. Linson	C. Y. She
I. C. Chang	C. M. McIntyre	T. C. Simonen
M. Cowley	W. Nichparenko	J. E. Simpson
D. R. Dobrott	M. Omura	H. Sonnenberg
G. Francois	L. M. Osterrink	J. Tellefsen
A. S. Halsted	T. Paoli	J. L. Uebbing
J. Hosea		

PUBLICATIONS AND REPORTS

(1 April through 30 June 1964)

PAPERS PRESENTED AT MEETINGS

Conference on Instabilities due to Streams or Currents, Berkeley, Calif., April 6, 1964.

D. A. Dunn, A. S. Halsted, and P. Burger, "Computer Experiments on Beam-Generated Plasmas." Contract AMC-00094(E).

Toronto Meeting of Electrochemical Society, May 7.

W. W. Anderson, "Photoluminescent Properties of Rare-Earth Doped II-VI Compounds." Contract AFOSR 62-286.

22nd Conference on Electron Device Research, June 24

W. W. Anderson and S. Razi, "Electroluminescent ZnS Doped with Rare Earths, a Possible Laser System." Contract SC-90839.

ARTICLES PUBLISHED

D. A. Dunn and I. T. Ho, "Computer Model of a Beam-Generated Plasma," *Bull. Am. Phys. Soc.*, **9**, 325, Mar. 23, 1964.

TECHNICAL REPORTS ISSUED BY EDL

(1 April through 30 June 1964)

Air Force Contract AF33(657)-11144

No. 0309-2: D. A. Dunn and I. T. Ho, "Computer Model of a Beam-Generated Plasma."

Army Contract DA 36-039 AMC-00094(E)

No. 0358-2: H. A. Hogg, "Design for a Hollow-Beam Disc-Loaded Coaxial-Line Megawatt, Traveling-Wave Amplifier."

PERSONNEL OF THE SOLID-STATE ELECTRONICS LABORATORY

(1 April through 30 June 1964)

DIRECTOR - J. G. Linvill

FACULTY, SENIOR RESEARCH ASSOCIATES, AND RESEARCH ASSOCIATES

J. B. Angell	G. L. Pearson
D. Chauvy	R. L. Pritchard
J. F. Gibbons	W. Shockley
L. Jonasson	W. E. Spicer
J. G. Linvill	R. L. White
M. M. McWhorter	B. Widrow
J. L. Moll	

RESEARCH ASSISTANTS AND FELLOWS

P. Bardell	E. W. Fraser	R. Mehta
N. Berglund	J. W. Hill	K. C. Pant
A. Blodgett	M. J. C. Hu	R. Potts
M. G. Buehler	R. P. James	A. Rideout
Y. S. Chen	N. Kindig	M. A. Savageau
E. Duh	J. Knox-Seith	K. Shih
D. J. Cumin	J. Koike	J. Vilms
R. Eden	W. Krolikowski	R. Woodbury
J. Eggenberger	D. Loescher	B. P. F. Wu

PUBLICATIONS AND REPORTS

(1 April through 30 June 1964)

PAPERS PRESENTED AT MEETINGS

San Francisco Bay Area Chapter of The Association for Computer Machinery Meeting, June 19, 1964.

    J. B. Angell, "Adaptive vs Fixed Redundancy in Digital Systems."

New York University Colloquium Series, April 7, 1964.

    J. G. Linvill, "Microelectronic Reading Aid for the Blind."

<u>NASA-Round Table Discussion, April 27, 1964.</u>*

  W. E. Spicer, "Optical Detectors in Space."

<u>1964 Summer Meeting American Physical Society, June 27, 1964.</u>⁺

  N. B. Kindig and W. E. Spicer, "Photoemission Studies of Vacuum-
Cleaved CdS."

  W. E. Spicer and N. B. Kindig, "Surface Reactions and Band-Bending
in Photoemission Studies of CdS."

PAPERS AND ARTICLES ACCEPTED FOR PUBLICATION

  J. F. Gibbons and H. S. Horn, "A Circuit with Logarithmic Transfer
Response Over 9 Decades," accepted for publication in the September 1964
issue of the Professional Group on Circuit Theory.

  R. Stuart, F. Wooten, and W. E. Spicer, "Monte Carlo Calculations
Pertaining to the Transport of Hot Electrons in Metals," Physical Review.**

  F. Wooten and W. E. Spicer, "Surface Effects, Band Bending, and
Photoemission in Semiconducting Films of Cs_3Sb," Surface Science.**

ARTICLES PUBLISHED

  L. L. Chang† and G. L. Pearson, "Diffusion Mechanism of Zn in GaAs
and GaP Based on Isoconcentration Diffusion Experiments," <u>J. Appl. Phys.</u>,
35, pp. 1960-1965, June 1964.

  L. L. Chang† and H. C. Casey, Jr.,†† "Diffusion and Solubility of
Zinc in Indium Phosphide," Solid-State Electronics, <u>7</u>, pp. 481-485, (1964).

  H. K. J. Ihantola and J. L. Moll, "Design Theory of a Surface Field-
Effect Transistor," Solid-State Electronics, Vol. <u>7</u>, pp. 423-430, 1964.

  N. B. Kindig and W. E. Spicer, "Photoemission Studies of Vacuum-
Cleaved CdS," <u>Bull. Amer. Phys. Soc.</u>, <u>9</u>, 573, 1964.*

  J. G. Linvill and G. Danon, "Application de la Methode des Para-
metres Echantillonnes au Calcul et a la Realisation d'Amplificateurs
Transistores a Larges Bandes," <u>Proceedings of the International Symposium
on Nuclear Electronics</u>,November 25-27,1963, Paris, pp. 829-39. [Supported
in part by Nonr-225(24).]

  W. E. Spicer and N. B. Kindig, "Surface Reactions and Band Bending
in Photoemission Studies of CdS," <u>Bull. Amer. Phys. Soc.</u>, <u>9</u>, 573, 1964.*

TECHNICAL REPORTS ISSUED BY SSL

(1 April through 30 June 1964)

Air Force Contract AF33(616)-7726

No. 4711-1:   J. F. Gibbons and P. C. Prehn, "Epitaxial Vapor Growth of III-V Compounds."

No. 4714-1:   D. J. Dumin, "The Quantizer: An Application of Quantization of Trapped Flux in Superconductors."

Office of Naval Research Contract Nonr-225(24)

No. 4815-1:   G. Danon and K. Sorenson, "The Sampled Parameter Method and Design of Wideband Transistor Amplifiers."

Office of Naval Research Contract Nonr-225(44)

No. 4816-1:   John Knud Knox-Seith, "A Redundancy Technique for Improving the Realiability of Digital Systems."

Office of Naval Research Contract Nonr-225(31)

No. 4818-1:   Tsu-fann Shao, "Measurement of the Temperature Dependance of Minority Carrier Mobility in a Transistor Base Region."

Contract SD 87-4850-47

No. 5205-1:   C. N. Berglund, "Photoemission Studies of Copper and Silver."

PERSONNEL OF SYSTEMS THEORY LABORATORY

(1 April through 30 June 1964)

DIRECTOR - G. F. Franklin

FACULTY

N. M. Abramson	H. Mays
D. Huffman (visiting)	J. McFadden (visiting)
T. Kailath	
W. K. Linvill	R. W. Newcomb (on leave)
D. Luenberger	D. Tuttle
R. Mattson	B. Widrow

RESEARCH ASSISTANTS AND FELLOWS

K. A. Belser	G. Groner	L. Meier
R. J. Brown	P. H. Haley	C. Mosher
C. S. Burrus	T. J. Harrison	A. Nichols
N. Carlson	J. Hopcroft	Y. N. Patt
J. Chang	T. L. Humphrey	D. Peterson
R. Chow	M. J. C. Hu	J. Rosing
A. Cooper	C. A. Isberg	W. Rousseau
J. Cooper	Donlan F. Jones	E. A. Sautter
T. M. Cover	E. R. Jones	C. Shaffer
R. F. Daly	P. Kennedy	E. J. Skiko
R. P. Dolan	J. S. Koford	P. B. Skov
C. N. Dorny	G. N. T. Lack	F. W. Smith
R. Dressler	R. E. Larson	D. Spaulding
M. J. Ferguson	M. L. Liou	D. F. Specht
E. C. Fraser	J. W. McConnell	D. Starner
N. T. Gaarder	K. B. Magleby	L. R. Talbert
R. Geesey	J. P. Mantey	D. M. Ward
F. Glanz	P. Mantey	C. Weaver
B. Gragg	J. E. Matheson	

SEL-64-073

PUBLICATIONS AND REPORTS

(1 April through 30 June 1964)

PAPERS PRESENTED AT MEETINGS

IEEE Region 6 Annual Conference, April 29, 1964.

N. Abramson, "Pattern Recognition."

PAPERS AND ARTICLES ACCEPTED FOR PUBLICATION

T. Kailath, "Some Results on Singular Detection," Proceedings of
International Conference on Circuits, Microwaves and Information Theory.
(Done under Project 7050, Task 24).

ARTICLES PUBLISHED

N. Abramson, "Bandwidth and Spectra of Phase- and Frequency-Modulated
Waves," IEEE Transactions on Communication Systems, Vol. CS-11, No. 4,
pp. 407-414, Dec. 1963.

TECHNICAL REPORTS ISSUED BY STL

(1 April through 30 June 1964)

Office of Naval Research Contract Nonr-225(24)

No. 6204-1: J. A. Cooper, "Orthogonal Expansion Applied to the
Design of Threshold Element Networks."
No. 6762-1: Walter S. Buslik, "Seek Time Improvement in a Random
Access File by Application of an Adaptive Element."
No. 6302-3: David Thomas Magill, "Optimal Adaptive Estimation of
Sampled Stochastic Processes."
No. 6104-8: R. A. Scholtz, "Coding for Adaptive Capability in
Random Channel Communications."
No. 6302-4: James Blair Farison, "Identification and Control of
Random Parameter Discrete Systems."
No. 6302-5: Edward John Skiko, "Optimum Sampling and Control
Procedures for a Multiplexed Digital Computer."

U. S. Army X Project Office Contract DA 04(200) AMC 57(Z)

FINAL: Bernard Widrow and Richard L. Mattson, "Adaptive Decision
Techniques for Discrimination." (Report SECRET - Title Unclassified).

PERSONNEL OF RADIOSCIENCE LABORATORY

(1 April through 30 June 1964)

Only a small number of the personnel
have contributed to this manuscript;
therefore, only the contributors are
listed below.

DIRECTOR - O. G. Villard, Jr.

FACULTY, SENIOR RESEARCH ASSOCIATES, AND RESEARCH ASSOCIATES

L. A. Manning   A. M. Peterson

V. R. Eshleman

RESEARCH ASSISTANTS

D. C. Brown   R. Nowak

PUBLICATIONS AND REPORTS

(1 April through 30 June 1964)

PAPERS AND ARTICLES ACCEPTED FOR PUBLICATION

L. A. Manning, "The Theoretical Heights and Durations of Echoes
from Large Meteors," October 1964 issue of the Journal, Radio Science
(Section D of the NBS Journal of Research).

L. A. Manning, "The Experimental Determination of Meteoric Line
Densities and Attachment Rates," October 1964 issue of the Journal,
Radio Science (Section D of the NBS Journal of Research).

TECHNICAL REPORTS ISSUED BY RSL

(1 April through 30 June 1964)

Office of Naval Research Contract Nonr-225(64)

No. 87: John Ames, "The Spatial Properties of the Amplitude Fading
of Continuous 17-Mc Radio Waves."

No. 90: T. A. Croft, "Aspect and Deviation Angle."

No. S-17: D. P. Kanellakos, "Characteristics of Ionospheric Dis-
turbances--Part IV." (Report SECRET - Title Unclassified).

No. S-19: G. H. Barry and L. J. Griffiths, "To or Fro." (Report
SECRET - Title Unclassified).

National Aeronautics and Space Administration Grant NsG 30-60

No. 4: J. J. Angerami and J. O. Thomas, "The Distribution of Ions and Electrons in the Earth's Exosphere."

CONTENTS

*Subject area codes: P, Plasmas; QE, Quantum Electronics; SS, Solid-State; ST, Systems Theory; ET, Electron Tubes; RS, Radioscience. Where a double reference is given (SS-ST), the work is such that portions of it may appear in each of the laboratories listed.

SEL-64-073

Contents (Cont'd)

I. ELECTRON DEVICES LABORATORY (Cont'd)

Contents (Cont'd)

III. SYSTEMS THEORY LABORATORY (Cont'd)

ILLUSTRATIONS

CROSS INDEX

<u>Office of Naval Research Contract Nonr-225(24)</u>

Project	Title	*Subject Area	Leader	Page
	ELECTRON DEVICES LABORATORY			
0174	Microwave spectra of transition-group ions in semiconductor lattices	QE	Anderson	I-1
0255	Computer model of a 2-dimensional plasma	P	Buneman	I-39
0311	Pinch effects in plasma beams	P	Dunn	I-43
0414	Emission of electrons in solids	QE	Heffner	I-61
0415	Utilization of optical masers	QE	Heffner	I-64
	SOLID-STATE ELECTRONICS LABORATORY			
4715	Transient performance of transistor switches under high level injection	SS	Gibbons	II-9
4814	Performance limitations of photon coupled systems	SS	Linvill	II-11
4815	Transistor pulse amplifiers	SS	Linvill	II-12
5064	Studies of luminescence centers in semiconducting compounds	SS	Moll	II-35
5107	Properties of GaAs p-n junctions	SS	Pearson	II-59
5207	Radiative lifetime measurement in GaAs	SS	Spicer	II-67
	SYSTEMS THEORY LABORATORY			
6103	Pattern recognition and machine learning	ST	Abramson	III-1
6105	Information theory	ST	Abramson	III-10
6203	State-logic relations for sequential networks	ST	Epley	III-12
6206	Multi-tape sequential machines	ST	Epley	III-12
6209	Logical design of fast circuits	ST	Huffman	III-12
6301	Development of simulation facility	ST	Franklin	III-13
6302	The optimum static and dynamic control of multi-actuator systems	ST	Franklin	III-13
6552	Modeling of linear systems	ST	Luenberger	III-13
6557	Theory and design of nonlinear reactance subharmonic generators	ST	Grace	III-17
6657	Studies of the describing-function method of nonlinear network analysis	ST	Tuttle	III-17
6758	Analysis and synthesis of some adaptive networks	SS-ST	Widrow	II-69

Cross Index (Cont'd)

Office of Naval Research Contract Nonr-225(24) (Cont'd)

Project	Title	*Subject Area	Leader	Page
	SYSTEMS THEORY LABORATORY (Cont'd)			
6762	Adaptive systems	SS-ST	Widrow	III-19
6763	Adaptive computer diagnosis	SS-ST	Widrow	III-20
6950	Threshold logic elements and adaptive systems	SS-ST	Mattson	III-25
6952	A study of adaptive input-coding technique	ST	Mattson	III-26
7050	Communication theory	ST	Kailath	III-27
	RADIOSCIENCE LABORATORY			
3550	Meteor echo properties	RS	Manning	IV-1
3606	Ionospheric winds and irregularities in electron density in the ionosphere	RS	Peterson	IV-2

Office of Naval Research Contract Nonr-225(31)

Project	Title	*Subject Area	Leader	Page
	SOLID-STATE ELECTRONICS LABORATORY			
4818	Applications of electro-optical phenomena in solids	SS	Linvill	II-12

Office of Naval Research Contract Nonr-225(44)

Project	Title	*Subject Area	Leader	Page
	SOLID-STATE ELECTRONICS LABORATORY			
4813	Application of solid-state phenomena to microsystems	SS	Linvill	II-10
4816	Reliable systems with unreliable parts	SS	Linvill	II-12

Air Force Contract AF33(657)-11586

Project	Title	*Subject Area	Leader	Page
	SOLID-STATE ELECTRONICS LABORATORY			
4651	Physical principles of magnetic adaptive components	SS	Angell	II-1
4655	Fefet adaptive components	SS	Angell-Moll	II-3
4656	Integrated arrays of magnetic adaptive components	SS	Angell	II-3
4657	Self-repairing circuit techniques	SS	Angell	II-6
4711	Epitaxial growth	SS	Gibbons	II-8

Cross Index (Cont'd)

Air Force Contract AF33(657)-11586 (Cont'd)

Project	Title	*Subject Area	Leader	Page
	SOLID-STATE ELECTRONICS LABORATORY (Cont'd)			
4714	Circuit aspects of various cryogenic phenomena	SS	Gibbons	II-9
5059	Hot electrons in thin metal films	SS	Moll	II-28
	SYSTEMS THEORY LABORATORY			
6201	Adaptive network organization	SS-ST	Epley	III-11
6202	Logical properties of adaptive networks	SS-ST	Widrow	III-11
6767	Two-layer adaption studies	ST	Widrow	III-21
6772	Pattern recognition control systems	ST	Widrow	III-24

Air Force Contract AF04(695)-305

Project	Title	*Subject Area	Leader	Page
	ELECTRON DEVICES LABORATORY			
0581	Infrared modulation and demodulation techniques	QE	Siegman	I-74
0582	Optical phase- and frequency-modulation techniques	QE	Siegman	I-77

Signal Corps Contract DA 36-039 SC-85339

Project	Title	*Subject Area	Leader	Page
	SOLID-STATE ELECTRONICS LABORATORY			
5054	Study of hot electrons in silicon	SS	Moll	II-28

Center for Materials Research Contract SD-87-003

Project	Title	*Subject Area	Leader	Page
	SOLID-STATE ELECTRONICS LABORATORY			
5105	Rare earth impurities in semiconductors	SS	Pearson	II-57

Cross Index (Cont'd)

Cross Index (Cont'd)

Air Force Contract AF33(657)-11144

Project	Title	*Subject Area	Leader	Page
	ELECTRON DEVICES LABORATORY			
0309	Neutralized charged particle streams	P	Dunn	I-40
0312	Amplification in beam-generated plasmas	P	Dunn	I-43
0322	Noise generation in plasmas	P	Dunn	I-57
0576	Microwave light modulation methods	QE	Siegman	I-69
0908	Ion and plasma beam sources	P	Lagerstrom	I-119

Air Force Contract AF33(615)-1504

	ELECTRON DEVICES LABORATORY			
0816	Transient phenomena in low pressure gas discharge plasmas	P	Derfler	I-84

Signal Corps Contract DA 36-039 SC-90839

	ELECTRON DEVICES LABORATORY			
0178	Optical maser materials	QE	Anderson	I-16
0592	Laser photomixing studies	QE	Siegman	I-79

Army Contract DA 36-039 AMC-00094(E)

	ELECTRON DEVICES LABORATORY			
0313	Computer experiments on beam-generated plasmas	P	Dunn	I-49
0321	Electron beam focusing in ionized gases	P	Dunn	I-51
0558	Investigation of noise in electron guns	ET	Siegman	I-65
0577	Microwave phototubes and light demodulators	ET	Siegman	I-72
0832	RF behavior of plasma diodes	P	Derfler	I-99

Cross Index (Cont'd)

PROJECT 0173: OPTICAL SPECTRA OF IONS IN SEMICONDUCTORS

Air Force Office of Scientific Research Grant 323-63
Project Leader: W. W. Anderson
Staff: T. C. Lee

The object of this project is to investigate various semiconductor lattices as hosts for active optical maser ions. This will involve the incorporation of members of the 3d and 4f transition group ions into semiconductor lattices, an investigation of absorption and emission spectra, and a study of the mechanisms of energy transfer from the host lattice to the active ion.

During the past quarter, we have carried out photoluminescence experiments on Mn diffused GaAs at 4.2 °K. The GaAs we used was supplied by Monsanto Company. It was boat grown, oxygen compensated, and had a low electron concentration of 4×10^{15}/cc. The surface concentration of manganese was 10^{18}/cc. The photoluminescence measurement was recorded on a Perkin-Elmer 12-G spectrometer using a 600 line/mm grating and a spectral slit width to give 6Å resolution. After being filtered by a saturated $CuSO_4$ solution, light from a Pek 109 mercury arc lamp was focussed on the GaAs immersed in liquid helium. Fluorescence was collected from the same surface as the exciting radiation and was filtered by a Corning CS-2-64 filter to remove the incident light. The detector was a cooled DuMont 6911 photomultiplier. The spectrometer transmission and detector response characteristic were determined by a NbS calibrated tungsten lamp.

Figure 1 shows the emission spectrum at 4.2 °K. The most intense peak occurs at 1.4089 ± 0.00032 ev and is only .01 ev wide. If one takes the band gap of GaAs at 4.2 °K as 1.521 ev [Ref. 1], then the acceptor energy level of manganese is 0.112 ev above the valence band. There exists a shoulder 0.0089 ev below the main peak which we ascribe to a transverse

---

[1] We assume that the band gap of GaAs at 4.2 °K is the same as at 21 °K. See p. 770, Table 1; M.D. Sturge, Phys. Rev., 127, 768 (1962).
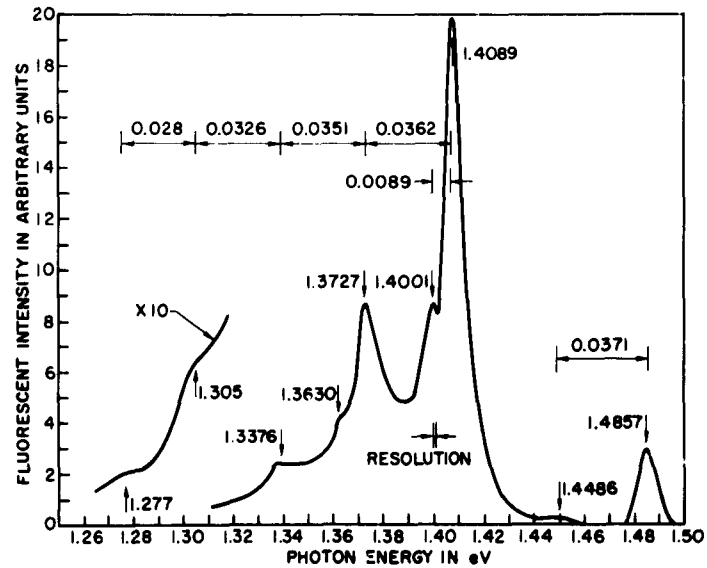
FIG. 1. PHOTOLUMINESCENCE OF Mn DIFFUSED GaAs AT 4.2 °K.

acoustic (TA) phonon emission [Ref. 2]. The next peak occurs at 1.3727 ± 0.0003 ev, which is 0.0362 ev below the main peak. This energy is very close to the LO phonon energy [Ref. 3] as measured in the Restrahlen band of GaAs. A shoulder 0.0097 ev below the peak of this line is also resolved, which again can be ascribed to TA phonon emission. The next three peaks are increasingly broadened and are separated from one another by approximately the LO phonon energy as indicated in Table 1. Contributions from the wings of the strong lines may influence the apparent locations of the peaks of the weaker lines.

In Table 1 we also compare the intensities of the various lines with the Poisson distribution as first suggested by Hopfield:

$$W_n \sim \frac{\bar{N}^n}{n!}$$

[2] W. Cochran, et al, J. Appl. Phys., 32, 2102 (1961).

[3] S. J. Fray, et al, Proc. Phys. Soc. (London) 77, 215 (1961).

[7] G. J. Lasher, IBM Journal, 7, 58 (1963).

where W_n is the probability of emission of n phonons with the photon and $\bar{N}$ is mean number of LO phonons emitted. In our case $\bar{N} = 0.43$ is chosen.

TABLE 1

n	measured peak height	$\dfrac{\bar{N}^n}{n!}$	location of peak (ev)	Difference (ev)
0	1.0	1.0	1.4089	0.0362
1	0.43	0.43	1.3727	0.0351
2	0.12	0.093	1.3376	0.0326
3	0.031	0.013	1.305	0.0280
4.	0.001	0.00015	1.277	
	Higher energy lines		1.485	0.037
			1.448	

As seen in the table, the comparison becomes poorer as the lines become weaker. One obvious reason for this is contributions from the wings of strong lines. Another reason is that the Poisson distribution is based on a simple model in which the trapped carrier interacts only with LO phonons which carry the ionic polarization. Actually, in our results, a TA phonon is obviously also involved in the interaction.

The two extra lines on the high energy side are also separated by the LO phonon energy. They may be due to other unintended impurities or surface defects. It seems improbable to correlate the first series and second series of lines although similar two-series phenomena also exist in the edge emission of CdS [Ref. 4] but have not been satisfactorily assigned.

---

[4] C. C. Klick, Phys. Rev., 89, 274, (1953).

The radius a of the trapped hole at a Mn center can be inferred from the following [Ref. 7]:

$$\bar{N} = \frac{e^2}{a}\ \frac{1}{\hbar\omega_{LO}}\ \frac{1}{\sqrt{2\pi}}\left(\frac{1}{\epsilon} - \frac{1}{\epsilon_o}\right)$$

where ϵ is the high frequency dielectric constant and ϵ_o the static dielectric constant. A Gaussian charge distribution has been assumed in deriving the above formula. The value of a turns out to be 5.35Å, which is compatible with the binding energy of 0.11 ev. The spread of virtual phonons in k space is about one-third the distance from the center to the edge of the first Brillouin zone.

We are also considering the possibility of optically pumping the Mn diffused GaAs sample to obtain laser emission at 4.2 °K. The scheme we propose is shown in Fig. 2. Pumping light shines directly on the front
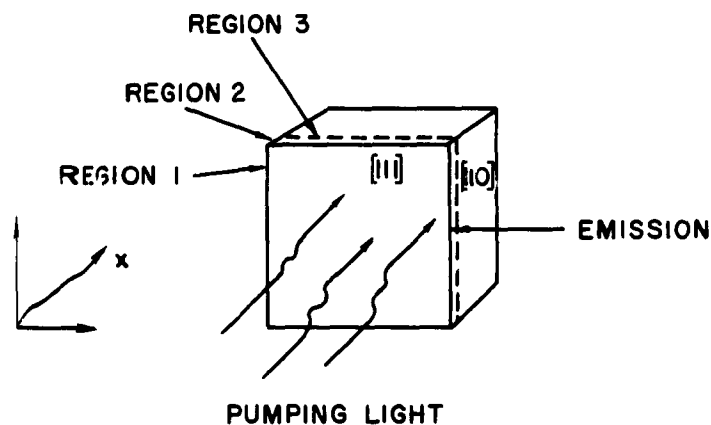
FIG. 2. A SIMPLE DRAWING OF A GaAs SQUARE TO BE OPTICALLY PUMPED.

surface, while the two cleaved surfaces form the end plates of a Fabry-Perot resonator. To estimate the threshold power required for obtaining lasing action, we have to take care of losses due to three mechanisms: 1) surface recombination; 2) bulk losses associated with diffraction; and 3) transmission losses at the end plates.

For a p-type semiconductor, the equation satisfied by an excess carrier density Δn is [Ref. 5]:

$$D_n \frac{d^2 \Delta n}{dx^2} - \frac{\Delta n}{\tau_n} = -Re^{-kx}$$ (1)

where:

D_n : diffusion constant of electrons

τ_n : lifetime of electrons

k : absorption constant for pumping light

$R = qk\bar{I}T/\bar{E}$

q : quantum efficiency of creating electron-hole pairs $\simeq 1$ in our case

$\bar{I}$: average incident power per unit area

T : transmission percentage of incident light

$\bar{E}$: $h\bar{\nu}$ average pumping photon energy

The boundary condition at $x = 0$ is that

$$D_n \frac{\partial \Delta n}{\partial x}\bigg|_{\alpha=0} = S\Delta n$$ (2)

where

S : surface recombination velocity.

Upon solving (1), one obtains

$$\Delta n = \frac{R\tau_n}{k^2 L_D^2 - 1} \left\{ \frac{kL_D^2 + S\tau_n}{L_D + S\tau_n} e^{-x/L_D} - e^{-kx} \right\}$$ (3)

where

$$L_D = (D_n \tau_n)^{1/2}: \text{ diffusion length}$$

5
R. A. Smith, Semiconductors, (Cambridge University Press), p. 310.

For GaAs in the pumping wavelength region, $k \gg 1/L_D$. Therefore, (3) can be simplified to

$$\Delta n = \frac{R\tau_n}{k^2 L_D^2 - 1} \cdot \frac{k L_D^2 + S\tau_n}{L_D + S\tau_n} e^{-x/L_D} \qquad (4)$$

In GaAs, we can take the following numbers

$$\frac{S\tau_n}{L_D} = 100 \qquad [\text{Ref. 6}]$$

$$L_D \simeq 2 \times 10^{-4} \text{ cm}$$

$$\bar{k} \simeq 10^5 \text{ cm}^{-1}$$

$$k L_D \simeq 20$$

$$\therefore \quad \Delta n \simeq \frac{R\tau_n}{\left(k L_D\right)^2} \times \frac{1.2}{2.72} \qquad (5)$$

where we have restricted the active region to be within one diffusion length. Now

$$g = \frac{\lambda^2}{8\pi n^2} F \qquad [\text{Ref. 7}] \qquad (6)$$

where

g: gain per unit length for the electromagnetic mode under consideration

F: Number of quanta spontaneously emitted per unit time per unit volume per unit frequency interval

_____

[6] The value of $S\tau_n/L_D$ ranges from 10 to 1000 depending on the material and the etching processes. (Private communication with J. Vilmes, Applied Electronics Laboratory, Stanford University.)

n: index of refraction

λ: wavelength in vacuum

Now that:

$$F = \frac{\eta \Delta n}{\tau_n \Delta \gamma} \tag{7}$$

where

η: quantum efficiency of radiation transition

$\Delta \gamma$: linewidth of spontaneous transition

Putting (5) and (7) into (6), renders:

$$g = \frac{\eta \lambda^2 R}{8 \, n^2 k^2 L_D^2 \, \Delta \gamma} \times \frac{1.2}{2.72} \tag{8}$$

Lasing threshold will be reached when

$$g = \alpha_S + \alpha_B \tag{9}$$

where

α_B = loss due to bulk of the inactive region, sometimes referred to as diffraction loss

α_S = loss due to transmission at surface.

From (8) and (9), one obtains

$$R = \frac{k\bar{I}T}{\bar{E}} = (\alpha_S + \alpha_B) \; 2.2 \; \frac{8\pi n^2}{\eta \lambda^2} \; k^2 L_D^2 \; (\Delta \nu)$$

or

$$\bar{I} = \frac{2.2}{T} \bar{E} \frac{8\pi n^2}{\eta \lambda^2} \Delta\nu (kL_D^2)(\alpha_S + \alpha_B)$$

(10)

$$= \frac{2.2}{T} kL_D^2 \cdot \frac{8\pi n^2 c\Delta E(\alpha_S + \alpha_B)}{\eta \lambda^2 \bar{\lambda}}$$

One can estimate α_B by using the equation [Ref. 8]

$$\frac{\sigma_2}{\omega_o \epsilon} = 3\sqrt{3/8} (k_o w)^2 \left(\frac{\sigma_{01}}{\omega_o \epsilon}\right)^2$$

(11)

The optical conductivity is related to absorption constant by

$$\frac{\sigma}{\omega \epsilon} = \frac{\alpha}{k_o}$$

(12)

where

$$k_o = \omega\sqrt{\mu\epsilon}$$

In (11), $\sigma_{01}/\omega_o \epsilon = \frac{\alpha_B}{k_o}$, $\frac{\sigma_2}{\omega_o \epsilon} = \frac{\alpha_2}{k_o}$. We therefore obtain

$$\alpha_B = \left\{ \frac{\alpha_2}{k_o} \frac{1}{w^2} \frac{1}{3\sqrt{3/8}} \right\}^{1/2} = \frac{0.736}{L_D\sqrt{k_o}} (\bar{\alpha})^{1/2}$$

(13)

where $\bar{\alpha} = \frac{\alpha_1 + \alpha_3}{2}$, is the average absorption constant in regions 1 and 3, and $w = L_D$ in our case.

---

[8] T. M. Quist, et al, Quantum Electronics III Conference, Paris, 1963, ed. Grivet and Bloembergen, V. II, p. 1833.

For the 0.9μ emission,

$$k_o = \frac{2\pi\sqrt{\epsilon}}{\lambda} = \frac{2\pi \times 3.3}{0.9 \times 10^{-4}} \simeq 23 \times 10^4 \ cm^{-1}$$

$$L_D \sim 2 \times 10^{-4} \ cm$$

$$\bar{\alpha} = \frac{\alpha_3}{2} \ (\because \ \text{there is no loss in region 1}) \sim 1 \ cm^{-1}$$

(14)

$$\therefore \qquad \alpha_B \simeq 8 \ cm^{-1}$$

If we coat the GaAs with silver so that transmission loss is around five percent, then

$$\alpha_S = \frac{0.05}{2mm} \simeq .25 \ cm^{-1} \qquad (15)$$

α_B dominates over α_S even if GaAs is not coated. 2mm is the length-wise dimension of the GaAs block. Together with (14) and (15), we can put the following numbers into equation (10).

$$kL_D \sim 20$$
$$\Delta E = 0.02 \ ev$$
$$\eta \sim 0.25$$
$$\bar{\lambda} = 0.69 \times 10^{-4} \ cm$$
$$\lambda = 0.9 \times 10^{-4} \ cm$$
$$\alpha_B + \alpha_S \sim 8 \ cm^{-1}$$
$$\therefore \qquad \bar{I} \simeq 10kw/cm^2$$

(16)

$\Delta E = 0.02 \ ev$ refers to the one phonon assisted transition, which though broader and less intense than the nonphonon line, will probably have lower lasing threshold due to the lack of loss associated with imcomplete inversion.

PROJECT 0174: MICROWAVE SPECTRA OF TRANSITION-GROUP IONS IN SEMICONDUCTOR LATTICES

Tri-Service Contract Nonr-225(24)
Project Leader: W. W. Anderson
Staff: I. C. Chang

A. INTRODUCTION

In the past few years there has been a great interest in the electron paramagnetic resonance of rare-earth ions in crystals of cubic symmetry. One reason (among others) is that some rare-earth ions in cubic fields will have a ground state that belongs to the Γ_8 representation of the cubic group. The Γ_8 state has many interesting features: it is of four-fold degeneracy and will split linearly into four unequally spaced levels when a magnetic field is applied. Transitions between any two levels are, in general, allowed; and, as pointed out by Bleaney [Ref. 1], the Γ_8 quartet has great potential in microwave maser applications.

Lea, Leask and Wolf [Ref. 2] have calculated the energy levels and wave functions of rare-earth ions in cubic fields. Their results conclude that Γ_8 quartet may be lowest for two cases: (1) Ce^{+++}, Nd^{+++}, Sm^{+++} and Dy^{+++} in the crystals of tetrahedral (4) or cubic (8) symmetry; (2) Nd^{+++} and Er^{+++} in the crystals of octahedral symmetry. Most of the rare-earth ions have been studied in the single crystals of CaF_2 and its isomorphs, [Refs. 3, 4] which are of cubic symmetry. Not too much work has been reported for rare-earth ions in octahedral sites, though Γ_8 quartet has been observed for Er^{+++} in the cubic fields of CaO [Ref. 5] and MgO [Ref. 6].

[1] B. Bleaney, Proc. Phys. Soc., (London) 73, 937 and 939 (1959).

[2] K. R. Lea, M. J. Leask, and W. P. Wolf, J. Phys. Chem. Solids, 23, 1381 (1962).

[3] W. Low, J. Phys. Soc. Japan, 17, Suppl. B-I 440, (1962).

[4] R. W. Bierig and M. J. Weber, Phys. Rev., 132, 164 (1963).

[5] W. Low and R. S. Rubins, Phys. Rev., 131, 2527 (1963).

[6] D. Descamps and Y. M. D'Aubigue, Phys. Rev. Lett., 8, 5 (1964).

In this report we discuss the EPR spectra of Er^{+++} in single crystals of CaO [Ref. 7]. The measurements were made at 35 kMc and at liquid helium temperatures. Measurements were also made at 9.3 kMc. The results are the same except for a scaling in the magnetic field, while the sensitivity of the spectrometer is considerably better at 35 kMc because of a better filling factor.

B. THEORY

The Hamiltonians describing the crystal field potentials of cubic symmetry are

$$\mathcal{H}_{cubic} = B_4(\tilde{O}_4^0 + 5\tilde{O}_4^4) + B(\tilde{O}_6^0 - 21\tilde{O}_6^4) \tag{1}$$

where $\tilde{O}_n^m$'s are Steven's operators transforming as the corresponding spherical harmonics [Ref. 8], B's are related to crystal field parameters and in the notation of Elliott and Stevens [Ref. 8], are equal to $\xi_n A_n^m \langle r^n \rangle$ where ξ_n is the operator equivalent factor α, β, γ for $n = 2, 4, 6$, respectively. For purely cubic fields, Lea, Leask and Wolf [Ref. 2] have plotted the energy levels of the rare-earth ions as a function of a parameter x defined by

$$\frac{x}{1 - |x|} = \frac{F(4)}{F(6)} \frac{B_4}{B_6} = \frac{F(4)\beta A_4 \langle r^4 \rangle}{F(6)\gamma A_6 \langle r^6 \rangle} \tag{2}$$

where the F's are multiplicative factors given in the paper by Lea, et al. From their diagrams one predicts that the ground state is a Γ_8 quartet if $x > 0.58$ for $J = 15/2$.

---

[7] The crystals were supplied by Semi-Elements, Inc., Saxonburg, Penn.

[8] R. J. Elliott and K. W. H. Stevens, Proc. Roy. Soc., (London) A 215, 437 (1952) and A 218, 553 (1953).

Bleaney [Ref. 1] has studied the Zeeman effect on a Γ_8 quartet and suggested a spin Hamiltonian

$$\mathcal{H}_s = g\beta(H_x S_x + H_y S_y + H_z S_z) + f\beta(H_x S_x^3 + H_y S_y^3 + H_z S_z^3) \qquad (3)$$

The matrix elements of this Hamiltonian are in one to one correspondence with the Zeeman operator $\Lambda\beta\vec{H}\cdot\vec{H}$ within the quartet. However, there are two alternative representations depending on the choice of correspondence. It is more convenient to choose two new parameters G and κ defined by the transformation

$$f = 4/3\ G\kappa$$

$$\qquad (4)$$

$$g = G(1 - 10/3\ \kappa)$$

The two equivalent representations are then related by $G' = G\kappa$, $\kappa' = 1/\kappa$. Thus, in the description of the resonance properties of the Γ_8 quartet, it is necessary to consider only values of $|\kappa| \leq 1$. Note for $\kappa = 0$, the Γ_8 behaves just like a free spin with $S = 3/2$. In terms of the parameters G and κ, the matrix representation of the spin Hamiltonian may be written as

$$(\mathcal{H}_s) = G\beta H \begin{bmatrix} (\frac{3}{2} - \frac{\kappa}{2})n & \frac{\sqrt{3}}{2}(1-\kappa)(\ell-im) & 0 & \kappa(\ell+im) \\ \frac{\sqrt{3}}{2}(1-\kappa)(\ell+im) & (\frac{1}{2} - \frac{3}{2}\kappa)n & (\ell-im) & 0 \\ 0 & (\ell+im) & (-\frac{1}{2} + \frac{3}{2}\kappa)n & \frac{\sqrt{3}}{2}(1-\kappa)(\ell-im) \\ \kappa(\ell-im) & 0 & \frac{\sqrt{3}}{2}(1-\kappa)(\ell+im) & (-\frac{3}{2} + \frac{\kappa}{2})n \end{bmatrix}$$

$$\qquad (5)$$

where (ℓ,m,n) are direction consines of H with respect to the cubic axis. The energy levels, derived from the diagonalization of the matrix (5), are, in terms of the parameters G and κ,

$$\left(\frac{E}{G\beta H}\right)^2 = \frac{1}{4}(5\kappa^2-6\kappa+5) \pm (1-\kappa)\sqrt{(1+\kappa)^2 - 12\kappa(\ell^2m^2+m^2n^2+n^2\ell^2)} \quad (6)$$

Numerical calculations of energy levels, wavefunctions, and transition probabilities, using a standard computer, were made. Resonance curves and maximum transition probabilities were plotted for various magnetic field orientations in the (001) and ($\bar{1}$10) plane respectively.

C. EXPERIMENTAL RESULTS

1. Cubic Spectra

Er[+++] in CaO has previously been studied by Low and Rubins [Ref. 5]. They observed only one line derived from cubic sites. From the angular variation of this line they concluded that it must be one member of the Γ_8 quartet and they identified this intense line to be the $\pm 3/2 \leftrightarrow \pm 1/2$ transitions. However, with this interpretation, they should observe a line $(+ 1/2 \leftrightarrow - 1/2)$ of similar intensity at higher fields. Since this line is missing, it is therefore more appropriate to attribute this line to the $+ 1/2 \leftrightarrow - 1/2$ transitions [Ref. 6]. This identification is correct and can be seen from the results of the measurements.

Three major resonances were observed in the EPR measurements at 35 kMc, and were identified as derived from the cubic fields. The theoretical and experimental angular dependence of the Γ_8 transitions for the magnetic field applied in the (001) and ($\bar{1}$10) orientations are shown in Fig. 3 and Fig. 4, respectively. The points shown in the figures are the observed resonances, while the solid lines represent the theoretical angular spectrum obtained from Eq. (7) with G = 3.85 and κ = -0.09. The g-values along the major directions are summarized in Table 1.
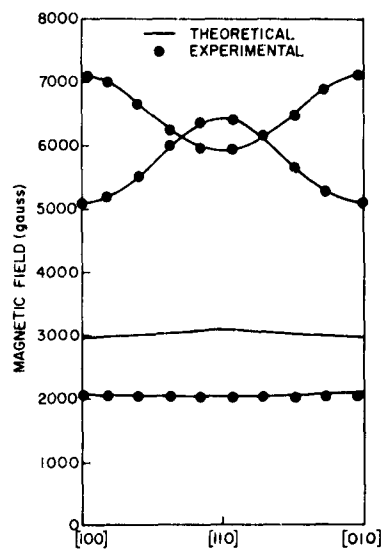
FIG. 3.   EXPERIMENTAL AND THEORETICAL
ANGULAR SPECTRUM OF Er^{+++} IN CUBIC
FIELD OF CaO FOR THE MAGNETIC FIELD
IN THE (001) PLANE.
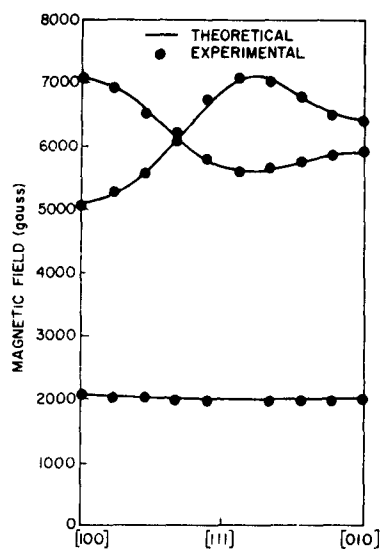
FIG. 4.   EXPERIMENTAL AND THEORETICAL
ANGULAR SPECTRUM OF Er^{+++} IN CUBIC
FIELD OF CaO FOR THE MAGNETIC FIELD
IN THE ($\bar{1}$10) PLANE.

The $+ 1/2 \leftrightarrow - \frac{1}{2}$ transition is an intense line with eight hyperfine lines
due to the nuclear isotope Er^{167} $\left(1 = \frac{7}{2}\right.$, natural abundance $22.82\%\left.\right)$.
The measured hyperfine structure constant is about 75 G. However, due
to the complexity of the spectra, the anisotropy of the hfs could not
be determined.

TABLE 1

Measured g-values for cubic spectra of Er^{+++} in CaO			
Transition	Magnetic Field Orientation		
	[100]	[110]	[111]
$+\frac{1}{2} \leftrightarrow -\frac{1}{2}$	4.90	3.87	3.49
$\pm\frac{1}{2} \leftrightarrow \pm\frac{3}{2}$	3.51	4.22	4.44
$+\frac{3}{2} \leftrightarrow -\frac{3}{2}$	12.20	12.66	12.00

The intensity of the $3/2 \leftrightarrow - 3/2$ line is much weaker (about 1 to 100 ratio compared to the $\frac{1}{2} \leftrightarrow -\frac{1}{2}$ transition). This result is predictable since the parameter $\kappa = -0.09$ is small. The accuracy of the g-values are poor due to the uncertainty in reading the magnetic fields.

The $\pm 3/2 \leftrightarrow \pm 1/2$ line are very broad (width ≈ 250 G). The broadening is due to random deviations from purely cubic fields. These random deviations will lift the zero field degeneracy and introduce small separations between the $\pm 1/2$ and $\pm 3/2$ levels, hence it will not affect the $1/2 \leftrightarrow - 1/2$ and $3/2 \leftrightarrow - 3/2$ transitions but will broaden inhomogeneously the $1/2 \leftrightarrow 3/2$ transitions [Refs. 6, 9]. This also explains why the much weaker $\Delta M = 2$ transition $(\pm 1/2 \leftrightarrow \mp 3/2)$ were not observed.

2. Axial Spectra

Two groups of axial spectra were observed. Their angular dependence in the (001) plane is shown in Fig. 5. The first set of lines, reported previously by Low and Rubins [Ref. 5], exhibits tetragonal symmetry about the cube axis. The measured g-values are $g_{\parallel} \approx 4.40$, $g_{\perp} = 7.93$. The second set also shows tetragonal symmetry about the cube axis but the g-values are very anisotropic; $g_{\perp} = 12.97$, $g_{\parallel} < 1$. From its temperature dependence, this set appears to be the transitions within the excited doublets. The tetragonal distortion most probably derives from the

[9] B. Bleaney, private communication.
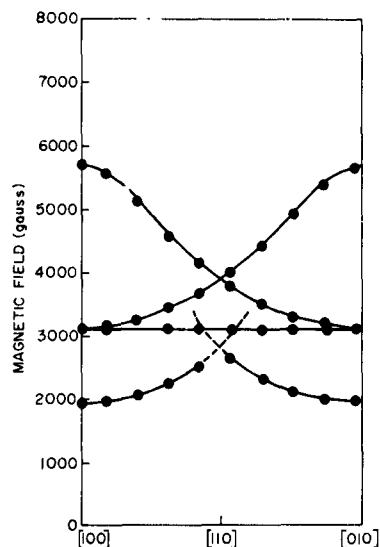
FIG. 5. ANGULAR DEPENDENCES OF
RESONANCES OF Er^{+++} IN AXIAL
FIELD OF CaO FOR THE MAGNETIC
FIELD IN THE (001) PLANE.

physical configuration in which charge compensation is fulfilled by one vacancy replacing one Ca^{++} ion on the cube axis next to the magnetic Er^{+++} ion.

PROJECT 0178: OPTICAL MASER MATERIALS

Signal Corps Contract DA 36-039 SC-90839
Project Leader: W. W. Anderson
Staff: ----

The object of this project is the study of new materials for solid-state optical masers, with particular emphasis on rare-earth ions in various lattices.

Work on the emission of the Tb^{+++} center in ZnS was continued this quarter. Computer solutions of the rate equations describing the ir stimulated emission given in the previous QRR were obtained. To obtain a good fit of experimental to theoretical results, the assumption of equal numbers of traps and recombination centers had to be discarded. The results are shown in Fig. 6 for a ratio of trap to recombination center density of:

$$\frac{N_t}{N_r} = 30$$
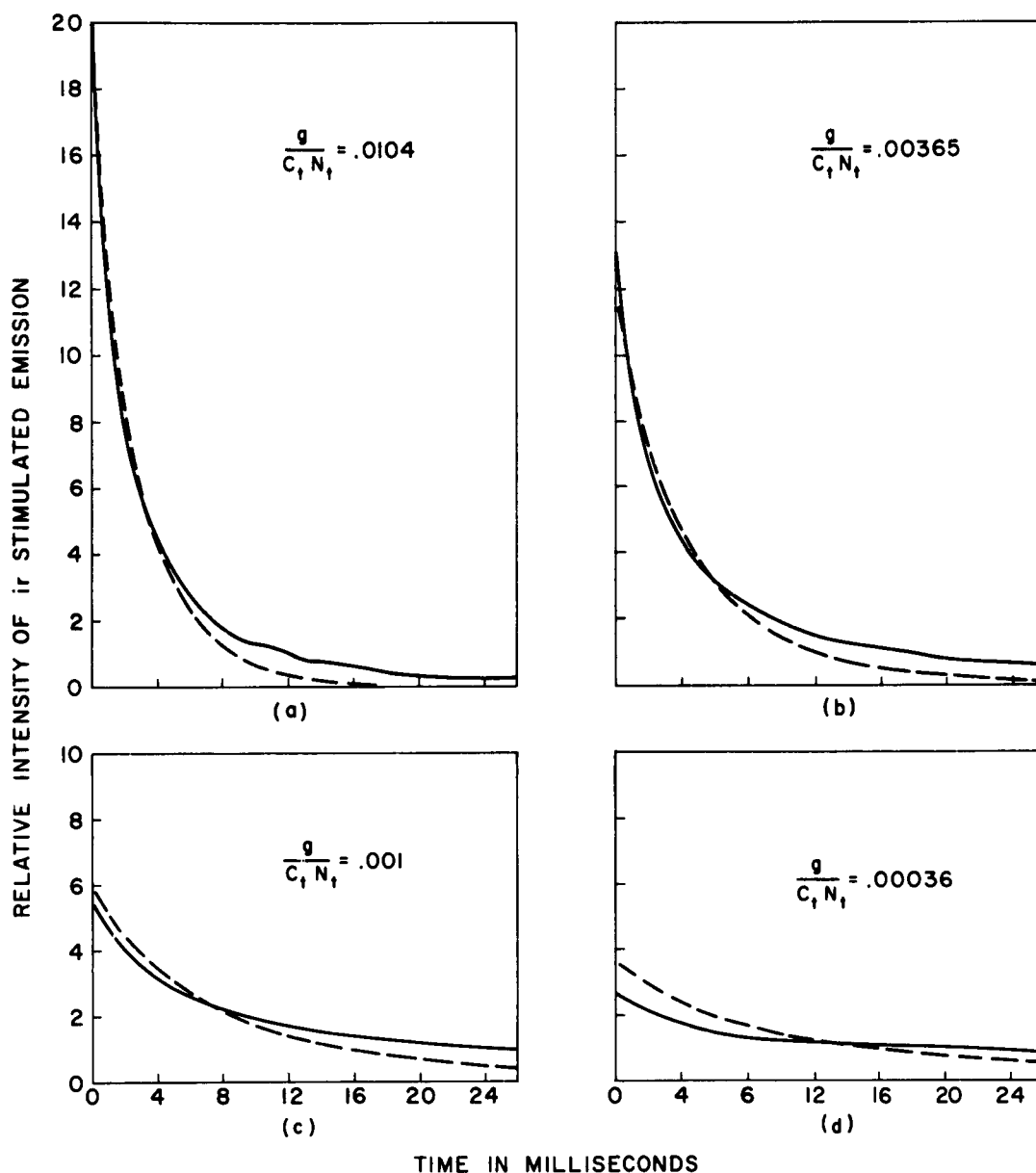
FIG. 6. DECAY CURVES OF INFRARED STIMULATED EMISSION.
Solid curves are experimental. Dashed curves cal-
culated with parameter values $N_t/N_r = 30$ and $C_r N_r =$
125 sec^{-1}.

and a recombination rate of

$$N_r C_r = 125 \ \text{sec}^{-1}$$

the trap rate, $N_t C_t$ is assumed to be very fast compared to the time
scale used in the experiment.

The departure of the experimental and theoretical curves in the tail
of the decay is probably due to a nonuniform doping. It was observed
that the crystals showed a nonuniform fluorescence. However, the agree-
ment of theory and experiment over a thirty to one range of excitation
intensities lends credence to the theory.

Electroluminescence of ZnS:Tb single crystals has been observed.
Under a-c or pulsed excitation, the Tb^{+++} emission is observed. How-
ever, under d-c excitation only a yellowish emission characteristic of
the ZnS lattice is observed. Electroluminescence occurs in the high field,
trap filling portion of the v-i curve. The power efficiency of the
Tb^{+++} emission is only 5×10^{-4} but this corresponds to a quantum effi-
ciency (photons per electron) of .07 which is rather high. Since the
current is increasing as about the eighth power of the voltage and the
emission is approximately proportional to the current, efficiency should
increase rapidly with voltage until the trap-filled region of the v-i
curve is reached.

The decay time of the Tb^{+++} emission was found to be about 50 μsec
by pulse excitation. This is an order of magnitude shorter than in most
other anhydrous Tb doped crystals and reflects the lack of inversion
symmetry at the Tb site.

PROJECT 0251:   AN I-F PLASMA EXPERIMENT

                      Air Force Office of Scientific Research Grant 323-63
                      Project Leader: O. Buneman
                      Staff: J. O. Hosea

The purpose of this project is to perform an experiment, or groups
of experiments, that will differentiate between "collective" and "in-
dividual" phenomena in plasmas.

A.   GRIDDED TUBE

The density between the grids of the gridded tube as measured vs
discharge current on "Piper" (QRR No. 1 and 2, Proj. 0253) is shown in
Fig. 7 for hydrogen at a pressure of 2μ and in a magnetic field of
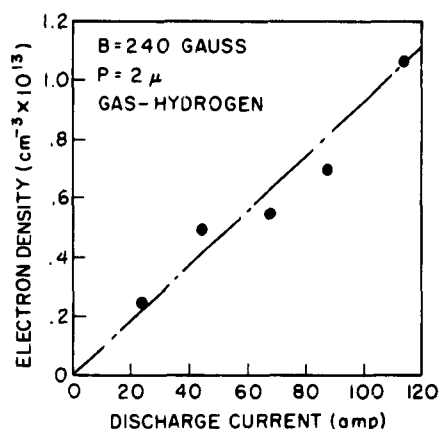
FIG. 7. ELECTRON DENSITY BETWEEN GRIDS ON PIPER AS A FUNCTION OF DISCHARGE CURRENT.

240 gauss. Densities on the order of 10^{13} cm^{-3} are obtained at reasonable discharge currents. The density is reduced by about a factor of 2 from the density obtained without the grids at any particular discharge current. The reduction is caused by the close spacing (0.2 inch) of the grid wires which is necessary to insure good rf shielding of the cavity fields. Nevertheless, the densities obtained are adequate for the cavity experiments on "collective" plasma phenomena.

B. CAVITY (WITH GRIDDED-TUBE) ON PIPER

Figure 8 shows the 140 Mc cavity placed on "Piper." Two magnets have been removed to make room for the cavity and in order to compensate their loss, a magnet has been placed inside the re-entrant shell of the cavity. The compensation is not complete; the variation of the magnetic field along the discharge tube is increased by a factor of two upon insertion of the cavity.

Figure 8 also shows the 8 mm interferometer which is used to measure the density between the grids of the gridded tube. Small holes in the cavity wall allow the interferometer horns to be inserted inside the cavity for density measurement and then withdrawn so that they do not perturb the cavity during the cavity experiments. The discharge on "Piper" is very stable from pulse to pulse so that density measurements made in the above manner are reliable.

FIG. 8. PIPER WITH 140 Mc CAVITY
IN PLACE. Also visible is an 8 mm
interferometer used for density
measurements.

C. FREQUENCY OF CAVITY VS PLASMA DENSITY

A calculation of the cavity resonant frequency vs electron density
has been made assuming the re-entrant cavity supports only its lowest
mode. This assumption is made for a first analysis because of the pres-
ence of the grids. For a cavity without grids a Fourier-Bessel analysis
must be used to match boundary conditions at the plasma (SEL Tech. Report
No. 251-2). Figure 9 shows the cavity cross-section. The quartz tube is
omitted in this analysis. It is assumed that the E-field is approximately
as shown in Fig. 9. In the region of the plasma the field is TM, whereas
in the base region of the cavity (see Fig. 9) the field is coaxial (TEM).
The transition region at the corner is taken into account by introducing
a discontinuity capacitance.

$R = 1/10\,a$ $d = 1.75$
$a = 5.25$ $l = 10$
$b = 14.5$
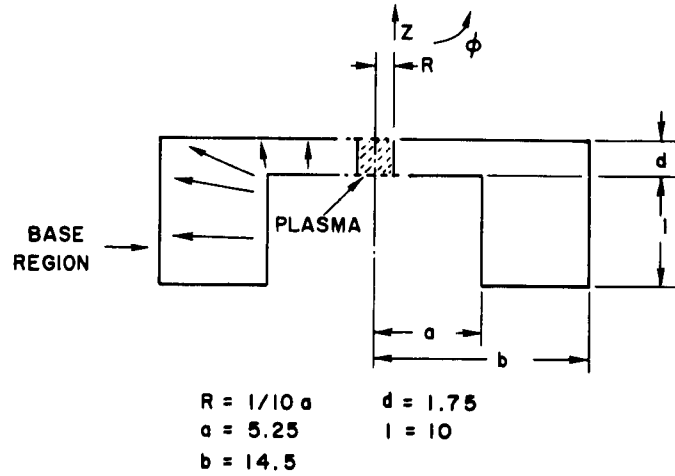
FIG. 9. CAVITY CROSS SECTION SHOWING THE
ASSUMED CAVITY ELECTRIC FIELD.

For $r < R$ $E_z = A_1 J_0\left(K_{zz}^{1/2}\, kr\right)$

$$H_\phi = \frac{j\omega K_{zz}^{1/2}\, \epsilon_0\, A_1}{k}\, J_1\left(K_{zz}^{1/2}\, kr\right)$$

(1)

$R < r < a$ $E_z = A_2 J_0(kr) + B_2 N_0(kr)$

$$H_\phi = \frac{j\omega\epsilon_0}{k}\,[A_2 J_1(kx) + B_2 N_1(kx)]$$

(2)

where A_1, A_2, B_2 are constants, $k = \omega\sqrt{\mu_0 \epsilon_0}$, and

$$K_{zz} = 1 - \frac{\omega_p^2}{\omega^2}$$

(3)

since a uniform cold plasma is assumed.

The base effect on resonant frequency may be approximated by assuming it to be a shorted coaxial line of length ℓ;

$$L = \frac{\eta}{2\pi\omega} \ln \frac{b}{a} \tan \omega \sqrt{\mu\epsilon} \, \ell \qquad (4)$$

where $\eta = \sqrt{\mu/\epsilon}$ and b, a, ℓ are indicated in Fig. 9. (The above formula is $L = (z_0/\omega) \tan \omega\sqrt{\mu\epsilon} \, \ell$ where z_0 is given by $(\eta/2\pi) \ln a/b$ as listed in Ramo and Whinnery, "Fields and Waves in Modern Radio," Chapter 9.) Assuming ℓ to be small compared to a wavelength in the coaxial base gives

$$L \simeq \frac{\mu\ell}{2\pi} \ln \frac{b}{a} \qquad (5)$$

The discontinuity capacitance may be approximated using techniques given in Moreno, "Microwave Transmission Design Data," pp. 96, 228, or it may be left as a parameter to be determined experimentally. For example, the cavity resonance frequency without the plasma present may be measured and then the discontinuity capacitance C_d determined by the resonance relation derived below.

Matching boundary conditions at $r = a$ gives

$$m \equiv \frac{B_2}{A_2} = - \frac{\left[\left(\frac{1}{\omega^2 L} - C_d\right) J_0(ka) - \frac{\epsilon_0 \, 2\pi a}{kd} J_1(ka)\right]}{\left[\left(\frac{1}{\omega^2 L} - C_d\right) N_0(ka) - \frac{\epsilon_0 \, 2\pi a}{kd} N_1(ka)\right]} . \qquad (6)$$

where a, d are indicated in Fig. 9. Matching boundary conditions at $r = R$ gives

$$\frac{K_{zz}^{1/2} J_1(K_{zz}^{1/2} kR)}{J_0(K_{zz}^{1/2} kR)} = \frac{[J_1(kR) + m N_1(kR)]}{[J_0(kR) + m N_0(kR)]} . \qquad (7)$$

Equation (7) may be solved by trial to give k for any particular value of K_{zz}.

For the 140 Mc cavity used for this project

$$L = 5.17 \times 10^{-8} \text{ h}, \qquad C_s \approx 12.5 \text{ pf}, \qquad \frac{R}{a} = \frac{1}{10} \qquad (8)$$

The resulting frequency vs density $[(\omega_p^2/\omega^2) \propto (n/\omega^2)]$ plot is shown in Fig. 10.
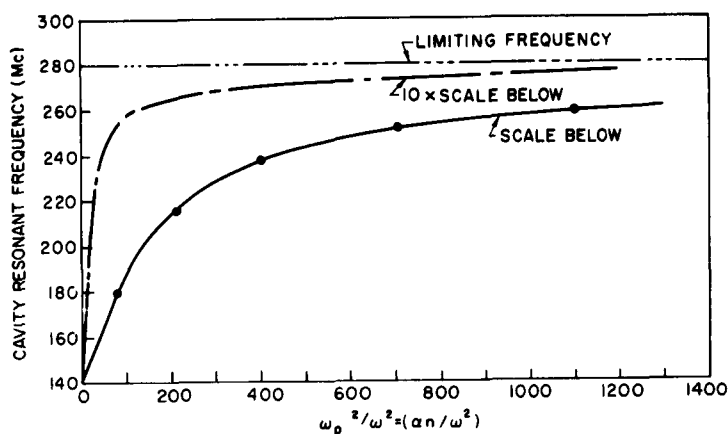
FIG. 10. DEPENDENCE OF CAVITY RESONANT FRE-
QUENCY ON PLASMA DENSITY.

The above analysis follows closely that of Buchsbaum, Mower, and Brown, "Interaction Between Cold Plasmas and Guided Electromagnetic Waves," in Physics of Fluids, Vol. 3, No. 5, 1960, p. 808. There, a cylindrical cavity is treated and thus the boundary conditions at r = a are those of a perfectly conducting wall. For a re-entrant cavity a suitable approximation must be made to account for the effect of the coaxial base.

D. EXPERIMENTAL PROGRESS

Experiments are now underway to check the resonant frequency of the cavity vs plasma density. The cavity Q is 18,000 with no plasma but drops drastically with the plasma present. This causes the resonant frequency to be very difficult to determine accurately.

As mentioned earlier the 140 Mc cavity perturbs the magnetic field significantly. In order to avoid this, a 1 kMc cavity which will fit inside the magnets on "Pipeᵢ" is being designed. Operation at a higher frequency will also decrease the effect of electron collision processes on the cavity operation. This should improve the Q of the cavity when the plasma is present.

PROJECT 0253:   ANOMALOUS CROSS-FIELD DIFFUSION

Atomic Energy Commission Contract AT(04-3)326
Project Leader: O. Buneman
Staff: D. Pigache, E. J. Powers, G. Reiter,
                    J. Hosea

The purpose of this project is the study of diffusion in a cylindrical discharge in a strong axial magnetic field. Measured diffusion rates across the field are higher than the rate proportional to $(1/B^2)$ predicted by binary collision theory. The observed anomalous diffusion rates can only be accounted for by some type of instability, and this project is concerned with a theoretical and experimental study of some of the possible instabilities in such a discharge and their effects on diffusion rates.

A. CONSTRUCTION AND PRELIMINARY RESULTS OF A TOROIDAL REFLEX DISCHARGE (BAGEL II).

The construction of an improved version of a toroidal reflex discharge, known as BAGEL II, has been completed during the past quarter and preliminary experiments have been performed. This machine is a significant improvement compared with the prototype model (BAGEL I).

A diagram and a photograph of BAGEL II are given in Figs. 11 and 12 respectively.

12
IDENTICAL
COILS

40

2.0 cm

GLASS TUBE

MS

MS

12

75
.TO 4 VACUUM
SYSTEM

VG

I_1

I_2

I_1

GI

R=45

7 5 cm ID

12
IDENTICAL
COILS

I_2

A   C

MS

14

34

MAGNETIC I_1
LINES I_2

A   ANODE
C   CATHODE
GI GAS INLET

MS METALLIC SPACER
VG VACUUM GAUGES
     (IONISATION AND ALPHATRON)
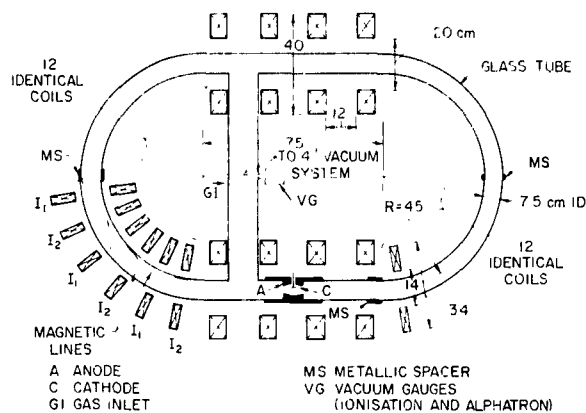
FIG. 11.   DIAGRAM OF BAGEL II.   Dimen-
sions in cm.   For typical bumpy field
configuration I_1 = 16 amps, I_2 = -4
amps (opposite direction), giving B_{ave} =
150 gauss and a mirror ratio   m = 2.1.
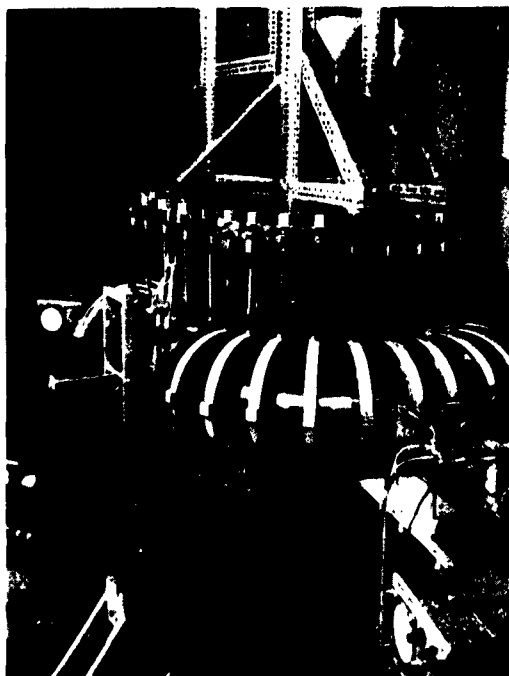
FIG. 12.   PHOTOGRAPH OF BAGEL II WITH
MIRROR RATIO   m = 2.1   CAUSING
PLASMA TO BULGE AS SHOWN.

A magnetic field of 2,000 gauss is delivered by 32 coils--4 coils for each straight section--12 coils for each bent section. When perfectly aligned these coils give a homogeneous field with only ±2 percent ripple on the axis. However, each coil of the bent section has 5 degrees of mechanical freedom--3 translations and 2 rotations (the only rotation which is not possible would be around the axis of the coil and would provide no change in the magnetic field configuration). Also 10 independent power supplies allow us to adjust the current individually in each coil. (The current in the adjacent coils can be in the opposite direction.) This versatility will permit the study of the confinement given by different magnetic-field configurations (bumpy and undulating magnetic field.)

The plasma chamber is 7.5 cm diameter with a 450 cm glass-tube circumference. The cathode-anode box is perfectly symmetrical and the diameter of both cathode and anode can be changed easily. The largest possible anode diameter is 6 cm.

The vacuum is provided by a 4" pumping system giving a base pressure (when the cathode is heated at 1000 °C) of $p = 5 \times 10^{-7}$ mm Hg.

A new SCR pulse generator rated at 600 volts and 1000 amps during 400 μs has been constructed and tested. A discharge current of 300 amps has already been obtained with a cathode whose active area was only 24 cm^2. This area can be increased by a factor of 3 (and hence, tripple the current) without changing significantly the discharge geometry, thus solving the cathode problem. The high discharge power available should provide a high density and a nearly fully ionized plasma. Also, if there is good confinement the plasma should be considerably warmer than in the previous machine.

Preliminary Experiment

Delivery of the power supplies for the magnets has been considerably delayed so that the experiments performed so far have been made with a smaller power supply (previously used for the PIPER machine). Consequently, the maximum magnetic field is presently 400 gauss instead of 2000.

a. Experiments with the homogeneous field.

As outlined in the Technical Report 0253-4 relating an experiment made on BAGEL I it is possible to establish a plasma all the way around the torus in spite of the plasma drift (due to the curvature of the magnetic field). In BAGELL II the minimum field required is only 100 gauss.

Measurements of plasma density yield 9×10^{13} electrons/cm^3 near the cathode box (see interferometer measurement, paragraph B) and 3×10^{13} in the straight section opposite the cathode box. Langmuir probe measurements have also been made giving an electronic temperature at low plasma density $(n \approx 10^{12})$ of 4 ev in argon and 7 ev in Helium.

b. Experiments with the bumpy field.

A bumpy toroidal magnetic field which consists of 12 mirror machines arranged along the two bent sections has been established with the current distributed as shown in Fig. 11. The mirror ratio was adjustable from 1.04 ($\sim$ homogeneous field) to 3. For higher mirror ratios the average field (150 gauss in this experiment) would be too small for practical application. Other magnetic field configurations are possible and will be tested later.

The plasma confinement has been studied with a Langmuir probe and an 8 mm interferometer. The probe was biased at a sufficiently negative potential to be in the ion saturation region where the ion saturation current is proportional to the plasma density times the square root of the electronic temperature. Thus, the observation of the ion current is a convenient way to test the effectiveness of the confinement which is indicated by a slower decay in the afterglow of both plasma density and electronic temperature.

It has been observed that the ion saturation current decay is slower as the mirror ratio is increased from 1 to 3, keeping the average magnetic field constant. This is shown in Fig. 13 which gives oscilloscope traces of the ion current for mirror ratios of 1 and 2. Using the 8 mm interferometer, which measures the average density in a plasma cross section
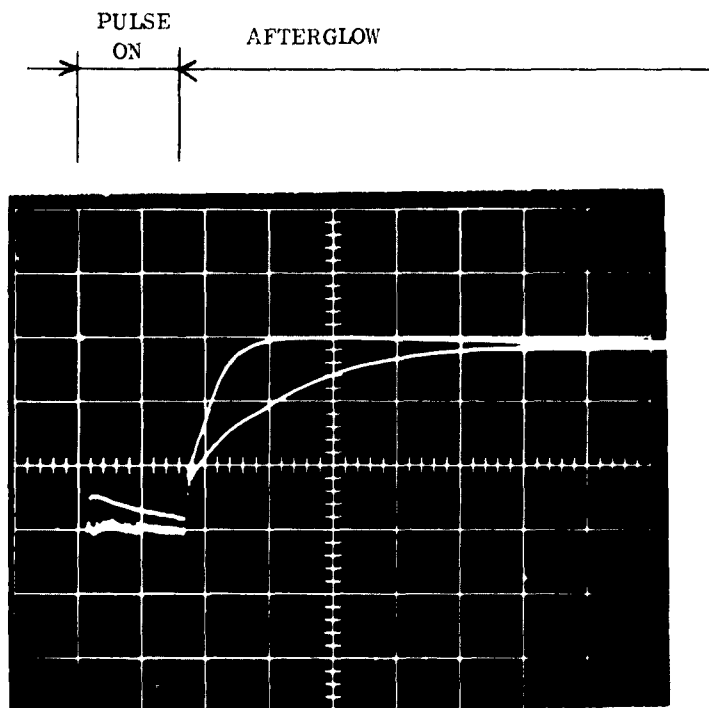
FIG. 13. OSCILLOSCOPE TRACES OF THE ION SATURATION
CURRENT IN HELIUM WITH THE LANGMUIR PROBE IN THE
MIDDLE OF ONE BENT SECTION AND ON THE AXIS OF THE
GLASS TUBE. Time scale 100 μs/cm, p = 3.5 × 10^{-4}
mm Hg, I_d = 7 amps, V_d = 240 volts, B = 150 gauss.
Upper trace is with the homogeneous field, lower
trace is with the bumpy field--mirror ratio m =
2.1.

and is independent of the electronic temperature, we can see that the
density decay time is much longer with the bumpy field than with the
homogeneous field (see Fig. 14).

From these experiments we can see that the bumpy field definitely
improves the confinement. However, it is not yet clear whether this
improvement is due to a reduction of the losses on the anode after dif-
fusion along the magnetic field or to a reduction of the drift caused
by the curvature of the magnetic field.

PULSE
ON   AFTERGLOW
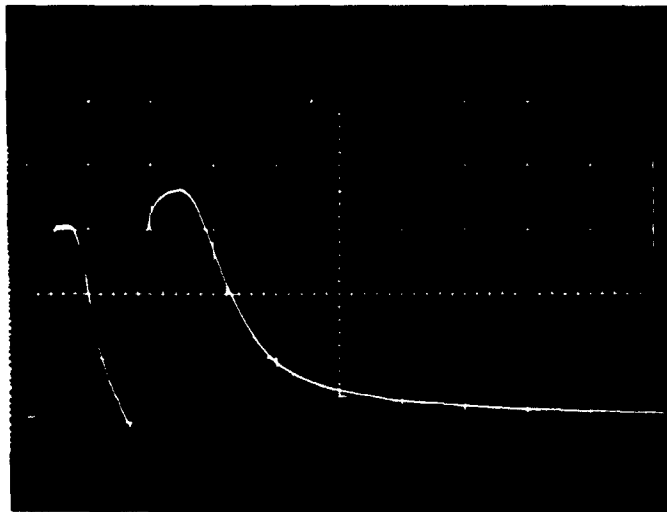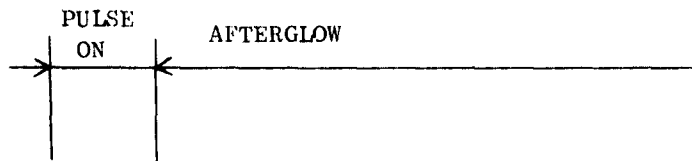
a. With the homogeneous field

PULSE
ON   AFTERGLOW
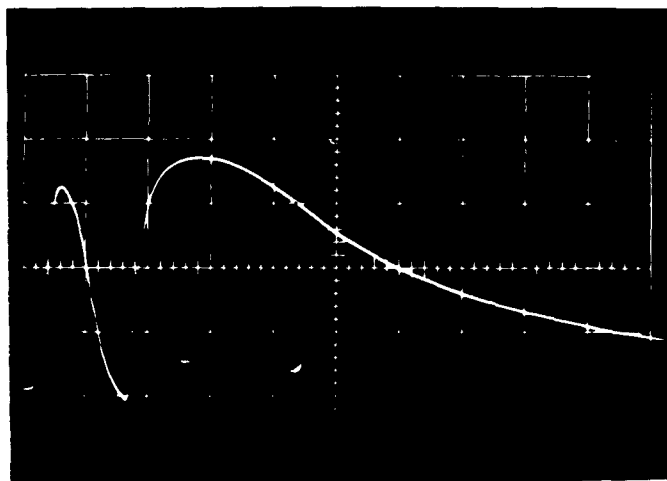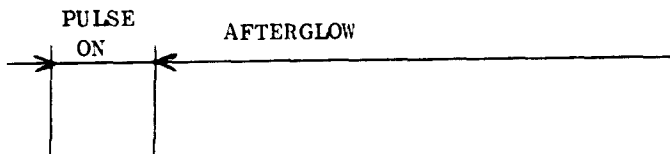
b. With the bumpy field

FIG. 14. 8 mm INTERFEROMETER TRACES, FOR p = 3.5×10^{-4} mm Hg. Time scale 100 μs/cm, Average field B = 150 gauss. Discharge conditions were adjusted in order to get the same plasma density at the end of the discharge

B. 2.5 MM INTERFEROMETER

The 2.5 mm interferometer is completed and is now in use. Figure 15 shows the interferometer on its stand. The stand allows density profiles to be taken on the BAGEL II plasma device. That is, the indicated screw allows the interferometer to be pivoted about the lower end of the two-bar optical bench on which the interferometer is assembled.

FIG. 15. PHOTOGRAPH OF THE 2.5 mm INTERFEROMETER.

The operation of this interferometer is essentially the same as that of the 8 mm interferometer built earlier. Basically, the operation involves beating the "plasma" beam (signal through plasma which is placed between lenses) with a reference signal (signal through waveguide around plasma) and noting the change in phase of the "plasma" beam as a function of plasma electron density. For a detailed description of this type of interferometry see Plasma Physics, J. E. Drummond, Chapter 12, "Micro-wave Diagnostics for Controlled Fusion Research," C. B. Wharton.

The primary differences between the 2.5 mm and 8 mm interferometers are that lenses are used to focus the plasma beam in the 2.5 mm case

and that the "cutoff" density (density above which the interferometer cannot be used) is 1.6×10^{13} at 8 mm and 1.75×10^{14} at 2.5 mm. The focusing effect of the lenses is illustrated in Fig. 16. A .05" diameter rod (16 AWG) was used to perturb the "plasma" beam and the decrease in transmitted power was observed. Fig. 16a gives a transmission pattern at the center plane between the lenses. It is found that the smallest spot size of the beam is 8.9 mm in diameter. Fig. 16b shows the variation of the spot size along the beam. The average spot size over a one-inch
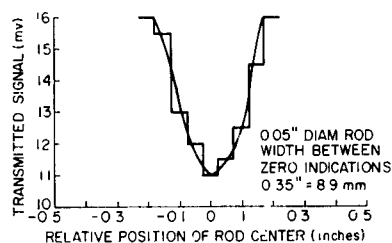
FIG. 16a. TRANSMISSION PATTERN AT CENTER PLANE BETWEEN THE LENSES.
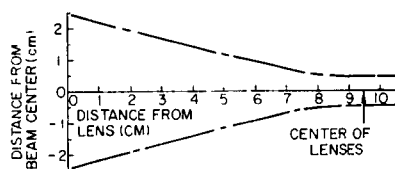
FIG. 16b. VARIATION OF SPOT SIZE ALONG THE BEAM.

plasma is slightly under 1 cm. This allows perhaps three density positions to be used transverse to the plasma column and gives good resolution along the column. Larger plasma diameters would enhance the use of this interferometer for transverse scanning. For plasma columns greater than perhaps 1.5" in diameter, lenses of greater curvature would be needed to give a longer "small spot" region.

This interferometer is particularly useful for measuring densities up to 1.75×10^{14} electrons/cm^3 in the center region of the plasma column. Here the curvature of the plasma surface over the interferometer beam width is relatively small and the conditions approach those required by the "sheet" theory [C. B. Wharton above] used for relating phase shift to the density of the plasma. Figure 17 shows a trace taken on BAGEL II with a weak field (300 gauss) and a discharge current of 300 amps. The
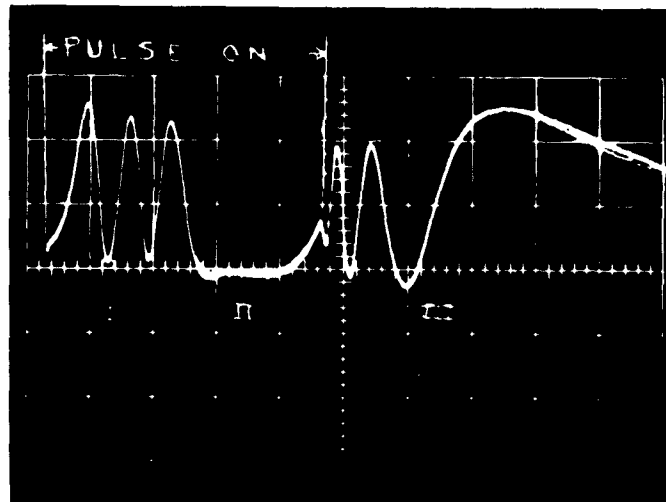
FIG. 17. 2.5 MM INTERFEROMETER.

number of fringes $(2\pi$ phase shifts$)$ to the equilibrium position is found to be 3. A plasma of 1" diameter was used. Assuming a "sheet" plasma with uniform density, the density is found to be

$$n = n_c \left[\frac{2N}{N_{co}} - \left(\frac{N}{N_{co}} \right)^2 \right] \tag{1}$$

where n_c = cutoff density = $\dfrac{f^2}{\left(8.97 \times 10^3 \right)^2}$ = 1.75×10^{14}

N_{co} = max. number of fringes = $\dfrac{d}{\lambda_0}$ = 10

$N = 3$ as stated above

This gives $n = 9 \times 10^{13}$.

Densities much higher than this are expected to be obtained on BAGEL II when higher fields and currents are used.

C. ENHANCED DIFFUSION IN AN RF DISCHARGE

In practically every experiment where some form of anomalous diffusion seems to be present the enhanced rate of escape of charged particles across a magnetic field is accompanied by noise and fluctuations in the frequency range between a few kilocycles and a few megacycles. Often noise in the microwave band is also observed. A number of workers [Refs. 1, 2, 3] have pointed out that randomly fluctuating electric fields are capable of enhancing the diffusion of charged particles across a magnetic field. Although there is a certain amount of evidence that the motion of the plasma is related to the fluctuations, the connection between the two has not been established conclusively. For these reasons we are con-tinuing our study of the fluctuations which accompany or precede the onset of anomalous diffusion in an rf discharge.

In QRR No. 7 we compared the rf discharge data with those obtained by other investigators in both dc and ac positive columns. At that time we only had rf discharge data for a 2.3 cm tube; thus it was un-known whether or not the rf discharge critical magnetic fields scaled with pressure and radius in the same way as the dc data did.

To obtain this information a new experiment was set up which allowed us to easily interchange tubes of different radii. This experiment is basically the same as that described in QRR No. 6 with the exception that the discharge is now being fed by an unbalanced system (one electrode grounded, the other hot) rather than a balanced system.

We have systematically studied the onset of the fluctuations in 29.3 Mc helium and argon discharges over a pressure range of 0.050 to 1.0 mm Hg in tubes of 1.70, 2.31 and 3.51 cm radii. We find that the critical field data for noise onset scale with pressure and radius in the same way as the dc positive column data do in the sense that all the rf data lie on, or reasonably close to, a single curve in the B/p, pR plane. The results for helium and argon are presented in Figs. 18 and 19. It is important

[1] L. Spitzer, Jr., Phys. Fluids, 3, 659 (1960).

[2] J. B. Taylor, Phys. Rev. Letters, 6, 262 (1961).

[3] S. Yoshikawa and D. J. Rose, Phys. Fluids, 5, 334 (1962).
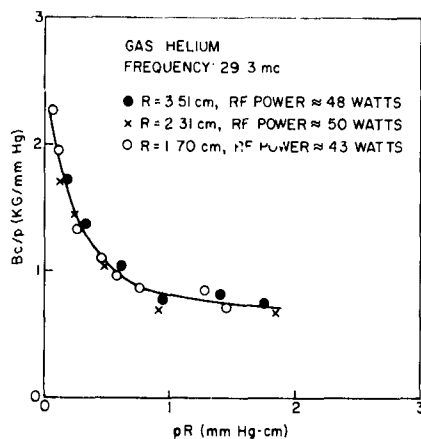
FIG. 18. PLOT OF THE CRITICAL MAGNETIC
FIELD FOR NOISE ONSET DIVIDED BY PRES-
SURE VS THE PRODUCT OF PRESSURE AND
RADIUS FOR RF HELIUM DISCHARGES.
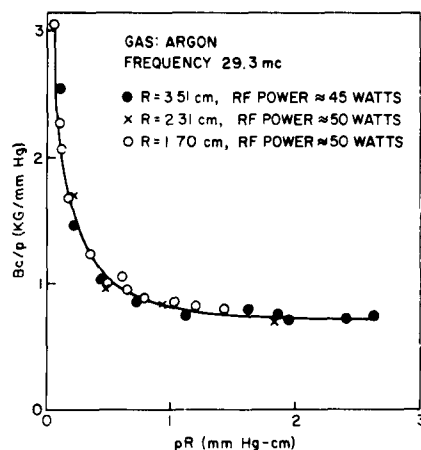
FIG. 19. PLOT OF THE CRITICAL MAGNETIC
FIELD FOR NOISE ONSET DIVIDED BY PRES-
SURE VS THE PRODUCT OF PRESSURE AND
RADIUS FOR RF ARGON DISCHARGES.

to note that although the same scaling laws are obeyed in the dc and
rf case, comparison of Fig. 18 with Fig. 9 in QRR No. 7 indicates that
the critical field for noise onset in an rf discharge is smaller than
the critical field in the dc discharge for the same pressure and radius.

The frequency spectrum of the emitted noise and oscillations has been
studied using a Panoramic SPA-3/25 spectrum analyzer which covers the
range from 200 cps to 25 Mc. The noise pickup consisted of strips of
copper foil (1.5 cm × 0.4 cm) which were taped to the outside surface
of the glass tube. In argon (tube radius 3.51 cm) we find that the onset
of the fluctuations is characterized by a very broad pip centered at 50
or 60 kc. In helium (tube radius 3.51 cm) the onset is often much more

coherent and is characterized by frequencies which are harmonically re-lated, the fundamental frequency being of the order of 50 or 60 kc. The behavior of the pure frequency onset with magnetic field is not readily observed because the range of field over which it occurs is quite narrow. Increasing the magnetic field just beyond onset causes the pips to di-minish in amplitude and to break up into a more or less broad spectrum covering the range from a few kilocycles to a few megacycles. Further increases in the magnetic field result in the amplitude growing in the above frequency band by about 40 db. This growth corresponds to the regions of intense noise which were previously observed on an oscillo-scope and reported upon in QRR No. 6. The principal effect of increasing the field further is to introduce higher frequency components in the noise spectrum.

The signal received by a six-inch dipole located outside the glass discharge tube (but inside the solenoid) was fed to a Polarad Model TSA spectrum analyzer with a 10 to 1000 Mc tuning head. As expected, there are strong pips at the rf driving frequency and its harmonics. Above the critical magnetic field, however, "grass" appears around the base of the pips indicating that the low frequency fluctuations modulate the rf driving frequency and its harmonics.

We have also carried out the following experiments which indicate that some form of anomalous diffusion exists in an rf discharge. Dur-ing a run the pressure is held constant and the ion density is monitored using a double probe located on the axis of the tube. The ion density is held constant by adjusting the rf power input to the discharge as the magnetic field is increased. The rf voltage required to maintain the discharge is then measured using a high frequency VTVM and the ion flux to the wall is measured by a double probe. The probes are similar to those described in QRR No. 1. Some typical results obtained in helium in the 1.7 cm radius tube are presented in Fig. 20. We note that as the magnetic field is increased from zero both the rf potential required to maintain the density constant and the radial ion flux to the walls de-creases. This is as expected, because as the magnetic field is increased the radial loss of charged particles should be sharply reduced according to classical theory. Since the equilibrium density is being held constant
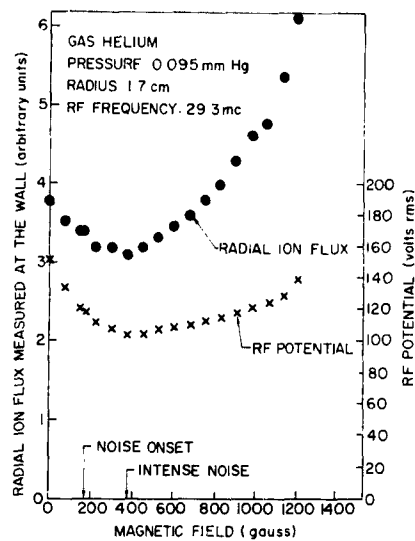
FIG. 20. PLOT OF RADIAL ION FLUX AND THE RF
POTENTIAL REQUIRED TO HOLD THE EQUILIBRIUM
DENSITY CONSTANT VS MAGNETIC FIELD.

the drop in loss rate must be accompanied by a corresponding drop in the
production rate which in turn implies a lower rf potential. Therefore,
on the basis of classical diffusion theory we would expect both the rf
potential and radial ion flux to decrease monotonically as the magnetic
field is increased. Examination of Fig. 20 shows, however, that the rf
potential and radial ion flux start to rise when the magnetic field exceeds
a certain critical value. We interpret this rise in the following way:
Above the critical field some mechanism of an unknown nature enhances the
rate at which particles are lost across the field. In order to maintain
the same equilibrium density the enhanced loss rate must be offset by an
increased production rate which is provided by an increased rf potential.

    At lower pressures the dips are sharper than that shown in Fig. 20,
whereas for higher pressures the dips are shallower. The fact that the
noise onset either precedes or coincides with the dip suggests that in
the rf discharge the onset of noise and anomalous diffusion are closely
related.

PROJECT 0254:   PLASMA THERMIONIC DIODES

The purpose of this project is to study the randomization of elec-
tron energies in thermionic diodes by computer methods.

The examination of the large signal behavior of a low pressure
thermionic converter was pursued further by computer calculations. We
have investigated how the applied potential influences the operation of
the converter when it exhibits large amplitude oscillations. We have used
a DEC (Digital Equipment Corporation) PDP-1 computer for our investiga-
tions. The output device of this computer has an oscilloscope. The
potential vs distance and the current vs time in the converter was dis-
played on this oscilloscope as the charged sheet calculations were carried
out. Figure 21 shows a photograph of the trace on the oscilloscope. The

**CURRENT
VS TIME**

**POTENTIAL
VS DISTANCE**
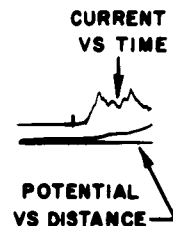
FIG. 21.   THE TRACES OF CURRENT VS TIME AND POTENTIAL
VS DISTANCE AS DISPLAYED ON THE OSCILLOSCOPE OF THE
DEC PDP-1 COMPUTER.   These quantities are the re-
sults of computer calculations done by this computer.

upper curve shows current vs time from the start of the calculations up
to the time when the display was made; the lower curve shows the potential
in the diode at the time of display. We have already shown in earlier
QRR's that the time of computations is measured in units of time steps
that refer to a real time interval of the order of $m\mu$ seconds. The
total length of the current trace shown is equivalent to 1024 time steps.

We have examined the behavior of the converter for different physical
parameters. The parameter α had a constant value of 2 (slightly ion-
rich) for all these calculations. Diode separation values of 30, 50,
100 λ_{DB} were chosen, and the value of the applied potential was varied.

First, the smallest positive potential was determined for which periodic
oscillations could be observed in the current. These oscillations re-
mained periodic when the potential was increased. until they disappeared
completely. By measuring the length of one period of the oscillating
diode current for different potential values, we have obtained a measure
for the frequencies of these oscillations as functions of applied poten-
tials. The measured points connected with smooth curves are shown on
Fig. 22.

FREQUENCY VS APPLIED POTENTIAL FOR
A LOW PRESSURE THERMIONIC CONVERTER
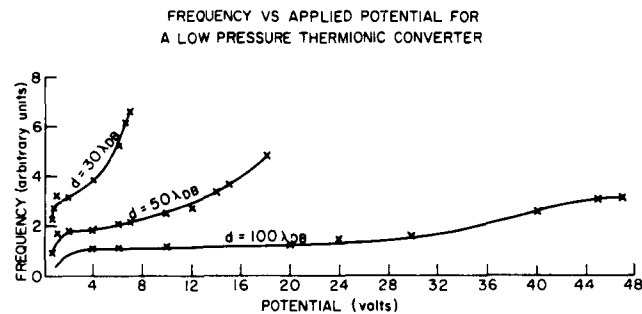
FIG. 22. FREQUENCY VS APPLIED POTENTIAL
FOR A COMPUTER SIMULATED LOW PRESSURE
THERMIONIC CONVERTER.

We can observe that periodic oscillations are present in the con-
verter when the applied potential is larger than 0.5 volts. The starting
point of oscillations is independent of the length of the converter. The
frequency of oscillations increases with increasing potential, until the
oscillations disappear. We believe that these oscillations are caused
by transit time effects and in order to show why the frequency of oscil-
lations increase with increasing applied potential we have to examine
the potential distribution in the converter during these oscillations.
Data for plotting these curves are collected at the present time.

PROJECT 0255: COMPUTER MODEL OF A 2-DIMENSIONAL PLASMA

Tri-Service Contract Nonr-225(24)*
Project Leader: O. Buneman
Staff: R. Hockney

The object of this project is programming simple 2-dimensional plasma problems into an IBM 7090, ions and electrons being simulated by rods of positive and negative charge which trace out their orbits in fully self-consistent fields.

A report SEL-64-056 (Technical Report 0255-1) has been distributed describing the numerical aspects of the 2-dimensional plasma program and this has been submitted to the Journal of the Association of Computing Machinery for possible publication.

The program modification permitting the potential to be any given function of 'x' at $y = 0$ and $y = \ell$ has been completed. The new program is slightly faster and just as accurate as the original program that assumed periodicity at $y = 0$ and $y = \ell$.

Numerical experiments on the passage of a beam of electrons through a plasma were made using the modified program and reported to the 'Plasma Instabilities' meeting at Berkeley on April 6-7.

A proposal has been prepared suggesting that the IBM 7090/PDP-1 computer combination could be used as an ideal experimental plasma. It is suggested that the experimenter type the parameters of his experiment on the PDP-1 computer; the IBM 7090 would then compute the experiment using the basic plasma program already developed under this project and then display the results on the PDP-1 oscilloscope. Any computed quantities such as field, particle density, or potential at a number of probe positions could be displayed or else the motions of the individual particles. Preliminary time estimates suggest that such a use of the computers is feasible.

A study of the process of simplified Fourier Analysis has brought about some minor improvements in the Fourier Analysis routine and suggested a systematic way of doing the analysis on larger numbers of points.

PROJECT 0256: CURRENT FLOW IN PLASMAS

Atomic Energy Commission Contract AT(04-3)326 P.A. No. 8
Project Leader: O. Buneman
Staff: D. Dobrott

The purpose of this project is the study of instabilities in a current sheet.

The orbit equation derived in previous QRR's have been used to examine the stability of the sheet pinch. Because of the application of a strong magnetic field, in the direction of the particle drift, a shear in the magnetic field exists. This shear as well as field and density inhomogeneities allow propagation of low-frequency waves across the strong applied field at the center of the sheet. Two modes, obtainable in the low β and finite orbit limits, occur. These modes prove to be evanescent. These modes occur whenever the pinch exists, and hence are of the "universal" character. Distinct from the usual "drift-wave" analogy, these universal modes are due to the peculiar motion of the particles near the minimum B-field (see QRR No. 7). For the $T_i > T_e$ case one finds that the frequency of the mode is

$$\omega \sim \beta^{1/2} \; \Omega_i \; \frac{k^2 R_i^2}{k\lambda}$$

where $\beta \ll 1$ is the ratio of particle pressure to magnetic pressure, Ω_i is the ion gyro-frequency, R_i is the ion gyro-radius, k is the wave number and λ is the width of the sheet. This mode is evanescent with a decay rate proportional to $\sqrt{\frac{m}{M}} \, \omega$.

PROJECT 0309: NEUTRALIZED CHARGED PARTICLE STREAMS

Air Force Contract AF33(657)-11144
Project Leader: D. A. Dunn
Staff: P. Burger

The purpose of this project is the study of neutralized streams of electrons or ions in a field-free space.

The new routines described in the last QRR were introduced into the computer program in order that it could be used to simulate the ionizing process of an electron beam in a gas. We have chosen the same initial

state for the study of the ionization process as that shown in QRR No. 7,
i.e., and electron beam shot into a semi-infinite space. After the initial
transient has died out, namely the first electron sheet has returned to
the injection plane, the creation of electron-ion pairs was started (see
Fig. 23). We set the ratio of the beam potential to the ionization poten-
tial $\left(V_o/V_i\right)$ equal to 100. The frequency of ionization was so chosen that
an electron traveling with a velocity higher than the threshold velocity
$\left(2\sqrt{eV_i/kT_e}\right)$ created an electron-ion pair after it spent a time interval
T_o in the semi-infinite space under study.
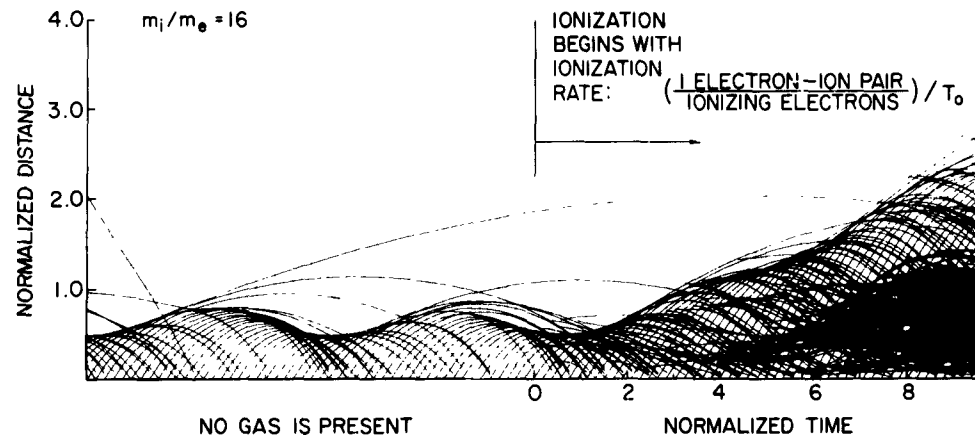
FIG. 23. COMPUTER CALCULATED TRAJECTORIES OF BEAM AND
PLASMA ELECTRONS FOR AN ELECTRON BEAM SHOT INTO A GAS.

The trajectories of the ionizing beam electrons as well as the
created plasma electrons are plotted on Fig. 23 for a time interval of a
few T_o after the creation of ion-electron pairs has begun. The normali-
zation of distance and time has already been described in QRR No. 7. We
could see that the beam electrons could not penetrate into an empty space
very far and most beam electrons were turned back before they could travel
a normalized distance of 1 into the evacuated space. After the ionization
process has begun, however, the space where electrons can be found expands
rapidly. We can observe (see Fig. 23) that the front of this space travels
with a constant velocity.

The fast penetration of an electron beam into a gas, shown in Fig. 23, can be explained with a very simple mechanism observed in the computer simulated model. Before ionization has begun in the semi-infinite space, a large negative space charge is present near the injection plane. The negative space charge sets up a positive electric field which decelerates the injected beam electrons and eventually turns them back. Naturally, ionization occurs in this region, since the ionizing electrons are located here. The first ions created in this space are in a region where a large positive field is present, hence they are accelerated through this negative space charge region and leave it with a positive velocity of the order of $\sqrt{m_e/m_i} \cdot u_o$, where u_o is the velocity of the beam electrons. After the ions have started to stream into the empty space, they are not influenced much by electric fields because the beam electrons which reach the front of the streaming ions neutralize the space charge of the ions. This mechanism which is actually the space charge neutralization of an ion beam by electrons was studied by Dunn and Ho [Ref. 1] and their work can be directly applied here. Consequently, unless some beam-plasma interaction sets in which could alter the initial behavior of the ionization process just described here, we can expect that the front of the beam penetrates into a semi-infinite space filled with gas with a velocity of the order $\sqrt{m_e/m_i} \cdot u_o$.

The results of computer calculations have shown that the velocity of the front of the penetrating electron beam is proportional to $\sqrt{m_e/m_i}$. Furthermore, we found no change in the behavior of the system as far as we could follow our calculations. The number of charge sheets were rapidly increasing during these calculations and the core memory of the IBM 7090 computer was exhausted after calculating the behavior of the system for a time interval of $30T_o$. A new computer program has to be developed before we can study the behavior of this system for longer runs.

[1] D. A. Dunn and I. T. Ho, "Computer Experiments on Ion-Beam Neutralization with Initially Cold Electrons," S.E.L. Technical Report No. 0309-1 (1963).

PROJECT 0311: PINCH EFFECTS IN PLASMA BEAMS

Tri-Service Contract Nonr-225(24)
Project Leader: D. A. Dunn
Staff: J. W. Christie

The purpose of this project is the study of transients and insta-
bilities in beam-generated plasmas.

A report on the work to date is in preparation.

PROJECT 0312: AMPLIFICATION IN BEAM-GENERATED PLASMAS

Air Force Contract AF33(657)-11144
Project Leader: D. A. Dunn
Staff: J. E. Simpson, W. Nichparenko

The purpose of this project is the study of the amplification of
waves on an electron beam resulting from the passage of the beam through
a plasma produced by the beam itself.

A. TWO STREAM AMPLIFIER THEORY FOR FINITE MAGNETIC FIELD

In the last two quarterly reports we have considered the theory of
wave propagation in a beam-plasma cylinder focused in a magnetic field.
In QRR No. 7 we showed the results of numerical calculation for the case
of a conducting pipe completely filled by the beam and the plasma. In
QRR No. 8, the computed results for a beam and plasma of the same diameter,
passing through a pipe of larger diameter than the beam plasma stream were
given. During the recent quarter, we have continued the latter calcula-
tion, in order to study the changes in the gain of the low frequency for-
ward wave mode as the various parameters are varied as indicated by the
dispersion relation.

During the last quarter changes of gain with pipe diameter were com-
pared. It was noted that the low frequency gain tends to increase until
the pipe is about 4 times the beam diameter, after which little change
occurs. We shall compare results for the 4:1 diameter ratio as represent-
ing all large pipe configurations.

In Fig. 24 dependence of gain on magnetic field is shown. So long
as the cyclotron frequency is below the plasma frequency, there is little
change in the peak gain value, but only a shift toward lower frequencies.
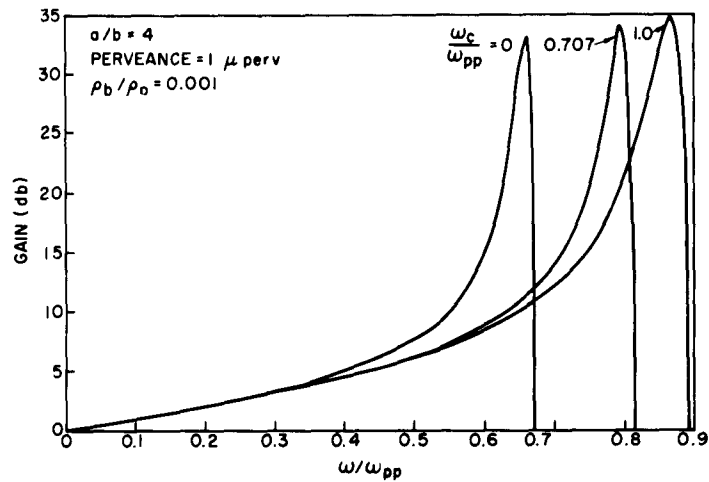
FIG. 24. COMPARISON OF GAIN PER BEAM CIR-
CUMFERENCE VS FREQUENCY FOR VARIOUS MAG-
NETIC FIELDS.

Figure 25 compares gain for several beam perveances. The peak gain is roughly proportional to the perveance at low perveance.
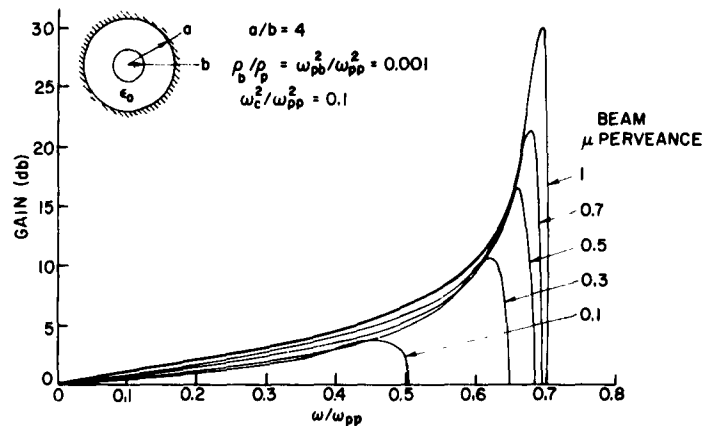
FIG. 25. GAIN PER BEAM CIRCUMFERENCE VS
FREQUENCY FOR VARIOUS BEAM PERVEANCES.

Fig. 26 compares gain for several beam density to plasma density ratios. The peak gain is proportional to ω_{pp}. For a fixed signal

frequency, as ω_{pp} is increased from zero (by increasing gas pressure, perhaps), there is at first no gain. Then the gain rises rapidly to a maximum but falls off at still higher plasma density.
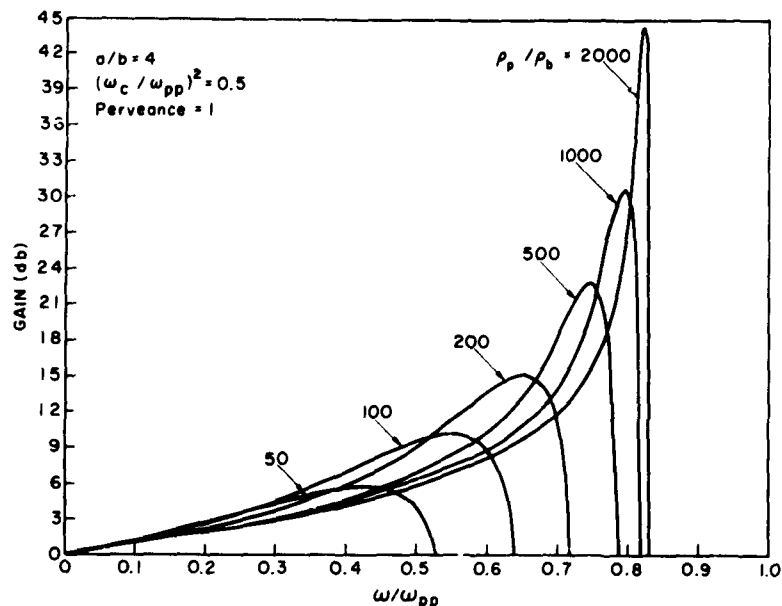
FIG. 26. GAIN PER BEAM CIRCUMFERENCE VS FRE-
QUENCY FOR VARIOUS PLASMA TO BEAM DENSITY
RATIOS.

B. EXPERIMENTAL

Observations this quarter were confined to extensive measurements of electron density in an Argon plasma. Figure 27 shows the experimental set-up used. A cylindrical cavity $(f_o = 2.3 \text{ GC.})$ operating in the TM_{010} mode was powered by a swept oscillator. The detected output appeared as a typical resonance curve when displayed on a oscilloscope. If the resonance peak is maintained on the central axis of the oscilloscope, the frequency shift of the cavity due to changes in plasma density, can be determined by varying the center frequency of the oscillator. The frequency of the oscillator is in turn measured by the transfer-oscillator, counter combination to ± 15 kc.

DIRECTIONAL
COUPLER

1.8-4.0 GC
OSCILLATOR

SAWTOOTH
GENERATOR

CYLINDRICAL
CAVITY

INPUT
LOOP

BEAM
GENERATED
PLASMA

OUTPUT
LOOP

TRANSFER
OSCILLATOR

500 Mc
COUNTER

SCOPE

CRYSTAL
DETECTOR
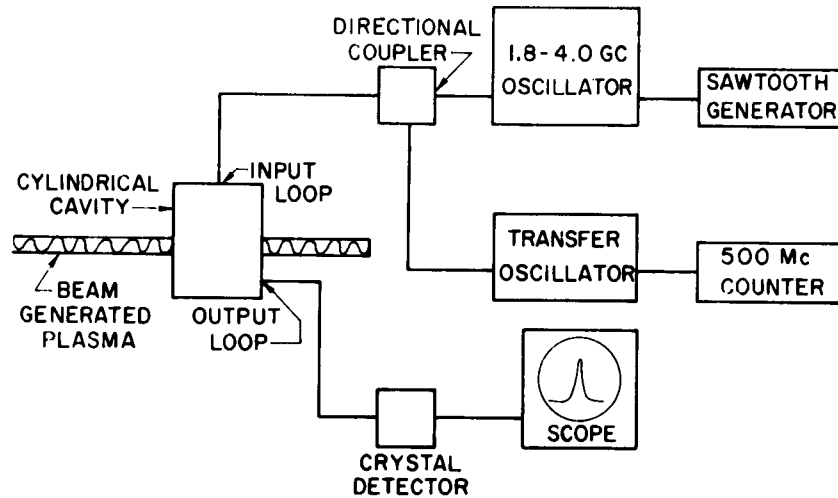
FIG. 27.   EXPERIMENTAL SETUP FOR MEASURING ELECTRON
DENSITY IN A BEAM-GENERATED PLASMA.

If the beam-generated plasma is considered to be a dielectric rod, of uniform density and diameter d, placed on the axis of the cavity, the resulting frequency shift Δf is given by:

$$\Delta f = \gamma N_e d^2 / f_o$$

$$N_e = \Delta f \, f_o / \gamma d^2$$

where

f_o = Resonant frequency of cavity.

γ = Constant evaluated by using rods of known dielectric constant and diameter.

N_e = Number of plasma electrons per unit volume.

This method has the limitation of measuring only the total number of electrons contained in the pipe.   If the radial variation of the plasma electron density is unknown, some assumption must be made in order to compute the actual number density.

Basically, there are two modes of tube operation. One where the plasma generated by the beam is confined to the beam radius. The other occurs when the beam-generated plasma completely fills the pipe. This is termed total glow. Figure 28 shows these two conditions graphically,
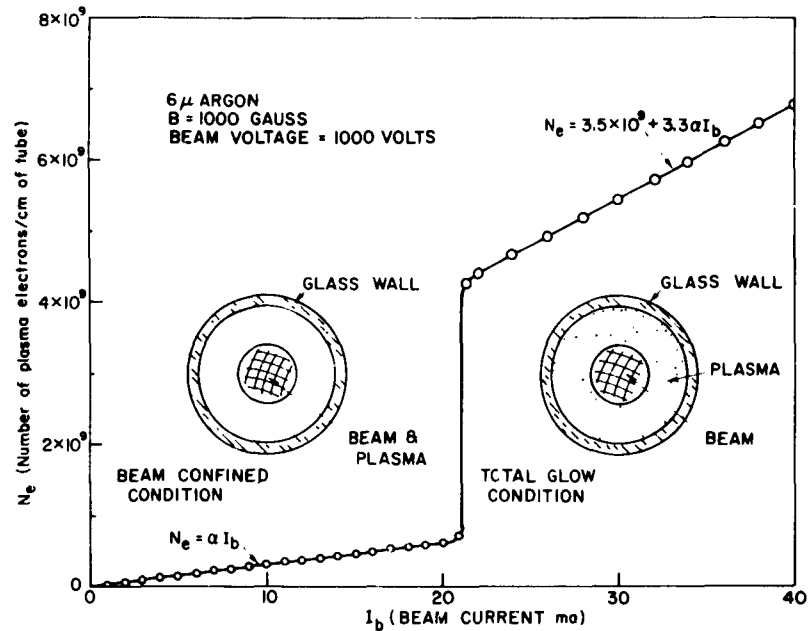
FIG. 28. PLOT OF ELECTRON NUMBER VS BEAM CURRENT SHOWING THE EFFECT OF TOTAL GLOW.

and the corresponding plot of N_e, the number of plasma electrons/cm of tube length vs beam current, I_b. A sharp rise in N_e occurs during the transition to total glow. Many such density measurements with varying tube parameters (beam voltage, gas pressure, magnetic field) were taken. If we write $N_e = I_b\, g(V_b,\, p,\, B)$ where V_b is the beam voltage, p is the pressure in Torr, B is the axial magnetic focusing field, and $g(V_b,\, p,\, B)$ is the measured generation function, we have found that the following statements hold.

1. During the sudden transition from beam-confined plasma to total glow, the amount of the sudden jump in N_e increases with increasing beam voltage, V_b, in the range of 500-1500 volts.

2. For the region of beam confined plasma below total glow, the N_e is linearly proportional to the beam current I_b.

3. In the linear region below total glow, the generation function $g(V_p, p, B)$ is a slightly increasing function of beam voltage, V_b, in the range of 500-1500 volts.

4. At high pressures, 9-15 μ Argon, the total glow transition no longer occurs very suddenly, but slowly spreads out from the beam til it fills the tube.

5. Persistent noise peaks were found at 1 and 2 Mc. Figure 29 shows spectrum analyzer photographs of these peaks. No explanation exists at the present for these peaks.

LOW FREQUENCY SPECTRUM
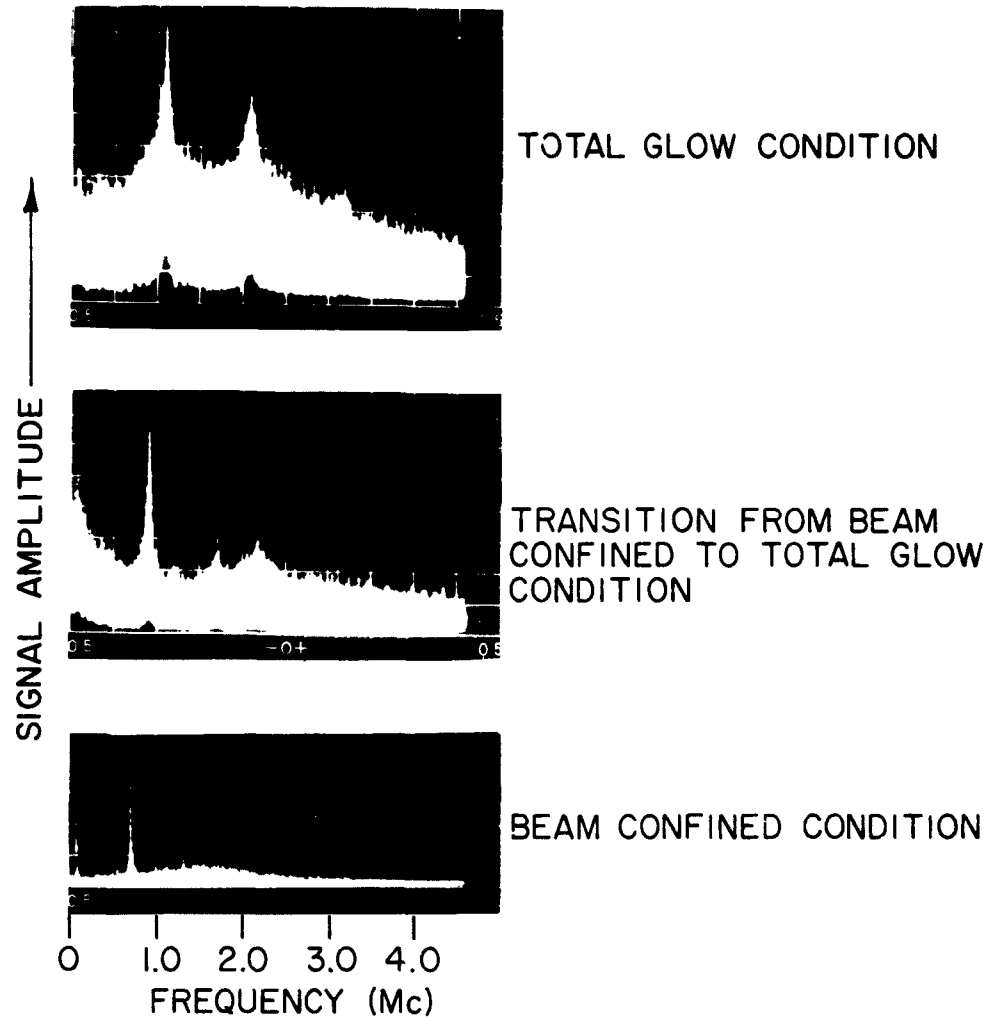
FIG. 29. SPECTRUM ANALYZER PHOTOGRAPHS SHOWING LOW FREQUENCY NOISE PEAKS UNDER NORMAL AND TOTAL GLOW CONDITIONS.

Work next quarter will consist mainly of forward gain and backward attenuation measurements along the beam.

PROJECT 0313:   COMPUTER EXPERIMENTS ON BEAM-GENERATED PLASMAS

Army Contract DA 36-039 AMC-00094(E)
Project Leader: D. A. Dunn
Staff: A. S. Halsted

The purpose of this project is the study of a beam-generated plasma using a computer model in which transverse motion of beam and plasma particles are allowed. Plasma oscillation and beam focusing effects are being studied on the computer.

The use of a computer model to investigate the behavior of a beam-generated plasma was discussed in the previous quarterly reports, and experimental results were given for the case of plasma generation by an electron beam of fixed density partially filling the space between two planar electrodes.

This study has now been extended to consider the effect of the self-focusing field on the beam. After an equilibrium condition is established with the beam fixed, the beam electrons are allowed to move under the influence of the self-focusing field, with the plasma generation propor-tional to the instantaneous beam density. The results of such an experi-ment are shown in Fig. 30. The system is initially in equilibrium with the beam confined to the center one quarter of the diode (see QRR No. 7 for a description of the equilibrium state for this case). At $T = 0$, the 128 charge sheets used to represent the beam are released and allowed to move in the direction normal to the direction of the drifting beam. Since the plasma is approximately one hundred times denser than the beam, the new distribution of the beam charge alone does not alter the fields in the diode. However, the plasma generation pattern determined by the beam will modify the fields and reduce the confining potential as shown in the lower figure. This process eventually allows the beam to spread until it fills the diode space. We shall use the term "generation instability" to describe such a process leading to the breaking up of the beam. Our object in future work will be to determine a time scale for such a generation instability which may then be compared to the characteristic times of other processes which cause the defocusing of the beam.

BEAM SHEET TRAJECTORIES

NORMALIZED TIME

POTENTIAL PROFILES

NORMALIZED TIME
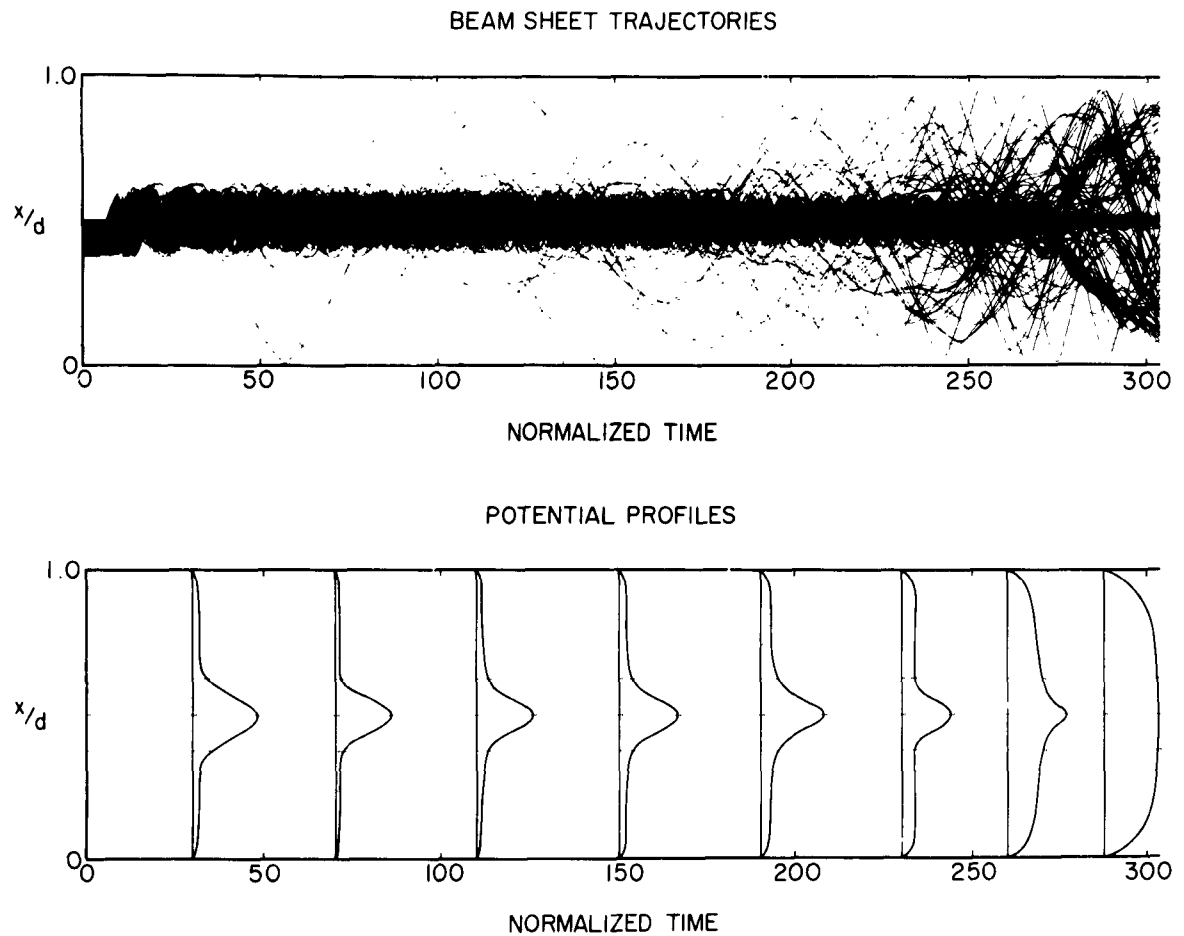
FIG. 30.   DEFOCUSING OF AN ELECTRON BEAM IN A BEAM GENERATED
PLASMA.

In addition to these studies using a computer model, work is also being done under this project to extend the static theory [Ref. 1] of a beam generated plasma in planar and cylindrical geometry.

---

[1] D. A. Dunn and S. A. Self, "Static Theory of Density and Potential Distribution in a Beam Generated Plasma," J.A.P., 35, 113 (1964).

PROJECT 0321: ELECTRON BEAM FOCUSING IN IONIZED GASES

Army Contract DA 36-039 AMC-00094(E)
Project Leader: D. A. Dunn
Staff: R. P. Lagerstrom, J. Bridges

Recent studies [Ref. 1] of the potential distribution in a beam-
generated plasma have indicated that a potential distribution is produced
in the vicinity of the beam that is self-focusing, i.e., beam electrons
are returned toward the axis if they start to leave the beam. This pro-
ject will be a theoretical and experimental study of this phenomenon with
a view toward the application of this focusing effect to beam-type electron
tubes.

A. 20 KILOVOLT PULSED MEASUREMENTS

Pulse equipment giving 20 kilovolt, 1,000 μsec pulses at repetition
rates up to 60 pps is 95 percent complete. The equipment behaved satis-
factorily at 10 kilovolts, with 500 μsec pulse length.

B. MOLECULAR-FLOW CALIBRATION OF THE BELL-JAR EXPERIMENT

This experiment basically involves: (1) a target-gas chamber; and
(2) an electron-gun chamber. These two regions are connected by the
anode hole, the conductance of which determines the pressure differential
between the two regions. The target region will operate between 10^{-6} to
10^{-3} torr, whereas the gun chamber would perferably operate at as low a
pressure as possible, but it may be quite high in the electron gun because
of the high conductance of the anode aperture. A tantalum emitter was
therefore employed that can withstand ion bombardment. Also, electrode
spacings were chosen that would allow 20-kilovolt operation without
breakdown even at pressures up to 1 micron.

The anode aperture and gun configuration play central roles in the
gas flow aspects of this experiment. The following experiments were per-
formed to understand better the characteristics of this region.

---

[1]D. A. Dunn and S. A. Self, "Static Theory of Density and Potential
Distribution in a Beam-Generated Plasma," J. Appl. Phys., 35, 113
(1964).

A detailed sketch of the experimental assembly was given in the last QRR [Ref. 2]. The sketch of Fig. 31 indicates the molecular flow paths through the bell-jar assembly and electron-gun. A flow, Q (torr-liters/ sec), is defined as the product of the volumetric flow rate dV/dt (liters/ sec) across a plane, and the pressure P (torr) at which it is measured,

$$Q = P \frac{dV}{dt} .$$
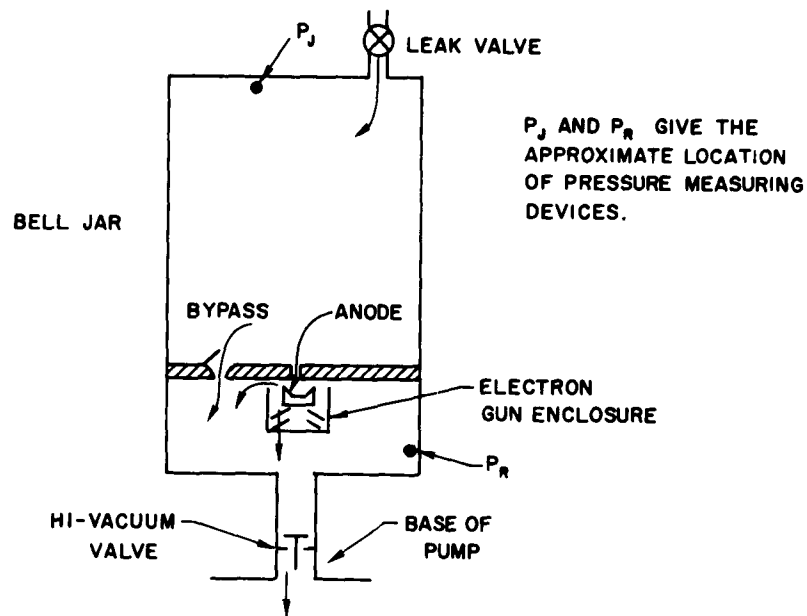
FIG. 31. SKETCH OF FLOW PATHS THROUGH BELL-JAR ASSEMBLY.

This is related to molecular flow by the ideal gas law,

$$Q = kT \frac{dN}{dt} ,$$

---

[2]QRR No. 7, 1 October through 31 December, 1963, Project 0321, p. I-44.

where   k   is the Boltzmann constant, T $(^\circ K)$ is the absolute tem-
perature and   dN/dt   is the rate at which molecules cross the plane.

The molecular conductance of a channel (pipe or orifice) can be
defined by the equation

$$G = \frac{Q}{P_2 - P_o} \; ,$$

where P_2 and P_1 are the entrance and exit pressures, respectively.
Noting that V/G has the dimensions of a time constant,   the equations
provide an analogy with circuit theory:

$$P \rightarrow \text{voltage}$$
$$Q \rightarrow \text{current}$$
$$G \rightarrow \text{conductance}$$
$$V \rightarrow \text{capacitance} \; .$$

A circuit model for the bell jar is shown in Fig. 32.   The pumping speed
in l./sec is represented as a conductance, g_p. An approximate calcula-
tion of these conductances was made on the basis of the following
formulae [Ref. 3].

For a circular opening of diameter   D:

$$G_{OD} = 2.86 \; D^2 \sqrt{\frac{T}{M}} \; \text{l./sec} \tag{1}$$

For a pipe of inside diameter   D   and length   L:

$$G_P = 3.81 \sqrt{\frac{T}{M}} \; \frac{D^3}{L} \; \text{l./sec} \tag{2}$$

---

[3] S. Dushman and J. M. Lafferty, Scientific Foundations of Vacuum
Technique, John Wiley and Sons, Inc., Chapter 2, 1962.

Q = LEAK VALVE CURRENT
V_J = VOLUME OF BELL JAR
V_E = VOLUME OF ELECTRON GUN ENCLOSURE
V_R = VOLUME REMAINING

CONDUCTANCE:
G_S - ENTRANCE
G_A - ANODE
G_B - BYPASS PORT
G_{A1} - AROUND GUN ENCLOSURE
G_{A2} - THROUGH GUN ENCLOSURE
G_O - EXIT
g_P - PUMPING SPEED
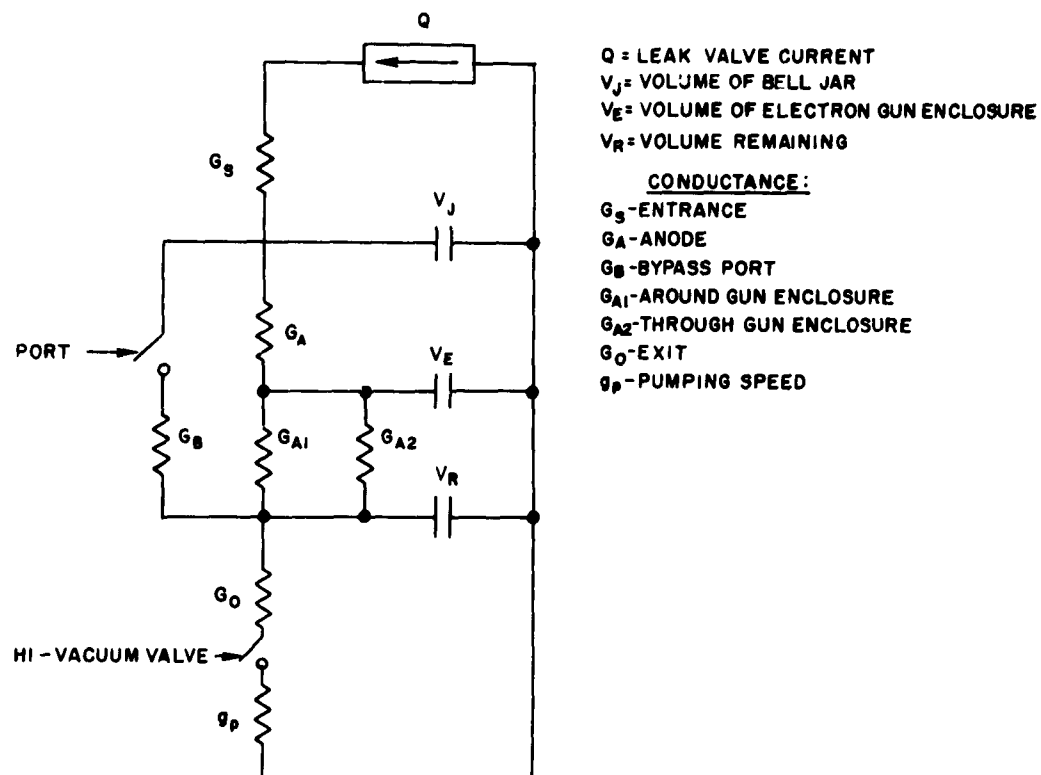
FIG. 32. AN ANALOGUE CIRCUIT MODEL FOR THE BELL-JAR
EXPERIMENT.

The common channel has a total conductance G_T given by

$$\frac{1}{G_T} = \frac{1}{G_{OD}} + \frac{1}{G_P} \quad .$$ (3)

In these formulae T is the absolute temperature and M is the molecular weight. Dimensions are in centimeters.

If the flow paths in the bell jar are highly idealized we have the approximate numerical results for argon at room temperature:

$$G_B \;=\; 133 \quad 1./sec$$

$$G_A \;=\; 4.5 \;\; 1./sec$$

$$G_{A1} \;=\; 18 \quad 1./sec$$

$$G_{A2} \;=\; 3.7 \;\; 1./sec$$

Considering these magnitudes as relative, then a simpler model can represent the flow problem. For the interesting case of the exhaust port closed and the leak valve open we have Fig. 33. This case may be further simplified by noting that the time constant for the leak filling
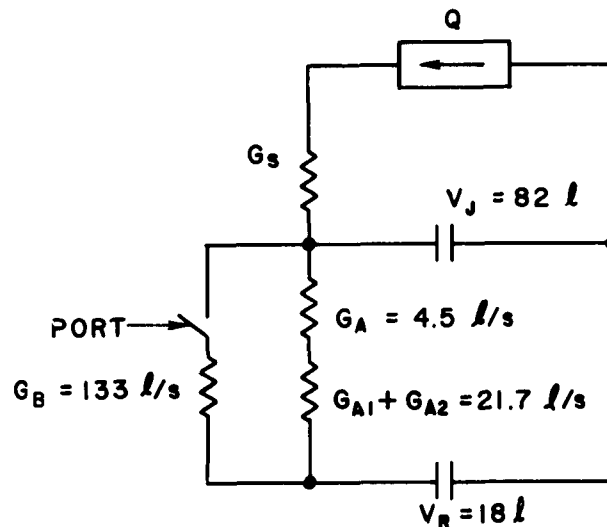
FIG. 33. SPECIAL CASE FOR CALIBRATING
LEAK VALVE.

the volume V_J was on the order of minutes, whereas the time constant $\left(V_R/G_B \text{ seconds}\right)$ of the lower section is tenths of a second. Therefore ignore G_B and add V_R to V_J as one volume. We now represent the flow problem by a single conductance G in series with $V = V_J + V_R$.

We shall show that this will permit an experimental determination of Q. Knowing Q we can experimentally determine G_B and G_A and compare with the values obtained from the formulae (1) through (3). Notice that the series combination of G_A plus G_{A1} and G_{A2} in parallel is essentially equal to G_A. If the exhaust port (hi-vacuum valve) is closed and leak valve open we have (for the simplified model)

$$+ V \frac{dP_J}{dt} = G(P_J - P_S) , \qquad (4)$$

where P_J is the pressure in the bell jar at any instant. It follows that, if P_S is the source pressure, and the initial pressure in the bell jar is assumed negligible, the pressure in the bell jar is given by

$$P_J = P_S(1 - e^{G t/V}) . \qquad (5)$$

For time small with respect to the time constant,

$$P_J \approx \frac{P_S G t}{V} .$$

Then the current Q is given by V times the slope of P_J vs time,

$$Q = P_S G .$$

Measurements taken for various settings of the leak valve were plotted as a calibration curve for the leak valve. Using the calibration curve along with measurements of P_R and P_J the formula

$$G = \frac{Q}{P_J - P_R}$$

gives G_A with the bypass port closed and gives $G_A + G_B$ with the by-pass port open. The following table summarizes the results

| leak valve | G_A (l./sec) | | G_B and G_A (l./sec) | |
dial	exp.	theor.	exp.	theor.
35	2.5	4	100	140
40	3.1	4	340	140
45	2.9	4	540	140

Because $P_J - P_R$ is very small with the bypass port open, the experimental determination of $G_B + G_A$ is very approximate. The net results, however, indicate that our calibration curve is probably correct to within a half-order of magnitude.

NEW PROJECT

PROJECT 0322:   NOISE GENERATION IN PLASMAS

Air Force Contract AF33(657)-11144
Project Leaders: O. Buneman and D. A. Dunn
Staff: K. Thomassen

The purpose of this project is the study of mechanisms of noise generation in plasmas and methods of coupling noise out of plasmas.

The first source we are investigating is a voltage tunable magnetron (VTM) obtained from Eitel-McCullough, Inc., San Carlos, Calif., which has been found to be noisy for certain conditions and coherent for other conditions. It is not without reason that we are studying the noise in this tube rather than in a plasma. Aside from being in some ways more simple than a plasma the tube is a crossed field device and the instabilities giving rise to noise in crossed field devices may also be present in plasmas in which crossed fields are present. The recent work of Knauer at Hughes Research Laboratories has shown that an unstable sheath exists in the Penning discharge at certain pressures as a result of the action of these crossed fields. This type of mechanism might explain the high diffusion of particles across the magnetic field in some plasmas. From this study we should also gain experience in making noise measurements and perhaps also arrive at a design for a practical noise source.

A. VTM DESCRIPTION

A VTM is very similar to an ordinary magnetron in that it has a cylindrical cathode (or sole) surrounded by a cylindrical anode r-f structure with an annular interaction region between them in which a beam rotates. The beam is modified through interaction with the r-f structure to give a rotating spoke like pattern. There are two essential differences however--the first is that the r-f structure consists of an interdigital line (a backward wave structure) which is nonresonant, thus allowing the output frequency to vary linearly with beam voltage as in a BWO. The second difference is that the cathode area exposed to the interaction region is not heated so the back-bombardment cannot cause fluctuations in the emission. Instead, the cathode cylinder is extended axially out of the interaction region and a portion of this part of the cathode is heated. Then, the electrons are injected into the region by a voltage applied to another anode (separated electrically from the r-f anode structure) surrounding this called the injection anode (see Fig. 34). Their path is then initially along the axis, or magnetic field direction, and then they are spun circumferentially by the crossed E and B fields.
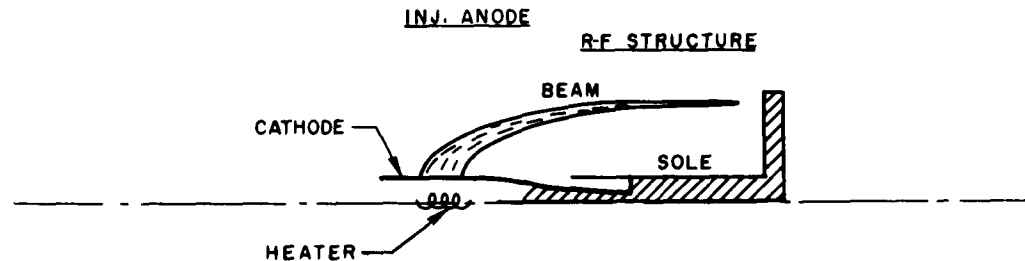
FIG. 34. VTM GEOMETRY.

It is obvious that the initial beam velocities are dependent on the magnetic field configuration at the cathode and on the injection voltage which can range from 0 - 400 volts above the cathode potential (anode voltages range from 0 - 2 kv). Indeed, one finds that bringing up the

injection anode voltage from zero causes the tube to break into noise
from its formerly coherent state. Also, slightly changing the position
of the tube with respect to the field in which it is immersed will again
cause the tube to be noisy. Further, it was found that tilting the
cathode some 5 degrees off axis toward the interaction region makes it
more difficult to bring the tube into a noisy regime.

It is fruitful to look more closely at the effects which occur when
one adjusts the tube position with respect to the magnetic field. In
Fig. 35 the field configuration for the magnet   is shown. The magnetic
is a permanent magnet with circular pole pieces about 3 cm apart. It is
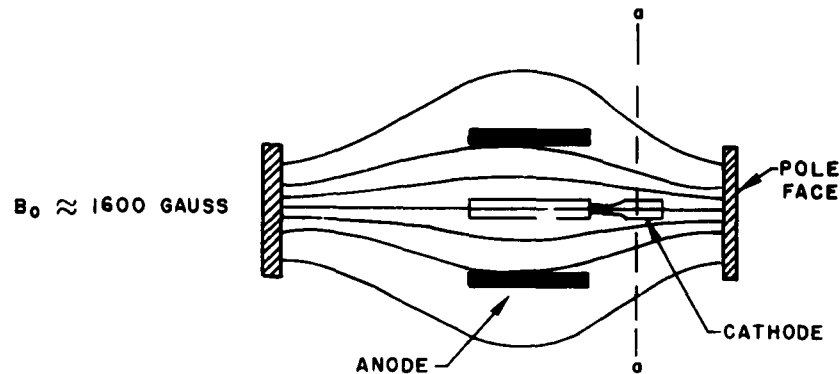
FIG. 35.   MAGNETIC FIELD CONFIGURATION.

found that if the tube is aligned with the axis of the magnetic poles the
output is the least noisy when the cathode is close to one pole piece
(plane a-a). This is very reasonable since in this position the magnetic
field diverges from the axis as does the electron beam in its course to-
ward the interaction region. Consequently, there is a minimum of dis-
turbance put on the beam due to trying to cut across the magnetic field.
Tilting the cathode also causes the beam to follow the magnetic field
lines more closely as was shown by Okoshi at Bell Labs in a recent
theoretical study, hence it is not surprising that the noise is reduced
under these conditions.

B. VTM CHARACTERISTICS

We have speculated on plausibility grounds as to the reasons noise
appears when it does. These suspicions should be put on firmer theoreti-
cal grounds and then accepted or disproved on the basis of conclusive
experimental evidence. We have begun our study by investigating the
experimental behavior of the tube.

The tube is supplied by an FXR regulated power supply with a regulated
heater voltage. The beam supply should be well regulated since the output
frequency varies linearly with this voltage and consequently may vary
according to the peak to peak ripple voltages.

A 20 db coaxial attenuator is placed directly on the output and the
attenuated signal is then analyzed. The easiest thing one can do is to
examine the frequency spectrum of the signal as a function of anode volt-
age under various conditions using either a spectrum analyzer or a narrow
band receiver. This was done for no injection voltage with the tube
placed so as to minimize the noise output. The plot in Fig. 36 shows
the output spectrum which consists of the main peak and a large number
of secondary outputs some 20 - 50 db weaker than the main signal. These
secondary outputs tune linearly in frequency with voltage.
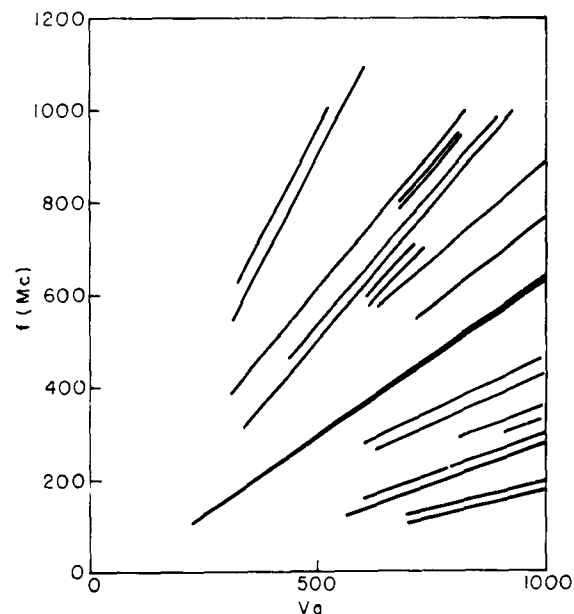
FIG. 36. VTM FREQUENCY SPECTRUM VS
ANODE VOLTAGE.

The spectrum for a given beam voltage changes when the injection anode voltage is increased from zero. At about 50 - 100 volts the coherent peaks break suddenly into noise of varying bandwidths centered about their former peak frequencies. As the injection voltage increases further the noise becomes less peaked in amplitude and more broadband in frequency. Bands of noise as large as 100 - 200 Mc centered at 700 - 800 Mc have been observed.

PROJECT 0414: EMISSION OF ELECTRONS IN SOLIDS

Tri-Service Contract Nonr-225(24)
Project Leader: H. Heffner
Staff: M. Cowley

The object of this project is to carry out experimental studies of emission of electrons from various substances with the aim of developing a practical cathode with high emission density.

A. [BARIUM-STRONTIUM] OXIDE - SILVER JUNCTION

Most of the past quarter has been devoted to the design and construction of a tube which will allow investigation of a [Barium-Strontium] Oxide - Silver ([BaSr]O-Ag) junction. Basically this consists of a structure which provides for the normal activation of a [BaSr]O thermionic cathode, with subsequent evaporation of a silver film to which an electrical contact is made. Figure 37 shows a schematic drawing of the
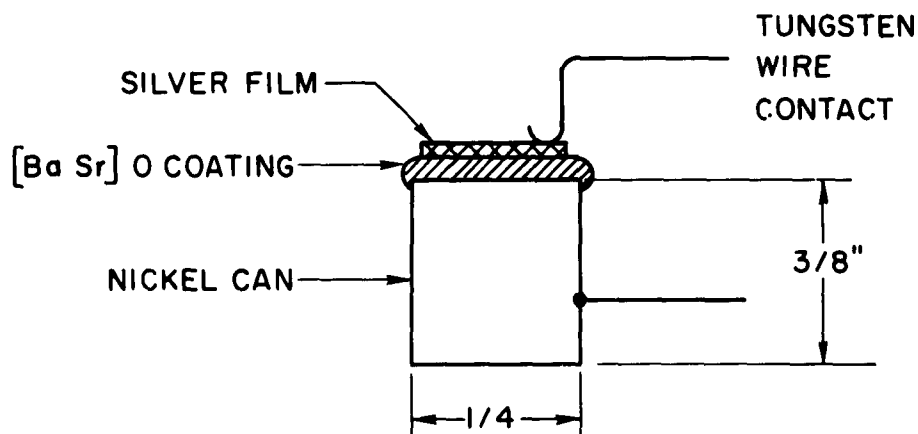
FIG. 37. SCHEMATIC DIAGRAM OF [BaSr]O-Ag JUNCTION.

[BaSr]O-Ag junction. Figure 38 is a drawing of the tube. Operation of
the tube is simple: After the cathode has been activated, and the silver
film has been evaporated, the fuse wire is burned by passing current
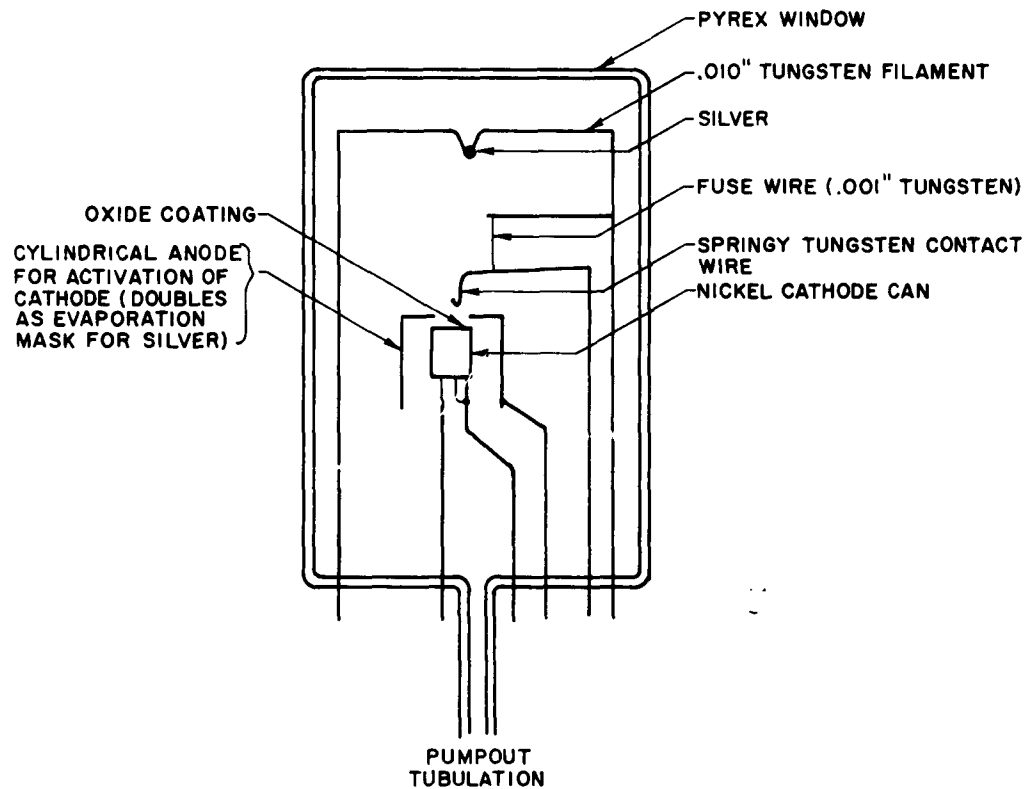
FIG. 38. [BaSr]O-Ag TUBE.

through it, allowing the springy tungsten wire to which it is attached to fall
onto the silver film. This provides an electrical contact to the silver film.
The [BaSr]O-Ag junction may now be studied using the standard techniques
for determining metal-semiconductor barrier heights. The junction can be
illuminated by shining light through the Pyrex window onto the silver
film, and electrical measurements can be made via the connections which
are brought outside the tube. One version of this tube has been built

and tested, with only partial success. The contacting scheme involving the fuse wire worked perfectly, but oxidation of the tungsten spring wire (probably during tube construction) caused a very poor contact to be made to the silver film. As a consequence of this, electrical tests were not possible. A second tube is in the process of construction; two contacts will be made to the silver film in this tube, so that electrical continuity between them may be checked. This will provide a check both on the contacts to the film and on the continuity of the film itself.

B. INVESTIGATION OF OTHER METAL-SEMICONDUCTOR SYSTEMS

Consideration has been given to the investigation of Zinc Oxide-metal surface barrier junctions. Zinc Oxide has a band gap of 3.3 ev, and is now available in wafer form from a commercial source. These wafers are n-type with resistivities ranging from 0.5 to 1.0 Ω-cm. Six wafers have been ordered, and experiments on ZnO-metal systems will begin upon their arrival.

C. THEORETICAL INVESTIGATION OF THE METAL-OXIDE-SEMICONDUCTOR SYSTEMS

Some preliminary results of a detailed theoretical investigation of the metal-oxide-semiconductor (MOS) system indicates that in the presence of surface states, it may be possible to raise the energy of electrons in the conduction band of the semiconductor above the Fermi level in the metal by an amount exceeding the zero-bias barrier height Calculations on a GaP-oxide-platinum junction indicate that electrons flowing into the platinum film might have energies as high as 1.8 ev above the Fermi level. If further investigation shows that this phenomena can be of use in an electron emission device, some experiments will be undertaken in an attempt to verify these calculations.

PROJECT 0415: UTILIZATION OF OPTICAL MASERS

> Tri-Service Contract Nonr-225(24)
> Project Leader: H. Heffner
> Staff: C. Y. She, H. Sonnenberg

The object of this project is to investigate possible ways of utilizing the unique properties of the laser.

A. QUANTUM COMMUNICATION PROBLEMS'

In previous issues of the QRR, the development of quantum statistical theory of simultaneous measurements and the result of its applications to obtain quantum noise and channel capacity of a typical communication system has been reported.

A final report is in preparation on this section.

B. SECOND HARMONIC GENERATION BY A METAL SURFACE

So far, a second harmonic could not be detected, even after slight modification to the experimental setup as proposed in the last report. In order to obtain any photomultiplier readings at all, it was found necessary to focus the incident and the reflected laser beams. With this modification, photomultiplier readings could be obtained, but unfortunately these were not proportional to the square of the intensity, (as the second harmonic must be), but rather appeared to be exponentially dependent on the intensity.

The observed photomultiplier response is probably due to thermal radiation from the metal surface. The fact that the surface was found to be damaged by the laser beam supports this belief.

Two methods of combating thermal radiation are to be persued: liquid nitrogen cooling of the metal surface; and liquid nitrogen cooling of the photomultiplier (since we are limited in sensitivity by the dark current of the tube). It is doubtful whether cooling the metal will decrease heating of the surface significantly, but because cooling is easily achieved, it is to be tried.

PROJECT 0558:   INVESTIGATION OF NOISE IN ELECTRON GUNS

> Army Contract DA 36-039 AMC-00094(E)
> Project Leader: A. E. Siegman
> Staff: M. O'Flynn

Technical Report No. 0558-1 by Michael O. O'Flynn, entitled "Monte Carlo Investigation of Noise in an Incipient Space-Charge Diode," is in process of publication. Upon its completion and distribution this project will be terminated.

PROJECT 0572:   INFRARED AND SUBMILLIMETER MASER STUDIES

> Air Force Office of Scientific Research Grant No. 323-63
> Project Leader: A. E. Siegman
> Staff: Guido Francois

This project presently aims at mixing in an appropriate crystalline material a visible laser output with infrared or far infrared radiation in order to obtain sidebands of the laser light. This will allow measurement of the relevant nonlinear dielectric matrix elements of various crystalline materials and evaluation of the possibilities for difference frequency generation at infrared frequencies and for optically pumped parametric oscillation. These are also important quantities for evaluating the light modulation capabilities of the materials.

Using the experimental setup described in previous quarterly reports (Fig. 39), we have been able to detect the second harmonic radiation generated in KH_2PO_4 by a few milliwatts of CW laser light at 6328$\overset{\circ}{A}$. Measurements have been made using different input powers and different combinations of collimating lenses.

From these measurements the following is apparent:

1. The measured output is generated second harmonic since:
    a. it is a quadratic function of the input power
    b. it is dispersed by the predicted angle from the fundamental by the prism (Fig. 39).
    c. its maximum occurs at the predicted crystal orientation
    d. it leaves a blue mark on color film (75 ASA-15 min. exposure).
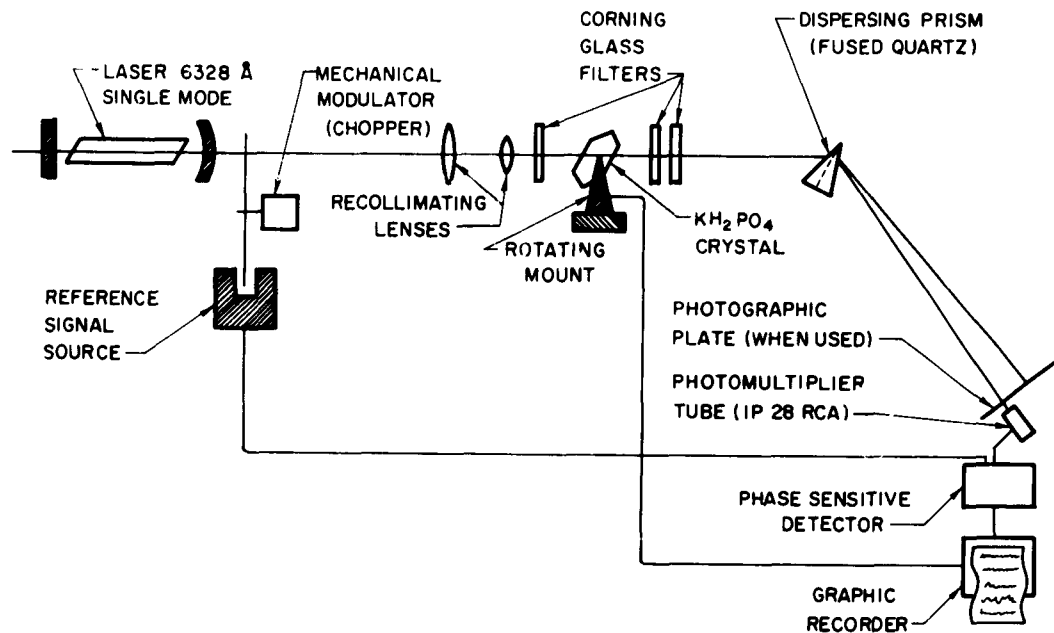
FIG. 39. SECOND HARMONIC GENERATING EXPERIMENT.

2. The theoretical $\left(\dfrac{\sin x}{x}\right)^2$ dependence of the output power on the angular orientation of the crystal was never obtained. Figure 40 gives a typical example of the second harmonic power vs crystal orientation. Depending on collimation, beam size and point of incidence on the crystal, single or multiple peaked curves are obtained. Sidelobes were never observed.

3. The sensitivity of the detecting system is at the present time of the order of 10^{-15} watt (corresponding to a signal to noise ratio = 1).

The absence of sidelobes and the variations of the shape of the output curve are due to crystal imperfections, causing the output to be a superposition of several theoretical lines. A better crystal is in preparation.

The excellent signal to noise ratio displayed in Fig. 40 has proven to be insufficient to repeat the experiment for doubling the 1.15μ line of the same laser. The lack of infrared lenses, appropriate laser mirrors and the lower frequency are responsible for this. We are now completing our experiment and examining the possibility of cooling the detector.
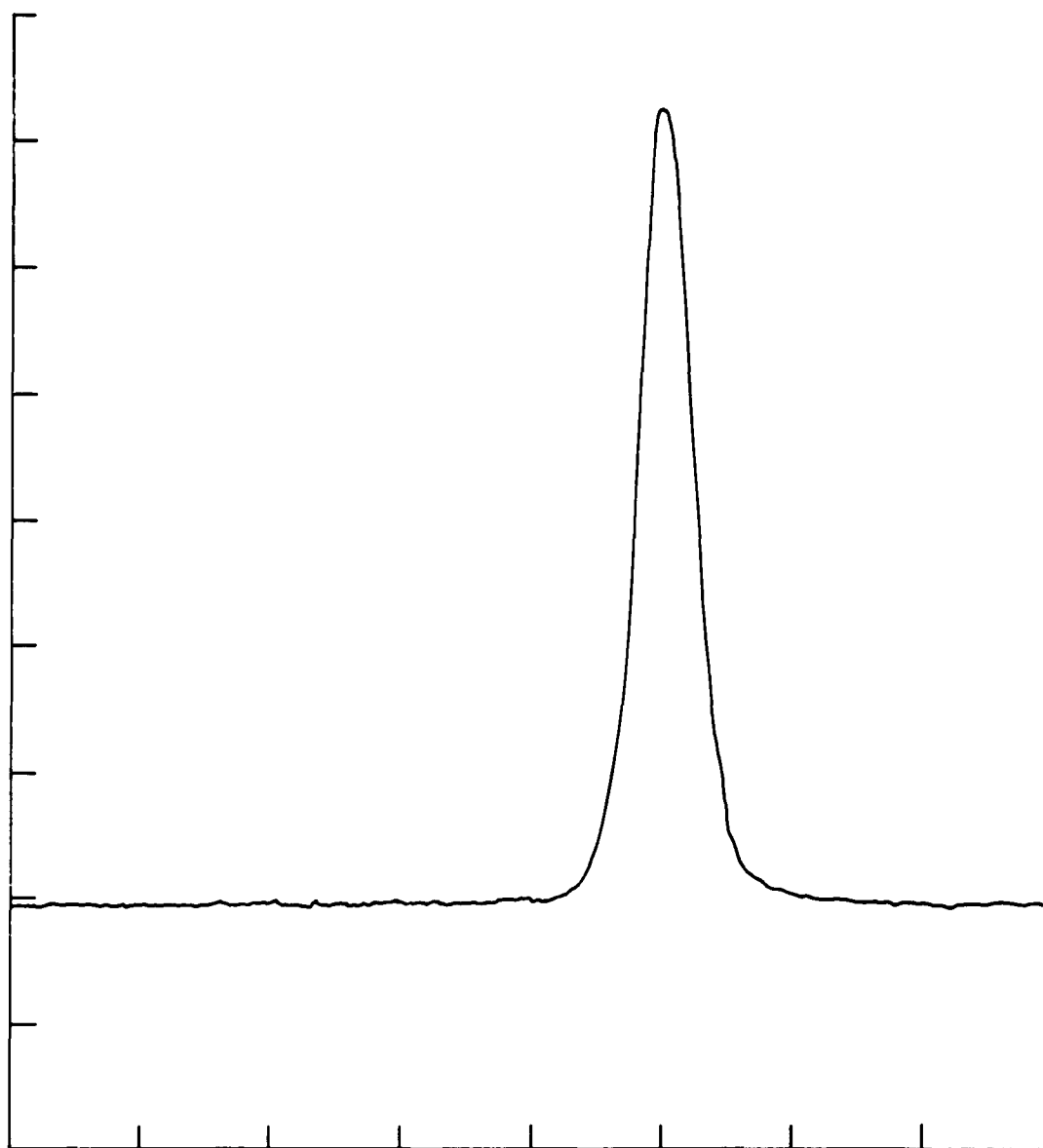
FIG. 40.   SECOND HARMONIC POWER VS CRYSTAL ORIENTATION INPUT
POWER: 4 MILLIWATTS AT 6328Å CROSS SECTION OF BEAM: 1.6 mm
MARGIN MARKERS OCCUR EVERY 1/4° OF CRYSTAL ROTATION. OUTPUT
POWER IS (AT PEAK) 10^{-12} WATT AT 3.164Å.

TABLE 1

		CRYSTAL CLASS	REFRACTIVE INDEX	BIREFR.
Alunite	$KAl_3(SO_4)_2(OH)_6$	3m	1.572	.020
Ammonium Dihydrogen Phosphate	$NH_4H_2PO_4$	$\bar{4}2m$	1.460	.040
Barium formate	$Ba(HCOO)_2$	222	1.573	.123
	$BaTiSi_3O_9$	$\bar{6}m2$	1.757	.047
Codeine	$C_{18}H_{21}NO_3 \cdot H_2O$	222	1.543	.141
Epsomite	$MgSo_4 \cdot 7H_2O$	222	1.433	.028
Goslarite	$ZnSO_4 \cdot 7H_2O$	222	1.457	.027
Lactose Monohydrate	$C_{12}H_{22}O_{11} \cdot H_2O$	2	1.517	.038
Lead dithionate	$PbS_2O_6 \cdot 4H_2O$	32	1.635	.018
Lithium Sulphate	$LiSO_4 \cdot H_2O$	2	1.460	.028
Metaldehyde	CH_3CHO	4	1.430	.100
Nickelsulphate heptahydrate	$NiSO_4 \cdot 7H_2O$	222	1.467	.025
Parahilgardite	$C_8B_{18}O_4 \cdot 4H_2O$	1	1.630	.034
Potassium Dihydrogenphosphate	KH_2PO_4	$\bar{4}2m$	1.468	.042
Potassium dithionate	$K_2S_2O_4$	32	1.455	.060
Quartz	SiO_2	32	1.544	.009
Rochelle Salt	$KNaC_4H_4O_6 \cdot 4H_2O$	222	1.494	.004
Rubidium dithionate	$Rb_2S_2O_6$	32	1.457	.050
Shortite	$Na_2Ca_2(CO_3)_3$	mm2	1.531	.039
Silver Nitrate	$AgNO_3$	222	1.729	.059
Sodium Silicate	Na_2SiO_3	2	1.513	.015
Sterrettite	$Al_6(PO_4)_4 \cdot 5H_2O$	222	1.572	.029
Strontium Chlorate	$Sr(ClO_3)_2$	mm2	1.516	.110
Strontium formate dihydrate	$Sr(HCOO)_2 \cdot 2H_2O$	222	1.484	.054
Sucrose	$C_{12}H_{22}O_{11}$	2	1.538	.033
Tartar Emetic	$KSbOC_4H_4O_6$	222	1.620	.018
Tartaric Acid	$(COOH)(CHOH)_2(COOH)$	2	1.495	.109
Urea	$CO(NH_2)_2$	$\bar{4}2m$	1.484	.122
Wurtzite	ZnS	6mm	2.356	.022

Our present efforts are also directed toward calibrating the various elements of equipment.

Parallel to this experimental research we have been searching for crystals that will allow the mixing of the 6328$\overset{o}{A}$ and 3.39μ lines of the HeNe laser. With the help of an undergraduate student, over 350 crystals have been examined. The materials on the preceding **page** have been selected on the basis of their crystal class (nonisotropic and no center of symmetry) and transparency in the visible part of the spectrum.

Data on the infrared transmission (at 3.39μ) are generally not available. However, the C-H bond is resonant at 3.4μ. This eliminates most of the organic materials.

We know that quartz is not sufficiently birefringent to allow compensation of its dispersion and index matching.

Many of the materials listed above are actually minerals and have a complicated formula which makes it hard to grow them articifically. Natural samples are seldom pure. Also, complex ions tend to absorb infrared radiation. Potassium dithionate and strontium chlorate are only available as powders. KDP and ADP absorb the infrared. Among the remaining materials, rubidium dithionate, silver nitrate, and urea have the highest birefringence. At present, we are trying to obtain single crystals of optical quality and sufficient size of silver-nitrate and urea.

PROJECT 0576: MICROWAVE LIGHT MODULATION METHODS

Air Force Contract AF33(657)-11144
Project Leaders: A. E. Siegman and S. E. Harris
Staff: C. M. McIntyre

This project will investigate methods for the modulation and demodulation of light at microwave frequencies, with particular emphasis on frequency-modulated light.

During this quarter, time was spent in preparing revised versions of the publications "Demodulation of Phase Modulated Light Using Birefringent Crystals," and "Conversion of Frequency-Modulated Light to Space-Modulated Light." Both of these publications have now been accepted.

An analysis of the birefringent demodulator described in M.L. Report No. 1156 has been made taking into account the fact that the optical carrier is not monochromatic. We assume that the input to the demodulator is given by:

$$Z(t) = X(t) \cos[\omega_c t + \theta + k \cos(\omega_m t + \phi)]$$

where

$X(t)$ = stationary, gaussian, random process with zero mean;

θ is a random variable uniformly distributed on the interval 0 to 2π;

ϕ is a random variable uniformly distributed on the interval 0 to 2π;

$X(t)$, θ, and ϕ are independent

Using the transfer function of the demodulator given in M. L. Report No. 1156, the input to the photodetector will be:

$$\begin{bmatrix} W_x(t) \\ \\ W_y(t) \end{bmatrix} = \frac{1}{2} \begin{bmatrix} Z(t - \frac{a}{2} - \frac{b}{2}) + Z(t + \frac{a}{2} - \frac{b}{2}) \\ \\ Z(t - \frac{a}{2} + \frac{b}{2}) - Z(t + \frac{a}{2} + \frac{b}{2}) \end{bmatrix}$$

The polarization insensitive photodetector will respond to the incident signal squared and low passed (intensity envelope). The incident signal squared is

$$W(t) = W_x^2(t) + W_y^2(t)$$

with autocorrelation function given by:

$$R_W(\tau) = E[W(t_1)W(t_1 + \tau)].$$

The term in this autocorrelation function corresponding to the discrete spectral component at f_m (the modulating frequency) is:

$$P_x^4 \rho_x^2(a)[\frac{1}{2} \sin^2 \omega_c a \; J_1^2(2k \sin \frac{\omega_m a}{2})(\sin^2 \frac{\omega_m a}{2}) \; \sin^2 \frac{\omega_m b}{2}] \cos \omega_m \tau$$

where P_x^2 is the power in the carrier and $\rho_x(\tau)$ is the normalized auto-correlation function of the random process $x(t)$.

The interesting result is that there is a discrete spectral component at f_m in the output even when the carrier is not monochromatic. It can be shown that this result reduces to that of a monochromatic carrier for the monochromatic case, except that it is multiplied by $P_x^4 \rho_x^2(a)$. Setting $P_x^2 = 1$, the multiplying factor will be less than or equal to one. That is, the main effect of the nonmonochromatic carrier is to reduce the power contained in the discrete spectral component of the output at the modulation frequency f_m. The reduction in power is dependent on the width of the power spectral density of $X(t)$. The wider the spectral distribution, the "narrower" the autocorrelation function will be, and therefore, the power in the discrete component will be smaller (since $\rho_x(a)$ will be relatively farther from the maximum which is $\rho_x(0) = 1$).

It should be noted that there will be a continuous portion of $S_W(f)$, the power spectral density of $W(t)$, centered at the modulation frequency $\pm f_m$. This means that narrow band filter considerations may be necessary to extract a "pure" signal if the spectral extent of $S_x(f)$ is appreciable.

It is interesting to see what magnitude of power reduction is obtained. Assume a rectangular shape for the power spectral density with bandwidth $2w$. Then $\rho_x(\tau)$ is of the form $\sin w\tau/w\tau$ and $\rho_x(a) = \sin wa/wa$. If the parameter a is chosen for optimum PM to AM conversion, using $\omega_m a/2 = \pi/2$, then $a = 1/2f_m$ and $\rho_x(a) = 2f_m/w \sin w/2f_m$. This will equal 0.7 (3 db down) for $w \approx \pi f_m$.

The above analysis can be repeated when the input signal is corrupted by the presence of additive noise with the result that the discrete component of the output spectral density at $\pm f_m$ is unchanged but the

continuous portion of the output spectral density centered at $\pm f_m$ will be increased due to the noise and to signal noise cross terms.

Effort during the coming quarter will be directed at examining methods of electro-optic frequency shifting.

PROJECT 0577:   MICROWAVE PHOTOTUBES AND LIGHT DEMODULATORS
            Army Contract DA 36-039 AMC-00094(E)
            Project Leader: A. E. Siegman
            Staff: J. R. Kerr

This project will investigate methods for demodulating coherent light signals which are carrying broadband microwave frequency or amplitude modulation, with particular emphasis on microwave phototubes, photomixers, and similar devices.

A.   DISTRIBUTED-EMISSION MICROWAVE PHOTOTUBES

No work was done on this topic during the past quarter

B.   TRANSVERSE-WAVE FM MICROWAVE PHOTOTUBE

In the last report, the preliminary experiments with the FM microwave phototube were described. A problem with microwave-leakage pickup was given as the principal obstacle to obtaining precise quantitative results. This problem has been solved through the development of a homodyne detection scheme which eliminates the nonlinear effect of the diode detector. This nonlinear element was responsible for the "cross-product" between the chopped, desired-signal and the unchopped leakage-pickup; the cross-product was effectively chopped and hence was detected by the phase-lock amplifier. The present system renders the phase-lock amplifier entirely insensitive to the leadage-pickup and hence eliminates "and effect," i.e., signal changes due to varying pick-up whenever any object near the tube is moved. It has the further advantage of providing a means of measuring the phase of the microwave signal.

Experiments using the above detection scheme have shown the presence of another effect: when the light is effectively apertured by misalignment, it can be seen from the swinging-beam picture that the total photo-current will vary with time. Thus some sort of an AM phototube effect can be expected in addition to the desired effect.

A complete, three-dimensional analysis of the "aperature effect" shows that it can be represented by a term which is added to the simple,

transverse center-of-gravity term. In the small-signal case, this term contributes a signal which reproduces the modulating signal, but opposes the desired detection mechanism in phase.

Mechanically, it is difficult to be certain that a condition of perfect alignment has been achieved, because the aperture sizes involved are very small (1 mm) and the tube is mounted inside a long solenoid. An attempt was made at verifying the analysis (and clearly separating the two detection mechanisms) by varying the mean position of the light beam relative to the tube, and recording the total detected signal as a function of d-c current, where the d-c current indicates, hopefully, the degree of misalignment for a given measurement. These measurements qualitatively verified the analysis. For instance, a mean position (with some misalignment) was found for which the net signal is zero, which was consistent with the analysis. However, due to the mechanical problems, and due to the complexity of the aperture-effect analysis for a circular aperture and an offset Gaussian spot, a new experiment has been devised, in which a knife-edge will be inserted into the beam external to the tube to cause a deliberate aperture effect. It will be relatively easy to ensure that this is the only effective aperture, and the aperture-effect expression becomes quite simple for this case. It is expected that this experiment, which will be undertaken immediately, will provide the complete quantitative verification of tube operation.

It is worth noting that the "aperture effect" does not in reality represent a mechanism which differs from the simple "transverse" interaction in principle; since individual electrons have no transverse velocities, the true interaction is longitudinal when considered on a microscopic scale. These ideas are clarified in a new theory, which explores the implications of a nonfilamentary, apertured beam in detail. It should also be noted that this aperture-effect mechanism could be used to detect FM light using a photodiode as well as a special phototube; and that a finite cathode with light "spilling off the edge" represents the same mathematical situation.

The FM space-conversion analysis has been extended to the finite-cathode situation by convolution. The result verified the above possibility of detecting FM light with a photodiode, with no distortion in

the small-δ case. It also verifies the validity of the swinging-beam viewpoint ("Quasi-steady-state") for a finite cathode, with the new requirement that $k\omega_H \ll \Delta X$, where ω_H is the highest significant modulation frequency, k is the dispersion in cm/sec, and ΔX is the cathode width in cm. This requirement is consistent with the results of a filter analogy which has been formulated to clarify the meaning of "quasi-steady-state" in the space-conversion case, as distinguished from the usual circuit case.

Upon completion of the experiment described above, work will continue on the analysis of the system for imperfect optics and incoherent light. It is expected that the new insights described above will aid in interpreting these results.

PROJECT 0581: INFRARED MODULATION AND DEMODULATION TECHNIQUES

Air Force Contract AF04(695)-305
Project Leader: A. E. Siegman
Staff: J. A. Tellefsen, Jr.

The objective of this project is to develop high-frequency modulation and demodulation techniques for IR (as opposed to visible) light waves. The program is motivated by the availability of numerous strong gas-laser lines in the IR. Initial efforts are being devoted to free-electron absorption for modulation, and fast photodiodes for demodulation.

A. CURRENT PROBLEMS

The current experimental problems on this project have been the design and construction of control and safety devices for the high-voltage power supplies; designing and constructing mechanical supports to accomodate the laser and the modulator tube on to an optical bench; locating and eliminating the expected high-voltage breakdown and arcing occurrences; improving the general performance of the modulator tube as far as electrical characteristics are concerned; testing the infrared detector system; and finally carrying out initial experiments with the modulator tube in a realistic setup.

B. CONTROL AND SECURITY DEVICES

The semiconductor sample in the tube is bombarded with 10 kv electrons emitted from a standard TV-gun. The grid focusing the plate voltages are obtained by using two high-voltage power-supplies, one at 2 kv for the grid and cathode potentials and one at 8 kv for the plate and beam-steering. To facilitate the interconnection and control of these lethal voltages, a completely enclosed control-box was constructed, incorporating interlocks and latching relays that will remove the power from the whole system if the box is opened or the filament voltage exceeds a certain upper limit. Fuses and potentiometers for beam-steering as well as two sets of batteries for deflecting and focusing the electron beam were placed on isulating stand-offs. The electrical system, when freed from corona discharge, can withstand 15 kv, this being an adequate protection in our case. To improve the focusing of the electron beam, we had to partially rewire the box.

C. MECHANICAL SUPPORTS

The laser was fitted to the optical bench via two aluminum brackets, with provision for micro-manipulating the direction of the laser beam. A stool to accomodate the modulator tube in a fixed position was constructed. Special care was given to the design of a precision heat contact so that heat developed in the sample during bombardment could be dissipated through a tight-fitting copper block imbedded in bakelite.

D. BREAK-DOWN AND ARCING

This proved to be a difficult point. By placing components at maximum distances from each other, and avoiding sharp edges and pointed contacts, we eliminated most of these problems. Breakdown between adjacent electrodes occured both outside and inside the tube itself. The outside breakdown was eliminated by imbedding the socket leads in insulating silicone. The interior arcing is probably caused by small amounts of impurities located on the surface of the electrodes. We plan to remove the impurities by a controlled discharge between the electrodes.

E. ELECTRICAL CHARACTERISTICS

The earliest tests of the modulator tube gave very small beam currents
and poor focusing as well as steering. By changing the potential of the
focusing electrode to be approximately the cathode potential, we were
able to get a controlled spot-size of 2 mm maximum diameter, which is
the order of magnitude we need. The beam-steering is now also good.
Using several μA-meters we could monitor the current flow at the various
electrodes. The effect of secondary electrons was negligible, which it
should be according to theory. Measuring the dynamic characteristics
of the tube under pulsed conditions is difficult because of the potential
differences involved, and we are working now to solve this problem.

F. DETECTOR SYSTEM

To get an independent picture of the performance of the chosen de-
tector under ideal conditions, several experiments have been planned.
Using the laser as light-source and chopping the beam with a small rota-
ting mirror, we were able to produce 10 μsec pulses. The signal from
the detector could be directly coupled to a regular oscilloscope without
pre-amplification. This way we discovered and studied some mode-
instabilities in the laser. Spatially distributed mode structures in
the laser beam were converted to temporarily distributed structures on
the scope-face.

G. MODULATION EXPERIMENTS

Plans were made for a set of thorough tests involving the modulator
and demodulator under actual conditions. This will be one of the main
objectives for the next quarter.

H. PLANS FOR THE NEXT QUARTER

The first modulator tube will be thoroughly tested and its charac-
teristics established. Plans are now under way for two more tubes in
this series. While the first tube employs a Gallium Antimonide target,
the two next will be equipped with a Germanium and a Silicon target

respectively. The light absorption of a semiconductor, which is the
principle of this modulation scheme, is directly proportional to the
conductivity of the sample. Therefore, a measure of how effectively
the conductivity can be modulated is of great importance for evaluating
the performance of the modulator as well as for understanding the physical
principles involved. The two new tubes will be so designed that we can
measure directly the conductivity modulation induced in the sample.
Finally, upon completion of these two tubes they will also be tested
and their performance evaluated.

PROJECT 0582:   OPTICAL PHASE- AND FREQUENCY-MODULATION TECHNIQUES

                Air Force Contract AF04(695)-305
                Project Leaders: A. E. Siegman, S. E. Harris
                Staff: C. M. McIntyre, L. M. Osterink

The revised objective of this project is the synthesis and develop-
ment of such linear optical components as narrowband filters with pre-
scribed transmission characteristics, optical equalizers and compensators,
optical discriminators and ratio detectors, and matched optical filters.

During this quarter, the synthesis technique for lossless crystals
of equal length has been perfected, and a technical report on this sub-
ject has been prepared. This report is entitled "Optical Network
Synthesis Using Birefringent Crystals," and is authored by S. E. Harris,
E. O. Ammann, and I. C. Chang. Subject to revision, this report has been
accepted for publication by the Journal of the Optical Society of America.

We now intend to direct our efforts toward the experimental problem.
The immediate objective is the construction of a six stage linear dis-
criminator. Each stage will consist of a 1 cm crystal of calcite, and
a very thin quartz compensating plate.

Of particular importance is the question of temperature stability
and tolerance.

The temperature control required depends on birefringence and length.
To keep changes in retardation less than 1/100 of a wave, the tempera-
ture of a 1 cm crystal of calcite must be constant to within 0.05 °C. A
test unit has been constructed which will support individual crystals in
an oil bath. The unit will be heated using a proporational temperature
controller to keep the temperature constant within 0.01 °C. The unit is

mounted so that it will rotate about each of the three orthogonal crystal axes. This unit is ready and will be used in conjunction with a Senarmont compensator to measure changes in retardation, prior to the construction of the linear discriminator.

Osterink has proposed a modification of our basis filter which allows its use with unpolarized light. This modification is based on a similar scheme used by Evans in conjunction with the Solc filter [Ref. 1]. The modification consists of using prism polarizers which, instead of completely eliminating one polarization, merely separates the two polarizations in space. Thus the input light is separated into two polarized beams, each of which traverses the filter. At the output the wanted light is recombined into one beam by the prism, whereas the unwanted light leaves the output prism as two separate beams, each separated in space from the wanted light. This modification is indicated schematically in Fig. 41.
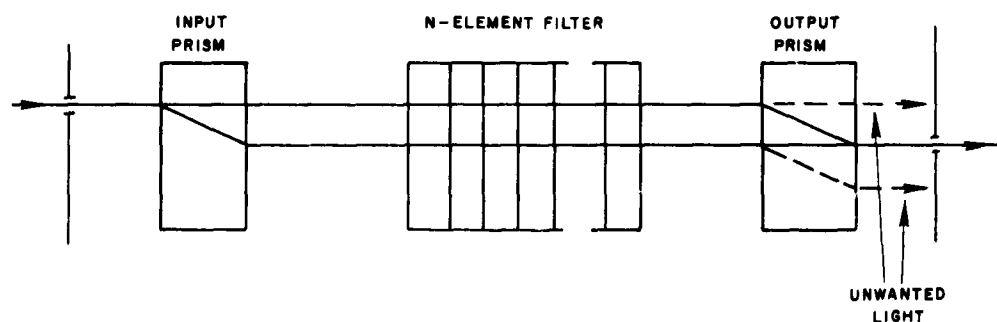
FIG. 41. MODIFICATION OF BASIC FILTER.

[1] John W. Evans, "A Birefringent Monochromator for Isolating High Orders in Grating Spectra," Appl. Optics, 2, 193 (1963).

The purpose of this project is to study optical maser characteristics via photoelectric mixing, particularly at microwave difference frequencies. Emphasis will be placed on the mixing of signals derived from two separate lasers, using one laser as a frequency reference for studying the other.

Our efforts continue to be directed toward single-transverse-mode laser operation. Because initial tests made on the rod with one end flat and the other end slightly divergent, as reported in the preceding ORR, were not as successful as anticipated, it was decided to check the curved end of the rod to determine if it had been ground properly. The method used is shown in Fig. 42. A gas laser beam, enlarged with a telescope, is
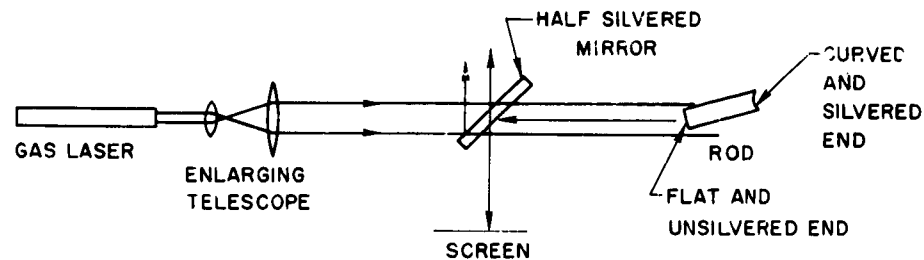
FIG. 42. ARRANGEMENT FOR CHECKING CONCAVE CURVED END OF ROD.

directed through a half silvered mirror at 45° to the beam onto the rod's flat end roughly along the longitudinal axis at the rod. Reflections from both the flat and curved end of the rod are detected on a screen after they are reflected from the half silvered mirror. From the pattern observed, and from measurement of appropriate distances, the radius of curvature and the angle from the rod axis at which the center of curvature is located may be found. Figures 43a and 43b summarize these results.
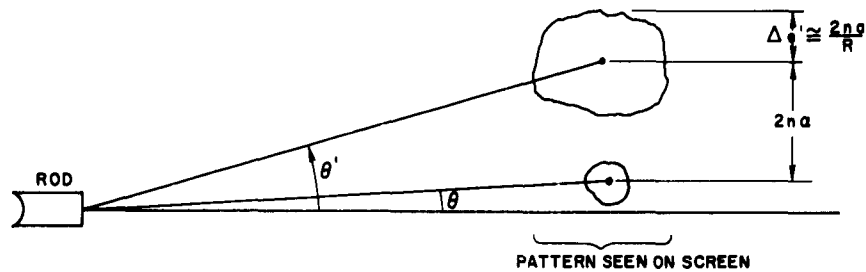
FIG. 43a. PATTERN SEEN ON SCREEN AND RESULTS OF ANALYSIS
IN CHECKING CONCAVE END OF ROD.
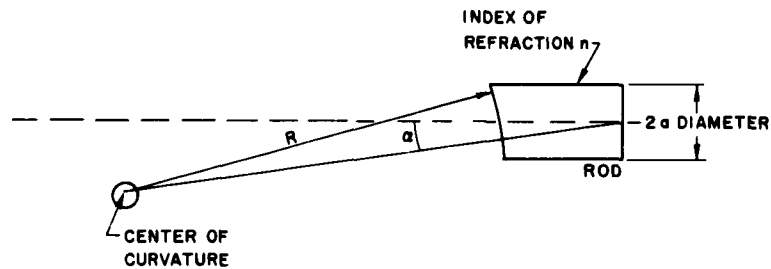
FIG. 43b. DEFINITION OF QUANTITIES IN FIG. 43a.

Measurements on our rod indicated that the center of curvature is located too far off the rod axis for the rod to work properly. Therefore, the rod is being corrected. By using this method of checking during the grinding process, we believe the grinding may now be done quite accurately.

Further investigation of the rings that are photographed in the output of our small-spot mirror mode-controlled rods has been made. We have reported previously that a plot of ring radius squared against ring index number has an essentially constant slope of about $3\lambda\lambda$, L being

the length of the rod, and that this is explained very well as being due to interference between single pass and triple pass rays from the silver spot. However, we have also occasionally observed a slope of about 1.7Lλ, a typical example being the plot shown in Fig. 44. The data shown was
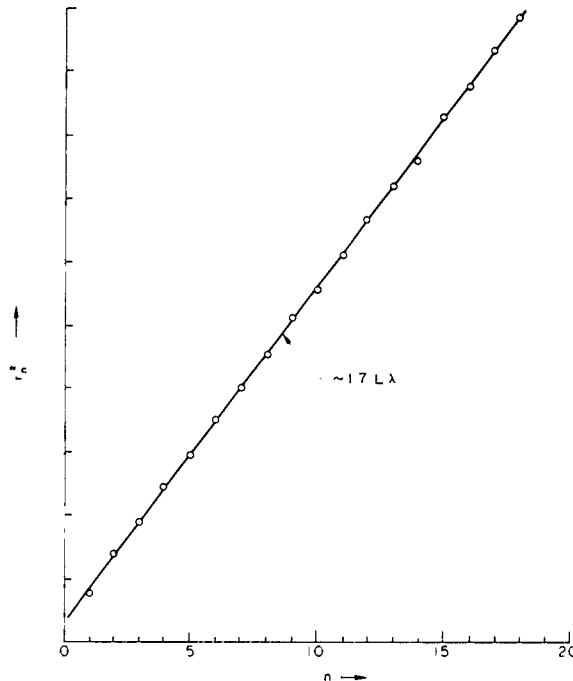
FIG. 44. PLOT OF DIFFRACTION RING RADIUS
SQUARED VS INDEX NUMBER SHOWING SLOPE OF
1.7 Lλ.

taken from a photograph of a rod whose spot was produced by pressing a cone-shaped piece of silver against the rod's end. As was reported in a previous QRR, this method of producing a spot was not successful, in that the rod began lasering not at the spot but in an outer part of the rod. A very interesting point, however, is that rings were still observed and that they were centered near the rod center, rather than at the point of strongest lasering.

We now believe these rings may be explained as being due to interference between rays reflected from the spot and rays reflected from one or more microscopic internal defects that act as scattering centers. This model is shown in Fig. 45.
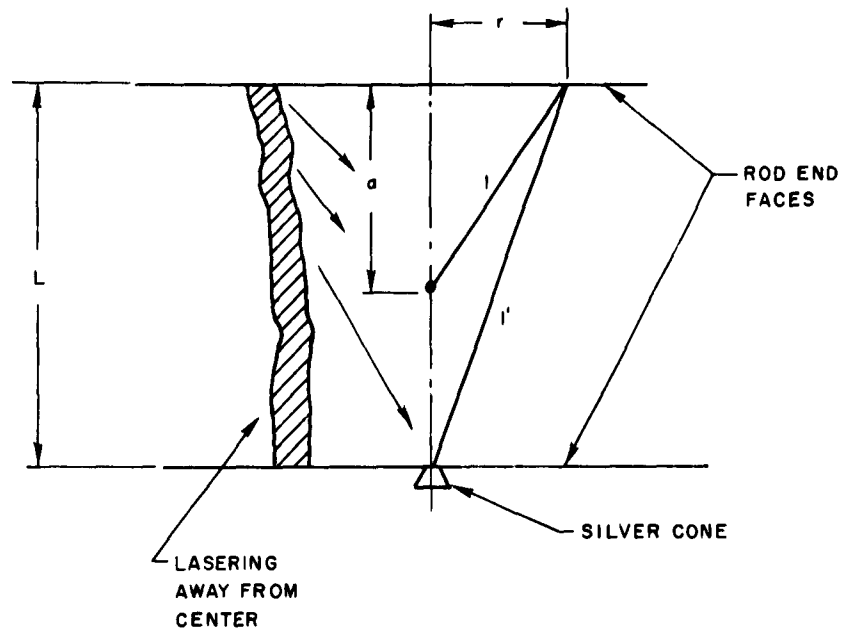
FIG. 45. SHOWING MODEL TO EXPLAIN THE DATA OF FIG. 44.

Using the notation of Fig. 45, the analysis is as follows:

$$\ell = \sqrt{a^2 + r^2} = a \left\{ 1 + \frac{r^2}{a^2} \right\}^{1/2} \simeq a + \frac{1}{2} \frac{r^2}{a}$$

$$\ell' = \sqrt{L^2 + r^2} = L \left\{ 1 + \frac{r^2}{L^2} \right\}^{1/2} \simeq L + \frac{1}{2} \frac{r^2}{L}$$

For constructive interference to take place at radius "r" the path length difference

$$\Delta\ell \overset{\triangle}{=} \ell' - \ell = (L - a) + \frac{1}{2} r^2 \left(\frac{1}{L} - \frac{1}{a} \right)$$

should equal λm, with $m = 0, 1, 2, \ldots$ Setting $\Delta\ell = m\lambda$, and solving for r yields

$$r^2_m = - \frac{2aLm\lambda}{L - a} + 2aL$$

From Fig 45 it is evident that the $m = 0$ case $(r_0 = 0)$ occurs only for $r \to \infty$. Therefore, the innermost and smallest ring must occur for some maximum value of m, denoted by M. If the rings are labelled by the index n from the smallest to the largest, then

$$m = M - n, \qquad n = 0, 1, 2, \ldots M.$$

Then

$$r_n^2 = \frac{-2(M - n)aL\lambda}{L - a} + 2aL$$

$$r_n^2 = \frac{2naL\lambda}{L - a} - \frac{2MaL\lambda}{L - a} + 2aL$$

It can be seen that the slope of the r_n^2 vs n plot will be constant and will equal $\frac{a}{L - a} \cdot 2L\lambda$. Therefore, experimental determination of the slope allows calculation of "a" which determines the location of the impurity in the rod. By focusing the camera at various planes along the rods length and photographing the rod while it is lasering, one should be able to detect such an impurity. One must be focused on the plane in which the impurity is located before the impurity is visible, in which case it would appear as a small bright spot. We have observed such a bright spot in a series of photographs taken of the rod used in this experiment.

Finally, using the same rod, but with an evaporated silver spot we have observed a change with pumping power of the slope of the r_n^2 vs n plot. This phenomenon is not completely understood at present, but it is plausible that the importance of impurity scattering and end face scattering in producing rings changes with pumping power and one predominates over the other, depending on the pumping level. We shall investigate this further during the coming quarter.

PROJECT 0816: TRANSIENT PHENOMENA IN LOW PRESSURE GAS DISCHARGE PLASMAS

Air Force Contract AF33(615)-1504
Project Leader: H. Derfler
Staff: T. Simonen

The purposes of this project is to study the excitation and detection of an impulse propagating through a plasma.

I. INTRODUCTION

This is the first quarterly report and covers the period for 3 February 1964 to 3 May 1964. It comprises a theoretical study of an impulse propagating through a simple one-dimensional plasma in the absence of magnetic fields. In this model the impulse is excited and detected with parallel plane pairs of grids immersed into the plasma. A set of two port equations relating the frequency spectrum of currents and potentials of the transmitter and receiver ends respectively is obtained. At this stage simplifying assumptions have been made to demonstrate the basic dispersion of an impulse which is carried through a plasma by means of Bohm and Gross type waves. These assumptions are infinitesimal size of transmitter and detector, stationary ions, neglect of drift, collisions and--due to the choice of a spherical shell distribution of electron velocities--also neglect of Landau damping. Then, with a Dirac-δ impulse applied to the transmitter, a simple analytic expression is obtained for the signal recorded at the detector. To what extent this ideal response can be obtained under more realistic conditions will be discussed in subsequent reports.

II. THEORETICAL WORK

A. THE PLASMA WAVE EQUATION

We consider longitudinal oscillations in an infinitely extended neutral plasma in the absence of magnetic fields. We shall use Boltzmann's

equation for the electrons and ions respectively with an approximation
to the collision integral due to Bhatnager, Gross and Krook [Ref. 1].

$$\left[\frac{\partial}{\partial t} + \vec{v}\cdot\frac{\partial}{\partial \vec{x}} \pm \frac{e}{m_\pm} \vec{E}\cdot\frac{\partial}{\partial \vec{v}} \right] F_\pm = - \nu_\pm (F_\pm - nF_{o\pm}) \tag{1}$$

Here

$F(t,\vec{x},\vec{v})$ = velocity distribution functions

$F_o(\vec{v})$ = suitable equilibrium distribution function
normalized to unity

n = number density

ν = collision frequency with neutral atoms

$\vec{E}(t,\vec{x})$ = electric field vector

Subscript $\pm$ refers to ions and electrons respectively.

Using a small signal approach, we linearize the distriubtion functions

$$F(t,\vec{x},\vec{v}) = n \, F_o(\vec{v}) + F_1(t,\vec{x},\vec{v}) + \ldots \tag{2}$$

and project them into one dimension by integrating over all velocities
perpendicular to the oscillating electric field $\vec{E} = (E,0)$, $\vec{v} = (v, \vec{v}_\perp)$

$$\int F(t,\vec{x},\vec{v}) \, d\vec{v}_\perp = n \, f_o(v) + f(t,\vec{x},\vec{v}) + \ldots \tag{3}$$

With $\vec{x} = (x,\vec{x}_\perp)$, the one dimensional BGK equation becomes

$$\left[\frac{\partial}{\partial t} + \nu_\pm + v \frac{\partial}{\partial x} \right] f_\pm(t,x,v) \pm \frac{en}{m_\pm} E \frac{d}{dv} f_{o\pm}(v) = 0 \tag{4}$$

Since all phenomena in nature occur with a finite speed of propagation,
at any given time a signal will be of finite extent and therefore we are
always entitled to Fourier analyze in space. On the other hand we cannot
rule out the occurrence of growing or even strictly periodic phenomena

[1] P.L. Bhatnager, E. P. Gross, M. Krook, <u>Phys. Rev.</u>, 94, 511 (1954).

and so we must use a Laplace transform in time. The following shorthand notation will be used for Fourier and Laplace transforms respectively:

$$f(t,k;v] = \int_{-\infty}^{+\infty} e^{ikx} \, f(t,x;v)dx \quad \text{reg. } |\text{Im}k| < \alpha \tag{5}$$

$$f[\omega,x;v) = \int_{0}^{\infty} e^{-i\omega t} \, f(t,x;v)dt \quad \text{reg. } \text{Im}\omega < \beta \tag{6}$$

We note that, according to the rules of Fourier and Laplace analysis, $f(t,k;v]$ and $f[\omega,x;v)$ must be regular analytic functions in a strip including the real k axis and in a lower frequency half plane respectively.

With this provision the BGK equation (4) can be analyzed in the t and x directions giving

$$f_{\pm}[\omega,k;v] = \frac{\mp \dfrac{en}{m} E[\omega,k] \dfrac{d}{dv} f_{o\pm} + f_{\pm}(0+,k,v]}{i(\omega - iv_{\pm} - kv)} \tag{7}$$

The double transform of the convection current is then obtained in the form

$$j[\omega,k] = e \int vf_{+}[\omega,k;v]dv - e \int vf_{-}[\omega,k;v]dv$$

$$= i\omega\epsilon_{o} \, E[\omega,k] \left\{ \frac{\omega_{p+}^{2}}{\omega} \int \frac{vdf_{o+}}{\omega - iv_{+} - kv} + \frac{\omega_{p-}^{2}}{\omega} \int \frac{vdf_{o-}}{\omega - iv - kv} \right\} \tag{8}$$

$$- ie \int \frac{vf_{+}(o+,k;v]}{\omega - iv_{+} - kv} \, dv + ie \int \frac{vf_{-}(o+,k;v]}{\omega - iv_{-} - kv} \, dv$$

where the plasma frequencies $\omega_{p\pm}$

$$\omega_{p\pm}^2 = e^2 n / \epsilon_o m_\pm \qquad (9)$$

have been introduced.

Now we use Maxwell's equation

$$(\nabla \times \vec{H})_x = j + \epsilon_o \frac{\partial E}{\partial t} = I \qquad (10)$$

and note that in a strictly one-dimensional problem the equation of continuity requires $\partial I / \partial x = 0$ and so I can be only a function of time. However, the equation of continuity is violated at a conducting surface which is transparent to particles but not to electric fields. Thus by introducing grids into the plasma I can be made a step function in space such as shown in Fig. 46. With this understanding we shall proceed to consider $I(t,x)$ a function of time and space. The double transform of (10) then reads

$$j[\omega,k] + i\omega\epsilon_o E[\omega,k] = I[\omega,k] + \epsilon_o E(o+,k) \qquad (11)$$
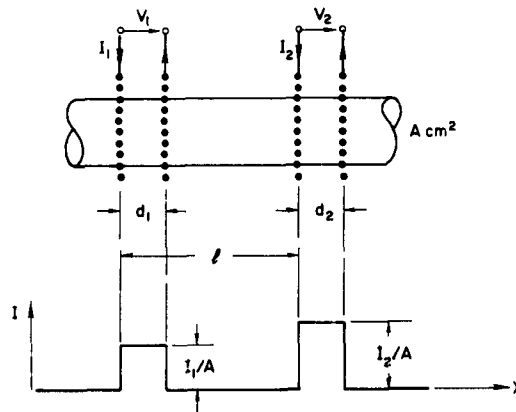
FIG. 46. PARALLEL PLANE PAIRS OF GRIDS
IMMERSED INTO A PLASMA COLUMN AND BELOW
TOTAL CURRENT DENSITY $I = j + \epsilon_o \partial E/\partial t$
AS A FUNCTION OF DISTANCE.

Now we use the space charge equation

$$\epsilon_o \frac{\partial E}{\partial x} = \rho = e \int f_+(t,x,v)dv - e \int f_o(t,x,v)dv \qquad (12)$$

Upon Fourier analyzing in space we have

$$-ik\epsilon_o E(t,k] = e \int f_+(t,k,v]dv - e \int f_-(t,k,v]dv \qquad (13)$$

and in the limit $t \to o+$

$$-ik\epsilon_o E(o+,k] = e \int f_+(o+,k,v]dv - e \int f_-(o+,k,v]dv \qquad (14)$$

Eliminating $E(o+,k]$ and $j[\omega,k]$ between equations (8), (11) and (14) we obtain finally the space-charge-wave equation

$$i\omega\epsilon_o E[\omega,k] = \frac{I[\omega,k] + \frac{ie(\omega-i\nu_+)}{k}\int\frac{f(o+,k,v]dv}{\omega-i\nu_+-kv} - \frac{ie(\omega-i\nu_-)}{k}\int\frac{f(o+,k,v]}{\omega-i\nu_--kv}}{1 + \frac{\omega_{p+}^2}{\omega}\int\frac{v\,df_{o+}}{\omega-i\nu_+-kv} + \frac{\omega_{p-}^2}{\omega}\int\frac{v\,df_{o-}}{\omega-i\nu_--kv}} \qquad (15)$$

Introducing the notation

$$\omega - i\nu_\pm = \omega_\pm, \qquad \omega_\pm/k = w_\pm \qquad (16)$$

and by using the identity

$$\frac{v}{v-w}\frac{df_o}{dv} = \frac{df_o}{dv} + w\frac{\partial}{\partial v}\frac{f_o}{v-w} + w\frac{\partial}{\partial w}\frac{f_o}{v-w} \qquad (17)$$

we can write the denominator of Eq. (15) in one of the more conventional forms

$$D(\omega, k) \equiv 1 - \frac{\omega_{p+}^2}{\omega k} \int \frac{v df_{o+}}{v - w_+} - \frac{\omega_{p-}^2}{\omega k} \int \frac{v df_{o-}}{v - w_-} \qquad (18)$$

$$= 1 - \left(\frac{\omega_{p+}}{k}\right)^2 \frac{\omega_+}{\omega} \int \frac{df_{o+}}{v - w_+} - \left(\frac{\omega_{p-}}{k}\right)^2 \frac{\omega_-}{\omega} \int \frac{df_{o-}}{v - w_-} \qquad (19)$$

$$= 1 - \left(\frac{\omega_{p+}}{k}\right)^2 \frac{\omega_+}{\omega} \frac{\partial}{\partial w_+} \int \frac{f_{o+} dv}{v - w_+} - \left(\frac{\omega_{p-}}{k}\right)^2 \frac{\omega_-}{\omega} \frac{\partial}{\partial w_-} \int \frac{f_{o-} dv}{v - w_-} \qquad (20)$$

$$= 1 - \left(\frac{\omega_{p+}}{k}\right)^2 \frac{\omega_+}{\omega} \int \frac{f_{o+} dv}{(v - w_+)^2} - \left(\frac{\omega_{p-}}{k}\right)^2 \frac{\omega_-}{\omega} \int \frac{f_{o-} dv}{(v - w_-)^2} \qquad (21)$$

We note that the zeros of the denominator $D(\omega, k) = 0$ are solutions of the plasma-wave dispersion relation.

B. TWO PORT EQUATIONS RELATING TRANSMITTER AND DETECTOR

We now use two pairs of grids immersed into a plasma column as transmitter and detector respectively. In this case the total current density $I(t, x)$ becomes a step function in space as shown in Fig. 46 and explained in Section A above. With the help of the unit step function defined by

$$H(x) \equiv \begin{cases} 1 & |x| < 1 \\ 0 & |x| > 1 \end{cases} \qquad (22)$$

We thus have

$$I(t, x) = \frac{I_1(t)}{A} H\left(\frac{x}{d_1/2}\right) + \frac{I_2(t)}{A} H\left(\frac{x - \ell}{d_2/2}\right) \qquad (23)$$

where

A = cross sectional area of plasma column

d_1 = spacing between input grids

d_2 = spacing between output grids

ℓ = spacing between input and output grids

I_1 = input current in Amps

I_2 = output current in Amps

The double transform of (23) is simply

$$I[\omega,k] = I_1[\omega] \frac{d_1}{A} \frac{\sin kd_1/2}{k\, d_1/2} + I_2[\omega] \frac{d_2}{A} \frac{\sin k\, d_2/2}{k\, d_2/2} e^{ik\ell} \qquad (24)$$

Now let us suppose that there is no initial perturbation of the plasma $f(o+,x,v) = 0$; then we obtain, by introducing Eq. (24) into Eq. (15),

$$E[\omega,k] = \frac{1}{i\omega\epsilon_o D(\omega,k)} \left\{ I_1[\omega] \frac{d_1}{A} \frac{\sin k\, d_1/2}{k\, d_1/2} + I_2[\omega] \frac{d_2}{A} \frac{\sin k\, d_2/2}{k\, d_2/2} e^{ik\ell} \right\}$$
$$(25)$$

To conform with the sign convention used in the theory of two-terminal-pair (two-port) networks, the potential across gap "1" is defined by

$$V_1[\omega] = \int_{-d_1/2}^{+d_1/2} E[\omega,x)dx = \frac{1}{2\pi} \int_{-d_1/2}^{+d_1/2} dx \int_{-\infty}^{+\infty} E[\omega,k]e^{-ikx}dk$$

$$(26)$$

$$= \frac{d_1}{2\pi} \int_{-\infty}^{+\infty} E[\omega,k] \frac{\sin k\, d_1/2}{k\, d_1/2} \quad dk$$

and similarly across the second gap "2"

$$V_2[\omega] = \int_{\ell-d_2/2}^{\ell+d_2/2} E[\omega,x]\,dx = \frac{d_2}{2\pi} \int_{-\infty}^{+\infty} E[\omega,k]\ \frac{\sin k\,d_2/2}{k\,d_2/2}\ e^{-ik\ell}\,dk \tag{27}$$

Introducing $E[\omega,k]$ as given by Eq. (25) into Eqs. (26) and (27) we obtain the following two-port equations:

$$V_1[\omega] = Z_{11}(\omega)\ I_1[\omega] + Z_{12}(\omega)\ I_2[\omega] \tag{28}$$

$$V_2[\omega] = Z_{21}(\omega)\ I_1[\omega] + Z_{22}(\omega)\ I_2[\omega] \tag{29}$$

where the impedance and transimpedance Z_{ik} are given by

$$Z_{11}(\omega) = \frac{d_1^2}{2\pi i\omega\epsilon_o A} \int_{-\infty}^{+\infty} \left(\frac{\sin k\,d_1/2}{k\,d_1/2}\right)^2 \frac{dk}{D(\omega,k)} \tag{30}$$

$$Z_{22}(\omega) = \frac{d_2^2}{2\pi i\omega\epsilon_o A} \int_{-\infty}^{+\infty} \left(\frac{\sin k\,d_2/2}{k\,d_2/2}\right)^2 \frac{dk}{D(\omega,k)} \tag{31}$$

$$Z_{12}(\omega) = \frac{d_1 d_2}{2\pi i\omega\epsilon_o A} \int_{-\infty}^{+\infty} \left(\frac{\sin k\,d_1/2}{k\,d_1/2}\right)\left(\frac{\sin k\,d_2/2}{k\,d_2/2}\right) \frac{e^{ik\ell}}{D(\omega,k)}\,dk \tag{32}$$

$$Z_{21}(\omega) = \frac{d_1 d_2}{2\pi i\omega\epsilon_o A} \int_{-\infty}^{+\infty} \left(\frac{\sin k\,d_1/2}{k\,d_1/2}\right)\left(\frac{\sin k\,d_2/2}{k\,d_2/2}\right) \frac{e^{-ik\ell}}{D(\omega,k)}\,dk \tag{33}$$

We note that in general $Z_{12}(\omega) \neq Z_{21}(\omega)$ as in the case of active networks. If, however, the distribution function of the plasma is isotropic, $f_o(v) = f_o(-v)$ and we prove immediately from Eq. (21) that $D(\omega,k) = D(\omega,-k)$ and so from Eqs. (32) and (33) that $Z_{12}(\omega) = Z_{21}(\omega)$.

C. THE DISPERSION OF AN IMPULSE DUE TO BOHM AND GROSS WAVES

We terminate the four-terminal network defined above by connecting it to an impedance $Z_2(\omega)$ used in the detecting circuit,

$$V_2[\omega] = -Z_2(\omega)\ I_2[\omega] \tag{34}$$

Eliminating the currents from Eqs. (28) and (29) we obtain

$$\frac{V_2[\omega]}{V_1[\omega]} = \frac{Z_{21}}{Z_{11} - \dfrac{Z_{11}Z_{22} - Z_{12}Z_{21}}{Z_2}} \tag{35}$$

In an ideal experiment we do not want our frequency response to depend on the load impedance Z_2 and so we stipulate the condition

$$Z_2 \gg (Z_{11}Z_{22} - Z_{12}Z_{21})/Z_{11} \tag{36}$$

Note that in realizing the condition Eq. (36) we can assist by designing the experiment properly. This conclusion is seen from $Z_{ik} \propto d_i d_k$. Thus by letting $d_i \to 0$ we obtain $Z_2 \gg 0(d_i)$ and in this limit $V_2[\omega]/V_1[\omega] \sim Z_{21}/Z_{11}$. In particular for $d_1 = d_2 = d$ we obtain

$$\frac{V_2[\omega]}{V_1[\omega]} \sim \int_{-\infty}^{+\infty} \left(\frac{\sin k\ d/2}{d/2}\right)^2 \frac{e^{-ik\ell}}{D(\omega,k)}\ dk \Bigg/ \int_{-\infty}^{+\infty} \left(\frac{\sin k\ d/2}{k\ d/2}\right)^2 \frac{dk}{D(\omega,k)} \tag{37}$$

Now let

$$D(\omega,k) = 1 + \frac{1}{P(\omega,k)} \qquad \frac{1}{D(\omega,k)} = 1 - \frac{1}{1 + P(\omega,k)} \tag{38}$$

and so with

$$\int_{-\infty}^{+\infty} \left(\frac{\sin k\ d/2}{k\ d/2}\right)^2 e^{-ik\ell}\ dk = \begin{cases} \dfrac{2\pi}{d}\left(1 - \dfrac{\ell}{d}\right) & |\ell| < d \\ 0 & |\ell| > d \end{cases} \tag{39}$$

we have:

$$\frac{V_2[\omega]}{V_1[\omega]} \sim \frac{-\int\left(\dfrac{\sin k\ d/2}{k\ d/2}\right)^2 \dfrac{e^{-ik\ell}\ dk}{1 + P(\omega,k)}}{\dfrac{2\pi}{d} - \int\left(\dfrac{\sin k\ d/2}{k\ d/2}\right)^2 \dfrac{dk}{1 + P(\omega,k)}} \tag{40}$$

As we decrease d further we may satisfy the condition

$$\frac{2\pi}{d} \gg \int\left(\frac{\sin k\ d/2}{k\ d/2}\right)^2 \frac{dk}{1 + P(\omega,k)} \tag{41}$$

and then Eq. (40) simplifies considerably

$$\frac{V_2[\omega]}{V_1[\omega]} \sim -\frac{d}{2\pi}\int\left(\frac{\sin k\ d/2}{k\ d/2}\right)^2 \frac{e^{-ik\ell}\ dk}{1 + P(\omega,k)} \tag{42}$$

Provided that the size of the transmitter and receiver is so small that for an appreciable range of wavelengths

$$\left(\frac{\sin k\ d/2}{k\ d/2}\right)^2 \sim 1 \quad \text{as} \quad d \to 0 \tag{43}$$

we have the ideal frequency response which is independent of the load impedance and geometry:

$$\frac{V_2[\omega]}{V_1[\omega]} = -\frac{d}{2\pi}\int_{-\infty}^{+\infty} \frac{e^{-ik\ell}}{1 + P(\omega,k)}\ dk \quad d \to 0 \tag{44}$$

We realize, of course, that some of the conditions Eqs. (36), (41) and in particular Eq. (43) may be difficult to satisfy in practice. But this manipulation was done in order to understand the basic principles governing the dispersion of an impulse propagating through a plasma. We shall remove these restrictions one by one in subsequent work. Let us then proceed with our idealized model and assume an electron plasma with a spherical shell distribution of velocities moving through a background of infinitely heavy ions. We also neglect the effects of drift and collisions.

Projecting the spherical shell distribution

$$F_o(\vec{v}) = \frac{1}{4\pi v_\theta^2} \; \delta(\vec{v}^2 - v_0^2) \tag{45}$$

into one dimension we have

$$f_o(v) = \frac{1}{2v_0} \; H\left(\frac{v}{v_0}\right) \tag{46}$$

where H is the unit step function defined by Eq. (22). Using this relation in Eq. (21) we obtain the dispersion relation

$$D(\omega, k) = 1 - \frac{\omega_p^2}{\omega^2 - (kv_\theta)^2} \tag{47}$$

At this stage it is convenient to measure frequency in units of plasma frequency and linear dimensions in terms of Debye lengths.

$$\omega/\omega_p = \Omega \qquad kv_\theta/\omega_p = K \qquad \omega_p \ell/v_0 = X \qquad \omega_p d/v_0 = D \tag{48}$$

We recognize by comparing (47) and (38) that $P(\omega,k) = K^2 - \omega^2$ and so Eq. (44) becomes

$$\frac{V_2(\omega)}{V_1(\omega)} = -\frac{D}{2\pi} \int_{-\infty}^{+\infty} \frac{e^{-iKX}}{K^2 - \omega^2 + 1} \, dK \tag{49}$$

We now solve the dispersion relation $D(\omega,k) = 0$ for frequencies on a Laplace integral path, that is for $\mathrm{Im}\,\omega < 0$:

$$K_{\pm} = \pm \sqrt{\omega^2 - 1} \tag{50}$$

It is convenient in this case to take the branch cut of the square root such that

$$\omega^2 - 1 = |\omega^2 - 1| \exp(-i\gamma) \quad 2\pi > \gamma > 0 \tag{51}$$

Then we have for all frequencies on a Laplace integral path as shown in Fig. 47

$$\mathrm{Im}K_{+} > 0 \quad \text{and} \quad \mathrm{Im}K_{-} < 0 \quad \text{for} \quad \mathrm{Im}\,\omega < 0 \tag{52}$$

With this provision the integral Eq. (49) is regular for real K and can be evaluated by the theorem of residues using the upper K-half plane for $X < 0$ and the lower K-half plane for $X > 0$. The result is

$$\frac{V_2(\omega)}{V_1(\omega)} = \frac{D}{2i} \frac{e^{i\sqrt{\omega^2 - 1}\,|X|}}{\sqrt{\omega^2 - 1}} \tag{53}$$

We notice that an extremely wide band of frequencies must be detected if the frequency response, Eq. (53), is to be recorded properly. Also we find that a spherical shell distribution of velocities does not exhibit the effect of Landau damping. We hope that with a more realistic distribution function and with collisions the requirement in bandwidth will be
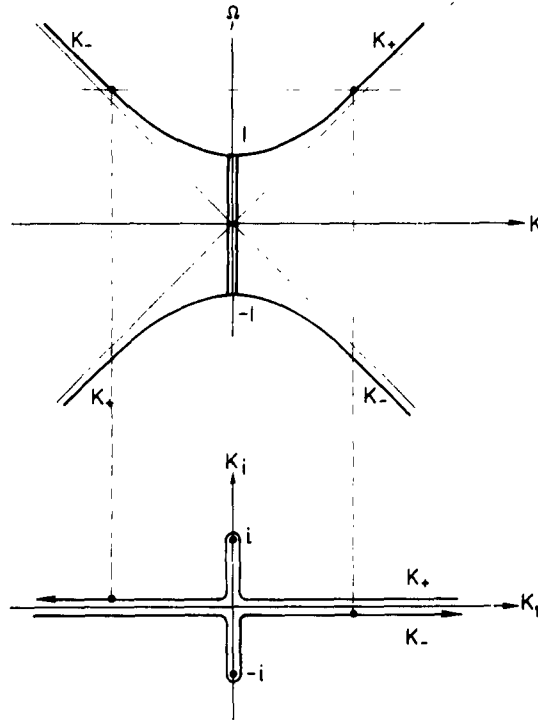
FIG. 47. PLASMA DISPERSION RELATION FOR
A SPHERICAL SHELL DISTRIBUTION OF VE-
LOCITIES IN THE ABSENCE OF DRIFT AND
COLLISIONS AND BELOW WAVE NUMBERS K_+
AND K_- FOR FREQUENCIES ON A LAPLACE
INTEGRAL PATH $\text{Im}\,\Omega = \sigma = \text{CONST} < 0$.

reduced drastically. For the present let us continue to investigate the
propagation of an impulse under ideal conditions. Upon applying a Dirac-δ
input on the input grids

$$V_1(t) = \Phi\delta(t) \quad \text{such that} \quad \int V_1(t)dt = \Phi \text{ Volt/sec} \tag{54}$$

We have $V_1(\omega) = \Phi$ and by the rules of Laplace analysis from Eq. (53)

$$V_2(t) = \omega_p\Phi \, D \, \frac{1}{4\pi i} \int_{i\sigma-\infty}^{i\sigma+\infty} \frac{e^{i\Omega T + i\sqrt{\Omega^2-1}\,|X|}}{\sqrt{\Omega^2-1}} \, d\Omega \quad \sigma < 0 \tag{55}$$

Taking · i·s we find from Laplace transform tables [Ref. 2] the simple answer

$$V_2(t) = \frac{1}{2} \, \omega_p \Phi D \begin{cases} J_0\left(\sqrt{T^2 - X^2}\right) & 0 < |X| < T \\ 0 & |X| > T \end{cases} \tag{56}$$

If p_ν are the zeros of the Bessel function $J_0(x)$ the nodes of the signal propagate along the hyperbolae $T^2 - X^2 = p_\nu^2$. This result is seen in Fig. 48 where we show snapshots of the propagating impulse and in Fig. 49 oscilloscope traces of the signal predicted at various distances from the antenna. These figures demonstrate clearly the dispersion of a Dirac-δ impulse due to Bohm and Gross type waves in a plasma.
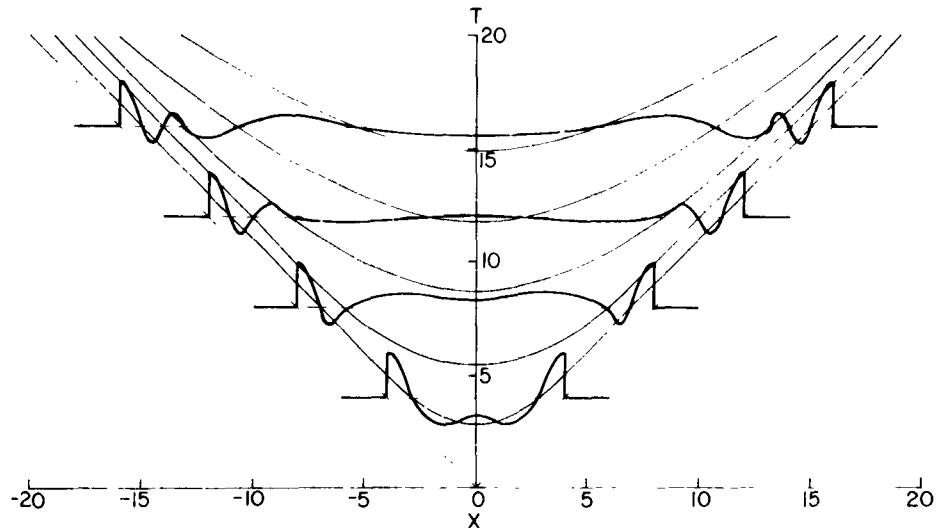
FIG. 48. DISPERSION OF A DIRAC-δ IMPULSE APPLIED AT TIME $t = 0$ AT THE TRANSMITTER LOCATION $X = 0$. Snapshots of the propagating signal at successive time intervals exhibit the characteristics of an evanescent wave pocket. $T = \omega_p t$. $X = \omega_p/v_0$.

[2] A. Erdelyi et al, Tables of Integral Transforms, Vol. 1, p. 248, McGraw-Hill Book Co., Inc., New York, 1954.
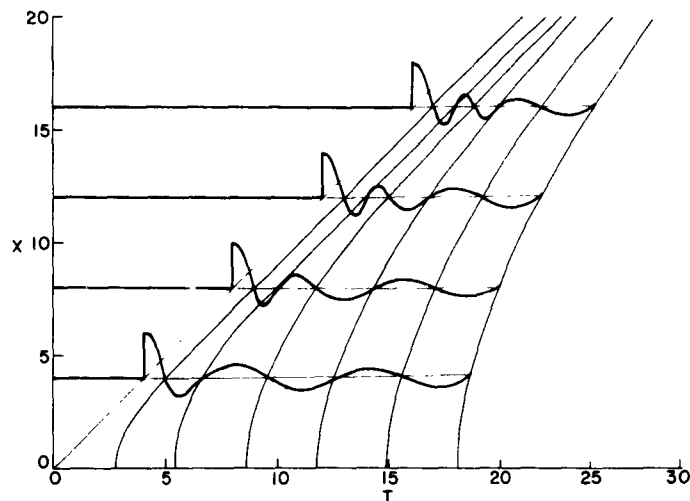
FIG. 49. OSCILLOSCOPE TRACES PREDICTED FOR
THE SIGNAL RECEIVED AT VARIOUS DISTANCES
AFTER A DIRAC-δ IMPULSE HAS BEEN APPLIED
TO THE TRANSMITTER. $T = \omega_p t$. $X = \ell \omega_p / v_0$.

III. DISCUSSION AND FUTURE WORK

Various assumptions have been made in order to predict the simple response of an electron plasma to a Dirac-δ impulse. We note that conditions Eqs. (36), (41) and in particular Eq. (43) impose an upper limit to the size (the gap width d) of antenna and transmitter. Preliminary results show that d must be of the order of one Debye length and then sheath effects may become important. We hope, though, that the effect of collisions and Landau damping will remove some of the problems associated with the broad-band design of the overall system. Most of these difficulties may be eliminated by measuring only the long-time response, that is to analyze the frequency observed for $t \rightarrow \infty$. The problems discussed above are subject to current investigations and will be analyzed in the next quarterly report. In addition we are solving the dispersion relation of an electron plasma with a gaussian distribution of velocities and collisions for real frequencies. These results are used to compute the impedance $Z_{ik}(\omega)$ for comparison with experimental results obtained

with parallel-plane grids immersed into a Mercury-vapor discharge tube. We also are planning to investigate experimentally the size effect discussed above by use of coaxial rf probes.

PROJECT 0832:   RF BEHAVIOR OF PLASMA DIODES

Army Contract DA 36-039 AMC-00094(E)
Project Leader: H. Derfler
Staff: M. Omura

The purpose of this project is the study of oscillations and waves in plasmas near thermodynamic equilibrium.

Plasmas produced in the laboratory differ in several respects from a true thermodynamical equilibrum plasma. In such nonequilibrium plasmas the energy distributions of the constituents (electrons, ions, neutrals and radiation) deviate significantly from Boltzmann's probability law (exp -E/kT). These deviations are an apparently inexhaustible source for discovery of new kinds of instabilities which are designed by nature to ultimately restore equilibrium. Theory and interpretation of experimental data frequently suffer from the fact that the deviations from equilibrium are never known exactly. To avoid the guesswork usually associated with the 'state' of the plasma we are looking for a situation in which all constituents are as close as possible to strict thermodynamical equilibrium and thus stable. This we believe we will find inside a long metal tube made of a refractory metal (i.e., Molybdenum) when heated in vacuum to the temperature of electron emission. We have shown theoretically [Ref. 1] on the basis of statistical mechanics that the small amount of metal ions emitted from the walls is sufficient to neutralize the electron space charge inside the tube such that a neutral plasma is formed. Unlike the situation in conventional plasmas, the electron density increases by several orders of magnitude near the wall. Since a classical electron and ion gas is antimagnetic, it is expected that this density distribution is independent of an applied magnetic field [Ref. 2] and those instabilities usually associated with such

---

[1] QRR No. 8, 1 Jan - 30 March 1964, Project 0832. (Page number not available).

[2] J. H. van Leeuwen, J de Physique (6) 2, p. 261, 1921.

fields do not arise. We propose to build such a tube and explore the
state of this plasma both experimentally and theoretically. These
studies are expected to lead to a better understanding of wave propa-
gation, Landau damping, 'Spitzer' resistivity, diffusion, and in particular,
noise and fluctuation phenomena.

A. NUMBER DENSITY CALCULATIONS FOR PLANAR GEOMETRY

In the previous QRR [Ref. 1] some numerical results for two infinite
parallel-plate molybdenum emitters were given. During this quarter
similar data have been obtained for tungsten as well as additional data
for molybdenum. In Fig. 50 electron density $n_-(0)$, ion density $n_+(0)$,
and Debye length λ_o at the midplane between the emitters and the neutral
density n_o vs $1/T$ are given for tungsten. The percent ionization is
a little less than 1 percent as was the case for molybdenum. The space
charge at the midplane becomes neutral above 2600 $°K$. In Fig. 51 plasma
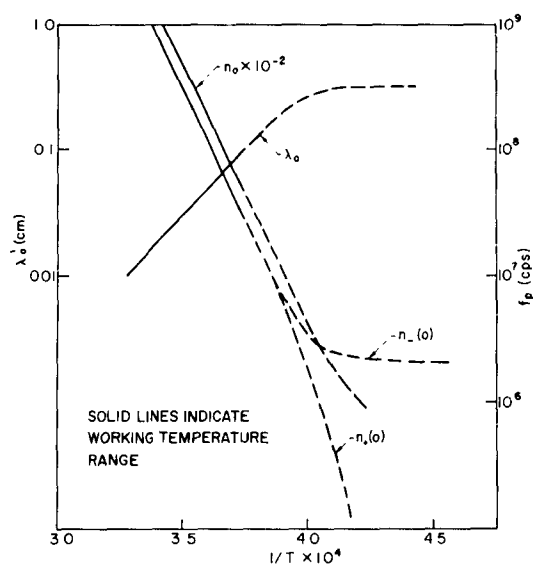
FIG. 50. ELECTRON DENSITY $n_-(0)$, ION
DENSITY $n_+(0)$, DEBYE LENGTH λ_o AT
THE MIDPLANE AND THE NEUTRAL DENSITY
n_o AS A FUNCTION OF $1/T$ FOR A PURE
TUNGSTEN EMITTER.
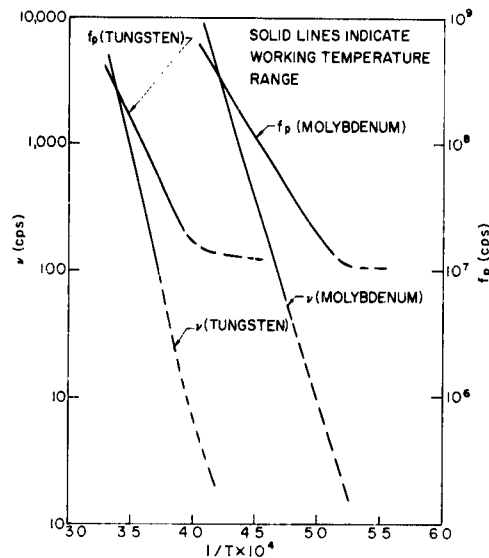
FIG. 51. PLASMA FREQUENCY f_p, AND COLLISION FREQUENCY ν VS $1/T$ FOR TUNGSTEN AND MOLYBDENUM EMITTERS.

frequency and collision frequency for both molybdenum and tungsten are plotted vs $1/T$. The collision frequencies were obtained by assuming hard sphere models for tungsten and molybdenum atoms. The data on neutral density were obtained from graphs provided by Honig [Ref. 3] and the following empirical formula as given by Smith [Ref. 4] was used to compute the ion density at the tungsten emicter.

$$\log_{10} J_+ + 0.363 \log_{10} T + 1.64 \times 10^{-4} T$$

$$= - \frac{e\phi_+}{2.303 \ kT} + 12.43$$

with $\phi_+ = 11.9$ volts. As was the case for molybdenum emitters, the electron number density increased by several orders of magnitude at the walls. The results for the two metals are qualitatively very similar.

---

[3] Honig, R.E., RCA Review, 18, 200 (June 1957).

[4] Smith, L. P., "Thermionic Emission," Handbook of Physics, edited by E. U. Condon and H. Odishaw, p. 8-78.

B. CONSIDERATIONS FOR THE EXPERIMENT

Experimentally, we must work with cylindrical geometry rather than a planar one. It was found, however, that Poisson's equation for the cylindrical system has no solution in terms of classical transcendental functions. Hence density and potential profiles must be obtained numerically for this case. Work is in progress to carry out the numerical analysis of the cylindrical system.

For the experiment, we plan to produce the plasma by heating a long molybdenum cylinder with electron bombardment. The plasma will be probed with electromagnetic waves by means of movable coaxial guides as shown in the schematic diagram of Fig. 52.
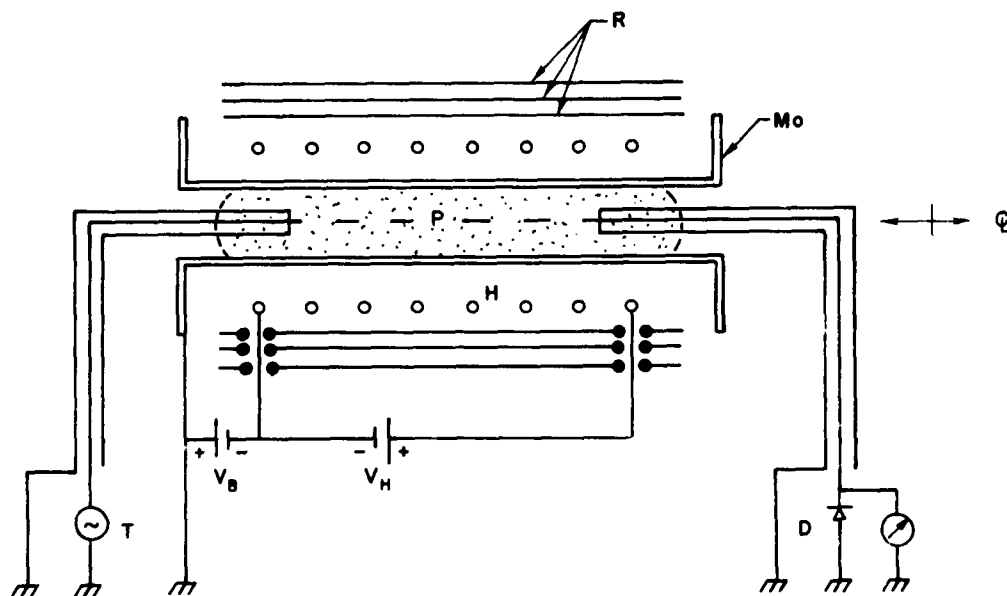
FIG. 52. SCHEME FOR PRODUCTION OF A MOLYBDENUM PLASMA.
P = Molybdenum vapor and plasma
H = Heater windings
M_O = Molybdenum tube
V_H = Heater voltage supply
V_B = Electron bombarder voltage supply
D = RF detector
T = RF transmitter
R = Heat radiation shield

In our plasma it will be difficult to measure the number density with conventional techniques (i.e., dc probe measurement) but the number density may be inferred from the propagation characteristics of the plasma-guide modes of the type discussed by Trivelpiece [Ref. 5]. An approximate theoretical dispersion relation for these modes was obtained by applying a quasi-static analysis to the model shown in Fig. 53. As
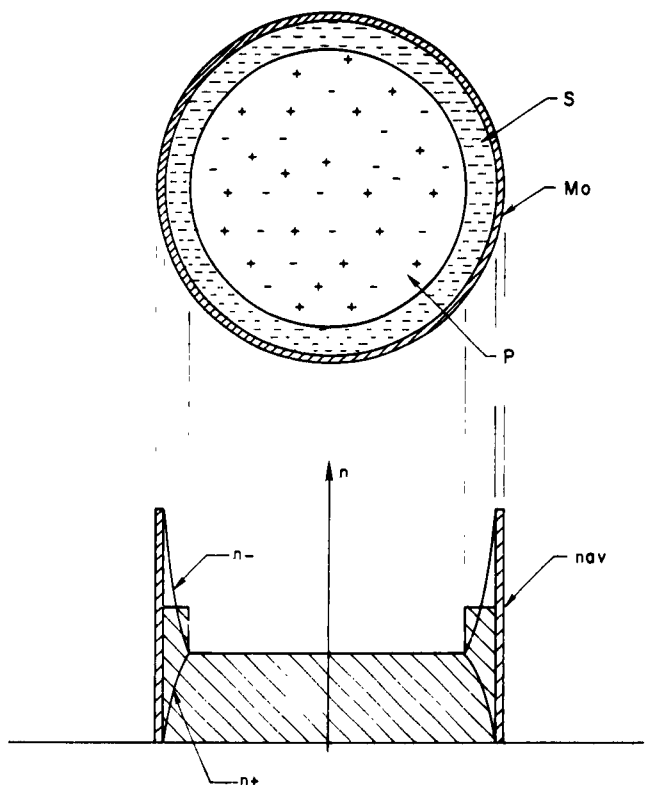
FIG. 53. MOLYBDENUM PLASMA AND THE DENSITY
         DISTRIBUTION OF ELECTRONS AND IONS.

n_{av} = average electron density in the sheath
M_0 = Molybdenum tube
S   = Electron sheath
P   = Neutral molybdenum plasma

[5] A. W. Trivelpiece, "Slow Wave Propagation in Plasma Waveguides," Technical Report No. 7, Electron Tube and Microwave Laboratory, California Institute of Technology (May 1958).

discussed in the previous QRR [Ref. 1], there is a steep rise of electron density near the emitting walls. This effect was taken into account in the model by a step discontinuity in the density, and thus the model consists of a uniform cylindrical plasma of radius b surrounded by a layer of uniform electron plasma with the density equal to the average density of the sheath. We realize that the model is very crude. A more thorough investigation will be carried out in the future, but for the time being we proceed to analyze the approximate model to get a rough idea of what is going to happen.

A quasi-static analysis of our model yields the following dispersion relation.

$$T_i \frac{J_n'(T_i a)}{J_n(T_i a)} = T_o \frac{J_n(T_o b)H_n'(T_o a) - J_n'(T_o a)H_n(T_o b)}{J_n(T_o b)H_n(T_o a) - J_n(T_o a)H_n(T_o b)}$$

where J_n and H_n are nth order Bessel function and Hankel function respectively, and the primes indicate derivatives with respect to the argument. T_i and T_o are radial wave numbers for inner and outer plasmas respectively and are given by

$$T_i^2 = -\beta^2 \left(\frac{1 - \dfrac{\omega_{pi}^2}{\omega^2}}{1 - \dfrac{\omega_{pi}^2}{\omega_c^2 - \omega^2}} \right)$$

$$T_o^2 = -\beta^2 \left(\frac{1 - \dfrac{\omega_{po}^2}{\omega^2}}{1 - \dfrac{\omega_{po}^2}{\omega_c^2 - \omega^2}} \right)$$

where

ω_{pi} = plasma frequency of the inner plasma

ω_{po} = plasma frequency of the outer plasma

ω_c = cyclotron frequency

p = longitudinal wave number

By using a computer program available [Ref. 6] the roots of the dispersion relation have been computed for the lowest order mode. As expected the dispersion characteristics were qualitatively similar to those modes discussed by Trivelpiece. In Fig. 54 we have plots of ω/ω_{pi} vs βa for different values of ω_{po}/ω_{pi} with a/b and ω_c fixed. The
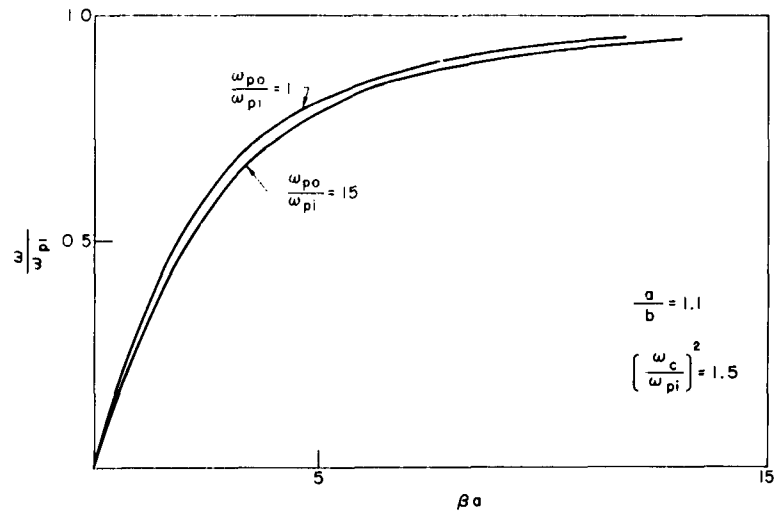
FIG. 54. DISPERSION RELATION ω/ω_{pi} VS βa WITH ω_{po}/ω_{pi} AS A PARAMETER FOR ω_c/ω_{pi} = 1.5 AND a/b = 1.1.

[6] QRR No. 8, 1 Jan - 30 March 1964, Project 0312, page I-43.

graph shows that when the outer plasma ring is thin, the variation of
the ratio ω_{po}/ω_{pi} has a very small effect on the dispersion relation.
The asymptotic value of ω/ω_{pi} goes to unity when $\omega_c > \omega_p$. In Fig. 55
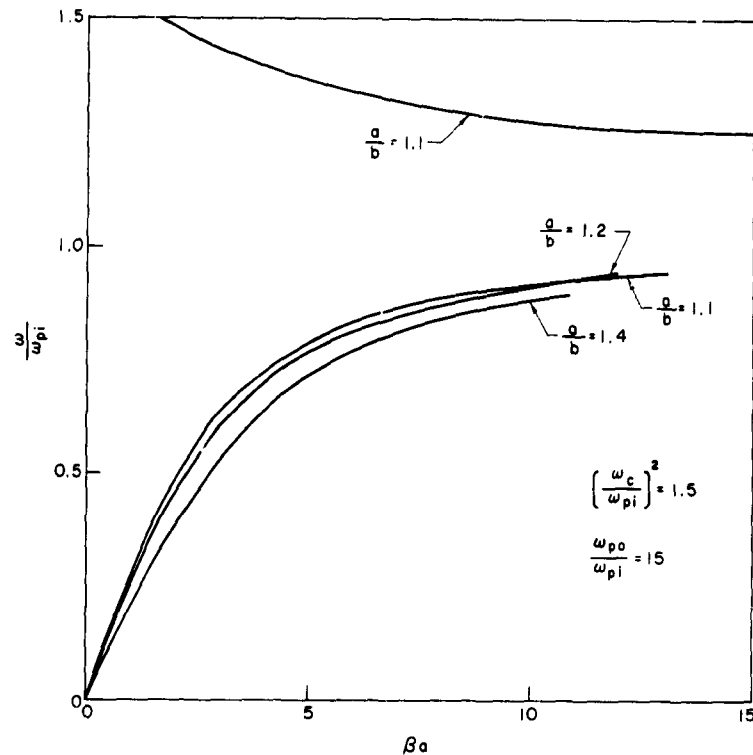
FIG. 55. DISPERSION RELATION ω/ω_{pi} VS βa WITH
a/b AS A PARAMETER FOR $\omega_c/\omega_{pi} = 1.5$ AND
$\omega_{po}/\omega_{pi} = 10$.

we have plots of ω/ω_{pi} vs βa for different values of a/b with
ω_{po}/ω_{pi} held constant. It can be seen that the variation of the ratio
a/b has a noticeable effect on the dispersion diagram. This latter
effect may be utilized to obtain information regarding the thickness of
the sheath. Also included in Fig. 55 is a plot of an upper passband
mode.

The above analysis, though a crude one, shows that the number density
and information regarding the sheath may be obtained from the experimental

dispersion curves, particularly from the asymptotic behavior and the initial slope. A more accurate analysis is needed to find the effects of the gradual rise in electron density near the wall.

The experimental tube is currently being designed.

PROJECT 0833:   DC STATES IN PLASMA DIODES

>   National Aeronautics and Space Administration
>   Grant NsG 299-63
>   Project Leader: H. Derfler
>   Staff: ----

The purpose of this project is the study of stationary potential distributions between parallel plane electron and ion emitting surfaces.

In view of the importance of charge-exchange collisions in certain phenomena related to low-pressure thermionic energy converters, the mobility of positive ions subject to such collisions has been reviewed. An expression due to Sheldon for the charge-exchange mobility at low electric fields is considered basically sound. However an equation for the drift velocity at high electric fields given by Sena has to be rejected because of his underlying assumption that the ions created start from rest. By properly balancing the momentum transfer in a charge-exchange collision we have arrived at an integro-differential equation for the ion distribution function. Work is in progress to solve this equation in order to find an expression for the charge exchange mobility at high electric fields.

A. INTRODUCTION

In an investigation of the open-circuit voltage of a cesium plasma diode, a theoretical expression for the mean velocity of ions subject to charge-exchange collisions was used. This expression

$$< v_+ > = \sqrt{\frac{\pi e E}{4 n_o m_+ Q}} \qquad (1)$$

was obtained by Sena [Ref. 1] subject to the conditions on the following page.

---

[1] L. A. Sena, J. Exp. Theor. Phys. (USSR) 16, 734, 1946.

1. The charge-exchange cross section Q_x is independent of the relative kinetic energy $\epsilon = M/2 \, (\vec{v} - \vec{V})^2$ of the approaching particles.

2. The temperature of the neutral particles is negligible $kT_o = 0$.

3. Each ion loses its kinetic energy completely upon impact with a neutral atom and so after charge exchange starts moving again from rest $\vec{v} = 0$ in the accelerating electric field $\vec{E}$.

4. The quantum-mechanical exchange energy is neglected.

It has been pointed our by Sheldon [Ref. 2] that the charge-exchange cross section Q_x is dependent on the energy ϵ of approach due to the large atomic polarizability $\alpha = 52.5 \cdot 10^{-24} \, cm^3$ [Ref. 3] of the neutral cesium atom. He uses an approximation of the type

$$Q_x = (A - B \, \ell n\epsilon)^2 + \frac{\alpha}{\epsilon}\left(\frac{e\pi}{2}\right)^2 (A - B \, \ell n\epsilon)^{-2} \tag{2}$$

Assuming that all collisions are head on, he then calculates an average cross section for momentum transfer

$$<Q> = \frac{1}{(kT)^3} \int_0^\infty \epsilon^2 Q_x e^{-\epsilon/kT} d\epsilon \tag{3}$$

and obtains a drift velocity

$$<\vec{v}_+> = \frac{3}{8}\sqrt{\frac{\pi m}{kT}} \frac{e\vec{E}}{mn_o <Q>} \tag{4}$$

[2] J. W. Sheldon, J. Appl. Phys., 34, 444 (1963).

[3] A Salop, E. Pollack and B. Bederson, Phys. Rev., 124, 1431 (1961).

[4] H. Derfler, QRR No. 7, page I-91, December 1963.

We note that in deriving Eq. (4) it is inherently assumed that the drift velocity is much smaller than the mean directed thermal velocity; that is $<v_+> << (8kT/\pi m)^{1/2}$ or by Eq. (4)

$$E_c \equiv \frac{16.2^{1/2}}{3\pi} \frac{kT}{e\lambda_+} >> E \qquad (5)$$

where $\lambda_+ = 1/n_o <Q>$ is the ion mean free path. There is no real discrepancy between Eq. (1) and Eq. (4) because Sena's expression is supposedly valid for large electric fields while Sheldon's expression applies for low electric fields. It is no wonder that the charge-exchange cross sections obtained from mobility measurements vary widely depending on whether the condition $E_c << E$ or $E_c >> E$ has been maintained experimentally and whether the proper Eq. (1) or Eq. (4) respectively has been used to compute $<Q>$.

When applying the concept of charge-exchange mobility to the low-pressure Cesium diode condition, Eq. (5) is almost always violated and so Sena's formula (1) must be used [Ref. 4]. There is, however, considerable doubt that Sena's assumption No. 3, which amounts to counting only head-on collisions, is still correct in the high-field limit. This doubt was the motivation for an investigation which shows that Sena's formula Eq. (1) is indeed on very weak ground. Work in progress to correct this situation is outlined below.

B. THE KINETIC EQUATIONS FOR CHARGE-EXCHANGE COLLISIONS

We attempt to calculate the charge-exchange mobility of positive ions in their own gas by dropping all of Sena's restrictions but 2 and 4. Neglect of the quantum-mechanical exchange energy allows us to treat a charge-exchange collision like an elastic collision with the only provision being that the identity of the particles has changed "after" collision. To illustrate exactly what is meant under "change of identity" we show in Figs. 56a and 56b direct and an inverse encounter between an ion and a neutral atom which does not lead to charge exchange. In Figs. 57a and 57b we show the same encounter with charge exchange taking place. We shall use the conventional symbols $\vec{v}$, $\vec{V}$ and $\vec{v}'$, $\vec{V}'$ for
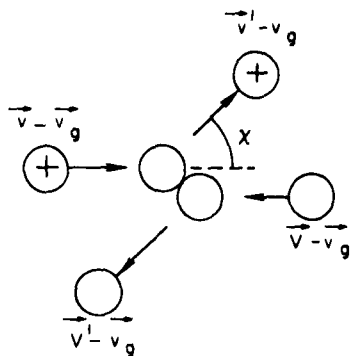
FIG. 56. DIRECT ENCOUNTER AND BELOW INVERSE ENCOUNTER WITHOUT CHARGE EXCHANGE IN THE CENTER OF GRAVITY SYSTEM. $\vec{v}_g$ = c.g. velocity, σ_{o+} = elastic scattering cross section.
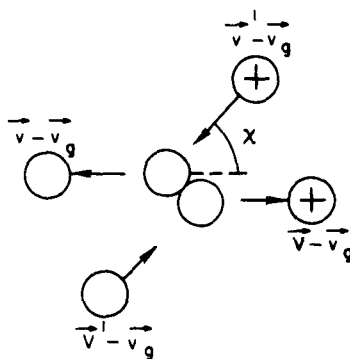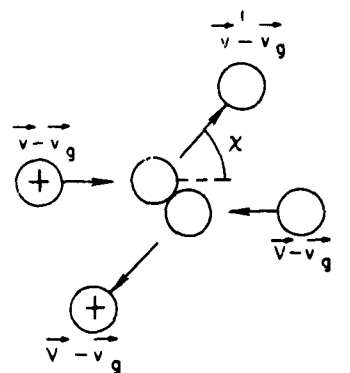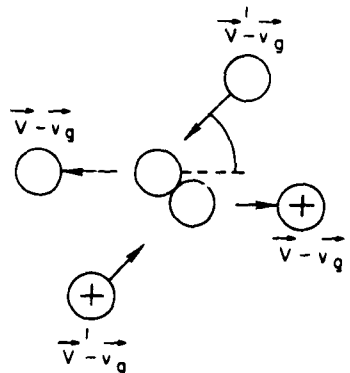
FIG. 57. DIRECT ENCOUNTER AND BELOW INVERSE ENCOUNTER WITH CHARGE EXCHANGE IN THE CENTER OF GRAVITY SYSTEM. $\vec{v}_g$ = c.g. velocity, σ_x = charge exchange cross section.

corresponding velocities of particles before and after collision, respectively. These velocities will not be labeled to indicate their charge as it is sufficient to identify their electrical nature by adding a subscript "o" for neutrals and "+" for ions to the distribution function in which they appear as argument. With this convention the Boltzmann equation for the ion distribution function is written in the form

$$\frac{d}{dt} \, f_+(\vec{v}) = \int\int \sigma_{++}(\chi)|\vec{v} - \vec{V}| \left\{ f_+(\vec{v'})f_+(\vec{V'}) - f_+(\vec{v})f_+(\vec{V}) \right\} \, d\Omega dV$$

$$+ \int\int \sigma_{+o}(\chi)|\vec{v} - \vec{V}| \left\{ f_+(\vec{v'})F_o(\vec{V'}) - f_+(\vec{v})F_o(\vec{V}) \right\} \, d\Omega dV$$

$$+ \int\int \sigma_x(\chi)|\vec{v} - \vec{V}| \left\{ f_+(\vec{V'})F_o(\vec{v'}) - f_+(\vec{v})F_o(\vec{V}) \right\} \, d\Omega dV$$

(6)

where

$$d\Omega = \sin \chi d\chi d\phi$$

(7)

is the solid-angle element of the scattering sphere and

$$\sigma_{ik}(\chi) = \frac{b_{ik}}{2 \sin \chi} \left(\frac{\partial b_{ik}}{\partial \chi} \right)_{|\vec{v} - \vec{V}|}$$

(8)

is the differential scattering cross section as defined by the impact parameter b_{ik} [Ref. 5]. Note that the first integral balances ion-ion collisions, the second, elastic neutral atom-ion collisions and the last, charge-exchange collisions between neutral atoms and ions. Note the important fact that the velocities $\vec{v'}$ and $\vec{V'}$ of the inverse collision in the 3rd integral are interchanged as compared with the 2nd integral. This is in fact the mathematical expression for the "change in density" due to the charge-exchange collision described above and shown in Fig. 57b. We cannot over-emphasize the fact that charge exchange appears only in the balance of inverse collisions!

[5] S. Chapman and T. G. Cowling, "The Mathematical Theory of Non-Uniform Gases," Cambridge University Press, 1952, Chapter 10.

We shall now take care of Sena's condition No. 2, assuming that the bulk of the neutral atoms is cold. Thus, restricting ourselves to the case of large applied electric field (compare Eq. 5), we use the Ansatz

$$F_o(\vec{V}) = n_o \delta(\vec{V}) + f_o(\vec{V}) \tag{9}$$

where $\delta(\vec{V})$ is a Dirac delta function representing the bulk of the neutral atoms and $f_o(\vec{V})$ is a small contribution due to "fast" neutral atoms. We also assume that the gas is only weakly ionized such that $f_+(\vec{v})$ is small and products like $f_o(\vec{V})f_+(\vec{v})$ can be neglected. With this provision also the ion-ion interaction can be neglected $\sigma_{++} = 0$ and to focus our attention to the charge exchange mechanism we also discard the elastic collisions between neutral atoms and ions $\sigma_{+o} = 0$. With these assumptions and Eq. (6) we linearize the Boltzmann equation (6) and find

$$\frac{d}{dt}f_+(\vec{v}) + n_o Q_x |\vec{v}| f(\vec{v}) = n_o \iint \sigma_x(\chi) \ |\vec{v} - \vec{V}| f_+(\vec{V'}) \delta_o(\vec{v'}) \ d\iota d\vec{V} \tag{10}$$

where

$$Q_x = \int \sigma_x(\chi) \ d\iota \tag{11}$$

is the total collision cross section for charge transfer as given, for example, by Eq. (2). This then is the kinetic equation describing the charge-exchange effect at large electric fields.

C. TRANSFORMATION OF THE COLLISION INTEGRAL

To make efficient use of the Dirac-δ function in the integrand of Eq. (10) we would like to integrate with respect to $\vec{v'}$ instead of $\vec{V}$. The Jacobian involved in this transformation has to be evaluated at constant $\vec{v}$, χ, ϕ and is found to be

$$\left\| \frac{\partial \vec{V}}{\partial \vec{v'}} \right\|_{\vec{v}, \, \chi, \, \phi} = \left| \frac{\vec{v} - \vec{V}}{\vec{v} - \vec{v'}} \right|^3 \frac{\sin \vartheta_r}{\sin \vartheta \cos(\psi_r - \psi)} \tag{12}$$

where ϑ_r, ψ_r and ϑ ψ are polar angles of $\vec{v} - \vec{V}$ and $\vec{v} - \vec{v}'$ with respect to a direction $\vec{e}$ fixed in space which we shall later identify with the direction of the electric field vector. Considerable time has gone into checking and double checking this Jacobian because Allis [Ref. 6] has obtained a Jacobian under similar conditions but missing the trigono-metrical factor given in Eq. (12).

Introducing Eq. (11) into Eq. (9) we find

$$\frac{d}{dt} f_+(\vec{v}) + n_o Q_x |\vec{v}| f(\vec{v}) = n_o \int\int \sigma_x(\chi) |\vec{v'}| f_+(\vec{v'}) \left\|\frac{\partial \vec{V}}{\partial \vec{v'}}\right\|_{\vec{v},\chi,\phi;\vec{v'}=0} d\mathcal{X}$$

(13)

We note that due to the restriction $\vec{v'} = 0$ arising from the Dirac delta function in integral Eq. (10) the velocities $\vec{V'}$ and $\vec{V}$, given $\vec{v}$, are no longer independent but functions of χ and ϕ. From the laws of Conservation of Momentum and Energy in an elastic collision, subject to the condition $\vec{v'} = 0$, we get a relation between the velocity vectors which is shown in Fig. 58. From this graph we find immediately that

$$\sin\frac{\chi}{2} = \left|\frac{\vec{v}}{\vec{v'}}\right| \qquad \frac{d\chi}{d|\vec{V'}|} = \frac{2}{|\vec{v'}|} \frac{\sin^2 \chi/2}{\cos \chi/2} d|\vec{V'}|$$

(14)

and thus we can choose to integrate Eq. (13) with respect to $|\vec{V'}|$ instead of χ. We also would like to change the variable ϕ to ϑ. The variation of ϕ with ϑ' when $\vec{v}$, $\vec{v'} = 0$, $|\vec{V'}|$ (that is χ) are held fixed is obtained from the orientation of the plane Fig. 58 with respect to an axis $\vec{e}$ fixed in space by considerations of spherical trigonometry. The result is given by

$$\left(\frac{d\phi}{d\vartheta'}\right)_{\chi,\vartheta} = \frac{\sin \vartheta \cos(\psi_r - \psi)}{\sin \vartheta_r \sin \beta \cos \chi/2}$$

(15)

---

[6]W. P. Allis, "Motion of Ions and Electrons," Article in "Encyclopedia of Physics" Springer Verlag, Berlin, 1956, p. 409.
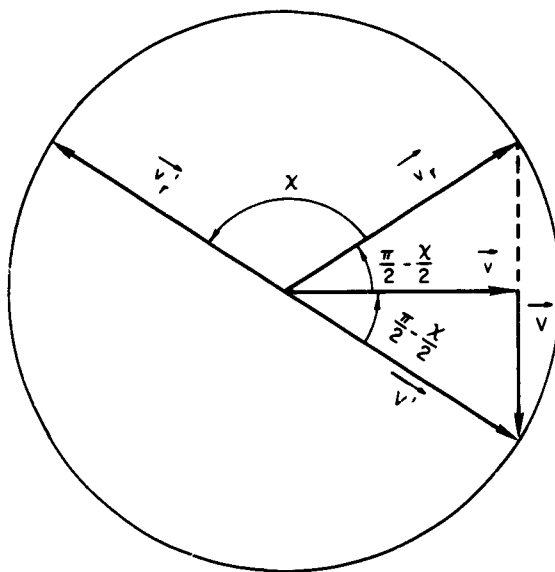
FIG. 58. VELOCITIES IN AN ELASTIC COLLISION
SUBJECT TO THE CONDITION THAT ONE OF THE
PARTICLES IS AT REST "AFTER"COLLISION $\vec{v}' =$
0. $\vec{v}_r = \vec{v} - \vec{V}$ relative velocity before
collision, $\vec{v}_r' = -\vec{V}'$ relative velocity
after collision, χ = scattering angle in
the c.g. system.

where β is the angle between the vectors $\vec{e} \times \vec{V}'$ and $\vec{v} \times \vec{V}'$

respectively.

Collecting Eqs. (7), (12), (14) and (15) we find

$$d\Omega \; \left\| \frac{\left|\partial \vec{v}\right|}{\left\|\partial \vec{v}'\right\|} \right\|_{\vec{v}, \chi, \phi; \; \vec{v}' = 0} = \frac{4 \; d\left|\vec{v}'\right| d\vartheta'}{\left|\vec{v}\right| \; \cos \chi/2 \; \sin \beta} \tag{16}$$

It is necessary to express β in terms of χ, ϑ and ϑ' which again
is done by means of spherical trigonometry.

$$\sin \beta = \frac{1}{\sin\vartheta' \; \cos \chi/2} \sqrt{\cos^2 \frac{\chi}{2} - \cos^2\vartheta - \cos^2\vartheta' + 2 \sin\vartheta \sin\vartheta' \sin \frac{\chi}{2}} \tag{17}$$

By introducing Eqs. (14), (16) and (17) into Eq. (13) we obtain

$$\frac{d}{dt} f_+(\vec{v}) + n_o Q_x |\vec{v}| \ f_+(\vec{v})$$

$$= \frac{4n_o}{|\vec{v}|} \iint \frac{\sigma_x(\chi, |\vec{v'}|) f_+(\vec{v'}) \ \sin\vartheta' \ d\vartheta' \ |\vec{v'}| \ d|\vec{v'}|}{\sqrt{1 - \left|\frac{\vec{v}}{\vec{v'}}\right|^2 + 2\left|\frac{\vec{v}}{\vec{v'}}\right| \ \sin\vartheta \sin\vartheta' - \cos^2\vartheta - \cos^2\vartheta'}}$$

(18)

which is identical with integral Eq. (10).

D.   THE CHARACTERISTICS OF THE DIFFERENTIAL OPERATOR EQ. (18)

In a homogeneous neutral plasma and under stationary conditions we have simply

$$\frac{d}{dt} f_+(\vec{v}) = \frac{e}{m} \vec{E} \cdot \frac{\partial}{\partial v} f_+(\vec{v}) = \frac{e}{m} E \frac{\partial}{\partial v} f_+(\vec{v})$$

(19)

It is convenient to introduce in Eq. (19) spherical coordinates in velocity space so that Eq. (18) becomes under said conditions:

$$L\left\{f_+(v)\right\} = \frac{4mn_o}{eE} \iint \frac{\sigma_x(\chi, |\vec{v'}|) f_+(\vec{v'}) \ \sin\vartheta' \ d\vartheta' \ |\vec{v'}| \ d|\vec{v'}|}{\sqrt{1 - \left|\frac{\vec{v}}{\vec{v'}}\right|^2 + 2\left|\frac{\vec{v}}{\vec{v'}}\right| \ \sin\vartheta \sin\vartheta' - \cos^2\vartheta - \cos^2\vartheta'}}$$

(20)

where the linear differential operator

$$L = |\vec{v}| \ \cos\vartheta \ \frac{\partial}{\partial |\vec{v}|} + \sin^2\vartheta \ \frac{\partial}{\partial \cos\vartheta} + \frac{mn_o Q}{eE} |\vec{v}|^2$$

(21)

has been introduced. Using the variables

$$|\vec{v}| = x \qquad \text{and} \qquad \cos\vartheta = y$$

(22)

the characteristic equations of the differential operator $L\{f\}$ can be written by means of an arbitrary parameter s:

$$\frac{dx}{ds} = xy \qquad \frac{dy}{ds} = 1 - y^2 \qquad \frac{df}{ds} = - \frac{mn_o Q}{eE} x^2 f \tag{23}$$

This set of linear differential equations can be solved by elementary means giving the characteristics

$$x = x_o[\cosh(s) + y_o \sinh(s)] \tag{24}$$

$$y = \frac{y_o + \tanh(s)}{1 + y_o \tanh(s)} \tag{25}$$

$$f = f_o\, e^{\dfrac{-mn_o Q}{2eE} x_o^2 \left[\left(1-y_o^2\right)s + \left(1+y_o^2\right)\sinh(s)\cdot\cosh(s) + 2y_o \sinh^2(s)\right]} \tag{26}$$

Note that for $s = 0$ we obtain the "initial values" $x = x_o$, $y = y_o$, $f = f_o$. By prescribing the initial values in the form

$$x_o = x_o(t) \qquad y = y_o(t) \qquad f = f_o(t) \tag{27}$$

where t is a suitable parameter we may introduce Eq. (27) into the characteristic Eqs. (24), (25) and (26) and eliminate s, t to obtain the general solution $f(x,y)$ of the linear differential equation

$$L\{f(\vec{v})\} = 0 \tag{28}$$

One solution of Eq. (28) which will be discussed further below is

$$f = f_o\, e^{-\dfrac{mn_o Q}{2eE} x^2\left\{y + C(1-y^2) + (1-y^2)\,\ell n\sqrt{\dfrac{1+y}{1-y}}\right\}} \tag{29}$$

where C is an arbitrary constant.

Actually we are not very much interested in solutions of the homogeneous Eq. (28) but we hope that by means of the characteristics Eqs. (24), (25) and (26) we can transform the differential operator (21) into an integral operator. In this way we try to transform the integro differential Eq. (20) into a pure integral equation which we hope to solve, if necessary, by numerical methods.

E. DISCUSSION

If we take Sena's condition No. 3 seriously each ion created will start from rest and move parallel to the electric field until it collides again head-on with a neutral atom. This amounts to replacing the "generation term," that is, the integral over the in verse collisions in Eq. (20), by a Dirac-δ function $\delta(\vec{v})$ and allowing only for positive velocities parallel to the electric field. In this case we have from Eqs. (18) and (19)

$$\frac{\partial}{\partial v_\parallel} f_+(v_\parallel) + \frac{mn_o Q_x}{eE} v_\parallel f_+(v_\parallel) = 0, \quad v_\parallel > 0 \tag{30}$$

The solution of this equation is

$$f_+(v_\parallel) = f_o e^{-\frac{mn_o Q_x}{2eE} v_\parallel^2}, \quad v_\parallel > 0 \tag{31}$$

from which the drift velocity of the positive ions is found to be

$$\langle v_\parallel \rangle = \frac{\int_0^\infty v_\parallel e^{-\frac{mn_o Q_x}{2eE} v_\parallel^2} dv_\parallel}{\int_0^\infty e^{-\frac{mn_o Q_x}{2eE} v_\parallel^2} dv_\parallel} = \sqrt{\frac{2eE}{\pi mn_o Q_x}} \tag{32}$$

Comparing this with Sena's Eq. (1) we find agreement apart from a numerical factor of order unity. The disagreement of the numerical factor must not be taken too seriously because Sena's formula was derived by little more than dimensional analysis. A serious objection to both Eqs. (1) and (32) arises by considering the effect of transverse velocities. Assuming with Sena that the "generation term" can be lumped into a Dirac-δ function $\delta(\vec{v})$, Eq. (28) is valid everywhere except for $\vec{v} = 0$ and the same holds for the solution Eq. (29). By substituting Eq. (22) into Eq. (29) and taking $C = 0$ we find that

$$ f = f_o \, e^{\frac{-mn_o Q}{2eE} \, |\vec{v}|^2 \left(\cos\vartheta + \sin^2\vartheta \, \ell n\left(\cot g \, \frac{\vartheta}{2} \right) \right)} \tag{33} $$
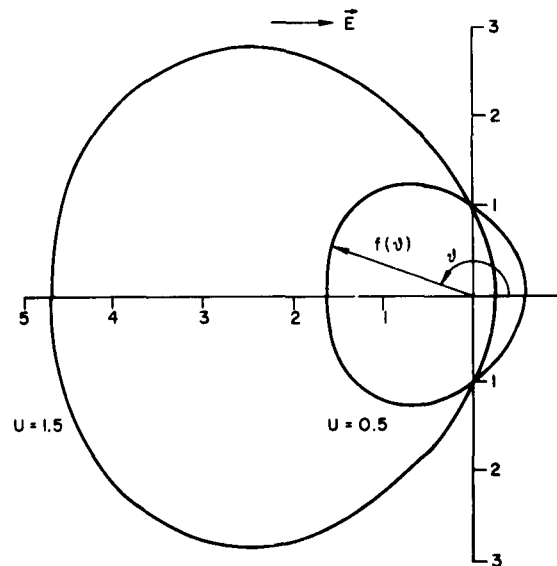
FIG. 59. POLAR DIAGRAM OF THE VELOCITY DISTRIBUTION
EQ. (33) FOR TWO VELOCITIES

$$ U = \frac{mn_o Q}{2eE} \, |\vec{v}|^2 $$

which for $\vartheta = 0$ agrees exactly with Eq. (31). It is not obvious why we should average Eq. (33) only over positive velocities as it was done in Eq. (32) to obtain the drift velocity. If instead we try to average (33) over all velocities we are in serious trouble because the distribution function Eq. (33) blows up for $|\vartheta| > \pi/2$ as shown in Fig. 59. From this figure we see that we get even more ions moving against the electric field than moving in its direction. This does not make sense physically and to find the correct distribution function we must solve the full integro differential Eq. (20) as outlined in Section D. Work along this line is now in progress.

PROJECT 0908: ION AND PLASMA BEAM SOURCES

Air Force Contract AF33(657)-11144
Project Leader: R. P. Lagerstrom
Staff: J. Shiue

The purpose of this project is to produce ion and plasma beam sources suitable for high-vacuum plasma experiments. Thermionic emission of lithium ions from lithium-alumino-silicates such as spodumene and eucryptite has been under specific investigation.

A final report is in preparation.

SEL-64-073

PROJECT 4651: PHYSICAL PRINCIPLES OF MAGNETIC ADAPTIVE COMPOUNDS

Air Force Contract AF33(657)-11586
Project Leader: J. R. Angell
Staff: R. C. Woodbury*

The purpose of this project is to study properties and basic operating mechanisms of square-loop magnetic materials suitable for use in magnetic adaptive components. Of particular interest is the 50 percent Ni-Fe grain-oriented material used by H. Crafts in his second-harmonic adaptive component.

To review briefly, the achievement of variable gain with memory stems from the correlation of magnetic remanence with the second-harmonic content of the time-varying flux when driven with a small sinusoidal H field. Adaption from one second-harmonic amplitude level, or gain state, to another is achieved by the application of a dc field, which causes the gross flux level to change linearly with time. The latter is achieved only if the material has a relatively square hysteresis loop and strong eddy-current damping.

Investigations during the quarter have been in the following areas:

1. The second harmonic output from a 50 percent Ni-Fe tape driven by a large, low-frequency transverse field (1 oersted, 2 kc) was found to be approximately 12 times greater than the anisotropy-predicted rotation of the magnetization. This indicates transverse domain motion. Low transverse fields ($H \approx 0.05$ oersted) were found to generate signals whose magnitude was closer to the normally expected rotation effect and hence suggests that the large-signal transverse domains were a result of the applied field and were not residual. The contribution from transverse domains in 2 mil tape was found to damp out above 10 kc.

2. The average spike domain radius in 4 mil 50 percent Ni-Fe tape was previously reported here to be approximately 6 micron. The average domain size in 1 mil tape was recently investigated with an experimental technique which was the same as previously reported.

---

*N.S.F. Faculty Fellow

It involved a correlation of the second-harmonic and fundamental flux components to the Bloch wall displacement and average spike radius. The Bloch wall displacement was determined by correlating the known displacement of simple planar walls to the minor hysteresis shape. The study yielded a spike radius of 0.6 - 1.0 micron for the 1 mil tape.

3. A knowledge of the damping phenomena in the tape is necessary to predict the power consumption and also to choose the best operating frequency for optimum second-harmonic output.

Figure 60 shows a plot of the actual fundamental flux response for longitudinal drive (0.04 oersted) in saturated 4 mil tape (curve A). Also shown for comparison is the response of a single-time-constant function, $1/1 + j\omega\tau$ (curve B). The response predicted by Maxwell's equations for a homogeneous material having sufficient permeability (400) to yield an output equal to the actual response at low frequencies is indicated by curve C. This function is of the form

$$\frac{\tanh ka}{ka}$$
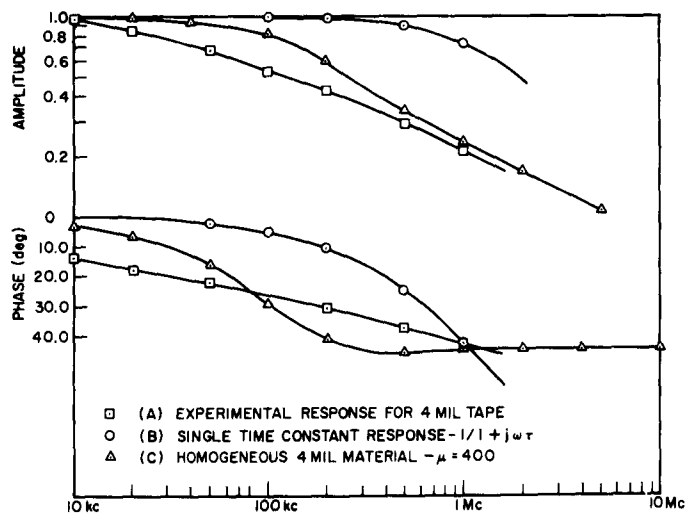
FIG. 60. FREQUENCY RESPONSE CURVES.

where

$a = 1/2$ the tape thickness

$k = 1/\delta + j/\delta$

$\delta = $ skin depth $\alpha\ 1/\sqrt{\omega}$

It is observed that the actual response amplitude varied inversely as $\sqrt{\omega}$ at the higher frequencies and compares favorably with the homogeneous case. The phase lag however shows greater deviation.

PROJECT 4655:   FEFET ADAPTIVE COMPONENTS

Air Force Contract AF33(657)-11586
Project Leader: J. B. Angell
Staff: R. P. James

This project is concerned with an adaptive component in which the surface conductance of a semiconductor layer is controlled by the field due to the remanent polarization of an adjacent ferroelectric layer.

This project has been inactive during the past quarter.

PROJECT 4656:   INTEGRATED ARRAYS OF MAGNETIC ADAPTIVE COMPONENTS

Air Force Contract AF(657)-11586
Project Leader: J. B. Angell
Staff: M. A. Savageau

This project is an experimental study aimed at developing suitable two-dimensional arrays of magnetic adaptive components. The project is an outgrowth of the work on project 4651.

The following results were obtained in the search for optimum operating conditions of the orthonal ladder structures previously described: Second harmonic output as a function of frequency, "Squareness" of the dynamic hysteresis loop as a function of frequency, and qualitative descriptions of performance. The second harmonic output of the orthonal ladder structure was found to reach a maximum at approximately 3.5 kc (see Fig. 61). However, this frequency of operation turns out to be undesirable from the standpoint of dynamic loop squareness.

With the AC drive current present, the amount of DC necessary to switch 90% of the flux divided by the amount necessary to switch 10% is defined as the squareness ratio, S (see Fig. 62).
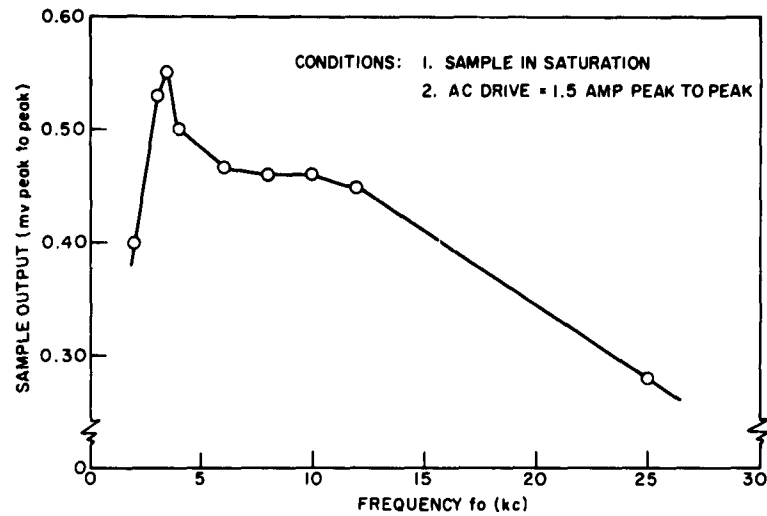
FIG. 61. SECOND HARMONIC OUTPUT VS FREQUENCY.

DYNAMIC HYSTERESIS LOOP AT 50 kc

$$S \triangleq \frac{b}{a}$$
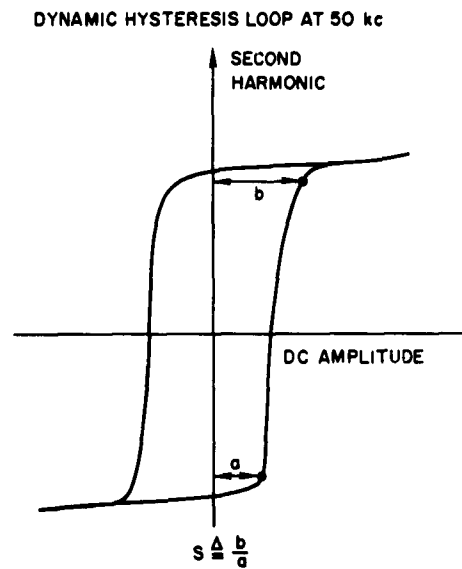
FIG. 62. DEFINITION OF SQUARENESS
RATIO, S.

At 50 kc the dynamic loop becomes very nearly square $(S \rightarrow 1)$ (see Fig. 63). Although the second harmonic output is well below the
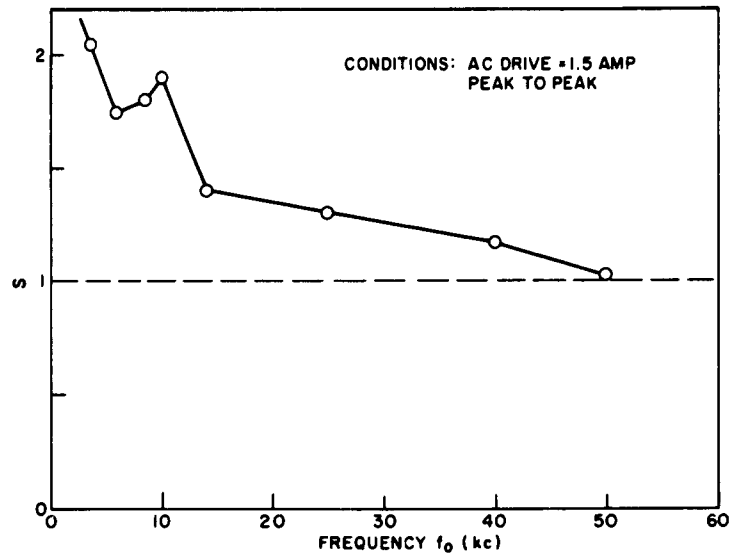
FIG. 63. SQUARENESS RATIO VS FREQUENCY.

3.5 kc level, it is still sufficient for detection purposes. A square
loop is probably the most desirable single property which the optimum
operating conditions should provide.

The best operating conditions at this time are:

AC Drive Current:

1) frequency = 50 kc

2) amplitude = 1.0 amp. peak

DC Adapt Pulse:

1) width   = 200 μs

2) amplitude = 200 ma

Under these conditions we find a fairly large number of stable states,
a large reverse jump (this is due more to the transverse technique than
to the loop squareness), and the coincident selection property is re-
tained. The training characteristic for these conditions is shown in
Fig. 64.

FIG. 64. TRAINING CHARACTERISTIC FOR THE BEST OPERATING
CONDITIONS TO DATE.

PROJECT 4657: SELF-REPAIRING CIRCUIT TECHNIQUES

Air Force Contract AF33(657)-11586
Project Leader: J. B. Angell
Staff: J. S. Eggenberger*

The objective of this project is to develop effective methods of using digital magnetic memory arrays in which there are some defective storage elements. For reasons outlined in a previous Quarterly Research Review,** emphasis is being placed on the use of error-correcting codes toward achieving this goal.

In particular, those block codes which can be decoded by a single layer of threshold devices, referred to as T-codes, are being studied. The defect model for individual storage elements is assumed to be describable by normally distributed zero and one outputs for a random element, and the decoding threshold devices threshold detect a weighted sum (over the field of real numbers) of the inputs.

A basic limit has been found on the decrease in defect probability which can be obtained by use of a T-code under these conditions. In essence, the bound implies that for a fixed redundancy, repetition of each variable is an optimum T-code.

---

*
I.B.M. Resident Scholar

**
QRR No. 7, page II-6, Stanford Electronics Laboratories.

FIG. 64. TRAINING CHARACTERISTIC FOR THE BEST OPERATING
CONDITIONS TO DATE.

PROJECT 4657: SELF-REPAIRING CIRCUiT TECHNIQUES

> Air Force Contract AF33(657)-11586
> Project Leader: J. B. Angell
> Staff: J. S. Eggenberger*

The objective of this projecu is to develop effective methods of
using digital magnetic memory arrays in which there are some defective
storage elements. For reasons outlined in a previous Quarterly Research
Review,** emphasis is being placed on the use of error-correcting codes
toward achieving this goal.

In particular, those block codes which can be decoded by a single
layer of threshold devices, referred to as T-codes, are being studied.
The defect model for individual storage elements is assumed to be de-
scribable by normally distributed zero and one outputs for a random
element, and the decoding threshold devices threshold detect a weighted
sum (over the field of real numbers) of the inputs.

A basic limit has been found on the decrease in defect probability
which can be obtained by use of a T-code under these conditions. In
essence, the bound implies that for a fixed redundancy, repetition of
each variable is an optimum T-code.

---

* I.B.M. Resident Scholar

** QRR No. 7, page II-6, Stanford Electronics Laboratories.

Considering the bound in detail, a quantity θ may be derived from the parameters of the output distributions such that Q_0, the single element defect probability, is given by:

$$Q_0 = A \text{ erfc } \theta$$

where

$$\text{erfc } y = 1 - \frac{2}{\sqrt{\pi}} \int_0^y e^{-T^2} dT$$

and

$$\frac{1}{2} \leq A \leq 1.$$

If n storage elements are used to store k variables in an (n,k) T-code, a set of parameters n_1, n_2, ... n_k may be defined such that Q_j, the probability that the jth decoded variable will be in error for some stored word, is bound by:

$$q_j \geq A_j \text{ erfc } \sqrt{n_j} \; \theta \; ,$$

and the n_j are bound such that:

$$n \geq \sum_{j=1}^{k} n_j \; .$$

It can also be shown that the only situation in which equality holds in the bound on the n_j is if the T-code consists of repetition of each variable.

Hence, for a fixed integral redundancy, repetition is the optimum T-code. It is interesting to note that for all T-codes which have been evolved to date, equal or lower defect probability can be achieved with equal or lower redundancy by use of repetition.

A report is being prepared covering the investigation of T-codes, including the derivation of the bound on their defect tolerance described above.

The other phase of the investigation has been concerned with the evaluation of various types of thin-film fuses atop glass or silicon-dioxide substrates. Various combinations of substrates and fuse metals were fabricated and measured during May. Substrates include glass, SiO_2 on polished silicon and SiO_2 on chemically etched silicon. Metals which have been tried are tin, gold, and lead. One objective was to determine how much thermal isolation could be achieved between the metal film and its substrate through a 'phonon mismatch.'

Measurement tests have shown that the time to blow, T_B, varies inversely as the inverse fourth power of the current for both tin and gold, as would be expected if significant cooling of the fuse by the substrate took place, and that the temperature of the metal is essentially that of the substrate surface, for blow times greater than 10^{-7} second. That is

$$T_B = K \ I^{-4}$$

The tin fuses, $400\overset{o}{A}$ thick and 0.001 inch wide, typically blew in 10 microseconds with 100 ma. The corresponding figure for gold fuses, $200\overset{o}{A}$ thick, was 100 microseconds for 100 ma. These blow times are about as short as can be achieved with practical films.

Thus, there seems to be little hope of forming an evaporated metal fuse atop a SiO_2 coating on silicon and obtaining a significant degree of thermal isolation.

PROJECT 4711: EPITAXIAL GROWTH

> Air Force Contract AF33(657)-11586
> Project Leader: J. F. Gibbons
> Staff: P. C. Prehn

The purpose of this project is to examine and control the crystal-lographic and electrical properties of the materials and structures

grown epitaxially by vapor deposition. Our interests have been concentrated on the materials Si, GaAs and GaP. Among the phenomena we plan to investigate are electroluminescence, the photovoltaic effect, and the properties of heterojunctions.

A final report has been distributed, TR 4711-1 by J. F. Gibbons and P. C. Prehn, dated October 1963, entitled "Epitaxial Vapor Growth of III-V Compounds." This project is now closed.

PROJECT 4714: CIRCUIT ASPECTS OF VARIOUS CRYOGENIC PHENOMENA

    Air Force Contract AF33(657)-11586
    Project Leader: J. F. Gibbons
    Staff: D. J. Dumin

This project has been undertaken to investigate and utilize cryogenic phenomena in the construction of new devices and circuits. Among the phenomena to be investigated will be the trapping of magnetic flux. Other low-temperature phenomena may be incorporated into this study as time progresses. Study of the properties of certain III-V compounds at low temperatures has been undertaken as part of this project.

The studies of quantization of trapped flux have been completed. A final report concerning these studies is in preparation.

A final report on this project has been distributed, TR 4714-1 by D. J. Dumin, dated December 1963, entitled "The Quantizer: An Application of Quantization of Trapped Flux in Superconductors." This project is now closed.

PROJECT 4715: TRANSIENT PERFORMANCE OF TRANSISTOR SWITCHES UNDER HIGH LEVEL INJECTION

    Tri-Service Contract Nonr-225(24)
    Project Leader: J. F. Gibbons
    Staff: P. Kamas

The purpose of this project is to study the transient behavior of transistor switches as they proceed from the OFF condition into the saturated condition.

This project has been inactive this past quarter.

PROJECT 4813:   APPLICATION OF SOLID-STATE PHENOMENA TO MICROSYSTEMS

Office of Naval Research Contract Nonr-225(44)
Project Leader: J. G. Linvill
Staff: Gerald Alonzo

The objective of this project is to apply physical phenomena of solids to systems which must be small to perform their necessary function. Further, the intent is to establish suitable models of the phenomena useful to the application and to evaluate the limits of performance which are imposed by the properties of the solids used.

Technical Report No. 4813-4, "Development of a Piezoelectric Dynamic Embosser for Use as a Reading Machine," by G. J. Alonzo was produced under date of March 1964 and is in distribution. The report describes the first version of a photomechanical device which presents a grainy, dynamically embossed version of printed material aimed to enable the blind to read ordinary printed material by touch.

The dynamic embosser described by Alonzo consists of a planar array of small photocells on which the image of letters is focused and of a set of piezoelectric reeds connected one-to-one with elements of the photocell array. A reed whose photocell is dark, the photocell being under the dark part of the letter image, is made to vibrate. A reed whose photocell is light does not vibrate. Thus the tips of the vibrating reeds present a grainy facsimile of the image on the photocells and provide a tactual presentation of printed characters to the sensing fingers of the blind reader. Tests made by Alonzo with this device insured that the photocell-piezoelectric reed combination was operable in the sense that the reeds were clearly made to vibrate in correspondence to the printed characters focused on the photocells. However, mechanical tolerances in the piezoelectric reed array were large enough that a definitive test of readability of material presented tactually by the piezoelectric array of reeds could not be made.

A definitive test of readability of material presented by a field of vibrating reeds has been made this quarter in cooperation with Dr. James Bliss and his colleagues of the Stanford Research Institute. Material presented tactually to a blind subject by means of an array of vibrating reeds was read at a rate exceeding 25 words per minute.

At SRI a research project in tactual perception is under way.* In particular, a computer has been programmed to control a tactual stimulator consisting of a rectangular array of air jets which can be turned on and off. Roman capitals can be presented on a field of 8 rows and 5 columns of the air-jet stimulators. Moreover, the letters can be presented in sequence and moved across the rectangular field consisting of 8 rows and 12 columns. At our laboratory a corresponding array of piezoelectric reeds, an 8 by 12 array, was constructed in a form which could be driven by the same signals used on the air-jet stimulators. The tests of the piezoelectric reed stimulator then were made, printed material being presented to the blind subject who read at the rate indicated above after a few hours of practice.

Thus, at this point, the preliminary tests on all parts of a photo-mechanical reading aid are successful. Support from agencies more concerned with its end use is being sought for further work. Under the present project, further work on the photocells and piezoelectric reeds in accordance with our stated objectives will continue.

PROJECT 4814:   PERFORMANCE LIMITATIONS OF PHOTON COUPLED SYSTEMS
Tri-Service Contract Nonr-225(24)
Project Leader: J. G. Linvill
Staff: I. Wunderman

The objectives of this project are to characterize the electrical performance of photodetective-luminescent systems, thereby enabling useful design criteria and a comparison with other devices. This is achieved by considering photon coupling between an emitting source and a radiation detector as a transport mechanism similar to drift and diffusion. The concepts are generic to numerous light sources and detectors. Neon glow lamps, injection luminescent diodes, photoconductors, photodiodes, and phototransistors are specifically considered in detail.

A final report in in preparation.

PROJECT 4815:   TRANSISTOR PULSE AMPLIFIERS

                      Tri-Service Contract Nonr-225(24)
                      Project Leader: J. G. Linvill
                      Staff: G. Danon

Detection and data transmission for experiments in high-energy physics require pulse amplifiers with hundreds of megacycles of bandwidth.

A final report has been distributed, TR 4815-1 by G. Danon and K. Sorenson, dated November 1963, entitled "The Sampled Parameter Method and Design of Wideband Transistor Amplifiers." The project is now closed.

PROJECT 4816:   RELIABLE SYSTEMS WITH UNRELIABLE PARTS

                      Office of Naval Research Contract Nonr-225(44)
                      Project Leader: J. G. Linvill
                      Staff: John Knox-Seith

The purpose of this project is to investigate techniques for building reliable digital systems from unreliable components.

Technical Report 4816-1 by John Knud Knox-Seith, dated December 1963, entitled "A Redundancy Technique for Improving the Reliability of Digital Systems," has been distributed. A final report is in preparation, and upon its distribution, this project will be closed.

PROJECT 4818:   APPLICATIONS OF ELECTRO-OPTICAL PHENOMENA IN SOLIDS

                      Office of Naval Research Contract Nonr-225(31)
                      Project Leader: J. G. Linvill
                      Staff: John W. Hill

The purpose of this project is to evaluate the presently available photo-optical solid-state components and to find ways of interconnecting these components to construct a set of static and dynamic logic circuits. "Circuits" in this case includes optical connections, the close proximity of photon emitting and detecting units, and also longer-range optic-fiber coupling.Conventional electrical circuit connections are used as well.

TRANSIENT RESPONSE OF FIBER OPTICS

Just as series resistance and leakage conductance in electrical transmission lines determine their rise time, the multiplicity of optical paths (modes) in an optic fiber determine a rise time too. The rays

that travel along the axis of the fiber take the least time to propagate through, while those that reflect from side to side as they go take longer, depending on their angle θ with the axis of the fiber. The time delay of a ray in a fiber of length ℓ and index of refraction n is

$$t = n\ell/c \ \cos \theta$$

where c is the velocity of light. Using this relation the impulse response and rise time of a length of fiber may be calculated. In fact, using the simple model of a straight fiber with a point source of light flux centered near one end and a detector that collects the flux coming from the other end, the impulse response is

$$h(t) = \begin{cases} \dfrac{n\ell}{ct^2} & ; & t \geq \dfrac{n\ell}{c} \\[4mm] 0 & ; & t < \dfrac{n\ell}{c} \end{cases}$$

Both impulse response and step response of the model are shown in Fig. 65.
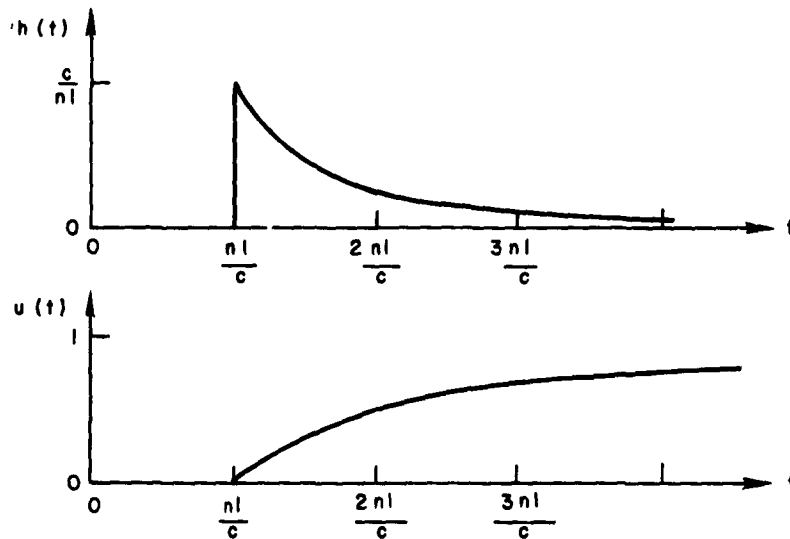
FIG. 65. FIBER IMPULSE AND STEP RESPONSE.

There are many additional factors that modify the impulse response of this model. If 0 is too large, light is lost through the sides of the fiber and hence no flux is transmitted with more than a certain angle or delay. There is also a limited angular input operative at the end of the fiber and again no flux can be transmitted with more delay than that corresponding to this angle. There is also attenuation in the fiber body, attenuation at each internal reflection, reflection on entering and leaving the fiber, nonuniformly emitting sources, and sources with finite size which affect the impulse response. Taking some of these effects into account and modifying the step response of the model accordingly shows that the rise times range from 10% to 50% of the fiber transit time delay, $n\ell/c$.

For example, in a 1-foot length of glass fiber, the rise time would be at least 0.15 ns corresponding to a pulse spacing of 0.60 ns and a pulse repetition frequency of 1660 Mc. In a 10-foot fiber the prf would be 166 Mc and correspondingly lower from longer fibers.

PROJECT 5002:   HIGH-FIELD TRANSPORT PROBLEM

This project is concerned with the theoretical studies of high-field transport properties in n-type semiconductors.

A set of differential equations that govern the expansion coefficients of electron distribution has been previously derived from Boltzmann's equation, i.e.,

$$F\left\{\frac{\ell}{2\ell+1}\left(n_\ell' + \frac{\ell+1}{p}n_\ell\right) + \frac{\ell-1}{2\ell-3}\left(n_{\ell-2}' - \frac{\ell-2}{p}n_{\ell-2}\right)\right\} + \frac{\ell-1}{c} = S_{\ell-1}$$

for $\ell \geq 1$

where $F = \dot{p}_z = e\mathcal{E}_z$ is the force due to the applied field $\mathcal{E}_z$. $n_\ell' = \frac{\partial}{\partial p}n_\ell(p)$ and $n_\ell(p)$ is the coefficient of the ℓth   polynomial in a Legendre polynomial expansion of $f(\bar{p})$.

This set of differential equations does not have a unique solution without further constraint, since there is always one more unknown function than there is equation. For this reason, any method of solution that arbitrarily chooses a functional form for $f(\bar{p})$ such as [Ref. 1] $f(\bar{p}) \propto \exp(|\bar{p} - \bar{p}_{zo}|^2/2m^*kT_e)$ can be made to satisfy this set of equations. Also, any arbitrary termination of the series expansion of $f(\bar{p})$ such as [Ref. 2] $n_2(p) \equiv 0$, or [Ref. 3] $n_2(p)/n_1(p) \equiv 5/3$ can be made to satisfy the set of equations.

It is quite unlikely that the apparent arbitrariness of functional form is inherent in the model of the physical problem. There are certain restraints that cannot be easily applied such as the requirement that $f(\bar{p})$ be everywhere positive and real. An arbitrary termination of the polynomial expansion may cause this condition to be violated. The choice of a positive function to force into the transport equation avoids negative values of distribution function but is unsatisfactory since certain gross features of the solution are assumed before the problem is started.

In the hope that some insight could be gained into the form of solution, we have considered a special case of scattering that seems most appropriate to electrons in very high fields--i.e., electric field $\mathcal{E}_z$, a phonon scattering cross-section that is zero for $E < E_r$ and is a constant for $E > E_r$ where E_r is the optical phonon energy. We also assume that an optical phonon quantum, E_r, is lost on each scattering.

With this model of scattering, the rate of change of carriers in a spherical volume of momentum space can be calculated as the sum of scattering and drift in momentum space. The result of this calculation is the first equation of equation set (1).

A similar calculation for the moment p_z results in the second equation.

A calculation for the rates of change of second moments p_z^2 and p_x^2 results in two equations that are linearly dependent on the first three

---

[1] H. Fröhlich and B. V. Paranjape, Proc.Phys. Soc. (London), B69, 1956, p. 21.

[2] P. A. Wolff, Phys. Rev., 95, 1954, p. 1415.

[3] G. A. Baraff, Phys. Rev., 133, No. 1A, 1964, p. A26.

equations of equation set (1) etc. It thus appears that the various terms
of the equation set (1) are identical with conservation conditions on
moments of the electron distribution. This result is reasonable since
specification of $n_0(p)$ determines the "zeroth" moment, $n_1(p)$ deter-
mines the first moment, $n_0(p)$, $n_2(p)$ determines the second moment,
etc.

Any arbitrary choice for one of the $n_\ell(p)$ results in an arbitrary
choice of one of the moments and thereby can have a drastic effect on
the calculated distribution.

During the next quarter we will attempt to find a suitable criterion
for uniquely determining electron distribution.

PROJECT 5003:   ELECTRICAL AND OPTICAL PROPERTIES OF III-V COMPOUNDS

National Science Foundation Contract NSF-GP 1033
Project Leader: John L. Moll
Staff: Douglas H. Loescher

The purpose of this project is the fabrication and testing of
gallium phosphide diodes. Both the electrical and the luminescent
properties of the diodes will be measured. Also, the effect of simul-
taneous application of high temperatures and large reverse biases will
be studied. Both alloyed and diffused diodes will be examined.

In order to fabricate the diodes it is necessary to have an etch
for gallium phosphide. The etchants most often referenced in the litera-
ture are combinations of nitric and hydrochloric acid. All of these
etchants suffer the fault of attacking the wax used as a mesa mask nearly
as rapidly as the gallium phosphide. Because these HCl, HNO_3 combina-
tions are somewhat useful, the etch rates of the particular combination
1 HCl: 1 HNO_3 were measured. The rate was calculated from measured
weight losses and from the area of the sample. The rates were: 0 °C
5 microns/min, 27 °C 10 microns/min, 70 °C 37 microns/min. These rates
are reproducible to ±30% and refer to etching only the B or phosphorus
face. The rates were not measured on the A face. An etchant consisting
of methanol saturated with chlorine gas was also tried. This etch is
very fast; 17.5 micron/min, at room temperature on the B face, and does

not seem to attack the masking wax. Of all the etchants tried this last one seems to give the best surfaces and also is the easiest to use.

Experiments have also been conducted to determine materials suitable for use as ohmic contacts. Tin was tried as an n-type contact but required temperatures in excess of 700 °C to alloy at all and even higher temperatures were required to achieve good wetting. At this time gold zinc, which wets fairly well, seems to be a satisfactory p-type contact. An alloy of silver and tellurium has proved to be a useful n-type contact.

In making the diffused diodes it has proved necessary to add excess phosphorus to the diffusion ampoule. By adding the phosphorus it has been possible to prevent damage to the crystal surface during the diffusion. Without the phosphorus the depth of the surface damage exceeded the calculated diffusion depth. Using excess phosphorus it has been possible to make a diffused diode with a reverse breakdown of ten volts.

PROJECT 5005:   BAND STRUCTURE OF GALLIUM PHOSPHIDE

The objective of this project is the experimental determination of the electronic band structure of gallium phosphide over a wide range of temperature.

The investigation of the band structure of this material will consist of three areas of effort: 1) the measurement of the optical absorption in the region of the band edge, 2) the measurement of the optical reflectivity of the material in the vacuum ultraviolet, and 3) the measurement of photoemission from the material in this same range of photon energy. The second and third portions of this effort are just being begun with the construction of a chamber for reflectivity measurements and a preliminary photoemission tube now in progress. The first area is essentially completed and is described herein.

A.   OPTICAL ABSORPTION OF GALLIUM PHOSPHIDE NEAR THE ABSORPTION EDGE

In this report, the theory of the optical absorption of an indirect semiconductor near the band edge is reviewed for a comparison with

experimental results. Equipment is described for the measurement of the transmission of crystals at temperatures up to 900 °K and the results of preliminary measurements made on a gallium phosphide crystal are presented. The band gap is found to vary as a function of temperature as $E_g = 2.312 - 4.2 \times 10^{-4}$ T electron volts where T is in degrees Kelvin. The energy of the phonon (or combination of phonons) involved in the transition is found to be about 0.034 ev for temperatures in the 200 °K to 600 °K range.

B. THEORY

The theoretical analysis of the optical properties of indirect semiconductors has been carried out by a number of workers [Ref. 1]. In a photon-induced transition between a valence band maximum at $k = 0$ and a conduction band minimum at $k_m \neq 0$, a phonon (or phonons) must be emitted or absorbed in the process in order to conserve momentum. Since the probability of the process going with the absorption of a phonon is proportional to the number of phonons present, N_s, and the probability of phonon emission is proportional to $N_s + 1$, the absorption coefficient for the material near the band edge should vary as

$$\alpha h\nu = \text{const} \left[N_s \left(h\nu - E_g + E_{ph} \right)^2 + \left(N_s + 1 \right) \left(h\nu - E_g - E_{ph} \right)^2 \right] \tag{1}$$

where $h\nu$ is the photon energy, α the absorption coefficient, E_g the energy gap, and E_{ph} the energy of the assisting phonon.

The number of phonons of energy E_{ph} is given by

$$N_s = N \frac{1}{e^{E_{ph}/kT} - 1} \tag{2}$$

which substituted into Eq. (1) gives

$$\alpha h\nu = \text{const} \left[\frac{\left(h\nu - E_g + E_{ph} \right)^2}{e^{E_{ph}/kT} - 1} + \frac{\left(h\nu - E_g - E_{ph} \right)^2}{1 - e^{-E_{ph}/kT}} \right] \tag{3}$$

---

[1]Smith, Semiconductors, Cambridge Press, London, pp. 201-210.

Expanding (3) and writing it in terms of the hyperbolic cotangent we have

$$\alpha h\nu = \text{const} \left\{ (h\nu - E_g)^2 \coth \frac{E_{ph}}{2kT} - 2(h\nu - E_g) E_{ph} + E_{ph}^2 \coth \frac{E_{ph}}{2kT} \right\} .$$ (4)

Since

$$\coth \frac{E_{ph}}{2kT} \left(h\nu - E_g - E_{ph} \tanh \frac{E_{ph}}{2kT} \right)^2$$

$$= \left(h\nu - E_g \right)^2 \coth \frac{E_{ph}}{2kT} - 2(h\nu - E_g) E_{ph} + E_{ph}^2 \tanh \frac{E_{ph}}{2kT} ,$$ (5)

we may approximate (4) by (5) in the higher absorption region where $\left(h\nu - E_g \right)^2 \coth \frac{E_{ph}}{2kT} \gg E_{ph}^2 \left(\coth \frac{E_{ph}}{2kT} - \tanh \frac{E_{ph}}{2kT} \right)$. Hence for $h\nu$ somewhat greater than $E_g + E_{ph}$ we have

$$\alpha h\nu = A \left(\coth \frac{E_{ph}}{2kT} \right) \left(h\nu - E_g - E_{ph} \tanh \frac{E_{ph}}{2kT} \right)^2 \quad \text{for} \quad h\nu > E_g + E_{ph} .$$ (6)

For photon energies between $E_g - E_{ph}$ and $E_g + E_{ph}$ the second term in Eq. (1) and Eq. (3) is zero and we have

$$\alpha h\nu = A \frac{\left(h\nu - E_g + E_{ph} \right)^2}{e^{E_{ph}/kT} - 1} \quad \text{for} \quad E_g - E_{ph} < h\nu < E_g + E_{ph}$$ (7)

where A is the same constant as in (6). For photon energies below $E_g - E_{ph}$, the absorption should be zero

From Eq. (6) and Eq. (7), we see a plot of $(\alpha h\nu)^{1/2}$ vs $h\nu$ should consist of two straight line segments as shown in Fig. 66. If both segments of this curve are experimentally observed at a single temperature then the value of the energy gap and assisting phonon energies may be calculated from the intercepts with the $\alpha h\nu = 0$ axis. If only the higher absorption segment of the curve is experimentally observed, then

THEORETICAL BAND EDGE ABSORPTION CURVE
FOR AN INDIRECT SEMICONDUCTOR

SLOPE B

$E_o - E_g + E_{pH} TANH \frac{E_{pH}}{2kT}$

$E_g - E_{pH}$

E_o

PHOTON ENERGY $h\nu$

$(\alpha h\nu)^{1/2}$
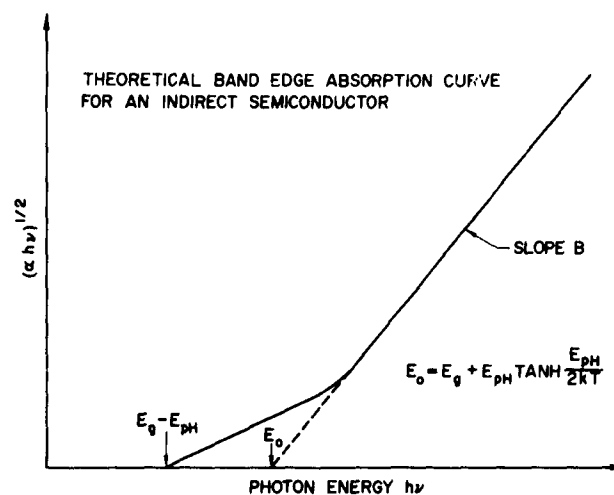
FIG. 66. THEORETICAL $(\alpha h\nu)^{1/2}$ vs $h\nu$ CURVE.

E_g and E_{ph} may still be obtained if measurements are carried out over a range of temperatures. The method of doing this is to observe that the slope of the $(\alpha h\nu)^{1/2}$ curve should be proportional to $(\coth E_{ph}/2kT)^{1/2}$ and hence the value of E_{ph} is selected which best fits the measured slope vs temperature relation. Knowing the value of E_{ph}, one may calculate the value of E_g as a function of temperature from the intercept of the curve.

C. MEASUREMENT EQUIPMENT

The experimental measurements were carried out on gallium phosphide, a semiconductor of special interest for its possible use at high temperatures. Because of this possible high temperature applicability, it was decided to study the material over a temperature range of from -50 °C up to 600 °C. In order to carry out useful measurements for the determination of E_{ph} and E_g, as described previously, good optical equipment combined with close temperature control of the sample is essential. In addition, for the higher temperatures the sample must be protected from deterioration by oxidation, etc.

In order to satisfy these measurement requirements, a vacuum dewar with a temperature-feedback-controlled sample heater was constructed for use in the Cary Model 14 recording spectrophotometer. The center tube

of the dewar is filled with liquid nitrogen to act as a coolant for
below-room temperature measurements and as a "cold finger" to maintain
a better vacuum. The gallium phosphide disc is mounted in a steel tube
(for a constant-temperature environment) which is loosely thermally
coupled to the cold finger. Two thermocouples are mounted near the
sample in the tube: one is used to monitor the sample temperature and
the other to provide the temperature feedback for the temperature-control
mechanism. The heater is wrapped around the outside of the sample tube
and is driven by a transistor amplifier. The feedback control mechanism
provides a stable sample temperature which may be easily kept within a
degree of any desired temperature.

D. EXPERIMENTAL RESULTS

The output of the spectrophotometer obtained at a given temperature
is a graph of optical density vs wavelength, where the optical density
is defined as

$$\text{optical density} = \log_{10}\left(\frac{\text{Incident Intensity}}{\text{Transmitted Intensity}}\right). \qquad (8)$$

The transmitted intensity will be less than the incident intensity due to
surface reflections, bulk absorption as described by Eq. 6 and Eq. 7,
and so-called "free carrier" absorption. Since we are interested only
in the second of these contributions, we wish to compensate for the re-
flection and free carrier contributions. We do this by noting that below
the absorption edge these are the only contributions to the sample absorp-
tion and that, ignoring multiple reflections, their contributions should
remain relatively constant in the region of the band edge. Hence the
optical density curve is corrected by extrapolating the below-band edge
absorption to the band edge region and subtracting this value from the
observed optical density to get the desired electronic contribution [Ref.
2]. The absorption coefficient defined by $I_x = I_0 e^{-\alpha x}$ is then given
by

$$= \frac{\log_e 10}{\alpha} \text{ optical density} = \frac{2.3026}{d} \text{ optical density} \qquad (9)$$

where d is the thickness of the sample.

[2] G. G. MacFarlane and V. Roberts, Phys. Rev., 97, 1714; ibid., 98, 1865

The measurements were made on a gallium phosphide sample grown by the float zone technique and sulfur doped to 0.1 to 0.2 ohm-cm resistivity at room temperature. A typical $(\alpha h\nu)^{1/2}$ vs $h\nu$ curve is shown in Fig. 67 for a temperature of 400 °C. It is noted that while the points
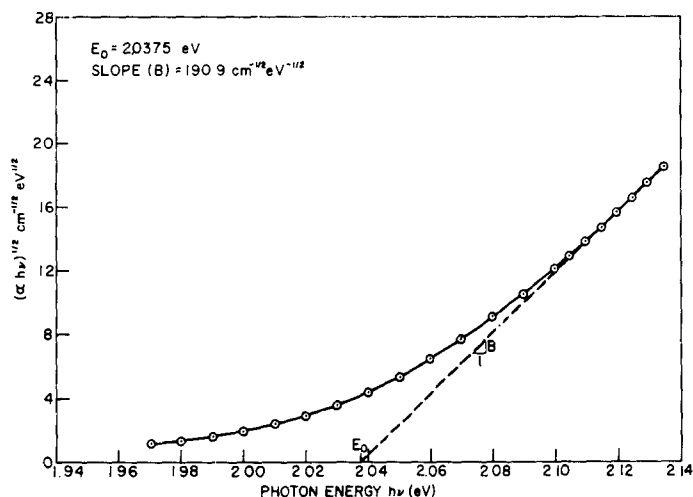
FIG. 67. $(\alpha h\nu)^{1/2}$ VS $h\nu$ FOR GaP SAMPLE AT 400 °C.

fit a nice straight line at higher values of α, on the low-energy end the curve tails off into an exponential. Figure 68 shows that for over an order of magnitude in absorption in this tail the curve fits an exponential very accurately. This $\alpha = \alpha_o e^{h\nu/s}$ type of dependence of absorption at low α is known as an "Urback tail" and is found in most of the less-pure semiconductors. The effect here is to make it impossible to see any distinct lower segment of the absorption curve and hence the second technique mentioned for evaluating E_{ph} and E_g must be used.

The absorption curves of $(\alpha h\nu)^{1/2}$ vs $h\nu$ for various temperatures are shown in Fig. 69. The slopes of these curves (squared) are plotted in Fig. 70 together with the "best fit" coth $E_{ph}/2kT$ curve which is obtained for $E_{ph} = 0.034$ ev. It should be noted that this value of E_{ph} fits the points accurately only up to about 400 °C whereupon the slopes fall below the expected values. The energy gap calculated using
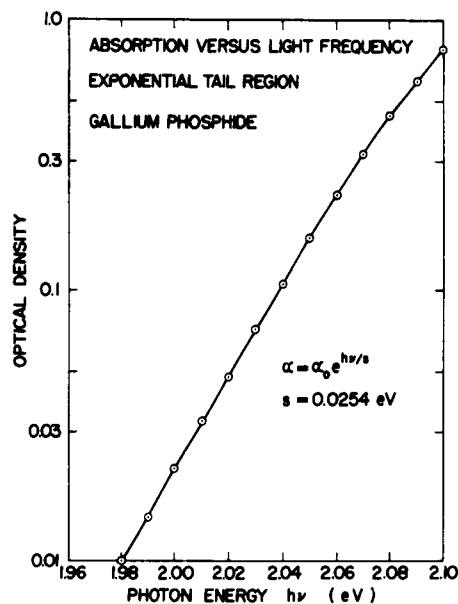
FIG. 68. OPTICAL DENSITY VS hν
FOR GaP AT 400 °C.
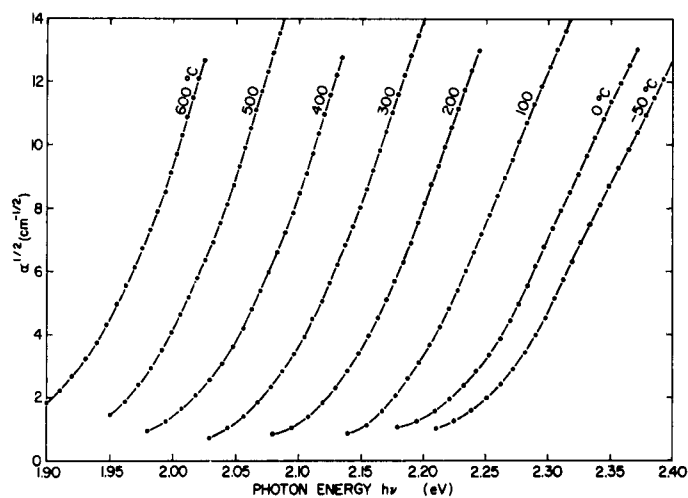
FIG. 69. TRANSMISSION CURVES OF GaP AT
VARIOUS TEMPERATURES $\alpha^{1/2}$ VS hν.

this value of phonon energy is graphed vs temperature in Fig. 71. For
temperatures up to 400 °C the energy gap relation is

$$E_g = 2.312 - 4.2 \times 10^{-4} \, T \text{ ev}$$
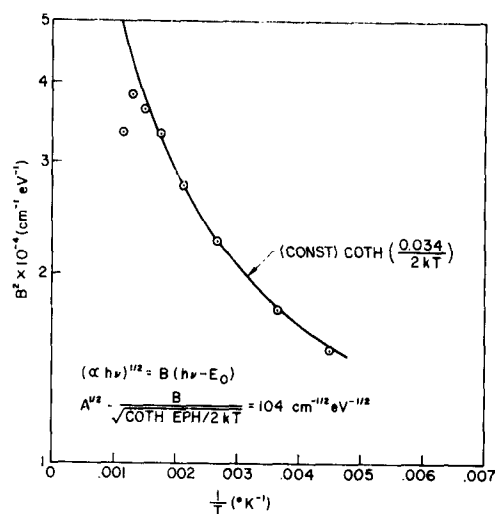
FIG. 70. SEMILOG PLOT OF B^2 AND
COTH $(0.034/2kT)$ PLOTTED VS $1/T$
DATA POINTS FOR GALLIUM PHOSPHIDE.
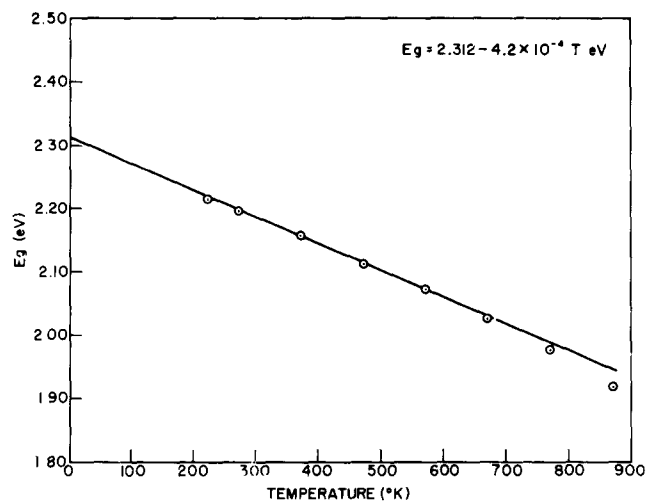
FIG. 71. ENERGY CAP VS TEMPERATURE FOR
GALLIUM PHOSPHIDE.

with all points within 0.005 ev of this. At higher temperatures the
energy gap drops below this curve (about 0.028 ev below at 600 °C).

E. DISCUSSION

The results of the measurements on the GaP sample agree very well
with the theory, perhaps even better than one would expect considering

the fact that the theory discussed considers only one type of assisting phonon whereas the phonon dispersion relation is actually quite complex and a number of different phonons could be involved in this transition. The fact that the slope data for temperatures between -50 °C and 400 °C can be fitted to good accuracy with a single phonon energy indicates that in this temperature range, one phonon (or combination of phonons) predominates in the transition. It is not particularly surprising that at higher temperatures (600 °C) this might change somewhat.

The only significant variation of the observed results from the theory is in the presence of the exponential tail on the absorption curve. This tail is probably due to the presence of impurities in the sample. One mechanism explaining the production of such a tail by charged impurities has been discussed by Redfield [Ref. 3]. Redfield calculates the effect on the absorption characteristic produced by high electric fields surrounding charged impurities acting on the crystal absorption through the Franz-Keldysh effect. For the case of a direct-bandgap material he finds the $\alpha(E_g)$ (the absorption coefficient at the energy gap) should vary as the nine halves power of the charged impurity density. His calculations are in good agreement with the measurements of Dixon and Ellis on InAs. Though the exponent would probably be different, the absorption in GaP ought to be similarly affected by changes in concentration of charged impurities. Since the number of charged impurities in GaP should vary with temperature for a reasonably deep impurity level, $\alpha(E_g)$ should likewise vary with temperature. In Fig. 72, $\alpha(E_g)$ decreases proportionally to $1/T$ which is what would be predicted for the contribution of a single donor level. Since the theory of this effect in an indirect transition semiconductor has not been worked out, no further correlations as to energy levels, etc., is possible.

In summary, the agreement between the measured band edge optical absorption of gallium phosphide and that predicted from theory is quite good. The value of the energy gap of $2.312 - 4.2 \times 10^{-4}T$ ev agrees well

---

[3]D. Redfield, Phys. Rev., 130, 916 (1963).
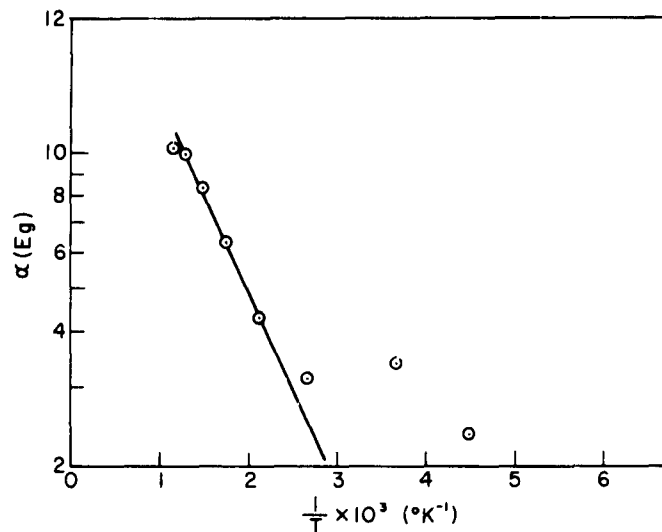
FIG. 72. $\alpha(E_g)$ VS $1/T$.

with that obtained by other workers [Ref. 4]. The energy for the con-
tributing phonon(s) in the transition of 0.034 ev is reasonable but
since neutron diffraction data on the phonon spectrum is not available
for GaP it cannot be accurately checked. It is hoped that purer samples
of GaP will become available for measurement to determine further the
effect of impurities on the observed exponential tail.

PROJECT 5006:   EPITAXIAL GROWTH OF GaP

National Aeronautics and Space Administration
Grant NsG 555
Project Leaders: J. L. Moll and G. L. Pearson
Staff: T. Koike

The purpose of this project is to apply the close-spaced epitaxial
growth technique to GaP in order to study its optical and electrical
properties.

4
M. Gershenzon, D. G. Thomas, and R. E. Dietz, Proc. International
Conference Semiconductor Physics, Exeter, 1962, The Institute of
Physics and the Physical Society, London, 1962, p. 752.

GaP is transported to a GaAs substrate as described in the previous report. The epitaxial deposition system is shown in Fig. 73. The quartz reaction tube contains two carbon blocks and in between these two carbon blocks the GaP polycrystalline source is separated by 20 to 40 mils from the GaAs substrate. The temperature difference is set by the relative position of the rf coil and the carbon blocks. The amount of water vapor is controlled by passing the hydrogen over ice which is maintained in the salt-ice bath.
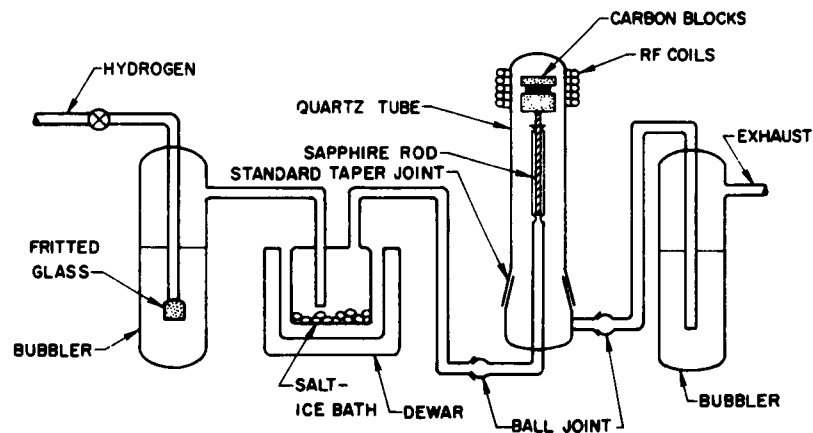
FIG. 73. THE EPITAXIAL GROWTH SYSTEM.

The system has been operated in most cases with considerable success and single crystal epitaxial layers of various thickness have been produced. Some of the grown crystals were tested by the Kossel line technique and were found to be high-quality single crystals. Although we have proved the feasibility of this technique, we have not yet acquired the best operating conditions because of many factors to be taken into consideration. Such factors are:

1. Source temperature
2. Substrate temperature
3. Temperature difference

4. Spacing

5. Flow rate and water content of the hydrogen gas

6. Substrate composition, etc.

Research on the interdependences of these factors is being continued to obtain a reproducible growing technique.

The future work is aimed at establishing this technique and applying it to the epitaxial growth of $GaP_x As_{(1-x)}$.

PROJECT 5054: STUDY OF HOT ELECTRONS IN SILICON

Signal Corps Contract DA 36-039 SC-85339
Project Leader: J. L. Moll
Staff: Gerald Lewis

During this quarter work was continued on the experiment to measure electron emission from cesiated clean silicon surfaces. Work was completed on a vacuum tube for etching and cesiating a silicon chip and measuring emitted currents under various conditions of bias.

A final report is in preparation.

PROJECT 5059: HOT ELECTRONS IN THIN METAL FILMS

Air Force Contract AF33(657)-11586
Project Leader: J. L. Moll
Staff: P. H. Bardell

This project is concerned with experimental and theoretical studies of high-energy electrons in thin metal films.

During the past quarter, the hot-electron range in thin copper films deposited on chemically cleaned silicon surfaces has been measured. These data have been combined with the resistivity data mentioned in QRR No. 8 to determine the electron-electron scattering length.

The measured resistivity of copper films deposited on chemically cleaned, mechanically polished (111) faces of silicon crystals is shown in Fig. 74. When the resistivity was measured at lower temperatures, it exhibited a higher temperature coefficient of resistivity than bulk material. This result was attributed to gross imperfections and discontinuities which resulted in a longer current path than expected from
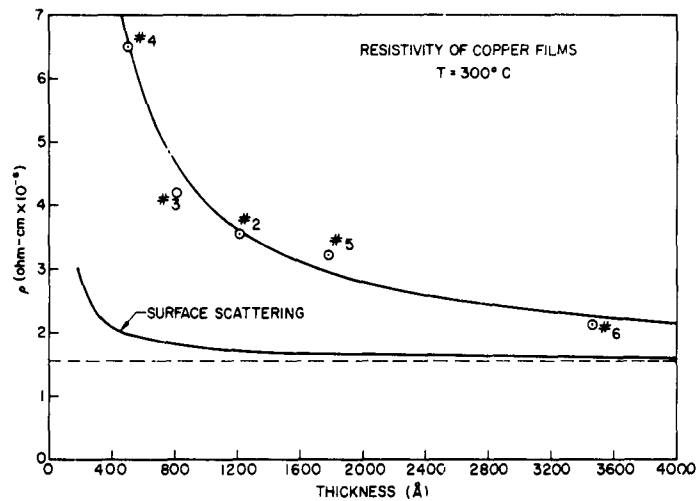
FIG. 74. RESISTIVITY OF COPPER FILMS (300 °K).

the geometry of the sample. When the resistivity was corrected for this geometrical factor, a large component of resistance remains, which is due to imperfection scattering. The scattering center density is constant for films up to 800Å thick, but decreases rapidly for thicker films. These data were used to determine a composite conductivity mean-free-path (ℓ_c) which varies with thickness and temperature. Figure 75 shows this result.
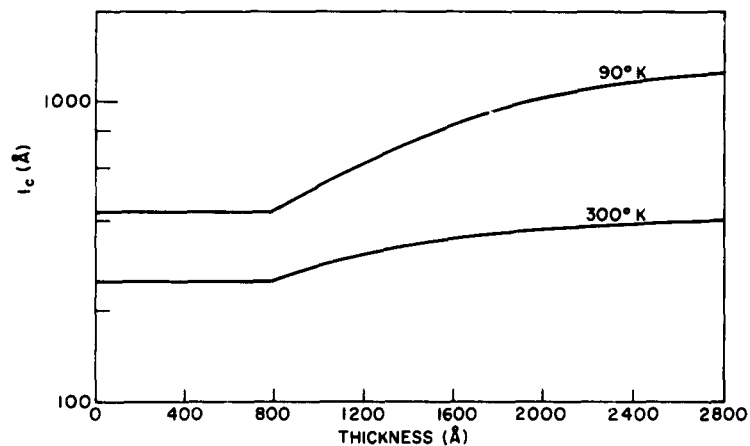
FIG. 75. CONDUCTIVITY MEAN-FREE-PATH FOR COPPER FILMS.

In order to extract the electron-electron scattering length (ℓ_e) from the measured values of hot-electron range, the transport process was analyzed using age theory and Monte Carlo techniques. Age theory predicts that the hot-electron range is a composite function of ℓ_e and ℓ_c,

$$L = \sqrt{\frac{\ell_e^2 \ell_c}{3(\ell_e + \ell_c)}} \qquad (1)$$

Under the assumption that $\ell_e \gg \ell_c$, Eq. (1) becomes

$$L \approx \sqrt{\frac{\ell_e \ell_c}{3}} \qquad (2)$$

When ℓ_c is a function of film thickness as is the case with the copper films studied, we have

$$L(w) = L_{ref}\sqrt{\frac{\ell w}{\ell_{ref}}} \qquad (3)$$

where ℓ_{ref} and L_{ref} are the conductivity mean-free-path and hot-electron range, respectively, for a film of a reference thickness. To plot the yield data in such a manner as to obtain a meaningful value of range, the data are normalized to a common scattering center density by defining an effective thickness in the following manner: The yield is written as,

$$Y_f = K\, e^{-\frac{w}{L_{ref}}} \sqrt{\frac{\ell_{ref}}{\ell w}} \qquad (4)$$

and we define $w' = w\sqrt{\ell_{ref}/\ell w}$. Thus L_{ref} is obtained from a plot of ln Y vs w' as shown in Fig. 76. In this manner, a hot-electron range of 280Å is obtained for electrons 0.61 ev above the Fermi level. The value ℓ_e which corresponds to this value of range was found to be 1100Å by both age theory and Monte Carlo analysis. This result, plus some range values at different energies is shown in Fig. 77.
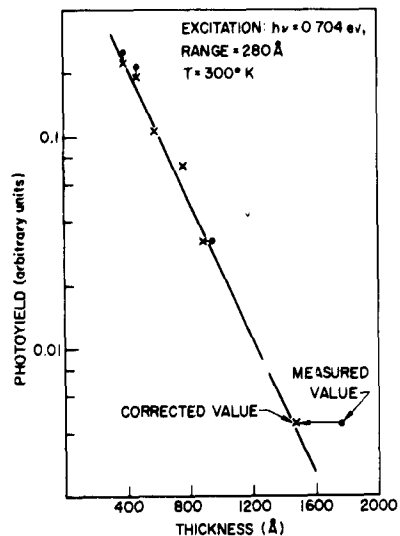
FIG. 76. PHOTOYIELD VS THICKNESS--300 °K COPPER FILM (CORRECTED FOR ABSORPTION AND SCATTERING NORMALIZED TO 800Å).
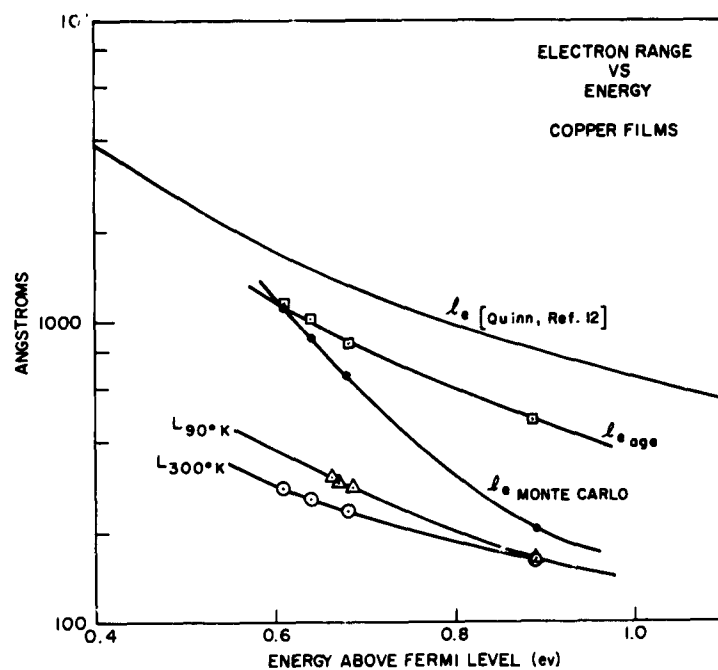
FIG. 77. ELECTRON RANGE AND ELECTRON-ELECTRON SCATTERING LENGTHS VS ENERGY.

The work on hot-electron transport in copper has been completed and a report is in preparation which gives full details of the experimental results and their interpretation.

In order to investigate the effects of surface preparation and sur-
face roughness on gold films deposited on silicon substrates, a series of
resistivity and photoyield measurements were made on gold films evaporated
onto chemically cleaned, mechanically polished surfaces.

The room-temperature resistivity of the gold films is shown in Fig.
78. Annealing effects at room temperature were noted on the films thinner
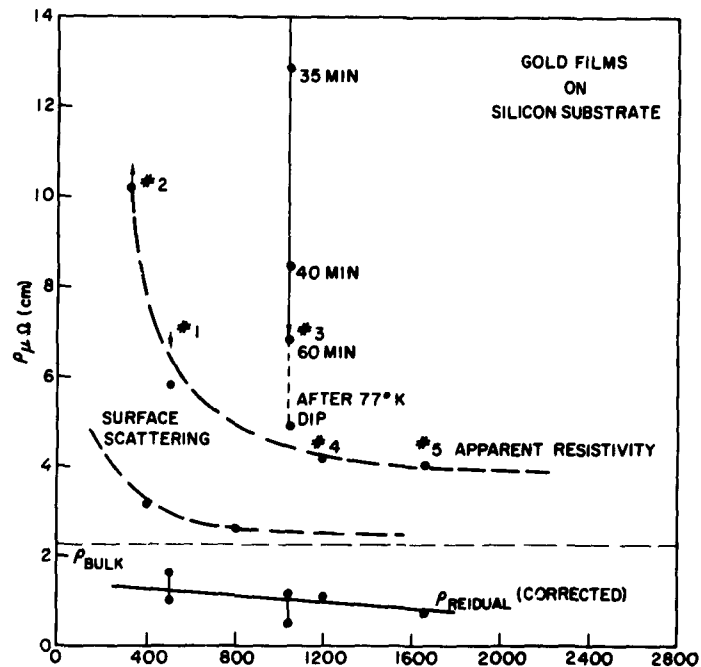
FIG. 78. RESISTIVITY OF GOLD FILMS (300 °K).

than 1100Å, especially the sample which was 1042Å thick. This sample
rapidly annealed to a resistivity of 6.76×10^{-6} ohm-cm according to
the relation

$$\rho - 6.76 = 500 \exp(-\alpha t) \times 10^{-6} \text{ ohm-cm} \qquad (5)$$

where $\alpha = 0.133 \text{ min}^{-1}$

After 24 hours, the film was immersed in liquid nitrogen and its 77 °K
resistivity was measured. Upon returning to room temperature, the

resistivity was 5.05 $\mu\Omega$-cm. This value of resistivity persisted after repeated temperature cycling.

The residual resistivity, determined in a manner similar to that for copper films, did not show any strong thickness dependence out to 1600Å, the limit of the measurements. This marked contrast with the copper resistivity data indicates that the structure of the gold films is different from that of copper. The conductivity mean-free path determined from the data is 260Å at 300 °K, independent of thickness.

Photoyield measurements were taken and the data appear in the form of Fowler plots in Fig. 79. Before the hot-electron range can be extracted from these data, it must be corrected for photon absorption. Crowell, et al [Ref. 1] measured the transmission and reflection of thin gold films deposited on quartz. The absorption calculated from these data is shown in Fig. 80. When the photoyield data is corrected for
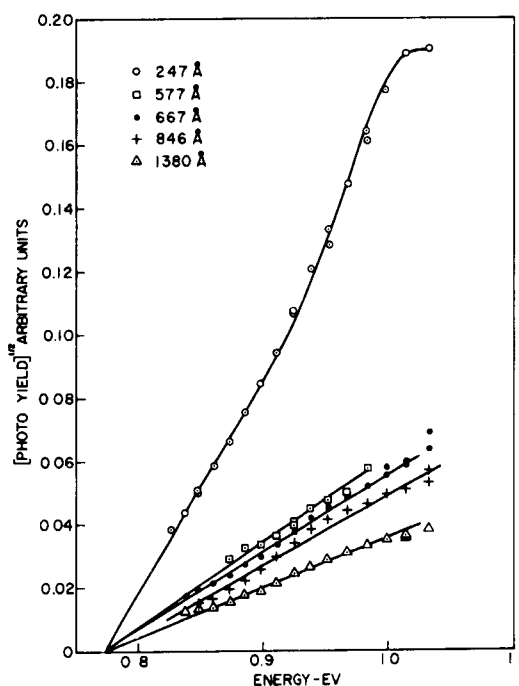
FIG. 79. FOWLER PLOT OF GOLD FILM PHOTOYIELD.

[1] C. R. Crowell, W. G. Spitzer, L. E. Howarth, and E. E. LaBate, "Attenuation Length Measurements of Hot Electrons in Metal Films," Physical Review, 127, p. 2006, 1962.
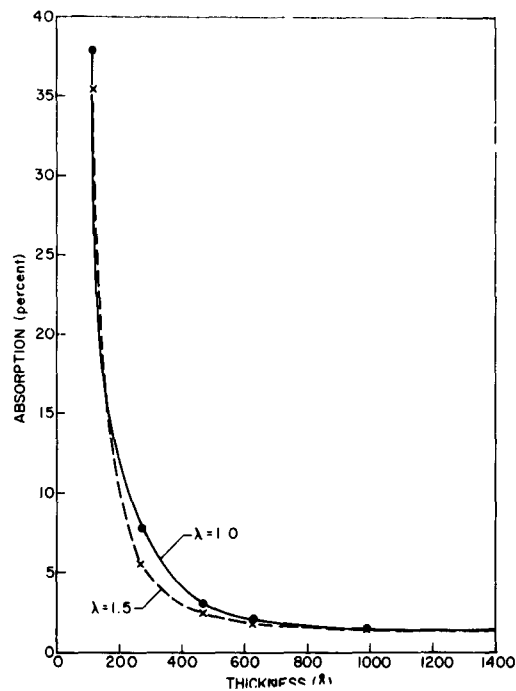
FIG. 80. MEASURED ABSORPTION OF
GOLD FILMS.

absorption, the yield vs thickness plot is as shown in Fig. 81. While
the indicated hot-electron range is in excess of 800Å, the actual value
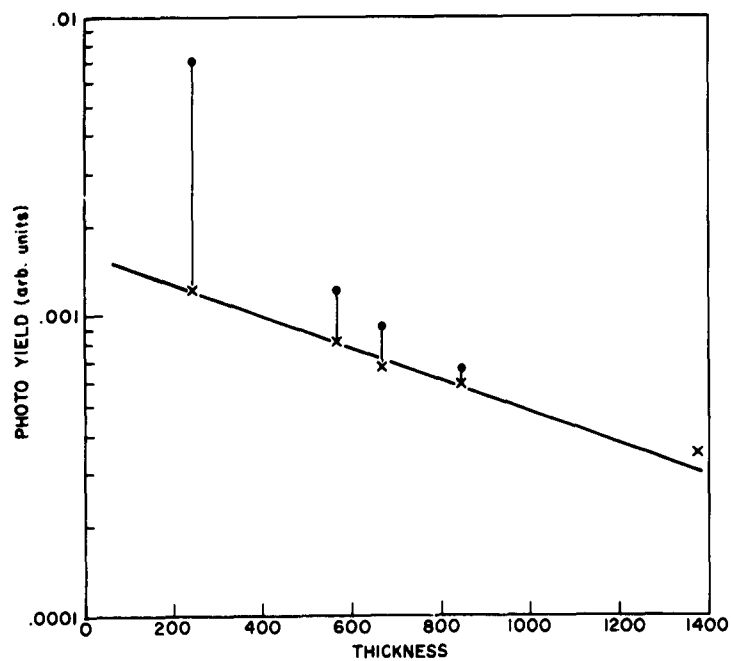
FIG. 81. PHOTOYIELD OF GOLD FILMS VS THICKNESS
(300 °K) CORRECTED FOR ABSORPTION.

is in some question. After testing, the gold films were examined visually under high-power magnification. The surface of the silicon substrates had quite a bit of roughness on a small scale in the form of scratches from polishing and pits of unknown origin. The photo response is very sensitive to surface irregularities of this type and therefore these results, which agree in general with those of Crowell, et al [Ref. 1] and Sze [Ref. 2], are not to be considered conclusive evidence of the attenuation length of hot electrons in gold films on silicon.

PROJECT 5064:   STUDIES OF LUMINESCENCE CENTERS IN SEMICONDUCTING
                COMPOUNDS

        Tri-Service Contract Nonr-225(24)
        Project Leader: J. L. Moll
        Staff: Bevan P. F. Wu

The purpose of this project is to study the properties of luminescence centers in semiconducting compounds.

A. GALLIUM PHOSPHIDE

    1. Electrical Measurement of GaP Crystals

The theoretical mobility of electrons and holes in GaP at different temperatures were calculated. The impurity-scattering-limited mobility of electrons and holes at different impurity concentrations were calculated by using the Conwell-Weisskopf formula;

$$\mu_I = \frac{3 \times 10^{15} \left(\frac{\epsilon}{\epsilon_o}\right)^2 T^{3/2}}{N_I \ln \left(1 + \frac{3 \times 10^6 \left(\frac{\epsilon}{\epsilon_o}\right)^2 T^2}{N_I^{2/3}}\right)} \tag{1}$$

where μ_I = impurity-scattering-limited mobility in cm^2/volt-sec

        $\left(\frac{\epsilon}{\epsilon_o}\right) = 10$

---

[2] S. M. Sze, "Hot Electrons in Thin Gold Films," SEL-63-032.

T = temperature in $^\circ K$

N_I = impurity concentration in cm^{-3}

In these calculations the ratio of effective mass of the carrier to the electron rest mass was assumed to be unity. The calculated curves of impurity-scattering-limited mobility vs temperature for GaP with different impurity concentrations are plotted in Fig. 82. The lattice mobility of electrons and holes at 300 $^\circ K$ were 110 cm^2/v-sec and 75 cm^2/v-sec respectively. The temperature dependence of lattice mobility
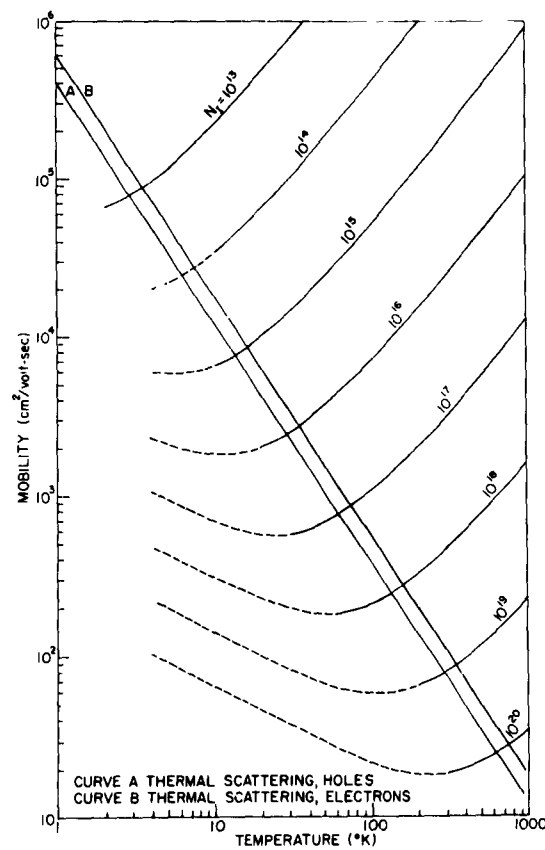
FIG. 82. IMPURITY AND LATTICE (THERMAL)SCATTERING VS TEMPERATURE FOR GaP (WITH m/m_{eff} = 1).

for both electrons and holes in GaP follow the temperature to the $-3/2$ power law. The averaging of lattice scattering effect and ionized impurity scattering effect on mobility was based on Conwell's relationship. The usual inverse averaging relationship, $1/\mu = 1/\mu_L + 1/\mu_I$ was also used for the purpose of comparison. The calculated curves of mobility vs temperature for GaP with different impurity concentrations are plotted in Fig. 83 and Fig. 84. The measured mobility data of solution grown GaP crystals are also plotted in Fig. 84.
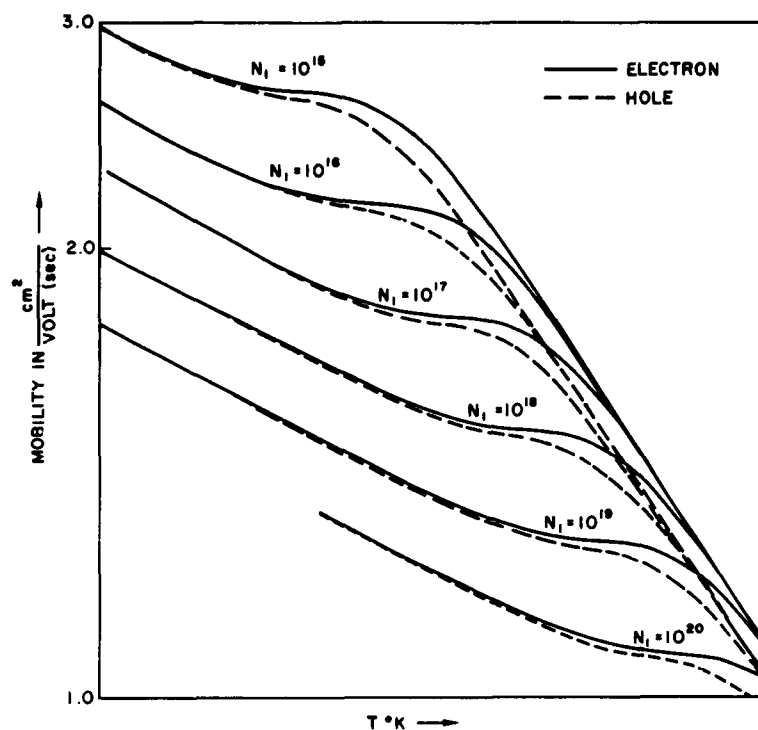
FIG. 83. MOBILITY VS TEMPERATURE CURVES FOR GaP
$\left(1/\mu = 1/\mu_L + 1/\mu_I \right).$
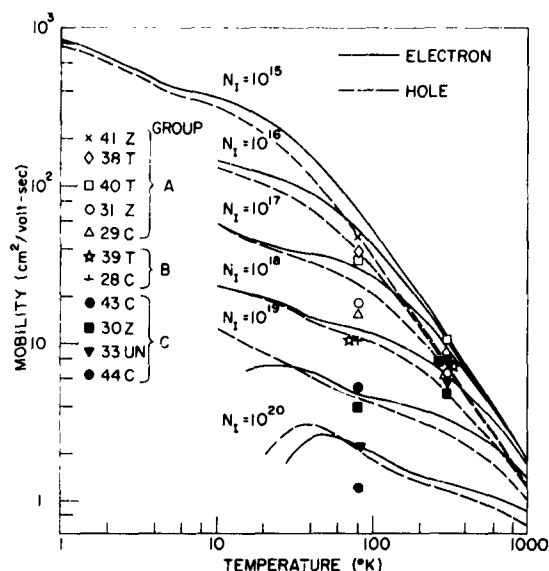
FIG. 84. MOBILITY VS TEMPERATURE CURVES
FOR GaP WITH MEASURED DATA OF SOLUTION-
GROWN GaP SAMPLES.

From the mobility data (see Fig. 84), the measured GaP crystals may
be divided into three following groups.

TABLE I

	Group A	Group B	Group C
Gap Sample Number	41Z 38T 40T 31Z 29C	39T 28C	43C 30Z 33UN 44C

For samples in Group A, the temperature dependences of measured mobility
values are generally in agreement with calculated values. For samples in
Group B, the measured results show deviation within an order of magnitude
at 77 °K from calculated values. The measured results of Group C samples
show more than an order of magnitude deviation at 77 °K. This phenomenon
suggests that the samples in Group C are highly compensated, i.e., the

effect of impurity scattering of $\left(N_A + N_D\right)$ is larger than that of N_A or N_D alone. In previous mobility calculations, only the scattering effect of N_A or N_D was assumed. N_A is the acceptor concentration, and N_D is the donor concentration in GaP crystals

2. Red Photoluminescence Measurement of GaP Crystals

The effects of excitation light intensity on red photoluminescence in GaP crystals are shown in Fig. 85 and Fig. 86. In Fig. 85 the intensity of the red photoluminescence peak was reduced as the intensity of excitation was reduced. From experimental data the following relation is deduced.

$$I_E = A \ I_R^{3/2} \tag{2}$$
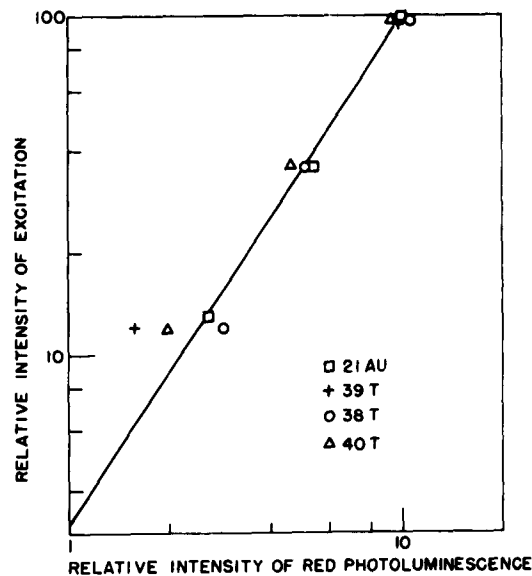
FIG. 85. RED PHOTOLUMINESCENCE
VS EXCITATION INTENSITY.

where

I_R = relative intensity of red photoluminescence peak

I_E = relative intensity of excitation light

A = a constant
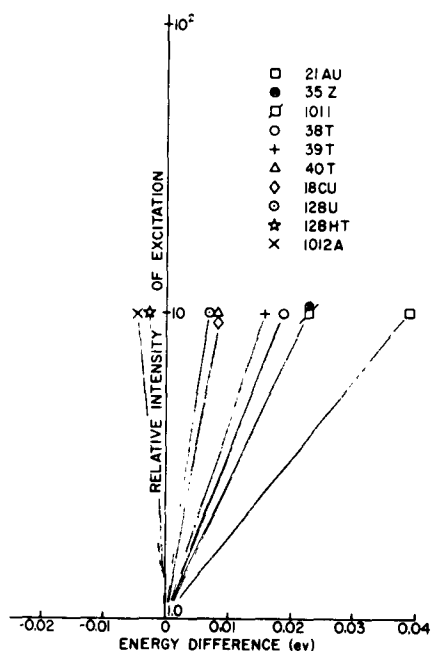
FIG. 86. THE SHIFT OF RED PHOTO-
LUMINESCENCE PEAK VS INTENSITY OF
EXCITATION.

In Fig. 86 the shift of the red photoluminescence peak vs relative ex-
citation intensity are plotted. In a majority of the GaP crystals the
red photoluminescence peak shifted to longer wave lengths as the inten-
sity of excitation was reduced. The exceptions were the two GaP poly-
crystals after heat treatment (No. 128 HT and 1012A). The red peak of
those two samples shifted to shorter wave lengths as the intensity of
excitation was reduced. The relative intensity of red photoluminescence
of different GaP cyrstals covered a wide range. The results are shown
in Fig. 87. The crystals may be grouped into three groups according to
their intensity of red photoluminescence. The Te-doped and Zn-doped GaP
crystals showed very strong red photoluminescence. The Cd-doped and Cd-
compensated (n-type) GaP crystal had medium intensity of red photolumi-
nescence. The Cu-doped and undoped GaP crystals had very weak red
photoluminescence.

TABLE II.

	Group I Relative Intensity $\sim 10^4$		Group II Relative Intensity $\sim 10^3$	Group III Relative Intensity ~ 10
Sample Number	41Z 39T 128U 40T 31Z 29C		28C 128HT 21AU 35Z 44C 30T 30Z	1012A 18CU 55 33UN
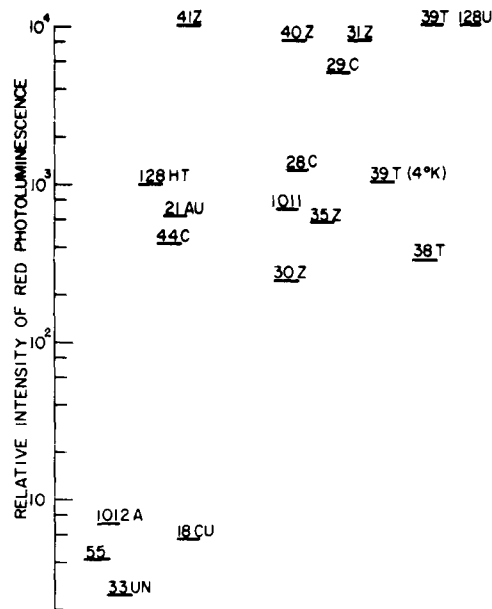
FIG. 87. RELATIVE RED PHOTOLUMINESCENCE OF DIFFERENT GaP CRYSTALS.

The data of relative intensity of red photoluminescence of GaP crystals with different concentration of doping are plotted in Fig. 88. The Zn-doped GaP has maximum intensity with a majority carrier concentration of 10^{17} cm^{-3}. The Te-doped GaP has a maximum intensity with a majority carrier concentration of 10^{18} cm^{-3}. These data give a general direction of doping in creation of red photoluminescence in GaP crystals.
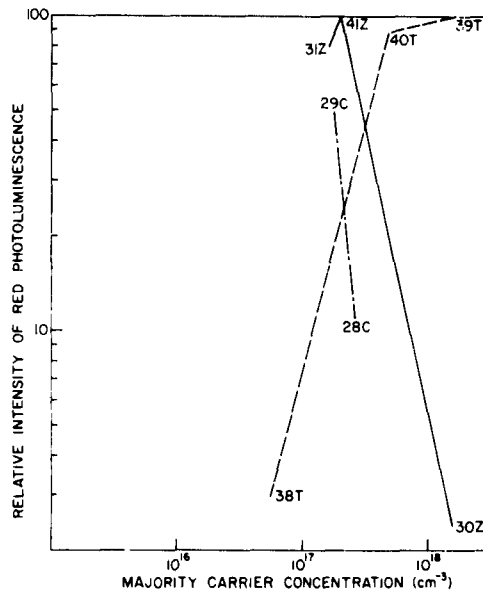
FIG. 88. RELATIVE INTENSITY OF RED
PHOTOLUMINESCENCE VS MAJORITY
CARRIER CONCENTRATION.

3. Optical Absorption Measurement

The optical absorption measurement of GaP was performed in the
following two regions:

1. Infrared region (2.0 to 15.0 micron in wavelength)
2. Visible region (0.45 to 0.7 micron in wavelength)

A Perkin-Elmer Model 21 double-beam spectrometer was used in the
infrared region for fast surveying measurements. The measured region
extended from 2.0 micron to 15.0 micron. If any absorption peak was
found in the infrared region by the surveying run, that particular region
was measured in detail by a Perkin-Elmer Model 112 single-beam spectrom-
eter. The sample-in and sample-out measuring technique was employed for
the single-beam machine. The absorption coefficient of the measured
sample was calculated by a computer from the measured data. Both spec-
trometers were constantly flushed by dry nitrogen gas during the
measurement.

A Carry Model 14 double beam spectrometer was used for absorption
measurement in the visible region.

Two dewars were used for the double beam spectrometer, one was placed in the path of the sample beam, and the other was placed in the path of the reference beam. The two dewars had the same aperture opening which restricted the area for the light beam to pass. Both dewars had the same kind of optical windows. In the case of the single beam spectrometer only one dewar was used. The sample-in and sample-out measuring processes were accomplished by rotating the sample holder of the dewar of 90 deg horizontally. A schematic diagram of the structure of the dewar is shown in Fig. 89.
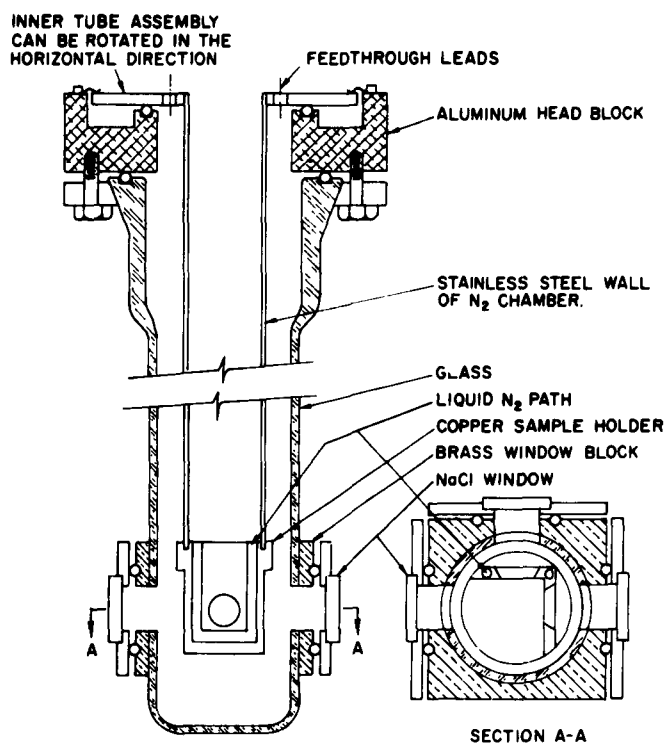
FIG. 89. LIQUID NITROGEN DEWAR FOR OPTICAL
ABSORPTION MEASUREMENT.

The GaP crystals for the optical absorption measurement were the same crystals used in the photoluminescence measurement. They were all optically polished on both surfaces, and were etched in aqua regia for 30 seconds. The thickness of the samples ranged from 0.001 cm to 0.1 cm.

The absorption of GaP crystals were measured at 100 °K and 300 °K. The absorption measurements in the visible region were attempted to find the optical absorption band corresponding to the red photoluminescence process. GaP samples with red photoluminescence were measured in the spectrum region from 6000$\overset{\circ}{A}$ to 4500$\overset{\circ}{A}$. No absorption band was found in any of the GaP samples in this region except the edge absorption near the energy band gap. It is possible that the absorption corresponding to the red photoluminescence was too small to be detected against the free-carrier absorption background. The physical size of the GaP sample also reduced the sensitivity by restricting the light-beam passage area to the size of the sample, which ranged from 2 mm^2 to 15 mm^2. Two typical absorption curves of GaP crystals in the visible region are shown in Figs. 90 and 91. They are not corrected for reflection. The infrared
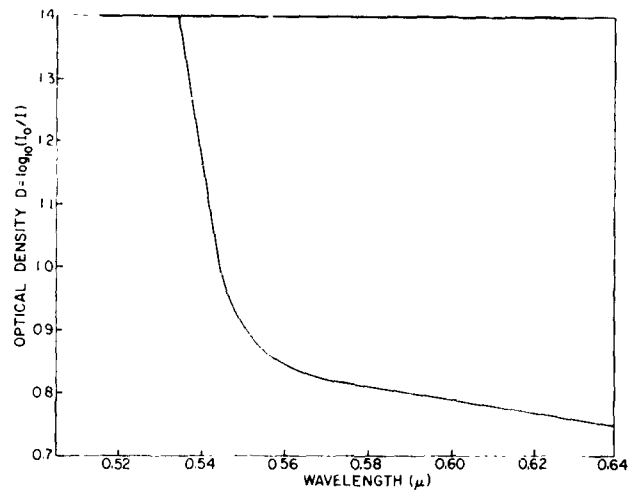
FIG. 90. ABSORPTION MEASUREMENT OF GaP
NO. 39T AT 300 °K.

absorption measurements were made between 2.0 micron and 14.0 micron in wavelength. The combination lattice absorption bands at 12.75μ, 13.25μ, 13.55μ, and 13.85μ were observed. These absorption bands were reported by Kleinman and Spitzer [Ref 1] One absorption band in the 1μ - 4μ region

[1]D. A. Kleinman and W. G. Spitzer, Phys. Rev., 118, 1960, p. 110.
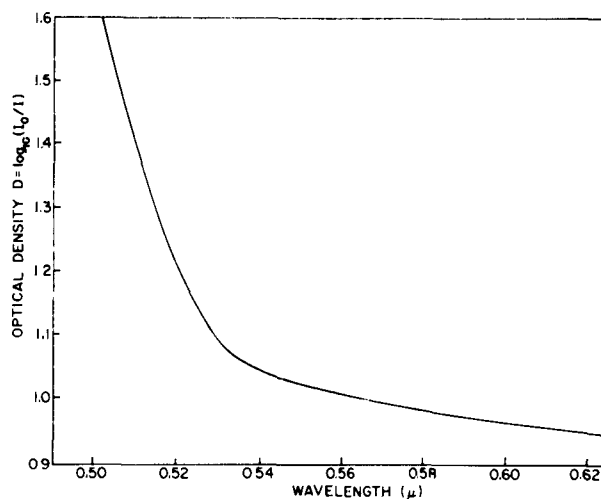
FIG. 91. ABSORPTION MEASUREMENT OF GaP
NO. 44C at 100 °K.

was observed for n-type GaP crystal only. This absorption band was also
reported by Spitzer et. al. [Ref. 2]. This band was ascribed to elec-
tron transitions between two sets of conduction band minima. If this
absorption band is due to the transition of electrons between two sets
of conduction band minima, the absorption should have the same tempera-
ture dependence as the electron concentration in the conduction band.
Figures 92 and 93 show the detail of the absorption peak of an n-type
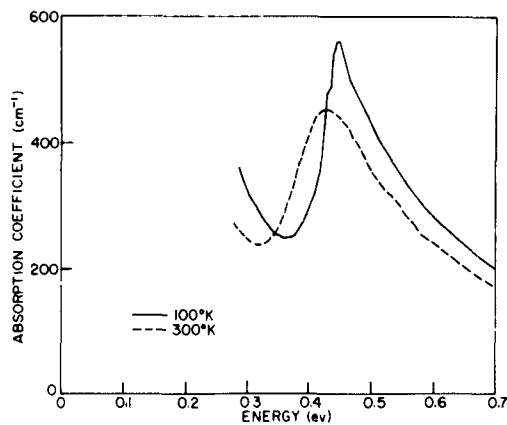
FIG. 92. ABSORPTION COEFFICIENT
VS ENERGY OF GaP NO. 39T.

[2] W. G. Spitzer, et al, J. Phys. Chem. Solids, 6, 1958, p. 173.
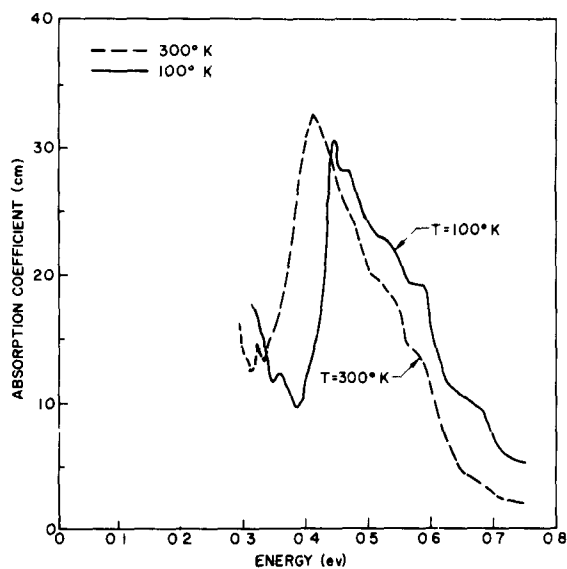
FIG. 93. ABSORPTION COEFFICIENT VS ENERGY
OF GaP NO. 28C.

GaP crystal in the 1μ - 4μ region (0.31 ev to 1.238 ev). Figure 94 shows the absorption of a p-type GaP crystal in the same energy range.
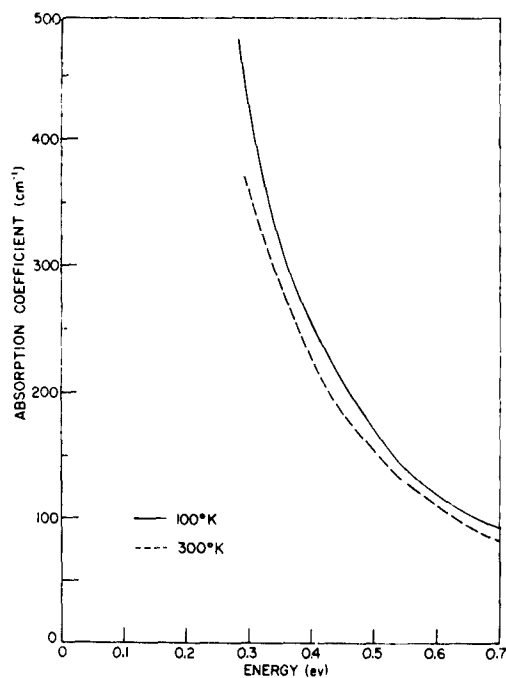
FIG. 94. ABSORPTION COEFFICIENT
VS ENERGY OF GaP NO. 30Z.

The absorption peak shifted to higher energies when the temperature was lowered. The bandwidth of the absorption peak became narrower at low temperature. The integrated area under the absorption curve after subtracting the free carrier absorption was measured. The integrated area has the expression:

$$\int_{E_1}^{E_2} \alpha dE \qquad (3)$$

where E_1 and E_2 are the end points of the absorption peak plotted in energy scale. The absorption data of GaP crystals are listed in Table III.

TABLE III. ABSORPTION OF GaP IN 1μ-4μ REGION

Sample Number	Absorption peak at 100 °K in ev	Absorption peak at 300 °K in ev	$A_1 = \int_{E_1}^{E_2} \alpha dE$ at 100 °K in(cm^{-1} ev)	$A_2 = \int_{E_1}^{E_2} \alpha dE$ at 300 °K in(cm^{-1} ev)	$(A_1 - A_2)$ in (cm^{-1} ev)
28C	0.44	0.412	3.26	3.8	-0.54
29C	0.481	0.425	1.03	1.603	-0.57
40T	0.455	0.43	11.1	11.8	-0.7
39T	0.45	0.42	47.7	43.35	+4.35
128UT	0.428	0.42	4.36	6.94	-2.58
128HT	0.435	0.422	3.45	3.05	+0.40
1101	0.435	0.415	8.77	8.83	-0.06
1012A	0.435	0.43	1.68	1.39	+0.29

The changes of integrated absorption from 300 °K to 100 °K are not correlated to the change of carrier concentrations in GaP from 300 °K to 100 °K. For example from the data of electrical measurements the carrier concentration of GaP sample No. 39T changed from 2×10^{18} cm^{-3} at 300 °K to 8×10^{16} cm^{-3}, and the integrated absorption increased by 10 percent only. This effect may be explained as the transition of electrons from

a shallow donor level to a conduction minimum at higher energy. It is also possible that the absorption peak in the 1μ-4μ region in n-type GaP was due to the transition of electrons from a deep donor level into the conduction band. The deep donor level then has to be located around 0.4 ev below the conduction band. The electron population at this deep level will not show a strong temperature dependence due to its high binding energy. In either of the above explanations the density of energy states at the conduction minimum has to be high in order to give an absorption peak. More detailed information about the band structure of GaP than the present knowledge of GaP energy bands is required to decide the origin of this absorption band. If the absorption band is due to a deep donor level, from the absorption data the deep donor concentration may be estimated by using the Smakula formula of Eq. (4).

$$N(cm^{-3}) = 0.821 \times 10^{17} \frac{n}{(n^2 + 2)^2} \frac{1}{f_{if}} \int \alpha dE \qquad (4)$$

The index of refraction, n, of GaP is 2.91. If the oscillator strength, f_{if}, is assumed to be 0.1, then Eq. (4) becomes

$$N(cm^{-3}) = 2.182 \times 10^{15} \int \alpha dE \qquad (5)$$

The estimated concentration of deep donors in different GaP samples are shown in Table IV on the following page.

A final report concerning the work on this project is in preparation.

TABLE IV. ESTIMATED DEEP DONOR CONCENTRATION OF
OF GaP CRYSTALS

Sample Number	Deep Donor Concentration in cm^{-3}	
	T = 100 °K	T = 300 °K
28C	7.1×10^{15}	8.3×10^{15}
29C	2.3×10^{15}	3.5×10^{15}
40T	24.2×10^{15}	25.8×10^{15}
39T	104.0×10^{15}	94.6×10^{15}
128U	9.5×10^{15}	15.2×10^{15}
128H	7.5×10^{15}	6.7×10^{15}
1011	19.2×10^{15}	19.3×10^{15}
1012A	3.7×10^{15}	3.0×10^{15}

PROJECT 5101: DIFFUSION OF IMPURITIES IN III-V COMPOUND SEMICONDUCTORS

The object of this project is to study the diffusion coefficients, solubilities, and distribution coefficients of II, IV, and VI column impurities in III-V compound semiconductors. In order to understand the diffusion mechanism of the Zn-InAs system, the number of electrically free carriers must be known, and one measure of the free carrier density is the Hall coefficient. This report presents, first, the feasibility of making resistivity and Hall measurements with point contacts on some semiconductors and, second, the details of measuring the resistivity and Hall coefficient on a circular sample with contacts mutually 90° apart and displaced a distance ℓ from the periphery.

To make electrical measurements on semiconductors it is convenient many times to place probes on the surface. However, to make potential-difference measurements, a low-impedance contact must be made to eliminate noise and stray pick-up. Using the apparatus shown in Fig. 96 the I-V of Fig. 95 was obtained for samples of Ge, GaAs and InAs. The I-V plot
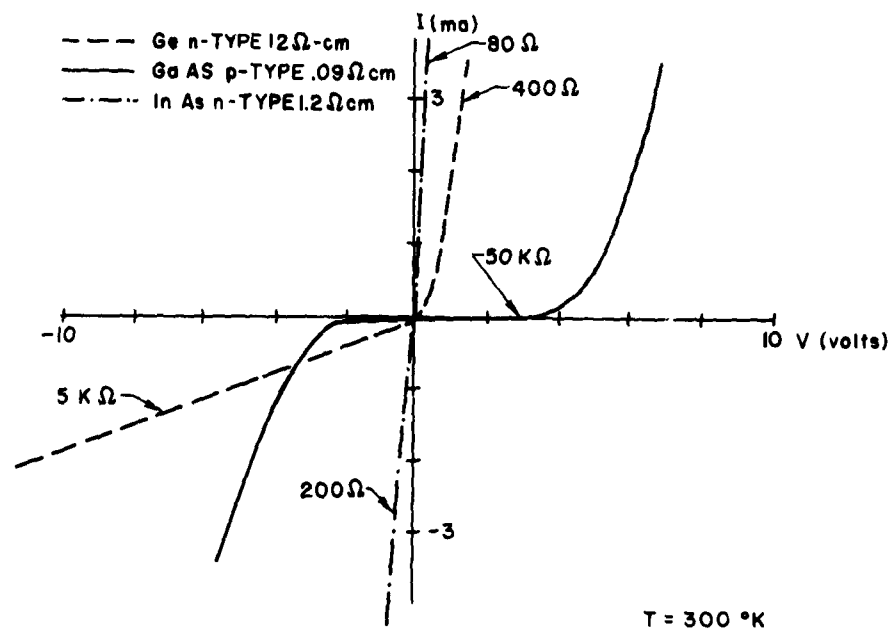
FIG. 95. CONTACT RESISTANCE OF A FOUR-POINT PROBE
ON SOME SEMICONDUCTORS.
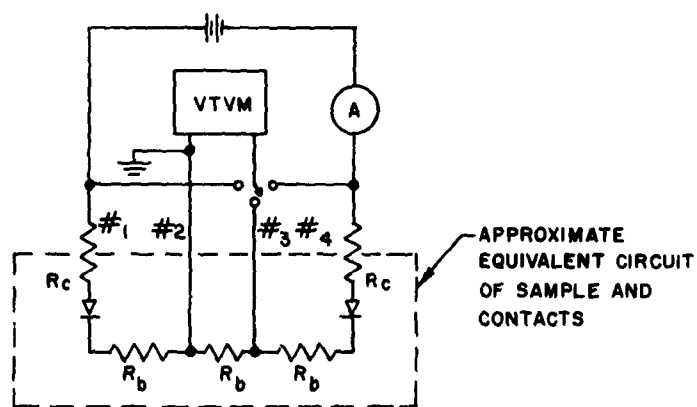
FIG. 96. EXPERIMENTAL CIRCUIT USED TO MEASURE CON-
TACT RESISTANCE. A standard four point probe was
used; R_c and R_b are contact and body resistors,
respectively.

was obtained by measuring the voltage between points No. 1, No. 4 and ground. It should be noted that the voltage of point No. 3 was never far from zero volts; in fact, the entire sample had a potential close to ground potential indicating that the body resistance was negligible compared to the contact resistance. The samples had rough surfaces (either lapped or sawed) and were less than 50 mils thick.

The parameters affecting contact resistance are: contact area, contact pressure, contact material, surface treatment, contact voltage, and temperature. By using the four-point probe, the first three parameters have been held fairly constant and the last two parameters are experimentally controllable. The surface treatment, however, is the parameter causing the deviations of the I-V characteristics in Fig. 95. The presence of an oxide layer and/or absorbed ions, which create a potential barrier at the surface, shield the semiconductor from the metal contact [Ref. 1] and give rise to high contact resistance.

From Fig. 95 it is seen that the contact resistance of GaAs is very high at low values of voltage. This makes direct probe measurements on GaAs very difficult. In contrast the contact resistance of the InAs is low and direct probe measurements are quite feasible.

Having resolved the feasibility of direct probe measurements on InAs, a sample holder was designed. Four-point contact are placed on a circular sample such that the contacts are mutually $90°$ apart and displaced a distance ℓ from the periphery. For this configuration the resistivity and Hall coefficient must be determined.

The first approximation to the measurement is that the problem is two dimensional. Uhlir [Ref. 2] explains that for a square array of points on an infinite slice, the resistivity is

$$\rho = \frac{2\pi d}{\ell n 2} \frac{\Delta V}{I_1} \left(d < \frac{S}{2}\right) \tag{1}$$

---

[1] Marton, L., ed., Methods of Experimental Physics, 6B, (1959).

[2] Uhlir, A., BSTJ, 34, 105 (1955).

where

        S = distance between points

        d = thickness of slice

The condition that $d < S/2$ is taken as the two-dimensional approximation.

    The relation for the resistivity, using the two-dimensional approximation, follows from Fig. 97. The sample represented by the unit circle
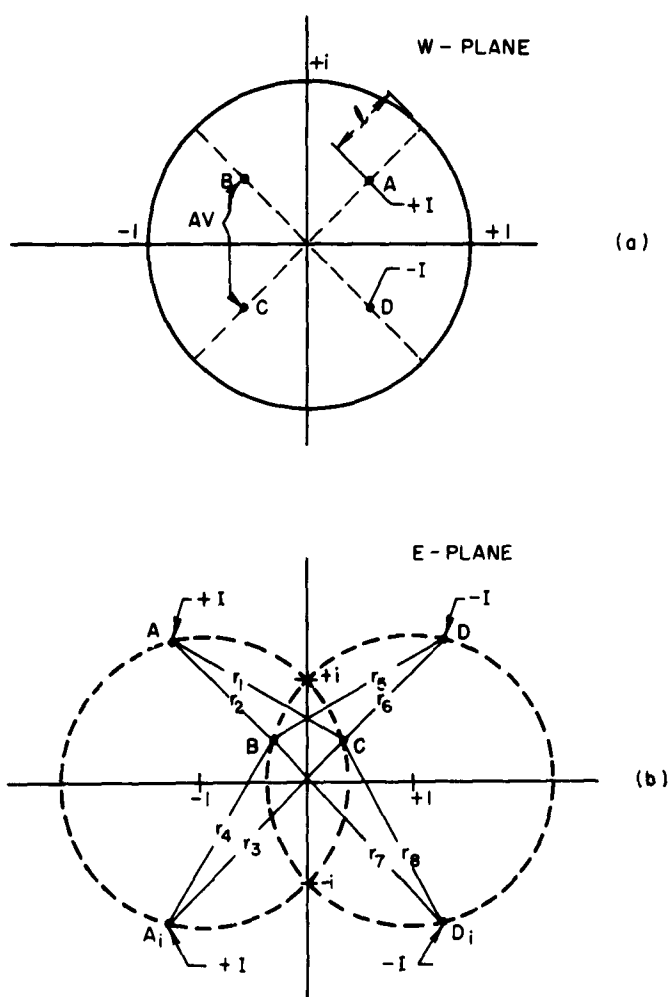
FIG. 97. RESISTIVITY MEASUREMENT ON A CIR-
CULAR SAMPLE WITH CONTACTS MUTUALLY 90°
APART AND DISPLACED A DISTANCE ℓ FROM
THE PERIPHERY.

in the W-plane is mapped into the upper half Z-plane by the bilinear transformation

$$Z = \frac{i(1 + W)}{(1 - W)} \quad .$$

Image currents are placed at A_i and D_i. The current from the contact at A is [Ref. 3]

$$J = \frac{I}{A} = \frac{I}{2\pi rd} = \frac{1}{\rho} E. \tag{2}$$

The potential difference between points B and C due to the current at A is

$$V_B - V_C = -\int_{r_1}^{r_2} E \, dr = \frac{I\rho}{2\pi d} \ln \frac{r_1}{r_2} \tag{3}$$

The potential difference between B and C due to all currents is

$$V_B - V_C = \frac{I\rho}{2\pi d} \ln \frac{r_1 r_3 r_5 r_7}{r_2 r_4 r_6 r_8} \quad . \tag{4}$$

But since $r_1 = r_5$, $r_2 = r_6$, $r_3 = r_7$, $r_4 = r_8$, the resistivity is

$$\rho = \pi d \frac{V_{BC}}{I_{AD}} \frac{1}{\ln \dfrac{r_1 r_3}{r_2 r_4}} \tag{5}$$

---

[3] van der Pauw, L. J., _Philips Technical Review_, 20, 220 (1958, 1959)

To develop a correction factor for the resistivity as the distance ℓ is increased consider the path of A in the Z-plane

$$Z(A) = \frac{-2(1 - \ell) + i\sqrt{2\ell}\,(2 - \ell)}{\sqrt{2}\,\ell^2 + 2(1 - \ell)(\sqrt{2} - 1)} \tag{6}$$

and for B

$$Z(B) = \frac{-2(1 - \ell) + i\sqrt{2}\,\ell(2 - \ell)}{\sqrt{2}\,\ell^2 + 2(1 - \ell)(\sqrt{2} + 1)} \tag{7}$$

Note that A and D and also B and C are symmetrical points. When $\ell = 0$, $Z(A) = -(\sqrt{2} + 1)$ and $Z(B) = -(\sqrt{2} - 1)$ so that

$$\ell n \,\frac{r_1 r_3}{r_2 r_4} = \ell n\,2. \tag{8}$$

Equation (5) is written

$$\rho = \frac{\pi d}{\ell n 2}\,\frac{V_{BC}}{I_{AD}}\,\frac{\ell n 2}{\ell n\,\dfrac{r_1 r_3}{r_2 r_4}} = \rho_0\,CF \tag{9}$$

where the correction factor (CF) is given as

$$CF = \ell n 2 / \ell n\,\frac{r_1 r_3}{r_2 r_4} \tag{10}$$

and

$$\rho_0 = \frac{\pi d}{\ell n 2}\,\frac{V_{BC}}{I_{AD}} \tag{11}$$

Eq. (11) is identical to Uhlir's relation Eq. (1) considering $I_{AD} = 2I_1$.

The correction factor was obtained graphically from Fig. 97b; values are tabulated in Table I for various values of ℓ. Figure 98 shows the data graphically and indicates three experimental check points. The
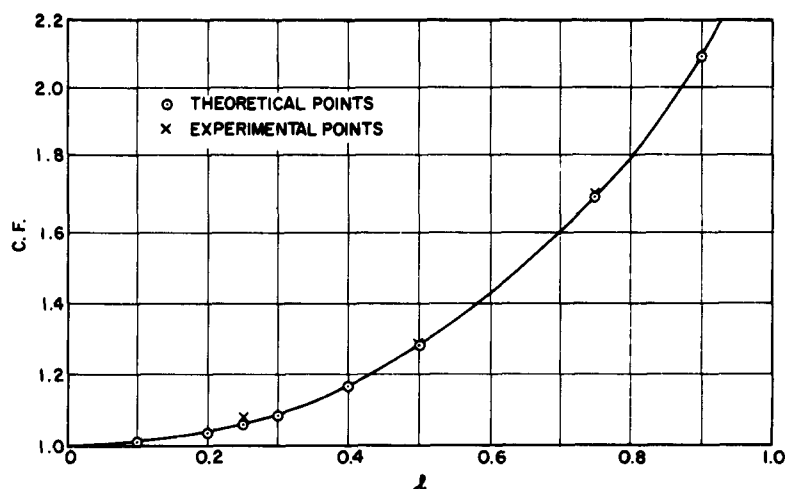
FIG. 98. CORRECTION FACTOR FOR THE RESISTIVITY
MEASUREMENT ON A CIRCULAR SAMPLE WITH CONTACTS
MUTUALLY 90° APART AND DISPLACED A DISTANCE ℓ
FROM THE PERIPHERY.

experimental points were obtained from a resistance-paper analog. A 16-inch-diameter sheet was used and the correction factor calculated from Eq. (9) as

$$CF(\ell) = \frac{V_{BC}(0)}{V_{BC}(\ell)} \qquad (12)$$

where I_{AD} was held constant. Good agreement is seen between experimental and theoretical points.

The Hall coefficient may be obtained from the same configuration by placing the current probes opposite each. Figure 99 illustrates simplifying transformations from the W-plane to Z-plane to P-plane. The Z to P transformation is

$$P = \ell nZ. \qquad (13)$$

SEL-64-073

W-PLANE   Z-PLANE   P-PLANE

(a)   (b)   (c)
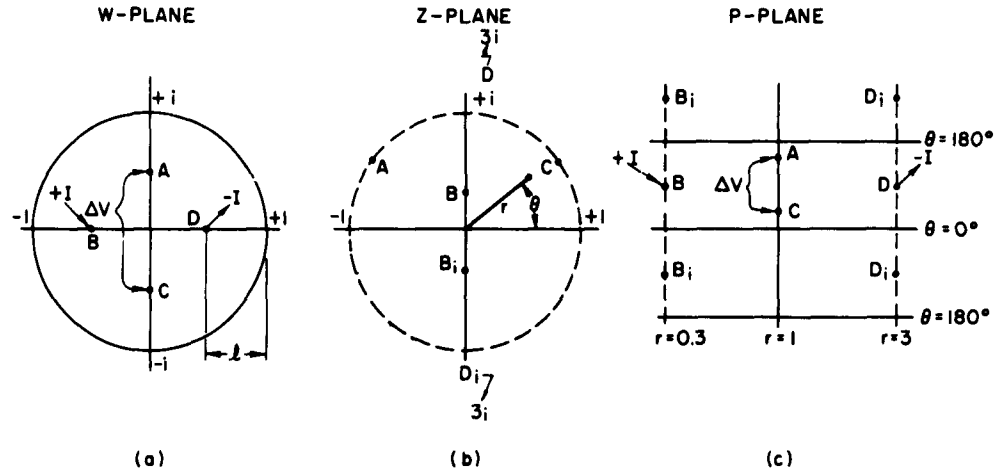
FIG. 99. HALL COEFFICIENT MEASUREMENT ON A CIRCULAR SAMPLE WITH CONTACTS MUTUALLY 90° APART AND DISPLACED A DISTANCE ℓ FROM THE PERIPHERY. Magnetic field is perpendicular to page.

In Fig. 99c the physical significance of the measurement is revealed. The voltage probes lie perpendicular to the current flow and measure the Hall voltage. The Hall voltage is given as

$$V_{AC} = \int_A^C E_H \, dS \tag{14}$$

where E_H = Hall field and S is taken along the equipotential line between A and C. But $E_H = JB/nq = JBR_H$ so that

$$V_{AC} = BR_H \int_A^C J \, dS \tag{15}$$

The current density is given as $J = I_{BD}/d \times 2$ where 2 is the diameter of the sample. The Hall coefficient is then

$$R_H \approx \frac{V_{AC}}{I_{BD}} \cdot \frac{d}{1 - \ell} \cdot \frac{1}{B} \tag{16}$$

The fraction of the total current flowing between the voltage points has been approximated by $(1 - \ell)$. Misalignment of the voltage probes may be taken into account by reversing the current flow and averaging the voltage measured.

During the next quarter it will be the purpose of this project to develop a correction factor for the Hall coefficient, to check the sample holder on a known sample of Ge, and to proceed with measurements on the InAs.

TABLE I. CORRECTION FACTOR

ℓ	C.F.
0.1	1.010
0.2	1.035
0.25	1.057
0.3	1.082
0.4	1.166
0.5	1.282
0.75	1.699
0.9	2.091

PROJECT 5103: ANOMALOUS DIFFUSION IN COMPOUND SEMICONDUCTORS

Office of Ordnance Research Grant DA 31-124 ARO(D)-155
Project Leader: G. L. Pearson
Staff: R. Mehta

The purpose of this project is to make a theoretical study of various parameters leading to anomalous diffusion characteristics of impurities into compound semiconductors.

A final report of this project is in progress.

PROJECT 5105: RARE EARTH IMPURITIES IN SEMICONDUCTORS

Center for Materials Research Contract SD-87-003
Project Leader: G. L. Pearson
Staff: H. C. Casey, Jr.

The purpose of this project is to study the fundamental electrical properties of column III-A impurities in elemental and compound semiconductors.

These may include solubilities, distribution coefficients, activation energies, and effective masses of such impurities in Ge, Si, GaAs and GaP.

The Final Report, SEL-64-036, has been issued and hence the project is closed.

PROJECT 5106: STUDY OF POINT DEFECTS IN SEMICONDUCTOR MATERIALS

               Office of Ordnance Research Grant DA 31-124 ARO(D)-155
               Project Leader: G. L. Pearson
               Staff: H. R. Potts*

The object of this project is to use the electron microprobe to generate x-rays and evaluate the resulting Kossel-line patterns in terms of lattice constant and, hence, defect structure on semiconductor materials of various preparation.

The project has been completed and a final report is in progress. The summary of conclusions of this report are given below.

The results of quenching experiments demonstrated an increase in lattice constant of the quenched GaAs samples as compared to the unquenched samples. The experimental value of the slope of log $(\Delta a/a)$ vs $1/T$ was 2.0 ev. This was interpreted as representing the formation of a defect structure in GaAs with an enthalpy of formation of 2.0 ev. The defects being observed were identified as mono-vacancies formed on only one sub-lattice, Ga or As.

Both room-temperature and high-temperature annealing were found to occur in at least two stages. The first stage annealing was quite rapid and did not have a well-defined activation energy. The second stage predominated after about 24 hours, comprised about 30 percent of the defects, and had an activation energy of about 1.0 ev. The interpretation of the data was that annealing first occurs by recombination of Frenkel pairs until essentially all of the interstitials are depleted. The second stage annealing the represents the annealing of the remaining vacancies to vacancy sinks such as the crystal surface or dislocations.

---

*IBM Fellow.

Increasing As pressure over the samples in the quenching experiments depressed the formation of defects. This was interpreted as indicating that the primary defects being observed were vacancies on the As sites and that significant Ga vacancies were not present.

A physical model of the defect structure was then formulated. The model describes the defect structure as comprised of As, Schottky vacancies and As, Frenkel pairs. The As vacancies are present in a concentration given by:

$$\frac{n_D}{N_a} \cong \frac{\Delta a}{a} = \exp(8.8) \ \exp(-\frac{2.0}{kT}) \left[\frac{P(As_4)}{P_{eq}(As_4)}\right]^{-\frac{1}{4}} \tag{1}$$

The model further proposes that annealing occurs first by vacancy-interstitial recombination and then by vacancy diffusion. Under the assumptions of the proposed model the enthalpy of formation of the vacancies on the As sublattice was found to be 2.0 ev. The activation energy associated with As vacancy mobility was 1.0 ev. The sum of these two gives an activation energy of 3.0 ev for the self-diffusion of As in GaAs by the vacancy diffusion process.

PROJECT 5107: PROPERTIES OF GaAs P-N JUNCTIONS

    Tri-Service Contract Nonr-225(24)
    Project Leader: G. L. Pearson
    Staff: D. J. Dumin

This project is concerned with the study of some of the properties of GaAs diodes. The temperature-dependent properties of the forward and reverse currents are being studied. Other diode properties will be incorporated into these studies as time progresses.

The tunneling model discussed in QRR No. 8 has been applied to the forward and reverse I-V characteristics of the GaAs diodes at 4.2 and 300 °K. Under the maximum field approximation the values of effective tunneling mass tabulated in Table 1 have been found. The masses tend to increase with increased doping density of the parent and with increased temperature.

TABLE 1. Effective tunneling mass at 4.2 °K and
300 °K for forward and reverse currents

Sample	Doping Density of parent	Reverse		Forward	
		$M_T(4.2 \ °K)$	$M_T(300 \ °K)$	$M_T(4.2 \ °K)$	$M_T(300 \ °K)$
D 10	$3.1 \times 10^{17}/cc$	$.030 \ m_o$	$.0377 \ m_o$	$.04 \ m_o$	
D160	$4.6 \times 10^{18}/cc$	$.0892 \ m_o$	$.1072 \ m_o$	$.079 \ m_o$	$.088 \ m_o$
D260	$4.3 \times 10^{18}/cc$	$.088 \ m_o$	$.118 \ m_o$	$.068 \ m_o$	$.068 \ m_o$
D290	$8.3 \times 10^{18}/cc$	---	---	$.188 \ m_o$	$.160 \ m_o$
D300	$2.1 \times 10^{18}/cc$	$.008 \ m_o$	---	$.004 \ m_o$	---
D310	$9.4 \times 10^{18}/cc$	---	---	$.068 \ m_o$	---
D340	$5 \times 10^{17}/cc$	$.0183 \ m_o$	$.0051 \ m_o$	$.032 \ m_o$	---
D350	$1.0 \times 10^{17}/cc$	$.0015 \ m_o$	---	$.017 \ m_o$	---
EN-01	$2 \times 10^{17}/cc$	---	---	$.047 \ m_o$	---

A direct comparison of the measured reverse current has been made
with the theoretical values predicted in QRR No. 8. The results of this
comparison are shown in Fig. 100 (on the following page) for reverse
current at 4.2 °K. The reduced hole-electron mass of $M_T = .063 \ m_o$ has
been used under the maximum field approximation.
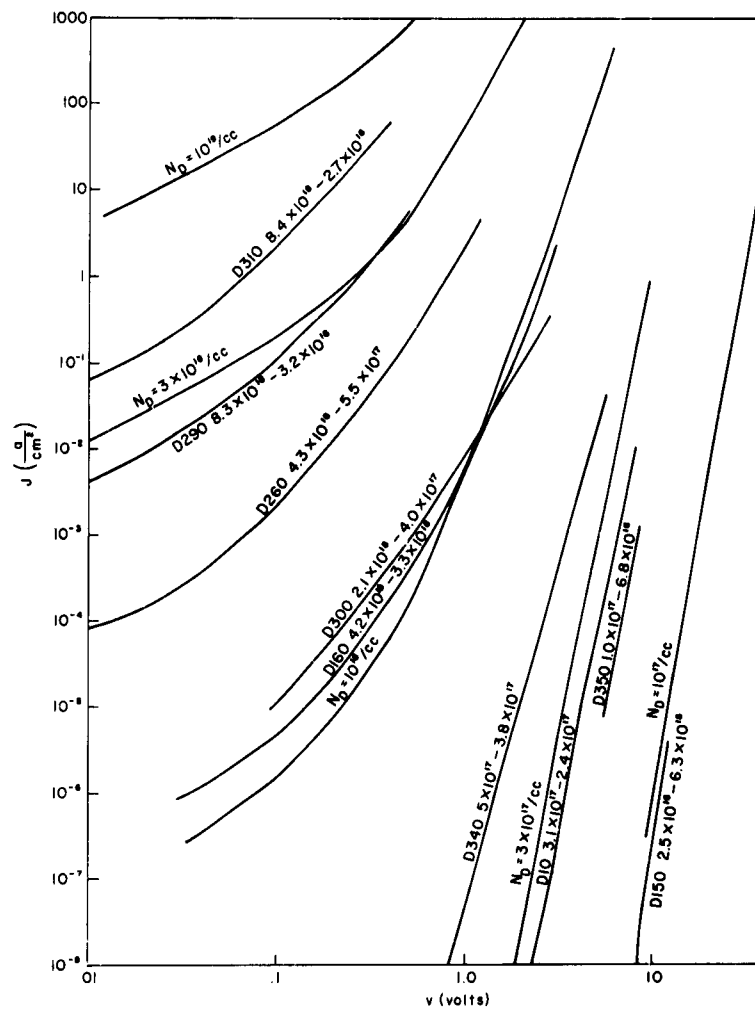
FIG. 100. REVERSE TUNNELING CURRENT VS
APPLIED VOLTAGE AT T = 4.2 °K.

PROJECT 5108: A STUDY OF GaAs$_x$P$_{1-x}$ ALLOY

The objective of this project is to evaluate the optical, electrical
and metallurgical properties of the GaAs$_x$P$_{1-x}$ alloy. Among evaluations
of particular interest to us are investigations of the crystal structure

and its imperfections by the Kossel line technique and by that of the lattice absorption spectra as the mole fraction of GaAs, x, varies from 0 to 1.

Recent results from measurements of lattice absorption bands in the spectral region between 10μ and 25μ are presented here. These are from samples of 75 percent As and 18 percent As, both from Merck Co.* The carrier concentration in these samples is of the order of 10^{16} - 10^{17} cm^{-3} n-type. The absorption coefficient α of the 75 percent As sample is plotted against the wave number in cm^{-1} in Fig. 101, while that of the 18 percent As sample is shown in Fig. 102. For convenience of
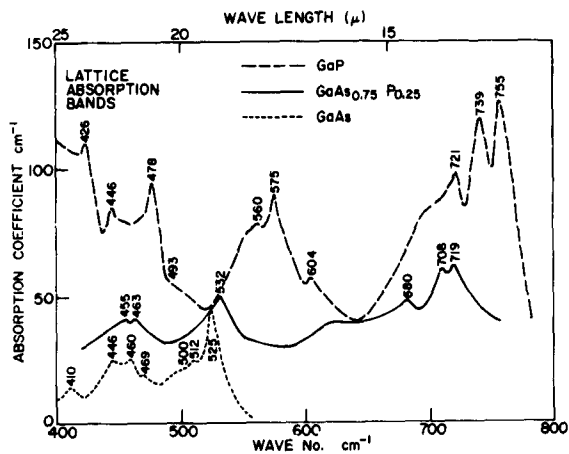
FIG. 101. LATTICE ABSORPTION BANDS
OF 75 PERCENT As SAMPLE.
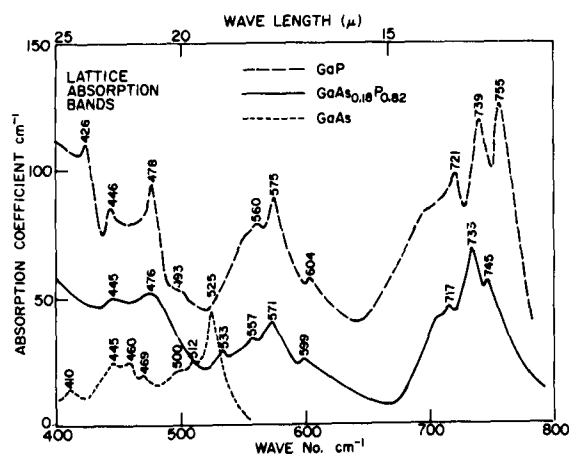
FIG. 102. LATTICE ABSORPTION BANDS
OF 18 PERCENT As SAMPLE.

---

*The 18 percent As sample was borrowed from H-P Associates, Palo Alto.

comparison, we have also plotted in each figure the absorption bands of GaAs and GaP [Ref. 1]. Each peak is described by its measured wave number in cm^{-1}. These samples were also checked for transmission in the visible region to determine the band gap; and by the Kossel line technique to determine lattice constant and defect structure.

The following information is obtained from our data:

1. Generally, the lattice absorption bands of $GaAs_xP_{1-x}$ are a mixture of the bands of GaP and GaAs in the corresponding wave number region. The peaks are shifted, however, those of GaP towards lower wave number and those of GaAs toward higher wave number.

2. In particular, we see the peak at 525 cm^{-1} (100 percent As) has shifted to 532 cm^{-1} (75 percent As) and further to 533 cm^{-1} (18 percent As). There is no doubt that the peak at 533 cm^{-1} is from GaAs since GaP has an exceedingly low absorption in this region.

3. The peaks at 604 cm^{-1} (0 percent As) left out by Kleinman and Spitzer [Ref. 2] in their assignment of combination bands is still present in the GaP rich crystal but shifted slightly to 599 cm^{-1}. Thus we think the 604 cm^{-1} band must be characteristic of GaP rather than due to the molecular vibrations of an unidentified impurity as suggested by Kleinman [Ref. 2].

4. The peaks at 680 cm^{-1}, 708 cm^{-1}, and 719 cm^{-1} (75 percent As) must be from the peaks characteristic of GaP, as again GaAs has an exceedingly low absorption in this region. This result leads us to believe that we will see a gradual shift of all peaks as the value of x varies from 0 to 1 in the mixture. This was not the case, however, in Braunstein's work [Ref. 3] on Ge-Si alloys; there, the combination bands become somewhat smeared in the region x ≅ .50.

---

[1] See SEL QRR No. 8 on the same project.

[2] D. Kleinman and W. Spitzer, "Infrared Lattice Absorption of GaP," Phys. Rev., 118, 110, (1960).

[3] R. Braunstein, "Lattice Vibration Spectra of Ge-Si Alloys," Phys. Rev., 130, 879 (1963).

Earlier work by Braunstein, Moore, and Herman [Ref. 4] showed that the equivalent temperature of phonons involved in the indirect band gap electronic transition in Ge-Si alloys varied with composition as shown in Fig. 103. They tried to interpret the result through short-range order in the crystal lattice, but were unsuccessful in giving any physical reason why the S-shaped curve shown in Fig. 103 is followed rather than any of three other curves which were also derived from their model.
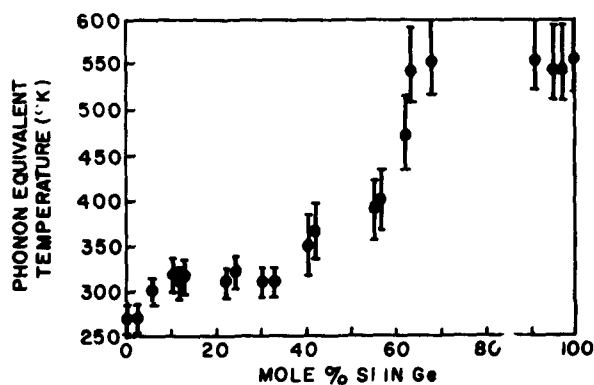
FIG. 103. THE CHARACTERISTIC TEM-
PERATURE OF PHONONS PARTICIPATING
IN THE NONVERTICAL TRANSITIONS IN
Ge-Si ALLOYS AS DETERMINED BY
BRAUNSTEIN, MOORE, AND HERMAN [REF.
4] FROM THE INTRINSIC ABSORPTION
EDGES.

From the data by Braunstein [Ref. 3] on Ge-Si alloy and that presented here on $GaAs_x P_{1-x}$, it is apparent that the short-range order in the crystal as proposed in Ref. 4 cannot explain our results, simply because of the fact that the corresponding modes of the constituents of the alloy do not merge as shown by the S-shaped curve. In fact, there was no evidence that the S-shaped curve in Ref. 4 represents a unique mode or combination of modes of lattice vibration. We are, instead, in

---

[4] R. Braunstein, A. Moore and F. Herman, "Intrinsic Optical Absorption in Ge-Si Alloys," Phys. Rev., 109, 695 (1958).

favor of the assumption that clustering of GaAs and GaP may exist through-
out the alloy system and consequently, the vibrational modes are charac-
teristic of pure GaAs and GaP aggregates.

It is known that both GaAs and GaP are somewhat ionic, thus we should
be able to detect the reststrahlen band of the mixtures as well as the
combination bands. The restrahlen band is due to the creation of long-
wavelength optical phonons through interaction with the radiation field.
We plan to investigate this point in order to evaluate the effect of
alloy composition on the long-wavelength phonons.

In the coming quarter, we shall also investigate the possibility of
growing the mixed crystals needed in this project. The most promising
method is that reported by Gibbons and Prehn [Ref. 5]. This technique
has two advantages: 1) it is a synthetic method so that source-material
is no problem, 2) most important of all, crystals grown by this method
exhibit exceedingly high purity.

PROJECT 5109: EPITAXIAL GROWTH OF III-V SEMICONDUCTOR COMPOUNDS

National Aeronautics and Space Administration
Grant NsG 555
Project Leader: G. L. Pearson
Staff: D. Chauvy

The purpose of this project is to examine and control the crystal-
lographic and electrical properties of III-V compound semiconducting
materials grown epitaxially by vapor deposition. Our interests have
been concentrated on the compounds GaP and GaAs and on the determination
of the chemical reactions involved in the deposition of these compounds
from the vapor phase.

In order to obtain more information on the chemical reactions
involved in the synthesis of GaP when Ga and PCl_3 are used as starting
materials, the system Ga (excess) - Cl_2 has been studied by optical
absorption at high temperatures. The absorption spectra show absorption

---

[5] J. F. Gibbons and P. Prehn, "Epitaxial Vapor Growth of III-V Compounds,"
TR No. 4711-1, SEL, Oct. 1963.

band systems which are characteristic of GaCl (Fig. 104). The height of the 3350Å peak is a measure of the concentration of GaCl. From its variation with temperature, the equilibrium constant for the reaction

$$GaCl_3(g) + 2Ga(l) \longleftrightarrow 3GaCl(g)$$
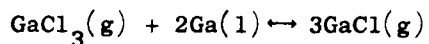
has been deduced as a function of temperature (Fig. 105).
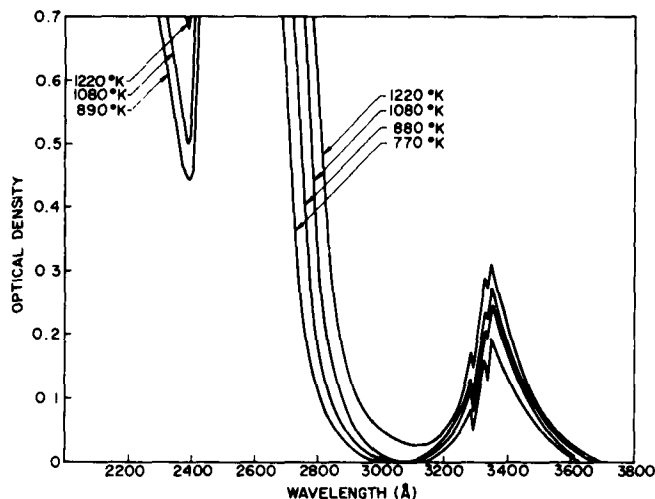
FIG. 104. OPTICAL DENSITY OF THE SYSTEM
Ga(excess) - Cl_2 VS WAVELENGTH.

Some of the published thermodynamical data for the gallium chlorides are either uncertain or have been empirically determined. As the equilibrium constant calculated from these data [Ref. 1] does not fit our measurements, new values have been deduced for the absolute entropy of $GaCl_3$ gas and for the enthalpy of GaCl gas.

---

[1] R. R. Fergusson and T. Gabor, **J. Electrochem. Soc.**, **111**, 585, (1964).
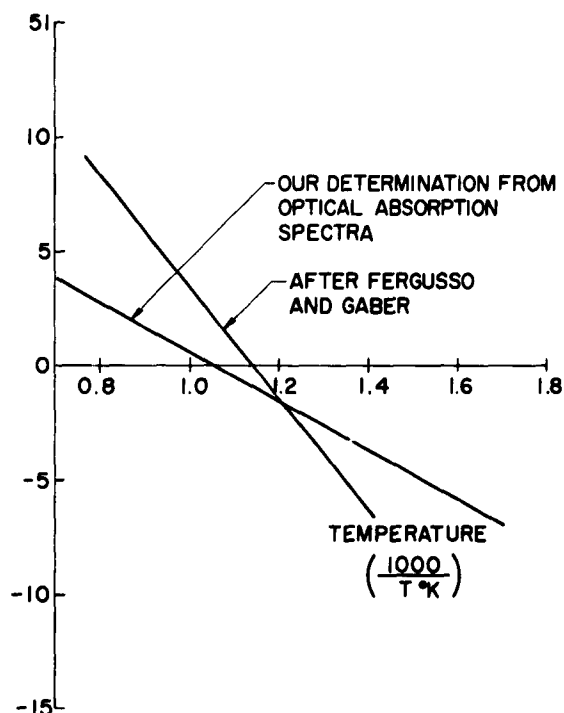
FIG. 105. NATURAL LOGARITHM OF THE
EQUILIBRIUM CONSTANT FOR THE RE-
ACTION $GaCl_3(g) + 2Ga(l) = 3GaCl(g)$
VS RECIPROCAL TEMPERATURE.

Specie	This work	Fergusson & Gabor [Ref. 1]
GaCl(g)	$H_f^o 298 = -24.7$ kcal/mole	-16.2 kcal/mole
$GaCl_3(g)$	$S^o 298 = 110$ e.u.	79.7 e.u.

PROJECT 5207: RADIATIVE LIFETIME MEASUREMENT IN GaAs

Tri-Service Contract Nonr-225(24)
Project Leader: W. E. Spicer
Staff: Juri Vilms

The purpose of this project is to study the relative strong inter-
action of radiation with electronic states in such materials as gallium
arsenide and other III-V compound semiconductors. A detailed understand-
ing of this interaction is of interest for analysis and development of

semiconductor diode light sources. The interaction manifests itself in both radiative recombination and in optical absorption and hence lends itself to experimental study by way of two different approaches: one concerned mainly with absorption of radiation, and the other with emission of radiation by recombining excess carriers. This project, embracing the latter approach, consists of a study of radiative lifetime in uniformly doped p-type gallium arsenide as a function of temperature and acceptor concentration, by means of photoluminescence and electron lifetime measurements.

Project efforts during this quarter were chiefly concerned with improvement of experimental apparatus, in preparation for a more extensive series of measurements following the program and utilizing the techniques developed during a previous quarter.

In particular, suspension of the sample in vacuum and more stable temperature control in the 80 $^\circ$K to 150 $^\circ$K range were realized through use of the sampleholder and liquid N_2 dewar arrangement shown in Fig. 106. Significant improvement in the photoluminescence data was achieved
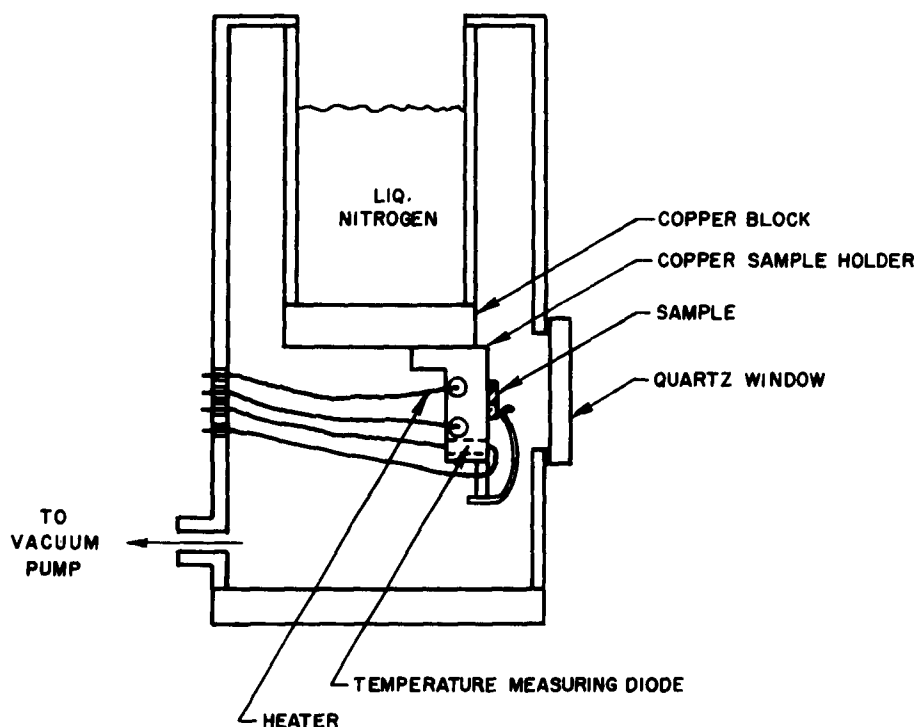
FIG. 106. DEWAR CROSS-SECTION.

as a result of cooling the photomultiplier with dry ice to reduce its noise. A Leeds & Northrup pen recorded was incorporated in the instrumentation in order to speed up data collection.

Some time was spent in setting up provisions for optical transmission measurement by means of the sample-in--sample-out method. This measurement had to be included in the present program since the published absorption-coefficient data are not adequate in the below-band-edge range of photon energies, a range in which a reliable knowledge of the absorption coefficient is necessary in order to obtain the minority-carrier diffusion length from the surface photovoltage measurements. Below the band edge, the absorption coefficient has a large dependence on both temperature and impurity content and hence needs to be measured for each sample at each temperature. For photon energies above the band edge, such effects are small and the data of M. D. Sturge (Phys. Rev., 127, p. 768) are satisfactory.

Work during the next quarter will be a direct continuation of the present and the previous quarter's work.

PROJECT 6758: ANALYSIS AND SYNTHESIS OF SOME ADAPTIVE NETWORKS

                Tri-Service Contract Nonr-225(24)
                Project Leader: B. Widrow
                Staff: Donlan Jones

The objective of this project is to attempt to find a mathematical technique which will facilitate the analysis and synthesis of some adaptive networks composed of Adalines and fixed logic.

Further analysis has indicated that a mathematical device called the generalized inverse can be useful in representing least-square-error tranining procedure applied to Adalines. It is believed that interpretation of this will apply to Ridgway training of Adalines. Investigation of this mathematical device in the synthesis of Adaline networks is being continued.

Not only has the generalized matrix inverse (g.i.) been shown to be a model of least-mean-square-error training of Adalines, but it has also been used to derive necessary and sufficient conditions for the realizability of a set of patterns used to train Adalines according to

Ridgway adaption. Further, rules have been derived using the g.i. which allow for the systematic synthesis of a number of different types of adaptive networks. These networks are Adalines feeding OR, AND, and MAJORITY GATES (Madalines), and also cascaded networks of Adalines.

Present investigation includes the possibiltiy of an Adaline being a matrix generalized inverse taker. Also, relationship of Adalines to the general theory of generalized inverses is being investigated.

PROJECT 6103: PATTERN RECOGNITION AND MACHINE LEARNING

Tri-Service Contract Nonr-225(24)
Project Leader: N. Abramson
Staff: D. Allais, S. Estes, J. McLauglin,
S. Fralick

The purpose of this project is to develop theoretical approaches
to various problems of pattern recognition and machine learning.

A. MEASUREMENT LEARNING IN PREDICTION - D. Allais

This portion of Project 6103 is concerned with the investigation of
indicator projection as a technique of measurement learning in pattern
recognition or projection.

Recent theoretical results have shifted the emphasis of the subproject
to measurement learning for prediction. The thesis outline given below
summarizes the work to date. Experiments on the statistical aspects of
measurement learning are continuing concurrently with the writeup of
previous results.

1. The prediction model and its extension to pattern recognition

    a. The Problem of Prediction

        The prediction problem and related terminology are defined.
        Concepts of mean square error, linear prediction and the
        normal model are discussed. The performance (m.s.e.) of
        an arbitrary linear predictor is derived.

    b. Pattern Recognition Using Indicator Predictands

        The p.r. problem is defined and known optimum solutions
        pointed out. Pattern recognition by means of indicator pre-
        dictands is suggested, and some experimental comparison is
        made with other techniques. The main virtue of this method
        is its close relationship to prediction and hence the appli-
        cability of techniques for selecting predictors.

2. The maximum likelihood predictor using prescribed normal
measurements

    a. Performance of the M. L. Predictor

        The maximum likelihood predictor for jointly normal measure-
        ments with unknown mean and covariance is given. Its per-
        formance (m.s.e.) is derived as a function of the number and
        quality of measurements, and of the sample size. Some im-
        plications of this result are illustrated by hypothetical
        curves of performance vs number of measurements.

b. Estimating Predictor Performance from the Sample Data

An unbiased estimate of expected (m.s.e.) is given and shown to be independent of the coefficients in the m.l. predictor.

3. A modified maximum likelihood predictor

a. A Simple Modification of the M. L. Predictor

A modified predictor is proposed in which a single constant is used to attenuate the coefficient vector of the m.l. predictor. The optimum constant is shown to be a function of the number of measurements, the sample size, and the multiple correlation between the set of measurements and the predictand.

b. Performance of the Modified Predictor When the Multiple Correlation is Estimated

Theoretical performance is derived for a special case. Some numerical results based on theory are presented for the case where the variance of the predictand is known. Experimental results are cited to further suggest the desirability of using the modified predictor.

4. Measurement evaluation

a. Correlation as a Basic Figure of Merit for Measurements

A direct correspondence is shown between m.s.e. and the multiple correlation between measurements and the predictand. The partial correlation between a measurement and the predictand is shown to be a natural conditional figure of merit. A critical partial correlation is derived for measurements used in the m.l. predictor.

b. A Geometrical Viewpoint

A vector space is defined in which correlation is equivalent to projection. The m.l. predictor is expressed as a sum of orthogonal vectors in this space. This interpretation facilitates the evaluation of individual measurements.

c. Systematic Procedures for Choosing a Good Set of Measurements

With a large number of candidate measurements, it is impossible to examine all subsets of measurements. Constructive procedures are outlined which are able to select a set of measurements having a large sample multiple correlation with the predictand. The procedures are justified theoretically for the case of random measurements.

5. Selecting measurements to minimize the error of prediction

    a. Choosing Predictors from a Preordered List of Measurements

    Given an ordered list of measurements and a sample of size N, consider the class of predictors using only the first p measurements. A procedure is given for determining that p which minimizes the expected error of prediction.

    b. Performance Degradation Resulting from Simultaneous Measurement Selection and Parameter Learning

    Combined measurement selection and parameter learning yields greater prediction error than parameter learning alone. This increase in error due to measurement selection is shown theoretically for the special case where measurements are independent of the predictand. The cost of measurement selection is illustrated more generally by experimental results.

    c. Selecting Measurements for Optimum Performance

    (The detailed contents of this section depend on forthcoming experiments and analysis.)

6. Conclusions

    a. Some Theoretical Details

       1. The variance in performance of the maximum likelihood predictor.

       2. The variation between experimental performance using new data and expected performance using separate learning data.

       3. Some distributions associated with a random unit vector.

B. SELECTION IN PATTERN RECOGNITION - S. Estes

Two criteria for the quality of a set of measurements are being investigated. The first is an extension of Mahalanobis' generalized distance function, D^2, from 2-classes to m-classes. D^2 is the distance from the sample mean of the individual classes to the mean of the composite sample of all classes measured in the metric of the within-class variations. D^2 is given by

$$D^2 = \sum_{i=1}^{m-1} \lambda_i$$

where λ_i are the m-1 eigenvalues of

$$\left| K_B - \lambda K \right| = 0$$

K_B is the between class sample covariance, and K is the total within-class sample covariance

The second criterion is a dispersion ratio, V^2, which is roughly analagous to the ratio of the "square of the volume" occupied by the composite sample to the sum of the "squares of the volumes" occupied by the individual class samples. In the sense that it is used here, "square of the volume" is measured by the determinant of the sample covariance about the sample mean. V^2 is given by

$$V^2 = \frac{\left| K_B + K \right|}{\left| K \right|}$$

For known parameters and normal distributions, these criteria may be derived as approximations to the mutual information, $I(\Omega;\overline{X})$, between the class alphabet $\omega_i \in \Omega$ and the observed measurements $x \in \overline{X}$. Here $i = 1, \ldots, m$, and $\overline{X}$ is the p-dimensional real space R^P.

For unknown parameters of normal distributions some progress has been made in the statistical significance of observed values of D^2 or V^2 and of comparisons for D^2 or V^2 corresponding to different observed measurements x or y where perhaps x and y are of different dimensions and have some individual measurements in common.

Given the criterion D^2 or V^2 it is then necessary to find how individual measurements contribute to the criterion and how they interact with other measurements to affect the criterion of goodness for the whole set. Considerable progress has been made in this area for D^2 but work remains to be done for V^2.

The value of any criterion of quality of a set of measurements depends on our ability to utilize it as well as its theoretical foundation. Special attention has been given to the computational aspects of these criteria for large-dimension problems (i.e., large p) and a number of classes, m, at least an order of magnitude less than p. Present plans

call for utilization of these results in a limited experimental program
to illustrate the instrumentation and to uncover possible practical
variations or modifications of the procedures.

C. MACHINE RECOGNITION OF BINARY PATTERNS - J. McLaughlin

Suppose each pattern is represented by a measurement vector X consisting of d binary digits. In this study, X is regarded as an element of the d-dimensional linear vector space V over the field of integers modulo 2. Although no inner product exists for this space, the simplicity of analysis and computation in V and encouraging experimental results strongly motivate the present approach.

Let W be the linear subspace of V spanned by a set of vectors $X_1, X_2, X_3, \ldots, X_N$, that is, W consists of all linear combinations of $X_1, X_2, X_3, \ldots, X_N$ (using mod-2 scalar arithmetic). If the vectors are random points in V, then the dimension of W is approximately N for N less than d, and approximately d for N greater than d. Experiments with some voice data and with handwritten character data show that the subspace spanned by vectors taken from a single pattern class tend to grow more slowly. The patterns are clustered in the sense that they belong to a subspace which is a very small fraction of V, even for N greater than d. For example, with $d = 160$, $N = 192$, a typical subspace has a dimensionality of 120. The subspace contains approximately one part in 10^{12} of the entire space V, yet contains all 192 training vectors.

If a subspace W_i is found in the above manner for each class i, classification of an unknown vector X can be attempted by finding which subspaces X belongs to. If X belongs to one and only one subspace, then X is assigned to the corresponding class. Computationally, this test is carried out by computing the value of $f(X)$ for each function f belonging to a basis for the annihilator of W_i. X belongs to W_i if and only if $f(X) = 0$ for every f in the annihilator of W_i.

If X belongs to more than one subspace, the ambiguity can usually be resolved by testing against smaller subspaces obtained by omitting training vectors one at a time (there are computationally convenient

methods for making these tests, based on keeping track of functionals which were zero on the training set every time but once). If an ambiguity still exists, there are additional methods that can be applied. These methods, and methods of resolving the ambiguity of X not belonging to any subspace, are currently under study.

D. LEARNING WITHOUT A TEACHER - S. Fralick

In the last quarterly report on this portion of project 6103 we reported a system synthesis technique for the solution of decision problems involving unclassified learning sequences (the "learning without a teacher" problem). During the last quarter the investigation has concentrated on two techniques for evaluation of the performance of such systems in the transient state. Although neither of these investigations are complete, the general approach which has been taken will be summarized below.

The performance investigation has followed two parallel paths. First a performance evaluation technique was developed as an extension and application of Shannon's unpublished paper "Bounds on the Tails of Martingales and Related Questions." Second, the performance of systems which learn to detect one of a set of orthogonal signals was investigated.

The technique based on Martingale sequences is applicable to Bayes optimum systems which learn (with or without a teacher), since they may be described by the equation (see previous report)

$$\ell_K = \ell(X_K | O_{K-1}) = \int \ell(X_K | \theta) \, p(\theta | O_{K-1}) \, d\theta$$

where

X_K = current observation (2TW dimensional vector)

$O_K = X_1 \ldots X_K$ = past (learning) observations

$\ell(X_K | \theta)$ = likelihood ratio given knowledge of θ

θ = unknown parameter

This sequence of likelihoods is a Martingale sequence since $E\left\{\ell_K \middle| O_{K-1}\right\} = E\left\{\ell_K \middle| \ell_{K-1} \cdots \ell_1\right\} = \ell_{K-1}$. It may be centered at its expectation by considering the "gain" at each new observation. We let $y_i = \ell_i - \ell_{i-1}$. Then $\ell_K = \sum\limits_{i=1}^{k} y_i$. Shannon has applied Chernoff's bounding technique to such Martingale sequences, and his work is almost directly applicable in this case.

Bounds on the tail probabilities of exceedence may be written as inequalities involving bounds on the semi-invariant generating functions for the martingale sequence. For example, we may let $v_K(S/H_q) =$ moment generating function for ℓ_K conditioned on H_q being true for X_K. $\left(H_1 = \text{hypothesis signal present}, H_2 = \text{hypothesis signal absent}\right)$ that is

$$v_K(S\ H_q) = \int \cdots \int e^{S\sum\limits_{1}^{K} y_i}\ d\ P(y_1,\ y_2\ \cdots\ y_K \middle| H_q)$$

Now define bounding functions by the relations

$$\gamma_i(S) \geq \int e^{Sy_i}\ d\ P(y_i \middle| y_{i-1}\ \cdots\ y_1)$$

$$\gamma_K(S \middle| H_q) \geq \int e^{Sy_K}\ d\ P(y_K \middle| y_{K-1}\ \cdots\ y_1,\ H_i) \qquad q = 1,2$$

and

$$\mu_i(S) = \log \gamma_i(S)$$

$$\mu_K(S \middle| H_q) = \log \gamma_K(S \middle| H_q) \qquad q = 1,2$$

Suppose that we can find a single bound for all $i \leq K - 1$, call this $\mu_o(S)$, then we can show that:

$$P_r\left\{\ell_K \geq (K-1)\mu_o'(S) + \mu_K'(S \middle| H_i)\right\} \leq e^{(K-1)\left[\mu_o(S) - S\mu_o'(S)\right] + \mu_K(S \middle| H_i) - S\mu_K'(S \middle| H_i)}$$

$$0 \leq S \leq b$$

$$P_r \; \ell_K S(K-1)\mu_o'(S) + \mu_K(S|H_i) \; \le \; e^{(K-1)\left[\mu_o(S) - S\mu_o'(S) - S\right] + \mu_K(S|H_i) - S\mu_K'(S|H_i)}$$

$$-a \le S \le 0$$

for some a, b > 0, real.

One technique for finding a suitable $\mu_o(S)$ is to find two cumulative distribution functions $\phi_1(y)$ and $\phi_2(y)$ which bound $P(y_i|y_{i-1} \cdots y_1)$ above and below for all y_i. We then choose $\phi_o(y)$ such that

1. $\phi_o(y) = \phi_1(y)$ $y \le \alpha$
2. $\phi_o(y) = \phi_2(y)$ $y \ge \beta$
3. $\phi_o(y) = K$ $\alpha \le y \le \beta$
4. $\int y \, d\phi_o(y) = 0$

Define

$$\mu_o(S) = \log \int e^{Sy} \, d\phi_o(y)$$

then $\mu_o(S)$ is a bound of the desired type. We can use this same approach to bound $\mu_K(S|H_q)$ by conditioning $\phi_1(y|H_q)$ and $\phi_2(y|H_q)$ on H_q. Unfortunately at this point the technique requires specification of the particular problem in more detail; i.e., the distribution of $\lim_{\to\infty} \ell_K$ and ℓ_o must be specified. Although this is in general possible, for the case of detection of an unknown signal in Gaussian noise both distributions are log-normal, and the moment generating functions do not exist for any S-interval. This problem may be overcome by noting that any practical system to compute ℓ_K has a finite dynamic range, and truncating the distribution at this limit. Such truncation makes evaluation of the bounds very difficult. Numerical solutions may, of course, be found for any particular problem by means of a computer solution; however, the results can only be expressed numerically, and will most likely shed little light on the question of performance in general.

The second technique, based on the assumption that the unknown parameter is vector-valued, and has only m possible discrete orthogonal values, is much less general in applicability, but much more illuminating. As an example we consider the following problem:

PROBLEM: We wish to detect the presence of one of a set of m orthogonal signals in white Gaussian noise. Let

$\left\{S_i\right\}$ = set of possible signals i = 1,2, ... m

X_K = observation (M-dimensional vector)

$O_K = X_1 \ldots X_K$ = past

$\hat{S}$ = actual signal transmitted

$S_i^t S_j = S_{ij} P^2$ (Orthogonality condition, super t indicates transpose)

$K = \sigma_n^2 I$ (Noise covariance matrix)

2TW = M

$\sigma^2 = M\sigma_n^2$

P_1 = probability that X will contains S

$P_2 = 1 - P_1$

SYSTEM SOLUTION: The Bayes optimum learning system computes

$$(X_{K+1} | O_K) = \sum_{i=1}^{m} \ell(X_{K+1} | S_i) \, p(S_i | O_K)$$

SYSTEM PERFORMANCE BOUNDS: One type of performance comparison, which is interesting for its intuitive value as well as the quantitative results, consists of a comparison of the optimum learning system with the optimum system given that the signal were known. We define

$\hat{\rho}$ = average risk of system when S is known.

ρ_K = average risk of learning system after K learning observations.

$\hat{p}_K = p(S | O_K)$

$R = \dfrac{P^2}{\sigma^2}$ = signal-to-noise ratio

$R' = \dfrac{R}{1 + P_1 P_2 R}$

With these definitions we may show that

$$\hat{\rho} \leq \rho_K \leq \hat{\rho} + p_1 \ P_r\left\{\hat{p}_K \leq \tfrac{1}{2}\right\}$$

Since

$$1 - \sqrt{\frac{m-1}{m}\left(\frac{1}{Kp_1^2 \ R'}\right)} \leq E\left[\hat{p}_K\right] \leq 1$$

and

$$0 \leq E\left\{\left(\hat{p}_K - 1\right)^2\right\} \leq \frac{1}{kp_1^2 \ R'}$$

we may evaluate the effect of variation in p_1, m, **K**, and R on the rate at which the system converges by applying a Chebysher-type bound to $P_r\left\{\hat{p}_K \leq \tfrac{1}{2}\right\}$. We obtain

$$\hat{\rho} \leq \rho_K \leq \hat{\rho} + \frac{4}{p_1 KR' - 4\sqrt{\left(\frac{m-1}{m}\right) KR'} + \frac{8}{p_1}}$$

PROJECT 6105:   INFORMATION THEORY

Tri-Service Contract Nonr-225(24)
Project Leader: N. Abramson
Staff: J. McFadden

STATIONARY POINT PROCESSES

The study of the entropy of a stationary point process has been continued. As mentioned previously, there are two kinds of entropy: (1) a discrete portion, associated with the number of events in a given interval; (2) a continuous portion, associated with the location of the points within the interval. The total entropy for a given interval is the sum of these two.

As mentioned previously, the discrete portion, or "numerical entropy," is maximized (for a given mean rate) when the number of events obeys a geometric distribution. As for the continuous portion, or "locational entropy," the conclusions reached in the previous report were incorrect.

The following new result has been proved for a general (non-stationary) point process. Let $\beta(t)$ dt be the marginal probability of an event in $(t, t + dt)$, with multiple events being neglected. For a given function $\beta(t)$, the total entropy for any fixed interval is maximized when the point process is the inhomogeneous Poisson. The study of the corresponding locational entropy will be continued.

A related result concerns the "mixed Poisson process," or mixture of Poisson processes, as described recently by Nawrotzky in _Mathematische Nachrichtem_, 24, 201-217 (1962), see also _Mathematical Reviews_, 27, 822-823 (1964). The new result is that the mixed Poisson process is a simple birth process having stationary increments. In fact, under fairly broad conditions, if the birth process is Markov and has stationary increments then it has been shown that the process must be mixed Poisson.

A formal translation has been given of the paper, "On the Mathematical Theory of Correlated Random Points," by P. I. Kuznetsov and R. L. Strationovich, Izo, Akad. Nauk SSSR, Ser. Mat., 20, 167-178 (1956).

PROJECT 6201:   ADAPTIVE NETWORK ORGANIZATION

                Air Force Contract AF33(657)-11586
                Project Leader: D. L. Epley
                Staff: J. S. Koford

The purpose of this project is a relation between the organization and capabilities of an adaptive switching network.

A final report on this project is in process of publication.

PROJECT 6202:   LOGICAL PROPERTIES OF ADAPTIVE NETWORKS

                Air Force Contract AF33(657)-11586
                Project Leader: B. Widrow
                Staff: R. J. Brown

The objective of this project is to study the logical capability of adaptive switching systems and the factors that determine and influence it.

A final report for this project has been written and the project is now closed.

PROJECT 6203: STATE-LOGIC RELATIONS FOR SEQUENTIAL NETWORKS

Tri-Service Contract Nonr-225(24)
Project Leader: D. L. Epley
Staff: D. L. Starner

This project is a study of the relations between the combinational logic and state-behavior of sequential networks. The goal is a state assignment algorithm, capable of being programmed for a computer, which will handle medium-sized flow tables and capable of producing good results with the expenditure of a reasonable amount of computer time.

The first draft of a final report has been completed, which should be published soon.

A second draft of a final report is being prepared.

PROJECT 6206: MULTI-TAPE SEQUENTIAL MACHINES

Tri-Service Contract Nonr-225(24)
Project Leader: D. Epley
Staff: C. A. Isberg

This project is an investigation of sequential machines with multiple input and output tapes, and their application to sequential transducers involving storage.

A second draft of the final report is being prepared.

PROJECT 6209: LOGICAL DESIGN OF FAST CIRCUITS

Tri-Service Contract Nonr-225(24)
Project Leader: D. A. Huffman
Staff: ----

The purpose of this project is the development of synthesis procedures by which the response time of logical circuits can be made as low as is theoretically possible. It has application to the design of all digital circuits including a wide variety of coding, control, and other information processing circuits in which the data is encoded in binary form.

This project was inactive the past quarter.

PROJECT 6301: DEVELOPMENT OF SIMULATION FACILITY

                Tri-Service Contract Nonr-225(24)
                Project Leader: G. F. Franklin
                Staff: Tom Redfern

The purpose of this project is to report, from time to time, the changes and growth of the computer simulation facility available to SEL, maintained by the Systems Theory Group. The purpose of the facility is to permit experimental testing of control and filtering schemes, and data reduction from analog tapes.

This project has been inactive during the past quarter.

PROJECT 6302: THE OPTIMUM STATIC AND DYNAMIC CONTROL OF MULTI-ACTUATOR
                SYSTEMS

                Tri-Service Contract Nonr-225(24)
                Project Leader: G. F. Franklin
                Staff: R. Larson, J. Farison

The purpose of this project is to study some of the more fundamental questions raised by the control of multivariable systems by a digital computer.

Technical Report No. 6302-6 by R. E. Larson titled "Dynamic Programming with Independent Variable" dated April 1964 is in process of publication.

PROJECT 6552: MODELING OF LINEAR SYSTEMS

                Tri-Service Contract Nonr-225(24)
                Project Leader: D. Luenberger
                Staff: Lewis Meier

The purpose of the project is to investigate the logical formulations and solutions of the problem of approximating a given linear dynamic system by means of a linear dynamic system of lower order than in the model.

A. APPROXIMATION OF A MATRIX BY A DYAD

If we have a discrete system operating for a finite time, then the input and output can be represented by vectors. In this case, we can represent the system by a matrix; if the system is causal, then the

matrix is lower triangular. In this case a first-order system is the lower triangular part of dyad (the outer product of two vectors). Hence, the problem of finding the best first-order approximation to such a system reduces to the problem of approximating a lower triangular matrix by the lower triangular part of a dyad.

Define an inner product norm on matrices by

$$\|A\|^2 = tr \ A^T \ A \qquad (1)$$

This norm is easily seen to be merely the square root of the sum of the squares of the components. Let us now consider the problem of finding the best approximation to a given matrix A by a dyad $a \ b^T$ (A is an $n \times m$ matrix, a is an $n \times 1$ matrix, and b^T is a $1 \times n$ matrix) in the sense of minimizing

$$\|A-a \ b^T\| = \sqrt{tr \ (A^T - Ba^T)(A - b^T)} \quad . \qquad (2)$$

We first assume that A is square and diagonal, with diagonal elements λ_i ordered in decreasing magnitude. By use of completion of the square and differentiation of expression (2), we find that the optimum is given by

$$a = \begin{bmatrix} 1 \\ 0 \\ \cdot \\ \cdot \\ \cdot \\ 0 \end{bmatrix} \quad b^T = \begin{bmatrix} \lambda_1, & 0, & \ldots & 0 \end{bmatrix} \quad a \ b^T = \begin{bmatrix} \lambda_1 & 0 & \ldots & 0 \\ 0 & 0 & \ldots & 0 \\ \cdot & \cdot & & \cdot \\ \cdot & \cdot & & \cdot \\ \cdot & \cdot & & \cdot \\ 0 & 0 & \ldots & 0 \end{bmatrix} \quad . \qquad (3)$$

And now consider a general $n \times m$ rectangular matrix A. It can be shown that any matrix of this form may be written as the product.

$$A = P \ D \ Q \qquad (4)$$

where P is n x n unitary, Q is m x m unitary, and D takes the form

$$D = \begin{bmatrix} \lambda_1 & 0 & . & . & 0 & . & . & 0 \\ 0 & \lambda_2 & . & . & 0 & . & . & 0 \\ . & . & & & . & & & . \\ . & . & & & . & & & . \\ 0 & 0 & . & . & \lambda_7 & . & . & 0 \end{bmatrix}$$

$$\lambda_1 \geq \lambda_2 \geq . . \tag{5}$$

We immediately note that

$$A^T A = Q^T D^T P^T PD \quad Q = Q^T D^T DQ$$

$$\text{tr } A^T A = \text{tr } D^T D \tag{6}$$

The best approximation to D can easily be seen from the above to be $a_o b_o^T$ where

$$a_o = \begin{bmatrix} 1 \\ 0 \\ . \\ . \\ 0 \end{bmatrix} \quad b_o^T = [\lambda_1, 0, ..., 0] \tag{7}$$

with a having n components and b having m. The best approximation to A is given by $a = Pa_o$ and $b^T = b_o^T Q$.

B. COMMENTS AND FUTURE PLANS

We have not succeeded with the above results in solving our given problem. We have solved the following problem: suppose we have a non-casual filter which is realized physically through the use of a delay followed by a dynamic system. Then we can find the best approximation in which the dynamic system is first order. We can use the above results to find first-order solutions to our approximation problems, but for the reasons given below it does not seem desirable to continue this path.

The idea of time variance can be related to dynamic behavior. In fact we may approximate a time-varying linear system by means of a non-linear system by making the varying coefficients state variables. In actual fact, the only convenient way to create time-varying coefficients is in effect to make them subsidiary state variables. The concept of time-varying linear system is really used only because of its mathematical convenience.

If we would succeed in solving the problem as previously formulated we may, for example, find that the best second-order approximation to a given time-invariant fourth-order linear system is a time-varying second-order linear system in which the dynamics of the time variation is third order. This result would not seem to be a significant simplification. What we really want to do is reduce the actual physical dynamic order and not the apparent but only mathematical dynamic order.

The simplest problem of this kind is the problem of finding the best approximation by a linear time-invariant system of given lower order to a given linear time-invariant system. One possible solution is to pick a system with sufficient undetermined coefficients to represent a general system of desired order. The error in using the approximation may be calculated as a function of these parameters and in theory the values which minimize any function of this error found. Unfortunately as the system increases in size, this method becomes rapidly impractical. If the dynamics are fixed, then finding the other undetermined coefficients is a linear problem.

In the next quarter, it is proposed to:

1. Formulate the above problem concretely.

2. Show that a unique solution exists.

3. Find an approximate procedure for iteratively finding this solution.

In addition, it is proposed to prepare a report summarizing and comparing the various methods of solving the linear estimation problem.

PROJECT 6557: THEORY AND DESIGN OF NONLINEAR REACTANCE SUBHARMONIC
GENERATIONS

Tri-Service Contract Nonr-225(24)
Project Leader: D. J. Grace
Staff: J. McConnell

A lumped model of the Linvill type has been developed for the junction
diode which, when used in the numerical integration computer program, gives
close agreement to experimentally observed subharmonic responses. In
addition to verification of the mechanisms involved in the experimental
circuit, the program and model have been used to illustrate transient
buildup of the subharmonic responses and to give some indication of the
principal effects of the losses in the diode.

The final report is ready for technical editing.

PROJECT 6657: STUDIES OF THE DESCRIBING-FUNCTION METHOD OF NONLINEAR
NETWORK ANALYSIS

Tri-Service Contract Nonr-225(24)
Project Leader: D. F. Tuttle
Staff: C. S. Burrus

This project is concerned with the analysis of lumped nonlinear
circuits. In particular, methods of generating and evaluating approxi-
mate solutions are being studied in hopes of extending and expanding the
idea of a describing junction.

An iterative method for finding an approximate solution to a dif-
ferential equation has been formulated. The procedure basically con-
sists of finding a special driving function for an auxiliary linear system
so that its response will approximate the true response of the nonlinear
system. It has been shown that Picard's successive approximations is a
special case of this method. This fact gives greater insight into Picard's
method. The uniform convergence of the method for restricted conditions
has been proven but it is hoped that less restrictive results can be
found.

An example initial-condition problem was worked with the method pro-
grammed for the B5000 computer. Rapid convergence occured for fairly
severe nonlinearities.

Presently the above method is being studied for the case of a sinu-
soidal driving function. It is hoped that comparisons with various
averaging methods will provide greater insight into both methods. Also
being studied is the question of what linear model to use for the most
rapid convergence.

PROJECT 6755:   DIGITAL ADALINES

        Army Contract DA 04(200) AMC-57(Z)
        Project Leader: B. Widrow
        Staff: M. E. Hoff, Jr.

Present plans call for the construction of a digital Madaline using
a high-speed ferrite-core memory. For initial testing a memory stack
consisting of four 32 × 32 planes has been obtained. While this memory
stack was designed for use with a 2-microsecond random-access cycle, the
read and adapt procedures in a digital Madaline would require a fixed
scan of the memory--it may therefore be possible to shorten the memory
cycle.

The overall components of the digital Madaline system are a finite-
core memory, used to store the weights, a master control clock, used to
select the proper sequence for reading out the weight bits, a set of
shifting accumulators each with a memory read-write circuit, and a com-
puter link. Each shifting accumulator becomes one digital Adaline, per-
forming summation, quantization, storing of the weight changes, and the
adaptation of the weights. The computer link enables reading Adaline
sums, reading weight values, writing patterns, writing initial weight
values, and writing adaptation instructions. Most of the internal
digital adaline arithmetic will be 16 bit binary, so the computer link
also includes a binary to B.C.D. connector and a B.C.D. to binary
converter.

A frame for holding the ferrite-core memory stack and the memory
driver cards has been completed. Because of the high currents (.45 amp)
and fast rise times (.05 μsec involved, it was necessary to keep lead
lengths in these circuits to an absolute minimum). The memory sequency
circuits have also been finished. Next the buffering circuits between

the memory sequency circuits and the memory drives will be constructed.
Several of the 32 memory driver circuits have been finished, and the
remainder are well under construction.

A capacitor storage shift circuit for the Adaline accumulators has
been developed, and design of the overall accumulator is well under
way. In addition, construction of the binary to B.C.D. arithmetic unit
for the computer link has been started.

PROJECT 6761:   SELECTION OF MEASUREMENTS FOR ADAPTIVE PATTERN RECOGNITION

Army Contract DA-04(200) AMC-57(Z)
Project Leader: B. Widrow
Staff: G. F. Groner

The objective of this project is to find optimum and nearly optimum
procedures for adaptive pattern recognition. This should include a study
of pattern generation by adaptive data processing, a study of the char-
acteristics of the adaptive system with those of the patterns.

The report mentioned in the previous QRR has been completed and will
be distributed during the next quarter, TR 6761-1 by G. F. Groner, entitled
"Statistical Analysis of Adaptive Linear Classifiers," dated April 1964.
This project will be terminated with the distribution of this report.

PROJECT 6762:   ADAPTIVE SYSTEMS

Tri-Service Contract Nonr-225(24)
Project Leader: B. Widrow
Staff: F. W. Smith, E. Fraser

Technical Report No. 6762-2 by Fred W. Smith, dated April 1964,
entitled "Contactor Control by Adaptive-Pattern-Recognition Techniques,"
is in process of publication. Upon its distribution, this project will
be terminated.

PROJECT 6763:   ADAPTIVE COMPUTER DIAGNOSIS OF ELECTROCARDIOGRAMS

Tri-Service Contract Nonr-225(24)
Project Leader: B. Widrow
Staff: Donald F. Specht

The purpose of this study is to discover, through adaptive pattern recognition techniques, a method of analyzing electrocardiograms with more accuracy than is presently obtained by the clinical diagnosis. This project is a continuation of an unsponsored project which resulted in a satisfactory method of separating normals from abnormals. Emphasis will now be placed on processing a sufficient number of cases for training of the adaptive computer so that the recognition rate of the machine will markedly exceed that of the present capability of human interpreters. An attempt will also be made to isolate the different diseases.

A report entitled "Vectorcardiographic Diagnosis Utilizing Adaptive Pattern Recognition Techniques," by D. F. Specht, has been prepared and is in process of publication. The report includes experimental results, a Madaline adapt procedure not previously published, and an efficient computer simulation program of a many-element Madaline which can accept analog inputs.

PROJECT 6764:   1000 WEIGHT MADALINE II

Army Contract DA-04(200) AMC-57(Z)
Project Leader: B. Widrow
Staff: M. E. Hoff, Jr.

The purpose of this project is the construction and use of Madaline II, a 1000-weight memistor Madaline. This machine - will be controlled by an IBM 1620 digital computer for use as a research instrument.

With the completion of Madaline II, accomplished with the installation of the last of the 1000 weights, the construction phase of this project has become relatively inactive. Some improvements in the machine will be made as is desirable, for example, a feature where various numbers of channels of the A-D converter may be read by the computer, has been installed. Where before each execution of a "read from A-D converter" instruction read to 20 channels, now 1, 2, 4, 8, 10, 20, 30, or 50 channels may be read, the number being selected by a switch on the Madaline console.

In addition to the Madaline improvements, work on the Flying Spot Scanner System continues with the installation and testing of the diffection amplifiers.

PROJECT 6766: CONDUCTION EFFECTS SUITABLE FOR ADAPTIVE DEVICES

           Army Contract DA-04(200) AMC-57(Z)
           Project Leaders: B. Widrow and H. Heffner
           Staff: G. Rosenberg

The purpose of this project is to examine the possibility of ionic conductivity in thin films of Al_2O_3, having in mind an adaptive memory device.

This project will be closing with the issuance of a final report.

PROJECT 6767: TWO-LAYER ADAPTION STUDIES

           Air Force Contract AF33(657)-11586
           Project Leader: B. Widrow
           Staff: F. Glanz

The purpose of this project is to find and investigate the properties of procedures for training a network of two layers of Adalines.

Because of the problem of relative minima in the error surface of many element networks, it would seem that an adaptive synthesis procedure might be more successful than the parallel adaption heretofore suggested. That is, one Adaline would be adapted until nonseparability was determined, then a second Adaline would be adapted to correct the errors made by the first, and so on, bring in new elements as needed. Several such methods have been suggested. The undesirable feature of this approach is that "minimum" networks cannot be assured. There is no reason to believe that there is any relationship between the separation a single Adaline could achieve and that which two Adalines together could achieve.

For example, consider the pictorial problem shown in Fig. 107. A single Adaline might realize plane A, making only two errors. Two more planes, B and C, would be required to cause complete partitioning. However, two planes, E and F, would completely partition this problem.
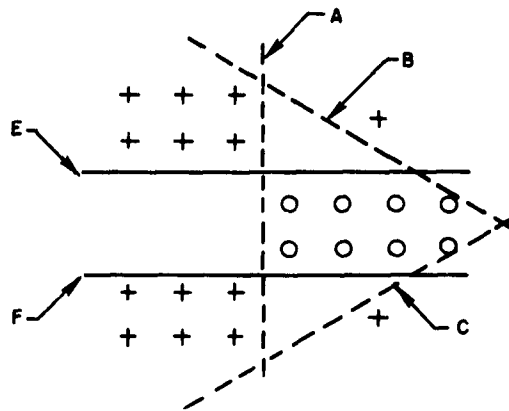
FIG. 107. PICTORIAL EXAMPLE SHOWING RE-
LATION OF MINIMUM ERROR SINGLE-ELEMENT
SOLUTION TO MINIMUM ERROR TWO-ELEMENT
SOLUTION.

The desirable feature of the synthesis approach is the fact that a
solution can be found if enough elements are used.

In a previous QRR it was mentioned that several multi-layer adapt
procedures have been experimentally tested and that none was found to be
satisfactory. It has been suggested that these procedures be recorded in
order to avoid duplication of "blind alleys" and to indicate the type and
breadth of approach.

A digital simulation was made of the following procedure for adapting
p Adalines feeding one Adaline. Start the p "first layer" Adalines
with zero weights but with a random threshold weight. Start the "second-
layer" Adaline with unity initial weights. Present a pattern to the
system and if the output is wrong adapt the second-layer Adaline in a
normal fashion (using the first-layer outputs as the input pattern) with
the following exception. If the weight with lowest magnitude is to be
decreased even more, then that weight is left alone and the Adaline feed-
ing it is adapted to change its output.

Since the second-layer weights are all positive initially and the
adapt increment is made small, the second-layer weights always remain
positive. It will be noted, however, that all possible solutions may be
obtained with the second-layer weights positive since a negative weight
may be made positive by complementing the weights of the corresponding
first-layer Adaline.

The above procedure was arrived at from the heuristic idea that if a weight is about zero, its input gives no information toward the classification and another input should be used. The procedure prevents any weight from becoming zero by decrementing the smallest weight and by forcing the Adaline feeding such a weight to take on different responses.

Simulation of the procedure led to three possibilities as outcomes. The procedure converged on small pattern sets less than 10 percent of the time. Most simulation runs ended with the second-layer weights growing without bound (or saturating) or with the weights bounded but no solution to pattern set. A few problems ended in a limit cycle. If limit cycles existed in the other runs, they were not detected because of their long length.

A second multi-layer adaption procedure which has been simulated by digital computer and found unsuccessful is the following:

Given a network of P Adalines feeding into Q Adalines, adapt the first layer for L adaptions and then the second layer for M adaptions. In adapting the second (or output) layer adapt those elements with wrong outputs in the usual manner, using the first-layer outputs as patterns. The procedure for adaption of the first layer becomes more complicated. With only one second-layer element $(Q = 1)$, we may use the straight-forward procedure of adapting the first-layer element with lowest confidence level in a direction which reduces the output error. With two or more second-layer elements we have trouble with the above procedure since one first-layer element feeds several second-layer ones. One method of deciding which element to adapt is to form "reverse sums" for each first-layer element.

This is shown in Fig. 108. For each of the p first-layer elements form $t_i = \sum_j b_{ij} d_j$: $i = 1, \ldots, P$.

Now if one t_i disagrees in sign with its corresponding first-layer output, a change of that first-layer output would, on the average, help attain the desired outputs. If more than one t_i disagreed with its corresponding first-layer output, the one adapted was the one with the largest negative ratio of t_i/c_i, where c_i is the first-layer confidence level corresponding to t_i. Heuristically this makes sense, since a low c_i makes t_i/c_i large and also means the smallest change in first-layer
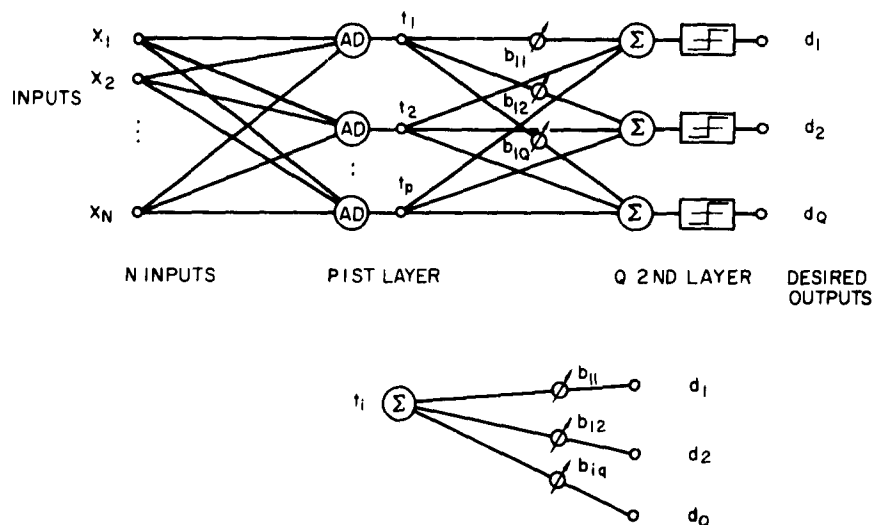
FIG. 108. ORGANIZATION OF SECOND MULTI-LAYER ADAPT
NETWORK SHOWING HOW "REVERSE SUM" t_i IS FORMED.

weights, while large t_i means large t_i/c_i and also will make a large change in output confidence levels (a change for the better, since t_i and c_i disagree in sign).

Unfortunately the aforementioned method converged only on a small number of the problems tried. The values of L, M, and the proportion-ality constants for each layer (thus allowing a wide range of time con-stants of adaption) were varied in hopes of finding ranges where convergence could be obtained every time. Modifications of the method to remedy the faults which were recognized became so involved and burden-some as to be completely impractical.

Presently a series of experiments on generalizing properties of Multi-Adaline networks is being run. The results will be given in a future QRR.

PROJECT 6772: PATTERN RECOGNIZING CONTROL SYSTEMS

Air Force Contract AF33(657)-11586
Project Leader: B. Widrow
Staff: E. Fraser

The objective of this project is the investigation of the feasibility and properties of a threshold logic controller for a dynamic system of

given order. Specifically, the question is whether such a controller may be trained to a configuration that will yield stable over-all system operation regardless of the initial state of either the controller or the dynamic system. This is to be accomplished by the simplest means possible.

A draft of a final report for the project was prepared. During this preparation, several areas were identified which warrant further investigation. Included are such items as a demonstration that a nonlinear switching surface may be successfully approximated by a hyperplane, and the susceptability of the system modeling technique to noise in the measurement of the state variables. These will be investigated during the coming quarter.

PROJECT 6950:   THRESHOLD LOGIC ELEMENTS AND ADAPTIVE SYSTEMS

Tri-Service Contract Nonr-225(24)
Project Leader: R. Mattson
Staff: G. Masters

This project investigates the area of sequential switching circuits which use adaptive threshold logic as the basic building block.

The concept of a sequential machine whose state diagram can easily be altered is being developed with several possible applications in mind. In one, the machine is used in an attempt to ascertain the statistical structure of a sequence of binary characters. In another, the same ideas are being applied to the problem of modeling an unknown machine which has both inputs and outputs by having the machine observe the response of the unknown to test sequences of binary characters. Some simple simulation experiments of this nature have been made.

A sequential threshold network whose properties are controlled by variable weights is being considered as a method of implementing this variable-state machine. In turn, this network lends itself to a simple weight-matrix description. When this matrix has certain symmetrical properties the corresponding network can be treated as a bilateral threshold net and some special theorems apply which may be helpful in the general case.

PROJECT 6952: A STUDY OF ADAPTIVE INPUT-CODING TECHNIQUES

Tri-Service Contract Nonr-225(24)
Project Leader: R. L. Mattson
Staff: J. D. Chang

This project is concerned with a study of quantizing the analog in-
puts of a threshold logic unit so that some nonlinearly separable func-
tions of analog variables can be realized.

Work during the last quarter was mainly devoted to the investigation
of workable synthesis procedures which will realize as many functions
as possible. Many ways have been tried. Among them, three seem feasible.
The first method is the so called moving-row-column method. The attrac-
tion of this method is the fact that the least number of coding variables
is required. However, this method is somewhat problem-oriented.

The second method is a synthesis procedure which is valid only for
a special kind of function. The requirements for this kind of function
are that the input vectors in the u-space must be different in at least
one coordinate value so that the vectors can be partitioned into sub-
sets in which all vectors have the same desired output. Then by coding
the subsets whose desired output is "1" into the largest subcube of the
Karnaugh map representation, any function of this kind is realizable by
a threshold element. The applicability of this synthesis procedure is
also limited; however, it is still of importance because it serves as
the stepping stone for another more useful synthesis procedure, i.e., the
third method. This method is the most useful one which evolves from a
deeper understanding of quantization. In the previous work, only quanti-
zation along the basis vectors was allowed. This is an unnecessary
restriction. The new method uses hyperplanes of different orientation to
partition the n-spaced into "slabs." Each "slab" contains vectors with the
same desired output. These "parts" can be mapped into a scaler to form a
new analog variable. Since the "parts" are disjoint, the equivalent
function defined on this new variable becomes a function belonging to
the kind discussed in the second method. Therefore, we can apply the
second method directly to this new input variable to realize the function.
Theoretically, this third method is valid for all functions of finite
number of points in finite dimensional space. The only limitation seems
to be the resolution power of the hyperplanes that we used for partition-
ing the n-space.

Further investigation about the third method is needed and an experiment will be planned.

PROJECT 7050: COMMUNICATION THEORY

        Tri-Service Contract Nonr-225(24)
        Project Leader: T. Kailath
        Staff: J. Omura and M. Gyi

The purpose of this project is to study basic problems in detection theory, with particular reference to time-variant channels.

A. TABULATION OF PROBABILITY DISTRIBUTIONS

Several probability-of-error calculations in radar, communications, pattern recognition and other applications of decision theory can be simplified and unified by relating them to certain canonical probability distributions, e.g., the chi-squared distribution, the distribution of the difference of two chi-squared variables, etc. We are attempting to tabulate various such useful distributions--this involves a literature search and also the development of some new distributions, e.g., the distribution for the difference of a central chi-squared variate of order two and a noncentral chi-squared variate of arbitrary even order. A report giving the results of this study together with various applications is being prepared.

B. DEMODULATION OF "FOLDED-FM" SIGNALS

With many tape-recorders, it becomes necessary to use FM signals with a bandwidth of the same (or larger) order as the carrier frequency. This causes a "folding-over" of the negative frequencies into the positive frequency part of the spectrum. Two methods of combatting the consequent distortion are being studied.

PROJECT 3550: METEOR ECHO PROPERTIES

Tri-Service Contract Nonr-225(24)
Project Leader: L. A. Manning
Staff: ----

The purpose of this project is to elucidate the mechanism of radi
reflections from meteor ionization trails, and to use meteoric echoes
investigate physical processes in the lower ionosphere.

As during the previous period, work was directed to the developme
of a simple but accurate theory relating the observed properties of
meteoric echoes to the properties of the ionospheric wind profile at
meteoric heights. One of the experimental findings is that the averag
rate of fading of meteoric echoes increases with time during much of t
echo duration. Study of the statistics of the fading rate increase in
terms of the autocorrelation function of the vertical wind profile for
a considerable variety of different shapes of profile has been used to
show by an iterative procedure that the average effect of correlation
may be neglected in computing the effective fading speed. With the ai
of this approximation, a new method of calculating expected fading spe
was developed based on combination of the statistics of occurrences of
reflecting glints with given frequency, and the expected velocity spre
within a sample of certain size in the velocity distribution. The ex-
pected fading rate increase as calculated on a digital computer was us
to develop a simple but precise approximate formula relating the rate
increase in fading speed to the mean values of the velocity and curvat
of-velocity with height in the wind profile. In addition, a measure i
obtained of the maximum possible number of reflecting glints per unit
height, equal to the number of relative maxima unit height in the velo
profile.

A modification of the new approach to the study of the fading-rat
increase has been applied to restudy the observed decrease in fading
speed at the end of a meteoric echo. The decrease results from the
shortening of the trail near the end of the echo, and hence a decrease
in the expected range of velocity sampled at the active glints. The
decrease in fading speed at the end is not used to yield measures of
the wind characteristics, but does confirm the theory ideas basic to t

rate increase at the start of the echo. The parameters used by the end-of-echo theory are the atmospheric scale height, fading speed for first echo cycle as a measure of mean wind velocity, and observed mean echo duration. With these parameters an excellent fit was obtained at the end of the echo, giving added confidence in the physical assumptions underlying the increase of fading speed at the start of the echo.

With the aid of the new results on the distribution of glints in groups of various frequencies, an analysis was also made of the relation between the expected and experimental delay to the start of fading. The mean value of the second derivative of the profile with respect to height obtained in this way is in good agreement with the results from the rate of increase of fading speed.

A new vector approach to a theory of the aspect sensitivity of the delay of echo appearance after the appearance of a visible trail was also developed. With this theory, an excellent agreement was obtained with the wind parameters found by the methods mentioned in the preceding paragraphs, and with the results of the diversity effect theory and experiments previously reported. Thus it is believed that a sound theory is now at hand for those properties of meteoric echoes related to distortions of the trails by ionospheric winds :. The results will be presented in a technical report as soon as the availability of project funds will permit.

PROJECT 3606:   IONOSPHERIC WINDS AND IRREGULARITIES IN ELECTRON DENSITY
                 IN THE IONOSPHERE

                 Tri-Service Contract Nonr-225(24)
                 Project Leaders: A. M. Peterson and V. R. Eshleman
                 Staff: R. Nowak and D. C. Brown

It appears possible that the winds may provide the driving force for generation of some large-scale irregularities such as sporadic-E patches, and the small-scale magnetic field-aligned irregularities which cause auroral and "northscatter" radio echoes. Some years ago at Stanford, a relationship was found between sporadic-E and E-layer-height field-aligned irregularities. It also appears possible that localized ionospheric-current systems may be generated by winds blowing ionization patches across the magnetic field. The recent theoretical work of

Buneman and others has shown that streaming electrons in ionospheric current systems can, under certain conditions, cause growing acoustic waves to develop. The acoustic waves in turn cause the equivalent to field-aligned irregularities which can be observed by radar means. Data are available at Stanford from past and presently operating experiments, which provide most of the inputs required for this study. In addition, winds at E-layer heights are measured using one of the Stanford IGY backscatter sounders suitably modified to measure the drift of meteor ionization trails.

Measurements with the specially constructed Doppler frequency measuring unit have been made for 18 consecutive days. Mean wind velocities were computed from these data, which were collected looking towards each of the four cardinal directions for four to five days. Since then, data have been collected switching every hour between two antennas, one pointing towards North, the other towards West.

Several other methods of measuring the Doppler shift have been investigated, e.g., digital filtering of taped data, parallel filtering of the Doppler signal, etc. Some of these methods have been simulated on an analog computer, and several appear feasible. Since all of these investigated methods depend on displaying magnitude and sign of the Doppler shift in one channel, a device is under construction which will offset the low frequency output by about 30 cps so that negative Doppler shifts are below the frequency, positive shifts above it.

Another study, closely related to the above, continues the work started by L. Colin on ion-gyro effects in strong field-aligned scatter (Colin, L., A. A. Burns, and V. R. Eshleman, "Radar Detection of Ionized Nitric Oxide in the Lower Ionosphere," J. Geophys. Res., 68, 4382-4387, 1963). The discovery of such ion-gyro effects is of considerable interest since it is related to fundamental problems in plasma instabilities, and it has application to plasma diagnostics using e.m. interactions. The initial discovery has raised more new questions than it has solved, however, and considerably more work is called for.

Echoes from field-aligned ionization in the E region are obtained using a pulse transmitter operating at 40-kw peak output at 23.1 Mc.

Normal operation of the transmitter is at 312.5 pps with a 300-μsec pulse width. The antenna system is a large array of Yagis, providing a 4° beamwidth pointing true north.

The detected output of the receiver is sampled at a frequency equal to the pulse repetition frequency of the transmitter, and the sampled echoes are recorded on magnetic tape. Through a process of re-recording, the original data track is translated upwards in a frequency and then processed on a commercial scanning spectrum analyzer. The output of the analyzer is further converted to a close approximation to (a portion of) the power spectrum of E-region echoes. An ion-gyro modulation component will result in a relative peak in this spectrum.

By use of a range-gated sampler, echoes from a restricted (in altitude) portion of the E region are recorded. Data have been obtained from five strata, each about 15 km in height. It is the intent of this portion of the study to observe the effects of ion-collision frequency on the relative strength of the ion-gyro frequency component of the spectrum. It is expected that the ion-gyro component of echoes received from the top of the E region will be stronger than that of echoes from the lower altitude portion. This effect is predicted because lower ion density in the higher strata will allow the ions to complete a higher average number of unimpeded periods of oscillation.

A semi-automated scheme for data reduction has been perfected during this period. Analog-to-digital conversion equipment samples the continuous output of the scanning spectrum analyzer, and an IBM 1620 computer performs a digital integration of the square of the filter output. The range of integration is the tape loop period. As the filter scans through a range of frequencies, a piecemeal approximation to a power spectrum is obtained.

The output of the 1620 is in punched card format. These cards are used as input data for an IBM 7090 program which yields a digitally plotted sample spectrum. These are provisions in the program for plotting an average of several data samples as well as plotting individual runs.

GOVERNMENT

U.S. Army

Commanding Officer
USAEL
Ft. Monmouth, N.J.
3 Attn: Continental Army Com.
    Liaison Officer
1 Attn: Director of Research
3 Attn: Chief, Tech. Info. Div.
1 Attn: Chf., Physical Elec. Br., SS
    and Freq. Cont. Div.
1 Attn: Chf., Circuit Functions Br.,
    SS and Freq. Cont. Div.
1 Attn: W. Matthei, Solid State and
    Freq. Cont. Div.
1 Attn: Rpt. Dist. Unit, SS and
    Freq. Cont. Div.
1 Attn: Dir., SS and Freq. Cont. Div.
4 Attn: A. P. LaRocque, SS and Freq.
    Cont. Div.
1 Attn: AMSEL-RD-DP
1 Attn: AMSEL-RD-X
1 Attn: AMSEL-RD-XE
1 Attn: AMSEL-RD-XC
1 Attn: AMSEL-RD-XS
1 Attn: AMSEL-RD-N
1 Attn: AMSEL-RD-NR
1 Attn: AMSEL-RD-NE
1 Attn: AMSEL-RD-ND
1 Attn: AMSEL-RD-NP
1 Attn: AMSEL-RD-S
1 Attn: AMSEL-RD-SA
1 Attn: AMSEL-RD-SE
1 Attn: AMSEL-RD-SR
1 Attn: AMSEL-RD-SS
1 Attn: AMSEL-RD-P
1 Attn: AMSEL-RD-PE
1 Attn: AMSEL-RD-G
1 Attn: AMSEL-RD-GF
1 Attn: AMSEL-RD-GD
1 Attn: AMSEL-RD-FU-1
1 Attn: AMSEL-RD/PR (Mr. Garoff)
1 Attn: AMSEL-RD/PRG (Mr. Zinn)
1 Attn: AMSEL-RD/PRT (Mr. Kaplan)
1 Attn: AMSEL-RD/PRM, Rec. File Cy.
1 Attn: Chf., Spec. Devices Br.
    (H. Brett)
5 Attn: AMSEL-RD/SL-SC
1 Attn: AMSEL-RD/SL-PRM
1 Attn AMSEL-RD/SL-PA
1 Attn: Dir. of Res. (H.A. Zahl)
1 Attn: ASRNE
1 Attn: Tech. Doc. Center
1 Attn: AMSEL-RD/SL-ADT-E
1 Attn: AMSEL-RD/SL-ADT
2 Attn: Communications Dept.
1 Attn: AMSEL-RD/SL-PEP (R.A. Gerhold)
1 Attn: AMSEL-RD/SL-TNR
1 Attn: Data Equip. Br.
1 Attn: AMSEL-RD/SL-PF (Dr. Jacobs)
1 Attn: AFSC Scientific/Tech.
    Liaison Office
1 Attn: Marine Corps Liaison Office
    AMSEL-RD/LNR
1 Attn: Corps of Engs. Liaison Off.
1 Attn: Logistics Div., AMSEL-RD/PRM
1 Attn: AMSEL-RD/PSM (Mr. Katzman)

CO, U.S. Army Signal Equip. Sup. Agcy.
1 Ft. Monmouth, N.J.

Chief Signal Officer
Dept. of the Army
Washington 25, D.C.
1 Attn: SIGRD

Director
U.S. Army Combat Dev. Command
Communications Electronics Agency
Bldg. 410
1 Ft. Monmouth, N.J.

Tech. Library
OASD (R and E)
Rm. 3E1065, The Pentagon
1 Washington 25, D.C.

Office of Chief of Ordnance
Dept. of the Army
Washington 25, D.C.
1 Attn: ORDTX-AR

Deputy President
U.S. Army Security Agency Board
Arlington Hall Station
1 Arlington 12, Va.

Commanding General
U.S. Army Combat Dev't. Command
Ft. Belvoir, Va.
1 Attn: CDCMR-E

CO, U.S.A. Comm. and Electronics
Combat Dev't. Agency
1 Ft. Huachuca, Arizona

Director, Ft. Monmouth Office
U.S.A. Comm. and Electronics
Combat Dev't. Agency
1 Ft. Monmouth, N.J.

CO, U.S.A. Elec. Materiel Sup. Agcy.
Ft. Monmouth, N.J.
1 Attn: SELMS-ADJ

CO, U.S.A. Missile Command
1 Redstone Arsenal, Ala.
1 Attn: Tech. Library

CO, U.S.A. Materiel Command
Washington 25, D.C.
1 Attn: R and D Directorate
1 Attn: AMCRD-RS-PE-E

U.S.A. Materiel Command Proj. Off.
Redstone Arsenal, Ala.
1 Attn: AMCPM-ZER-R

CO, Frankford Arsenal
Philadelphia 37, Pa.
1 Attn: ORDBA-FEL
1 Attn: Dr. Sidney Ross

CO, U.S.A. Sig. Mat. Sup. Agency
Ft. Monmouth, N.J.
1 Attn: SIGMS-ADJ

Engineering Procedures Br.
U.S.A. Sig. Mat. Sup. Agency
Ft. Monmouth, N.J.
1 Attn: Millard Rosenfeld

Electronic Warfare Div., USASCS
Ft. Monmouth, N.J.
1 Attn: Mr. H. Allem, EW Div.

U.S. Army Research Office
3045 Columbia Pike
Arlington, Virginia
1 Attn: Physical Sciences Div.

Office Chf. of R and D
Dept. of the Army
3045 Columbia Pike
Arlington 4, Va.
1 Attn: Mr. L. H. Geiger, Res.
    Planning Div.

U.S. Army Engineer R and D Labs
1 Ft. Belvoir, Va.
1 Attn: Tech. Doc. Center

Comm. General
U.S. Army R and D Activity
1 Ft. Huachuca, Arizona 85613

Signal Corps Liaison Office, MIT
77 Mass. Ave., Bldg. 26-131
Cambridge, Mass.
1 Attn: A. D. Bedrosian

CO, U.S.A. Ordnance Missile Comm.
1 Redstone Arsenal, Ala.
1 Attn: Tech. Library

Commander, Army Ord. Missile Command
Redstone Arsenal, Ala.
1 Attn: ORDXM-RFE, Mr. Lindberg

CO, Frankford Arsenal
Philadelphia 37, Pa.
1 Attn: ORDBA-1520

CO, Frankford Arsenal Library Br.
0270, Bldg. 40
Bridge and Tacony Streets
1 Philadelphia 37, Pa.

CO, Watertown Arsenal
Watertown, Mass.
1 Attn: OMRO
1 Attn: U.S.A. Mat. Res. Agency

Director
Ballistics Res. Lab
1 Aberdeen Proving Ground, Md.
1 Attn: V. W. Richard, BML

CO, U.S.A. Sig. Missile Sup. Agcy.
White Sands Missile Range, N. Mex.
1 Attn: SICWS-MEW

Commanding Officer
U.S. Army Electronics R and D Activity
1 White Sands, N.M.

CO, U.S.A. Elec. Proving Ground
Ft. Huachuca, Ariz.
1 Attn: Tech. Library

Dept. of the Army
Office, Chf. of R and D
Rm. 3D442, The Pentagon
Washington 25, D.C.
1 Attn: Res. Support Div.

CO, U.S.A. Res. Office(Durham)
Box CM, Duke Station
Durham, N.C.
3 Attn: CRD-AA-IP
1 Attn: Dr. H. Robl

Commanding Officer
Limited Warfare Lab.
Arberdeen Proving Ground
Aberdeen, Md. 21005
1 Attn: Tech. Dir.

CO, U.S.A. Electronics Command
Ft. Monmouth, N.J.
3 Attn: AMSEL-RD

Chief, Library Br.
Office of Chief of Engineers
Dept. of the Army
1 Washington 25, D.C.

OASD (R and E)
Rm. 3C-128, The Pentagon
Washington 25, D.C.
1 Attn: Tech. Library

Commanding Officer
Harry Diamond Labs.
Connecticut Ave. and Van Ness St., N.W.
1 Washington, D.C.

Director
Advanced Res. Projects Agency
1 Washington 25, D.C.

Commanding Officer
U.S. Army Security Agency
1 Washington 25, D.C.

U.S. Navy

Chief of Naval Research
Dept. of the Navy
Washington 25, D.C.
2 Attn: Code 437, Info. Syst. Br.
2 Attn: Code 427
1 Attn: Code 420

CO, ONR Branch Office
495 Summer St.
1 Boston 10, Mass.

CO, ONR Branch Office
1000 Geary St.
1 San Francisco 9, Calif.

Chief Scientist, ONR Br. Office
1030 E. Green St.
1 Pasadena, Calif.

ONR Branch Office
230 N. Michigan Ave.
1 Chicago 1, Ill.

CO, ONR Branch Office
207 W. 24th St.
1 New York 11, N.Y.

Officer-in-Charge
Office of Naval Research
Navy 100, Box 39
Fleet P.O.
16 New York, N. Y.

U.S. Naval Applied Science Lab
Bldg. 291, Naval Base
Brooklyn, N. Y. 11251
1 Attn: Tech. Library, Code 9832

Director, Naval Research Lab
1 Washington 25, D.C.
1 Attn: Code 5266 (G. Abraham)
1 Attn: Code 6430
6 Attn: Code 2000
1 Attn: Code 2027
1 Attn: Code 5200
1 Attn: Code 5266-GA
1 Attn: Code 5240
1 Attn: Code 5260
1 Attn: Code 5300
1 Attn: Code 5400
1 Attn: Code 5430

Chief, Bureau of Ships
Dept. of the Navy
2 Washington 25, D.C.
1 Attn: Code 732, A. E. Smith
1 Attn: Code 335
1 Attn: Code 684A, R. H Jones
1 Attn: Code 681A
1 Attn: Code 686
1 Attn: Code 687E
1 Attn: Code 687D
1 Attn: Code 681A1D
1 Attn: Code 607 NTDS
1 Attn: Code 607A, Cdr. E. B. Mahinske
1 Attn: Code 691A, A. H. Young
1 Attn: Code 681A-1
3 Attn: Code 670B
1 Attn: Code 691A1

Chief, Bur. of Naval Weapons
Dept. of the Navy
Washington 25, D.C.
1 Attn: RREN-3
1 Attn: RAAV-44
1 Attn: RAAV-6
1 Attn: ASM Detection and Cont. Div.
1 Attn: RUDC-1
1 Attn: RMWC Missile Weapons
           Control Div.
1 Attn: DIS-31
1 Attn: RAAV, Avionics Div.

Chief of Naval Operations
Dept. of the Navy
Washington 25, D.C.
1 Attn: Op-07T-12
1 Attn: Code Op 94T
1 Attn: Code Op-352
1 Attn: Op-945Y

U.S. Naval Weapons Lab
Dahlgren, Va.
1 Attn: Tech. Library
1 Attn: G. H. Gleissner, Head,
           Comp. Div.
1 Attn: Comp. and Analysis Lab

U.S. Naval Ordnance Lab
Corona, Calif.
1 Attn: R. Conger, 423
1 Attn: H. H. Wieder, 423
1 Attn: Library

AFSC Scientific-Tech. Liaison Off.
U.S. Naval Air Dev't Center
1 Johnsville, Pa.

CO, U.S. Naval Ordnance Lab
Silver Spring, Md.
1 Attn: Library

Ballistic Res. Labs
Aberdeen Proving Ground, Md.
1 Attn: K. A. Pullen
1 Attn: Chief, Computer Res. Br.

Commander
U.S. Naval Missile Center
Pt. Mugu, Calif.
1 Attn: Code N3232
1 Attn: Code N03022

Navy Dept.
U S. Naval Avionics Facility
Indianapolis 18, Ind.
1 Attn: Station Library

CO and Director
U.S. Naval Electronics Lab
San Diego 52, Calif.
1 Attn: Library

U.S. Naval Post Grad. School
Monterey, Calif.
1 Attn: Tech. Rpts. Librarian
1 Attn: Prof. Gray, Elec. Dept.
1 Attn: Dr. Harold Titus

Weapons System Test Div.
Naval Air Test Center
Patuxent River, Md.
1 Attn: Library

CO (ADL)
U.S. Naval Air Dev't. Center
1 Johnsville, Pa. 18974

U.S. Air Force

Hq. USAF (AFRDR-NU-3)
The Pentagon, Rm. 4D 335
Washington 25, D.C.
1 Attn: Mr. Harry Mulkey

Chief of Staff
U.S. Air Force
Washington 25, D.C.
1 Attn: AFDRT-ER

U.S. Army Signal Liaison Off.
Aeronautical Systems Div.
Wright-Patterson AFB, Ohio
1 Attn: ASDL-9

Commander, ASD
Wright-Patterson AFB, Ohio
1 Attn: SEQSS
1 Attn: ASRNC-21
1 Attn: ASRNC-23
1 Attn: ASRNCS-3
1 Attn: ASRNRD
1 Attn: ASRNE-2(D. R. Moore)
6 Attn: ASRNE-32
1 Attn: Electronic Res. Lab(ASRNEA)
1 Attn: ASRNE-2(Lt-Col. L.M. Butsch)
1 Attn: ASRNR-32
2 Attn: ASRNEM
2 Attn: ASRNET
1 Attn: ASNPRS-5
1 Attn: ASRNC-23
1 Attn: ASRNC-1

Commandant
AF Inst. of Technology
Wright-Patterson AFB, Ohio
1 At'n: AFIT(Library)

Executive Director
AF Office of Scientific Res.
1 Washington 25, D.C.

School of Aerospace Medicine
            Div. (AFSC)
USAF Aerospace Medical Center, ATC
Brooks AFB, Texas
1 Attn: SMAP

AFWL(WLL)
1 Kirtland AFB, New Mexico

Commander
Air Proving Ground Command
Eglin AFB, Fla.
1 Attn: APGTRI (Tech. Library)

Commander
AF Missile Dev't. Center
Holloman AFB, New Mexico
1 Attn: MDR

Director, Air University Lib.
Maxwell AFB, Ala.
1 Attn: CR 4582

Commanding General
Rome Air Dev't. Center
Griffiss AFB, Rome, N.Y.
1 Attn: RAALD
1 Attn: RAWCL
1 Attn: Doc. Lib (RAALD)
1 Attn: RALS/J. Fallik
1 Attn: RAWEC, T.J. Domurat
1 Attn: L. Sues (EMIAD)
1 Attn: Haywood Webb (RAWE)
1 Actn: RCWI, Major B.J. Long
1 Attn: RCLMA, J. Dove
1 Attn: RAOL
1 Attn: RAWED

Commanding General
AF Cambridge Res. Labs
Air Res. and Dev't. Command
L. G. Hanscom Field
Bedford, Mass.
1 Attn: CRB
1 Attn: CROTLR-2
1 Attn: CCRR
1 Attn: CCSD
1 Attn: CRZC
1 Attn: CRXL-R, Res. Library
1 Attn: CRXL, Scientific Library
1 Attn: CRTOTT-2, Electronics
1 Attn: Dr. L. M. Hollingsworth,
            Dir., Elec. Res. Directorate
1 Attn: CRW
1 Attn: Mr. Lawrence C. Mansur(CRW)

Data Sciences Lab (CRB)
AFCRL
L. G. Hanscom Field
Bedford, Mass. 01731
1 Attn: Dr. Zschirnt, Sr.Scientist

Commander
AF Ballistic Missile Div.
Hq., Air Res. and Dev. Command
USAF, AF Unit P.O.
Los Angeles, Calif.
1 Attn: WDLPM-1-TDC

Hq., AFSC
Andrews AFB
Washington 25, D.C.
1 Attn: SCSEI
1 Attn: SCTAE

Director, Res. and Dev.
Hq., USAF
Washington 25, D.C.
1 Attn: AFRDR-NU, Lt.Col. Raymond
            W. Booth

Electronic Systems Div. (AFSC)
Scientific and Tech. Info. Div.
L. G. Hanscom Field
Bedford, Mass.
1 Attn: ESTI

AFSC Scientific and Tech.
            Liaison Office
111 E. 16th St.
1 New York 3, N.Y.

AF Office of Scientific Res.
Washington 25, D.C.
1 Attn: Code SRPP
1 Attn: Code SREE

Foreign Technology Div.
Wright-Patterson AFB, Ohio
1 Attn: TD-C1 (T.M. Hay, J.R.)
1 Attn: TD-CIB
1 Attn: TD-E1

Commerce and Miscellaneous

Information Retrieval Sec., MS-112
Library Branch
Federal Aviation Agency
1 Washington 25, D.C.

Hq., USAF
Dir. of Science and Technology
Electronics Div.
Washington 25, D.C.
1 Attn: AFRST-EL/CS, Maj. Myers

U.S. Atomic Energy Commission
Research Division
Washington 25, D.C.
1 Attn: Mr. William C. Gaugh

Atomic Energy Commission
Project Matterhorn
1 Princeton, N.J.

NASA
G. C. Marshall Space Flight Center
Huntsville, Ala.
1 Attn: M-G and C-R

NASA
Langley Research Center
Langley Station
Hampton, Va.
2 Attn: Technical Library

NASA
Goddard Space Flight Center
Greenbelt, Md.
1 Attn: Dr. George H. Ludwig, Code 611
1 Attn: Chief, Data Systems Div.

NASA
Washington, D. C.   20546
1 Attn: Dr. H. Harrison

Assist. Secy. of Def. for Res.
   And Eng.
Information Office Library Br.
The Pentagon
2 Washington 25, D.C.

David Taylor Model Basin
Washington 7, D.C.
1 Attn: Technical Library

Census Bureau
Washington 25, D.C.
1 Attn: Office of Asst. Director
   for Statistical Services,
   Mr. J. L. McPherson

Program Director
Engineering Section
National Science Foundation
1 Washington 25, D.C.

U.S. AF Security Service
San Antonio, Texas
1 Attn: ODC-R

National Bureau of Standards
Washington 25, D.C.
1 Attn: R. D. Elbourn
1 Attn: S. N. Alexander
1 Attn: Librarian

National Security Agency
Ft. George G. Meade, Md.
1 Attn: Howard Campaigne

Diamond Ordnance Fuze Lab
Washington 25, D.C.
1 Attn: Library
1 Attn: ORDTL-450-638, R. H. Comyn
2 Attn: Dr. R. T. Young, ORDTL-930
1 Attn: T. M. Liimatainen

Central Intelligence Agency
2430 E St., N.W.
Washington 25, D.C.
1 Attn: Paul A. Borel

Assistant Secy. of Defense (R and D)
Research and Dev't. Board
Dept. of Defense
Washington 25, D.C.
1 Attn: Tech. Library

Office of Director of Defense(R and E)
Dept. of Defense
Washington 25, D.C.
1 Attn: Office of Electronics

Department of Defense
Defense Communications Agency
Washington 25, D.C.
1 Attn: Code 121A, Tech. Library

Institute for Defense Analyses
1666 Conn. Ave., N.W.
Washington 9, D.C.
1 Attn: W. E. Bradley

Director
Weapons System Evaluation Group
Rm. 1E875, The Pentagon
1 Washington 25, D.C.

Central Intelligence Agency
Washington 25, D.C.
1 Attn: OCR Standard Dist.

Advisory Group on Electron Devices
346 Broadway, 8th Floor East
New York 13, N.Y.
2 Attn: Harry Sullivan

Advisory Group on Reliability of
   Electronic Equipment
Office, Asst. Secy. of Defense
The Pentagon
2 Washington 25, D.C.

U.S. Dept. of Commerce
National Bureau of Standards
Boulder, Colorado
1 Attn: Library
2 Attn: Miss J. Lincoln, Chief,
   Radio Warning Services Sec.
1 Attn: Central Radio Prop. Lab.

The Director
U.S. National Bur. of Standards
Washington 25, D.C.
1 Attn: Sec. 14.1, Mr. G. Shapiro

Director
National Security Agency
Ft. George G. Meade, Md.
1 Attn: R-31
1 Attn: C-15
1 Attn: R-42
2 Attn: R-304
2 Attn: C3/TDL, Rm. 2C087

Chief, U.S.Army Security Agency
Arlington Hall Station
2 Arlington 12, Va.

CO, Harry Diamond Labs
Conn. Ave. and Van Ness Sts., N.W.
Washington 25, D.C.
1 Attn: Library, Rm. 211, Bldg. 92

Marine Corps Liaison Office
Bay 4D119, Hexagon
1 Ft. Monmouth, N.J.

Army Liaison Office
Lincoln Lab, P.O. Box 73
1 Lexington, Mass.

U.S. Coast Guard
1300 E St., N.W.
Washington 25, D.C.
1 Attn: EEE, Sta 5-5

Office of Tech. Services
Dept. of Commerce
1 Washington 25, D.C.

Advanced Res. Projects Agency
Office of Secy. of Defense
Washington 25, D.C.
1 Attn: Lt.Col. William B. Lindsay

U.S. Army Electronics Labs
Mt. View Office
P.O. Box 205
1 Mt. View, Calif.

CO, 9560 TSU
U.S.Army Signal Elec. Res. Unit
P.O. Box 205
1 Mt. View, Calif.

AF Systems Command Liaison Off.
Los Angeles Area
6331 Hollywood Blvd.
Hollywood 28, Calif.
1 Attn: Lt. Col. A. A. Konkel

DDC
Cameron Station
Alexandria, Va.
20 Attn: TISIA

Aerospace Res. Labs
Office of Aerospace Research, USAF
Wright-Patterson AFB, Ohio 45433
1 Attn: ARH

Scientific and Tech. Info. Facility
P.O. Box 5700
Bethesda, Md.   20014
1 Attn: NASA Rep. (SAK DL)

Universities

School of Engrg. Sciences
Arizona State U.
1 Tempe, Arizona

U. of Arizona
EE Dept.
Tucson 25, Arizona
1 Attn: Robert L. Walker
1 Attn: Dr. Douglas J. Hamilton
1 Attn: F. A. Lindholm, Assoc.Prof.

U. of California at Los Angeles
Dept. of Engrg.
Los Angeles, Calif.
1 Attn: Prof. Gerald Estrin

Calif. Inst. of Technology
Dept. of EE
1 Pasadena, Calif.
1 Attn: Dr. S. S. Penner
1 Attn: Prof. R. W. Gould
1 Attn: David Braverman

Calif. Inst. of Technology
Jet Propulsion Lab
4800 Oak Grove Dr.
Pasadena 3, Calif.
1 Attn: Documents Library
1 Attn: A. I. Bryan, Sr.Dev't Engr.

U. of California
Dept. of EE
Berkeley 4, Calif.
1 Attn: Dr. C. Susskind
1 Attn: Prof. J. R. Singer
1 Attn: Prof. R. M. Saunders

U. of California
Electronics Res. Lab
Berkeley 4, Calif.
1 Attn: Prof. Whinnery
1 Attn: T. Van Duzer, Asst. Prof.

U. of California
Radiation Lab, Info. Div.
Bldg. 30, Rm. 101
1 Berkeley 4, Calif.
1 Attn: Dr. R. K. Wakerling

U. of California
Tech. Info. Div.
Lawrence Radiation Lab
P.O. Box 808
1 Livermore, Calif.

University of California
Department of Engineering
Los Angeles 24, California
1 Attn: C.T. Leondes, Prof. of Eng.

University of California
College of Engineering
Electromagnetics Division
Los Angeles 24, California
1 Attn: R.S. Elliott

University of California, San Diego
School of Science and Eng.
Physics Department
LaJolla, California

Carnegie Inst. of Technology
E.E. Dept.
Schenley Park
Pittsburgh 13, Pa.
1 Attn: Dr. E.M. Williams

Case Institute of Technology
Engineering Design Center
Cleveland 6, Ohio
1 Attn: Dr. J.B. Neswick, Dir.

The University of Chicago
Institute for Computer Research
Chicago 37, Illinois
1 Attn: N.C. Metropolis, Dir.

University of Chicago
Lab. for Applied Sciences
Museum of Science and Industry
Chicago 37, Ill.
1 Attn: Library

Columbia University
Dept. of Physics
New York 27, N. Y.
1 Attn: Prof. L. Brillouin
1 Attn: Columbia Radiation Library

Columbia University
Columbia Radiation Lab.
538 W. 120th St.
New York, N. Y.
1 Attn: D. L. Harrow

Cornell University
Cognitive Sys. Res. Program
Hollister Hall
Ithaca, New York
1 Attn: Dr. E.F. Rosenblatt

DePaul University
1036 W. Belden Ave.
Chicago 14, Ill.
1 Attn: Dr. Julius J. Huppert,
        Prof. of Physics

Drexel Institute of Technology
Dept. of Electrical Engineering
Philadelphia 4, Pa.
1 Attn: Mr. F.B. Haynes

1 University of Florida
Dept. of Elec. Eng.
Gainesville, Florida
1 Attn: Prof. W.E. Lear
1 Attn: M.J. Wiggins

George Washington University
Electronics Res. Lab.
Washington 6, D.C.
1 Attn: Nelson T. Grisamore,
        Principal Investigator

Georgia Institute of Tech.
Atlanta 13, Georgia
1 Attn: Mrs. J.H. Crosland, Librarian
1 Attn: F. Dixon, Eng. Exper. Sta.

Harvard University
Tech. Rept. Collection
Rm. 303A, Pierce Hall
Cambridge 38, Mass.
2 Attn: Mrs. E. Farkas, Librarian

Harvard University
Pierce Hall 217
Cambridge 38, Mass.
1 Attn: Div. of Eng. & Applied Phys.
        Dean Harvey Brooks

University of Hawaii
Honolulu 14, Hawaii
1 Attn: Mr. Kazutoshi Najita, Ass't
        Prof., Elec. Eng. Dept.
1 Attn: Dr. Paul C. Yuen, Ass't Prof.,
        Elec. Eng. Dept.

University of Illinois
Department of Elec. Eng.
Urbana, Ill.
1 Attn: Dr. L. Goldstein
1 Attn: Tech. Ed., A. Albert
1 Attn: Antenna Lab.
1 Attn: William Perkins
1 Attn: Paul D. Coleman, Rm. 218

University of Illinois
Department of Physics
Urbana, Ill.
1 Attn: Dr. John Bardeen

University of Illinois
Digital Computer Lab.
Urbana, Ill.
1 Attn: Dr. .E. Robertson

University of Illinois
Coordinated Science Lab.
Urbana, Ill.
1 Attn: Prof. Daniel Alpert

University of Illinois
Urbana, Ill.
1 Attn: Lib. Serials Dept.

State Univ. of Iowa
Dept. of Electr. Engr.
Iowa City, Iowa
1 Attn: Prof. Donald L. Epley

Johns Hopkins University
Applied Physics Laboratory
8621 Georgia Ave
Silver Spring, Maryland
1 Attn: Doc. Library
1 Attn: Mr. A. W. Nagy
1 Attn: N. H. Choksy

Johns Hopkins University
Carlyle Barton Lab.
Charles & 34th St.
Baltimore 18, Maryland
1 Attn: Librarian
1 Attn: J.M. Minkowski

Linfield Research Institute
McMinnville, Oregon
1 Attn: Guy N. Hickok, Dir.

Marquette University
College of Engineering
1515 W. Wisconsin Ave.
Milwaukee 3, Wis.
1 Attn: Arthur C. Moeller

Massachusetts Institute of Tech.
Cambridge 39, Mass
1 Attn: J.B. Weisner
1 Attn: Mr. John E. Ward, Elec.
        Syst. Lab.
1 Attn: Res. Lab. of Elec., Doc. Rm.
1 Attn: Miss Aina Sils, Librn, LIR,
        Rm. 4-244, Lab for Insul. Res.
1 Attn: D.M. Baumann, Rm. 3-457,
        Dynamic Anal. & Control Lab.

1 Massachusetts Institute of Tech.
Lincoln Laboratory
P.O. Box 73
Lexington 73, Mass.
1 Attn: Library
1 Attn: Dr. Walter I. Wells
1 Attn: Navy Representative
1 Attn: Kenneth L. Jordan, Jr.

University of Maryland
Inst. for Fluid Dynamics & Appl.
  Mathematics
College Park, Maryland
1 Attn: Dr. J.M. Burgers

University of Michigan
Ann Arbor, Michigan
1 Attn: Electron Physics Lab.
1 Attn: Prof. Joseph E. Rowe, Elec.
        Eng. Dept.
1 Attn: Dir., Cooley Elec. Lab.
1 Attn: Tech. Doc. Service, Inst.
        of Science & Technology
1 Attn: Dr. Gordon E. Peterson,
        Dir. Communication Sci. Lab
1 Attn: W. Wolfe, IRIA, Inst. of
        Science & Technology
1 Attn: Communication Sciences Lab.

University of Minnesota
Dept. of Elec. Eng.
Institute of Tech.
Mineapolis 14, Minn.
1 Attn: Prof. A. Van Der Ziel

Missouri School of Mines & Metallurgy
Electrical Engineering Dept.
1 Rolla, Missouri

University of Nevada
College of Engineering
Reno, Nevada
1 Attn: Dr. Robert A. Manhart,
        Chairman Elec. Eng. Dept.

New York University
College of Engineering
New York 53, N. Y.
1 Attn: R.F. Cotellessa
1 Attn: Dr. Morris Kline

Northeastern University
The Dodge Library
Boston 15, Mass.
1 Attn: Joyce E. Lunde, Ref. Librn.

Northwestern University
Aerial Measurements Lab.
2422 Oakton St.
Evanston, Ill.
1 Attn: Walter S. Toth

North Carolina State College
Dept. of Electrical Eng.
Raleigh, North Carolina
1 Attn: Prof. R.W. Lade

University of Notre Dame
Electrical Eng. Dept.
South Bend, Indiana
1 Attn: Eugene Henry

Ohio State University
1314 Kinnear Road
Columbus 12, Ohio
1 Attn: Research Foundation
1 Attn: Dr. M.O. Thurston

Ohio State University
2024 Neil Ave.
Columbus 10, Ohio
1 Attn: Prof. E.M. Boone, Dept. of
     Elec. Eng.

Ohio State University
Dept. of Physics
174 W. 18th Street
Columbus, Ohio
1 Attn: Dr. M.L. Pool

Ohio University
College of Applied Science
Athens, Ohio
1 Attn: R.C. Quisenberry

Oregon State University
Elec. Eng. Dept.
Corvallis, Oregon
1 Attn: H.J. Oorthuys

Polytechnic Inst. of Brooklyn
Brooklyn, New York
1 Attn: Leonard Shaw, Elec. Eng. Dept.
1 Attn: Dr. R.A. Mareus
1 Attn: Dr. N. Marcuvitz, Vice Pres.
     for Res.

Polytechnic Inst. of Brooklyn
Graduate Center, Route 110
Farmingdale, New York
1 Attn: Librarian

University of Pennsylvania
Moore School of Elec. Eng.
200 South 33rd Street
Philadelphia 4, Pa.
1 Attn: Miss Anna Louise Campion

1 Princeton University
Elec. Eng. Dept.
Princeton, New Jersey
1 Attn: Prof. F.S. Acton

Purdue University
Elec. Eng. Dept.
LaFayette, Indiana
1 Attn: Library

Rensselaer Polytechnic Inst.
Troy, New York
1 Attn: Library-Serials Dept.
1 Attn: Plasma Res. Lab.,
     Mr. E. Howard Holt, Dir.
1 Attn: Prof. Kenneth E. Mortensen

Res. Inst. of Adv. Studies
7212 Bellona Ave.
Baltimore 12, Maryland
1 Attn: Dr. R.E. Kalman

University of Rochester
River Campus Station
Rochester 20, New York
1 Attn: Dr. Gerald H. Cohen,
     Gavett Hall

Rose Polytechnic Institute
Dept. of Elec. Eng.
Terre Haute, Indiana
1 Attn: Dr. C.C. Rogers

Rutgers University
Physics Dept.
Newark 2, New Jersey
1 Attn: Dr. Charles Pine

Stanford Research Institute
Menlo Park, Calif.
2 Attn: External Repts., G-037
1 Attn: Dr. C. Cook
1 Attn: H.D. Crane, Computer Lab.

Stevens Institute of Tech.
Hoboken, New Jersey
1 Attn: Dr. Bostick

Syracuse University
Syracuse 10, New York
1 Attn: Dept. of Elec. Eng.
1 Attn: Dr. Stanford Goldman

Temple University
Philadelphia, Pa.
1 Attn: Dr. J.L. Bohn

University of Tennessee
Dept. of Elec. Eng., Ferris Hall
1 Knoxville, Tennessee

Texas Technological College
Lubbock, Texas
1 Attn: Dir., Inst. of Science Engr.,
     Off. of Dean of Eng.
1 Attn: Prof. Harold Spuhler

University of Texas
Box 8029 Univ. Station
Austin, Texas
1 Attn: Def. Res. Laboratory

EERL
The Univ. of Texas
P O. Box 7789, Univ. Station
Austin, Texas   78712
1 Attn: Librarian, BFW

Tulane University
Elec. Eng. Dept.
New Orleans, La.
1 Attn: Dr. Nunn

University of Utah
Elec. Eng. Dept.
Salt Lake City, Utah
1 Attn: Richard W. Grow

Utah State University
Solid State Elec. Lab.
1 Logan, Utah
1 Attn: Mr. Craig M. Rushforth, Ass't
     Prof., Elec. Eng. Dept.

Santa Clara University
1 Santa Clara, California
1 Attn: Varsi Library

The University of Virginia
Charlottesville, Virginia
1 Attn: J.C. Wyllie, Alderman Lib.

University of Washington
Seattle 5, Washington
1 Attn: A.E. Harrison, Elec. Eng. Dept.

Wayne State University
Detroit, Michigan
1 Attn: Prof. Harry H. Josselson,
     Dept. of Slavic Languages

University of Wisconsin
College of Engineering
Dept of Elec. Eng.
Madison, Wis.
1 Attn: Mr. Thomas C. Gabriel

Worcester Polytechnic Inst.
Worcester, Mass.
1 Attn: Dr. H.H. Newell

Yale University
New Haven, Conn.
1 Attn: Dept. of Elec. Eng
1 Attn: Eng. Library
1 Attn: Sloane Physics Lab.

INDUSTRIES

Admiral Corporation
3800 Cortland St.
Chicago 47, Ill.
1 Attn: Edith N. Roberson, Librn.

Aero Chem Research Lab.
P.O. Box 12
Princeton, New Jersey
1 Attn: Dr. Calcote

Airborne Instruments Lab.
Comac Road
Deerpark, L.I., New York
1 Attn: John Dyer, Vice-Pres.
     Tech. Dir.

Amperex Corporation
230 Duffy Ave.
Hicksville, L.I., New York
1 Attn: S. Barbasso, Proj. Eng.

Argonne National Lab.
9700 So. Cass Ave.
Argonne, Ill.
1 Attn: Dr. O.C. Simpson, Dir.
     Solid State Science Div.

Auerback Corp.
1634 Arch St.
1 Philadelphia 3, Pa.

Autonetics
Div. of North American Aviation
9150 E. Imperial Highway
Downey, Calif.
1 Attn: Tech. Library, 3040-3

Avco Corp.
Research Lab.
2385 Revere Beach Parkway
Everett 49, Mass.
1 Attn: A. Kantrowitz
1 Attn: Dr. Gurdon Abell

Baird Atomic
33 University Rd.
Cambridge 38, Mass.
1 Attn: Dr. Hornig

Bell Telephone Laboratories
Murray Hill Laboratories
Murray Hill, New Jersey
1 Attn: Dr. J.K. Galt
1 Attn: Dr. J.R. Pierce
1 Attn: Dr. R.M. Ryder
1 Attn: Dr. M. Sparks
1 Attn: D.A. Chisholm
1 Attn: Mr. J.A. Morton
1 Attn: Dr. H. Loar
1 Attn: Dr. S. Darlington
1 Attn: A.J. Grossman

Bell Telephone Labs., Inc.
Technical Information Library
Whippany Laboratory
Whippany, New Jersey
1 Attn: Tech. Reports Librn.

Bendix Corporation
Research Laboratories Div.
Southfield (Detroit), Michigan
1 Attn: A.G. Peifer
1 Attn: Dr. W.N. Nunn, Jr.

Bendix Pacific Division
The Bendix Corporation
11600 Sherman Way
North Hollywood, Calif.
1 Attn: Engineering Library

Benson-Lehner Corporation
14761 California St
Van Nuys, Calif
1 Attn: George Ryan

Boeing Scientific Research Labs
P O. Box 3707
Seattle 24, Washington
1 Attn: G.L. Hollingsworth

Bomac Laboratories
Beverley, Mass.
1 Attn: Research Library

Chrysler Corp., Space Div.
P.O. Box 26018
New Orleans 26, La.
1 Attn: M.M. Holmes

Columbia Radiation Laboratory
538 W. 120th St.
1 New York 27, New York

Convair-San Diego
A Div. of General Dynamics Corp.
San Diego 12, Calif.
1 Attn: Engineering Library
        Mail Zone 6-157
        VIA: Air Force Plant Rep.
             San Antonio Air Materiel
             Area
             Convair-Astronautics
             San Diego 12 Calif.

Cook Research Laboratories
6401 W. Oakton St.
1 Morton Grove, Ill.

Cornell Aeronautical Labs., Inc.
4455 Genesee St.
Buffalo 21, New York
1 Attn: D.K. Plummer
2 Attn: Library

Eitel-McCullough, Inc.
301 Industrial Way
San Carlos, Calif.
1 Attn: Research Librarian
1 Attn: W.R. Luebke

Electronic Communications, Inc.
1830 York Rd.
1 Timonium, Maryland

Emerson Research Laboratories
Silver Spring, Maryland
1 Attn: Mr. S. Rattner

Electro-Optical Instruments, Inc.
125 N. Vinedo
Pasadena, Calif.
1 Attn: I. Weiman

Ewen Knight Corporation
East Natick, Massachusetts
1 Attn: Library

Fairchild Semiconductor Corp.
313 Fairchild Dr.
P.O. Box 880
Mt. View, Calif.
1 Attn: Dr. V. H. Grinich

Fairchild Semiconductor Corp.
545 Whisman Rd.
Mountain View, Calif.
1 Attn: Dr. R. Noyce

Federal Scientific Corp.
615 W. 131st St.
1 New York 27, New York

Geisler Laboratories
P.O. Box 252
Menlo Park, Calif.
1 Attn: Librarian

General Electric Co.
TWT Product Section
601 California Ave.
Palo Alto, Calif.
1 Attn: Tech. lab., C.G. Lob
1 Attn: Tech. Lib.
1 Attn: D.H. Goodman Manager
        Manufacturing Operations

General Electric Co.
Defense Electronics Division-LMED
Cornell University
Ithaca, New York
1 Attn: Library
        VIA: Commander, ASD
             W-P AFB, Ohio
             Attn: ASRNC-5,D.E.Lewis

Dr. Ervin J. Nalos
The Boeing Co.
Seattle 24, Wash.
1 Attn: MS-1331, ORG. 1-8000

General Electric Co.
Research Laboratory
P.O. Box 1088
Schenectady, New York
1 Attn: Dr Philip M Lewis
1 Attn: G.E Feiker
1 Attn: R. L. Shuey, Manager
        Info and Studies Section

General Electric Co.
Schenectady Tube Operation
1 River Rd.
Schenectady, N.Y.   12305
1 Attn: Mr. E.D. McArthur

General Electric Co.
Electronics Park Bldg. 3, Rm. 143
Syracuse New York
1 Attn: Doc. Librn., Yolanda Burke

General Electric Co.
Rectifier Components Dept.
Advance Rectifier Eng.
Auburn, New York
1 Attn: Gerald C. Huth

General Electric Co.
Evandale, Ohio
1 Attn: M.L. Ghai

General Electric Co.
Research Laboratory
Applied Physics Section
P.O. Box 1088
Schenectady, New York
1 Attn: V.L. Newhouse
1 Attn: Lab., L.M. E. Dept., Bldg
        28-501

General Electric Space Sciences Lab
Space Technology Center
King of Prussia, Pa.
1 Attn: Dr. David B. Miller

General Precision, Inc.
Link Group
1451 California Ave.
Palo Alto, Calif. , 94304
1 Attn: Technical Library

General Tel. and Elec. Lab.
Bayside 60, New York
1 Attn: L R Bloom

Gilfillan Bros.
1815 Venice Boulevard
Los Angeles, Calif.
1 Attn: Eng. Library

Goddard Space Flight Center
Greenbelt, Maryland
1 Attn: Code 611

Hallicrafters, Co.
4401 W. Fifth Ave.
Chicago 24, Ill.
1 Attn: William Frankart

Hallicrafters Co.
5th and Kostner Avenues
1 Chicago 24, Ill.

Hewlett-Packard Co.
1501 Page Mill Rd
1 Palo Alto, Calif

Hoffman Electronics Corp.
(Service Center)
700 Hoffman Dr.
1 Santa Barbara, Calif.

Hoffman Electronics Corp.
100 Hoffman Dr.
Santa Barbara, Calif.
1 Attn: Dr. D.M. Heinz
        Senior Scientist

Hoffman Electronics Corp.
Semiconductor Div
1001 Arden Drive
El Monte, Calif.
1 Attn: P.N. Russell,
        Technical Dir.

Hoffman Electronics Corp.
Military Products Div. Sys. Dept
3740 South Grand
Los Angeles 7, Calif.
1 Attn: L A. Saggiani

HRB Singer Inc.
Science Park
P.O. Box 60
State College, Pa.
1 Attn: Tech. Info Center

Hughes Aircraft Co.
Florence at Teale St.
Culver City, Calif.
1 Attn: Tech. Library
1 Attn: Solid State Group M107
1 Attn: Tech. Doc. Center
1 Attn: Mr. A.S Jerrems
        Aerospace Group
1 Attn: Dr N.I. Hall, Vice-Pres.
        Engineering

Hughes Aircraft Co.
Semiconductor Div.
P.O. Box 278
Newport Beach, Calif.
1 Attn: Library
1 Attn: Tech Librarian

Hughes Aircraft Co.
Bldg. 604, Mail Sta. C-213
Fullerton Calif.
1 Attn: Mr. A. Eschner, Jr
        Ground Systems Group

Hughes Aircraft Co.
3011 Malibu Canyon Rd
Malibu, Calif.
6 Attn: Mr. H.A. Iams, Res. Labs.

Huggins Laboratories
999 E. Arques Ave.
1 Sunnyvale, Calif.

International Business Machines
Product Development Lab.
Poughkeepsie, New York
1 Attn: E.M. Davis (Dept. 362)

International Business Machines
Data Systems Division
Box 390 Boardman Rd.
Poughkeepsie. New York
1 Attn: J.C. Logue

International Business Machines
Research Library, Box 218
1 Yorktown Heights, New York

IBM ASD × Res. Library
Bldg. 025
Monterey × Cottle Roads
San Jose, Calif.
1 Attn: Miss Marjorie Griffin
1 Attn: Dr. Mih Yin

International Business Machines
Tech. Reports Center
Space Guidance Center
Federal Systems Division
1 Owego, New York

ITT Laboratories
15151 Bledsoe Street
San Fernando, Calif.
1 Attn: F.E. Randle Librn.
1 Attn: C.V Stanley

ITT Federal Laboratories
500 Washington Ave.
Nutley 10, N.J.
1 Attn: Mr. Ellis Mount, Librn.
1 Attn: Mr. A.W. McEwan, Electron
     Tube Laboratory

ITT Federal Laboratories
390 Washington Ave.
Nutley, N.J.
1 Attn: Mr. T.J. Golden

International Tel. × Tel. Corp.
ITT Laboratories Div.
492 River Rd.
Nutley 10, N.J.
1 Attn: J. Le Grand

Jansky × Bailey
Systems Engineering Div.
Atlantic Research Corp.
Shirley Highway ; Edsall Rd.
Alexandria, Virginia   22314
1 Attn: John J. Renner

Korad Corporation
2520 Colorado Ave.
Santa Monica, Calif.
1 Attn: Mr. Fred P. Burns, Manager
     Semiconductor Division

Laboratory For Electronics Inc.
1075 Commonwealth Ave.
Boston 15, Mass.
1 Attn: Library

Laboratory For Electronics, Inc.
1079 Commonwealth Ave.
Boston 15, Mass.
1 Attn: Dr. H. Fuller

Lear Siegler, Inc.
3171 S. Bundy Dr.
1 Santa Monica, Calif.

LEL, Inc.
75 Akron Street
Copiague, L.I., New York
1 Attn: Mr. Robert S. Mautner

Lenkurt Electric Co.
San Carlos, Calif.
1 Attn: M.L. Waller, Librn.

Librascope Division
General Precision, Inc.
808 Western Ave.
Glendale 1, Calif.
1 Attn: Engineering Library

Litton Industries, Inc.
960 Industrial Rd.
San Carlos, Calif.
1 Attn: Tech. Library

Lockheed Aircraft Corporation
Georgia Division
Marietta, Georgia
1 Attn: Department 72-15

Lockheed Electronics Co.
Military Systems
U.S. Highway 22
Plainfield, N.J.
1 Attn: C.L. Opitz

Lockheed Aircraft Corp.
Missile & Space Div.
P.O. Box 504
Sunnyvale, Calif.
1 Attn: Dr. W.M. Harris, Dept. 65-70
     Bldg. 524
1 Attn: G.W. Price
1 Attn: Tech. Info. Center

Lockheed Missile × Space Div.
Dept. 5240, Bldg. 202
Palo Alto, Calif.
1 Attn: Mr. M.E. Browne

Loral Electronics Corp.
825 Bronx River Rd.
New York 72, New York
1 Attn: Louise Daniels, Librn.

Marquardt Aircraft Co.
16555 Saticoy St.
P.O. Box 2013-South Annex
Van Nuys, Calif.
1 Attn: Dr. Basun Chang, Res. Sci.

The Martin Co.
Baltimore 3, Maryland
1 Attn: Scientific-Tech. Lib.
     Mail J398

The Martin Co.
P.O. Box 5837
Orlando, Florida
1 Attn: Eng. Lib., M.P. 30

Maxson Electronics Corp.
460 West 34th St.
New York 1, New York
1 Attn: M. Simpson

Melpar, Inc.
3000 Arlington Blvd.
Falls Church, Va.
1 Attn: Librarian
1 Attn: W.T. Layton, Phys. Elec. Sec.

Micro State Electronics Corp.
152 Floral Ave.
Murray Hill, N.J.
1 Attn: A.L. Kestenbaum

Microwave Associates
North West Industrial Park
Burlington, Mass.
1 Attn: Librarian
1 Attn: Dr. Kenneth Mortenson

Microwave Electronics Corp.
3165 Porter Dr.
Palo Alto, Calif.
1 Attn: Stanley F. Kaisel
1 Attn: M.C. Long

Minneapolis Honeywell Reg. Co.
Semiconductor Prod. Lib.
1177 Blue Heron Blvd.
1 Riviera Beach, Florida

Minneapolis Honeywell Reg. Co.
Aeronautical Div, Los Angeles
1915 Armacost Ave.
Los Angeles 25, Calif.
1 Attn: Tech. Library

The MITRE Corp.
Bedford, Mass.
1 Attn: Library

Monsanto Research Corp.
Station B, Box 8
Dayton 7, Ohio
1 Attn: Mrs. Dorothy Crabtree

Monsanto Chemical Co.
800 N. Linbergh Blvd.
St. Louis 66, Mo.
1 Attn: Mr. Edward Orban
     Mgr. Inorganic Development

Motorola, Inc.
Military Electronics Div.
8201 East McDowell Rd.
Scottsdale, Arizona
1 Attn: Paul Stancik

Motorola, Inc.
P.O. Box 5409
Phoenix 10, Arizona
1 Attn: Dr. H.W. Welch, Jr., Gen.
     Mgr. Solid State Sys. Div.

Motorola, Inc.
Solid State Devices Lab
Scottsdale, Arizona
1 Attn: John Cacheris, Mgr.

Motorola Semiconductor Prod. Div.
5005 East McDowell Rd.
Phoenix Arizona
1 Attn: Dr. A. Lesk
2 Attn: Dr. R. M. Warner, Jr.
2 Attn: Library

Motorola, Inc.
Chicago Military Elec. Center
1450 North Cicero Ave.
Chicago 51, Ill.
1 Attn: Jo Goldyn-CMC Librn.
     VIA: Motorola, Inc.
          Chicago 51, Ill.
          Attn: Sec. Officer

National Biomedical Res. Inst.
8600 16th St.
Silver Spring, Maryland
1 Attn: Dr. R.S. Ledley

Norden Division
United Aircraft Corp.
Norwalk, Conn.
1 Attn: Alice Ward, Librn.

Nortronics
Palos Verdes Research Park
6101 Crest Rd.
Palos Verdes Estates, Calif.
1 Attn: Tech. Info. Center

North American Aviation, Inc.
Columbus Division
Engineering Data Services
4300 E. Fifth Ave.
1 Columbus 16, Ohio

Pacific Semiconductors, Inc.
14520 So. Aviation Blvd.
Lawndale, Calif.
1 Attn: H.Q. North

Philco Corp.
Tech. Rep. Div.
P.O. Box 4730
Philadelphia 34, Pa.
1 Attn: F.R. Sherman, Managing Ed.,
        Philco Techrep Div. Bulletin

Philco Corp.
Jolly & Union Meeting Roads
Blue Bell, Pa.
1 Attn: Mr. James P. Spratt
1 Attn: Dr. Marvin E. Lasser,
        Ass't. Dir.
1 Attn: C.V. Bocciarelli

Philco Corp.
Lansdale Division
Lansdale, Pa.
1 Attn: Dr. Clarence G. Thornton,
        Gen. Mgr. Spec. Prod. Op.

Philco Corp., Lansdale Div.
Church Rd.
Lansdale, Pa.
1 Attn. John R. Gordon

Polorad Electronics Corp.
43-20 Thirty-Fourth St.
Long Island City 1, N.Y.
1 Attn: A.H. Sonnenschein, Ass't
        to the President

PRD Electronics, Inc.
202 Tillary St.
Brooklyn 1, N.Y.
1 Attn: R. Casiano, Adv. Ass't.

Radiation, Inc.
Melbourne, Florida
1 Attn: Librarian

Radio Corp. of America
RCA Laboratories
David Sarnoff Res. Center
Princeton, N.J.
1 Attn: Dr. Jack Sklansky
1 Attn: Harwick Johnson

Radio Corp. of America
Defense Electronic Products
Missile & Surface Radar Eng.
Moorestown Eng. Library 127-221
1 Moorestown, N.J.

Radio Corp. of America
Missile Electronics & Controls Div
Woburn, Mass.
1 Attn: Library

Ramo-Wooldridge, A Div. of
Thompson Ramo Wooldridge, Inc.
8433 Fallbrook Ave.
Canoga Park, Calif.
1 Attn: Tech. Info. Services

The Rand Corp.
1700 Main St.
Santa Monica, Calif.
1 Attn: Helen J. Waldron, Librn.
1 Attn: Computer Sci. Dept.
        Willis H. Ware

Raytheon Manufacturing Co.
Research Division
Waltham, Mass.
1 Attn: Dr. Herman Statz
1 Attn: Mrs. Madaleine Bennett, Librn.
1 Attn: Res. Div. Library
1 Attn: J. M. Lavine

Raytheon Manufacturing Co.
Spencer Laboratory
Burlington, Mass.
1 Attn: Librn., Microwave & Pwr.
        Tube Div.
1 Attn: Dr. H. Scharfman

Raytheon Co.
P.O. Box 1542
Goleta, Calif.
1 Attn: Librarian

Raytheon Co.
Bedford, Mass.
1 Attn: Mrs. I. Britton Librn.

Raytheon Co.
Semiconductor Lib.
P.O. Box 280
Mountain View, Calif.
2 Attn: Leo M. Johnson

Raytheon Manufacturing Co.
1415 Boston-Providence Turnpike
Norwood, Mass.
1 Attn: Mr. L. Edwards

RCA Laboratories
Princeton, N.J.
1 Attn: Dr. W.M. Webster

Radio Corp. of America
Bldg. 108-134
Moorestown, New Jersey
1 Attn: H.J. Schrader

Radio Corp. of America
Surface Communications Div.
Front & Market St's., Bldg. 17-C-6
Camden, N.J.
1 Attn: K.K. Miller, Mgr. Minuteman
        Proj. Office

Sylvania Electronic Defense Lab.
P.O. Box 205
1 Mt. View, Calif.

Revere Copper & Brass, Inc.
Foil Division
196 Diamond Street
Brooklyn 22, N.Y.
1 Attn: Vincent B. Lane

Rocketdyne
Canoga Park, Calif.
1 Attn: Dr. Boden

Sandia Corp., Sandia Base
Albuquerque, New Mexico
1 Attn: Mrs. B.R. Allen, Librn.

S.F.D. Laboratories, Inc.
800 Rahway Ave.
1 Union, New Jersey
1 Attn: Dr. J. Saloom
1 Attn: Dr. Feinstein

The STL Tech. Library
Doc. Acquisitions
Space Tech. Labs., Inc.
One Space Park
1 Redondo Beach, Calif.

Sperry Rand Res. Center
North Road
Sudbury, Mass.
1 Attn: Alan Steeves, Librn.

Sperry Electron Tube Div.
Sperry Rand Corp
Gainesville, Florida
1 Attn: Librarian

Sperry Microwave Electronics Co.
Clearwater, Florida
1 Attn: John E. Pippin Res.
        Sec. Head

Sperry Gyroscope Co.
Div. of Sperry Rand Corp.
Great Neck, L.I., N. Y.
1 Attn: Leonard Swern (M.S. 3T105)
1 Attn: Mr. Robert L. Wathen
1 Attn: K. Barney, Engr. Dept. Head
        Mail Station F7

Socony Mobil Oil Company
Field Research Laboratory
P.O. Box 900
Dallas 21, Texas
1 Attn: Librarian

Sylvania Electric Products Inc.
P.O. Box 188
1 Mt. View, Calif.
1 Attn: Tech. Library
1 Attn: J.B. Gaenzle-M.T.L.
1 Attn: Dr. R. G. Hutter, Microwave
        Components Lab. Bldg. 4
1 Attn: Dr. H.W. Bandel

Sylvania Electric Products, Inc.
Tech. Info. Services
1 Mountain View, Calif.

Sylvania Electronic Def. Lab.
P.O. Box 205
1 Mt. View, Calif.
1 Attn: Donlan Jones
1 Attn: Optics Dept., Bldg. 4

Sylvania Electric Products, Inc.
Waltham Laboratories
100 First Ave.
Waltham 54, Mass.
1 Attn: Librn., Sylvania Electronics
        Systems
1 Attn: John Donner
1 Attn: Mr. Ernest E. Hollis

Sylvania Electric Products, Inc.
500 Evelyn Ave.
Mt. View, Calif.
1 Attn: Mr. E.O. Ammann

Technical Research Group
Route No. 10
1 Melville, New York   11749

Texas Instruments, Inc.
P O. Box 5012
Dallas 22, Texas
2 Attn: Semiconductor Components Lib.
1 Attn. Tech. Repts. Service, MS-65

Texas Instruments, Inc.
P.O. Box 6015
Dallas 22, Texas
1 Attn Apparatus Div., M.F. Chun

Texas Instruments Inc.
Corporate Res.   Eng.
Tech. depts. Service
P O. Box 5474
1 Dallas 22, Texas

Textronix, Inc.
P.O. Box 500
Beaverton, Oregon
4 Attn Dr. Jean F. DeLord, Dir.
          of Research

Tucor, Inc.
59 Danbury Rd.
Wilton, Conn.
1 Attn Mrs. Marion E. Osband

Varian Associates
611 Hansen Way
Palo Alto, Calif.
1 Attn: Tech. Library

Vitro Laboratories
200 Pleasant Valley Way
West Orange N.J.
1 Attn: Miss B.R. Meade, Librn.

Warnecke Electron Tubes Inc
175 W Oakton St.
Des Plaines, Ill.
1 Attn: Frank Voltaggio, Jr.
           Dir of Marketing

Watkins-Johnson Co.
3333 Hillview Ave.
Palo Alto, Calif.
1 Attn: Dr. H.R. Johnson

Weitermann Electronics
4549 North 38th St.
1 Milwaukee 9, Wisconsin

Westinghouse Electric Corp.
P.O. Box 284
Elmira, New York
1 Attn: Shelden S. King
1 Attn: Carl Miller, Elec. Tube Div.

Melbourne J. Hellstrom, Supv. Eng.
Westinghouse Electronics Corp.
Molecular Electronics Div.
Box 1836
1 Baltimore, Maryland   21203

Westinghouse Electric Corp.
Westinghouse Air Arm Div.
Box 746
Baltimore 3, Maryland
1 Attn: H.B. Smith, Mgr. Eng. Dept.
1 Attn: Tech. Info. Center
           Mrs. A.E. Battaglia, Supt.
1 Attn: G. Ross Kilgore

Westinghouse Electric Corp.
R & D Center, Bldg. 501
Beulah Rd.
Pittsburgh 35, Pa.
1 Attn: Dr. G.C. Sziklai
1 Attn: J. G. Castle, Jr. 401-1B5
1 Attn: R.E. Davis

Zenith Radio Corp.
6001 Dickens Ave.
Chicago 39, Ill.
1 Attn: Joseph Markin

Laboratory of Automatic Control Sys.
Tech. Univ. of Denmark, Lundtofte
1 Lyngby, DENMARK
VIA: ONR London

The University of Adelaide
Adelaide, SOUTH AUSTRALIA
1 Attn: BARR Smith Library
           VIA: ONR London